ANALYSIS AND CONTROL OF SHUNT COMPENSATOR IN DISTRIBUTION SYSTEM

by
PRAKASH CHITTORA
Department of Electrical Engineering

Submitted

In partial fulfillment of the requirements for the award of degree of

DOCTOR OF PHILOSOPHY

DEPARTMENT OF ELECTRICAL ENGINEERING
DELHI TECHNOLOGICAL UNIVERSITY
DELHI-110042, INDIA

November, 2018

CERTIFICATE

This is to certify that the thesis entitled "**Analysis and Control of Shunt Compensator in Distribution System**" being submitted by **Mr. Prakash Chittora** for the award of degree of Doctor of Philosophy in the Department of Electrical Engineering, Delhi Technological University, Delhi, is the record of students own work carried out by him under our supervision. The contents of this research work have not been submitted in part or fully to any other institute or University for the award of any degree.

Date:

Prof. Alka Singh
Department of Electrical Engineering
Delhi Technological University, Delhi
Shahbad Daulatpur, Delhi-110042, India

Prof. Madhusudan Singh
Department of Electrical Engineering
Delhi Technological University, Delhi
Shahbad Daulatpur, Delhi-110042, India

ACKNOLEDGEMENTS

I would like to express my deep and sincere gratitude to my supervisors **Prof. Alka Singh** and **Prof. Madhusudan Singh** for their valuable guidance and continuous monitoring of my research work. It was great honor for me to pursue my research work under their supervisions. Prof .Alka Singh has been the main motivating and inspiring factor behind my research work. It's her vigor and hunger to perform in adverse situation, which has inspired me to thrive for excellence and nothing less. Continuous monitoring by Prof. Madhusudan Singh, valuable guidance and input has always been a driving force to complete my research work. Also his support as the Head of the Department was invaluable. It is a life time experience to work under both of my supervisors.

I would also like to convey my sincere gratitude to **Mr. Ram Bhagat**, Assistant Professor, DTU, who has taught me the relevant course work. I would like to thank the SRC members mainly **Prof. B. Das**, who have given me valuable guidance and advice to improve quality of my research work. I am extremely grateful to **Prof. Pragati Kumar**, **Prof. Mukhtiar Singh** for their valuable assistance and support. I am extremely thankful to staff members of Power System Lab, DTU, Delhi for providing me immense facility and assistance to carry out my research work. I would like to thank other office staff, Central library and Computer Centre staff, for their valuable co-operation and support.

I would like my sincere thanks to **Dr. Manoj Badoni**, who has guided me to develop hardware at initial level of research work. His research publications have guided me during all time of my research work. I am extremely grateful to my research group and friends Hemant Saxena, Suryakant Shukla, Ashutosh Trivedi, Ambrish Devanshu, Imran quadri, Tausif Ahmad, Priyanka Choudhary, Nikita Gupta, Vivek Rewani, Rajat raj Singh, Rajat Kesharwni, Kuldeep Singh for their valuable assistance, co-operation and great source of learning.

If I get any success today for my research work, the entire credit should go to my mother Smt. Laxmi Chittora, wife Saloni Chittora, my elder bother Deepak Chittora and my elder sister Jyoti Chittora. I would like to express my deep concern to my lovely daughter, Miss Harshni Chittora for her consideration during long hours of absence from home. I would also like to thank my friend Vikas Bagla, for his extreme moral support during my research period. I would like to thank other family members supporting me directly or indirectly to carry out my research work.

I thank to almighty, the father of all for his blessing to accomplish my research work successfully.

Date:
Place: Delhi

Prakash Chittora
(2K14/Ph.D/EE/01)

ABSTRACT

Electrical Power distribution systems suffer from power quality (PQ) problems such as poor power factor, load unbalancing, harmonics, distortion in voltage etc. The contribution of non-linear loads incorporating power electronics devices viz. switch mode power supply, variable frequency drive (VFD), lighting loads (CFL, LED) etc. in power distribution systems is high. This leads to higher PQ problems into the system such as harmonics injection in voltage and current, high neutral current etc. Since the continued presence of PQ problems deteriorates the quality of power at the end user level, hence it becomes important to find solutions to overcome power quality problems.

Conventional methods to improve PQ in distribution system include the installation of capacitors, tap changing transformers, reactors, capacitor banks etc. However, these are slow compensation techniques and do not provide active load compensation, so new custom power devices have been designed. Shunt Active Power Filter (SAPF) is one such solution aimed to provide load compensation. The SAPF can mitigate several PQ problems such as load unbalancing, current harmonics, poor power factor of load etc. A SAPF can be realized using Voltage Source Converter (VSC) with a DC link capacitor. Three leg VSC for three-phase, three wire (TPTW) and four leg VSC for three-phase, four wire (TPFW) configuration are conventionally used VSC configurations.

TPFW systems may have additional requirement of neutral current compensation due to the presence of unbalanced loads. The SAPF with four legs can be realized for TPFW system, however, the system cost increases. A low cost solution is to use zigzag transformer configuration to mitigate excess neutral current and the conventional TPTW SAPF configuration.

The proposed work has been divided into four parts and deals with compensation in TPTW and TPFW distribution systems, distorted three-phase grid systems and single –phase systems without/ with PV integration. Detailed system design, development and analysis of new control algorithms have been investigated. Simulation as well as experimental results have been analyzed and tabulated with linear as well as non-linear loads. Conventional control techniques viz Synchronous Reference frame Theory (SRFT), Power Balance Theory (PBT) and Instantaneous Reactive Power Theory (IRPT) have been initially tested on the prototype system developed in the laboratory.

Three new control algorithms have been developed on TPTW distribution system which include Notch Filter, Kalman-LMS and Hopfield neural network based algorithm. These have been developed and implemented using dSPACE 1104 as Digital Signal Processor (DSP). Various PQ issues such as load unbalancing, current harmonics and supply current power factor have been considered. Detailed simulation results are recorded and verification of these results on the experimental setup is performed. Simulation has been performed in MATLAB/SIMULINK environment.

PQ problems in TPFW distribution system have been studied. The control algorithms developed for this system are Self Tuning Filter (STF), Modified Recursive Gauss Newton (MRGN) and Chebyshev polynomial based algorithms. A conventional three leg configuration of VSC has been used as SAPF; however zigzag transformer has been designed and used for neutral current compensation. The experimental setup has been controlled using dSPACE 1104. PQ issues such as load unbalancing, current harmonics, supply current power factor and neutral current compensation have been considered with different loads. Experimental results of all techniques have been analyzed in details.

In electrical power distribution system, the presence of distortion in the grid voltages is also a major PQ problem. The supply voltages may have high distortion due to presence of large source impedance. The TPFW experimental setup with distorted grid and unbalanced linear and non-linear loads has been investigated. PQ issues such as load unbalancing, current harmonics, supply current power factor and neutral current compensation have been mitigated successfully for distorted Point of Common Connection (PCC) voltages. Both simulation and hardware results using Multiple Complex Coefficient Filter (MCCF) and Second Order Generalized Integrator (SOGI) control algorithms have been analyzed and compared.

Next, PQ problems in a single phase grid connected system have been analyzed and the system has been developed in the laboratory. Two aspects discussed in this chapter are the integration of PV and mitigation of PQ problems. Three control algorithms viz SRFT, Notch Filter and second order generalized integrator (SOGI) based algorithm have been developed to mitigate PQ problems.

Solution of PQ problems in single-phase, TPTW, TPFW distribution systems using different SAPF configurations and new control techniques is the highlight of this thesis work.

TABLE OF CONTENTS

LIST OF FIGURES

LIST OF TABLES

LIST OF SYMBOLS

E_a, E_b, E_c	Three phase AC supply voltages
v_{sa}, v_{sb}, v_{sc}	Phase a, b, c PCC voltages
i_{sa}, i_{sb}, i_{sc}, i_{sn}	Phase a, b, c and neutral supply currents
i_{La}, i_{Lb}, i_{Lc}, i_{Ln}	Phase a, b, c and neutral load currents
i_{ca}, i_{cb}, i_{cc}	Phase a, b, c compensator currents
z_{sa}, z_{sb}, z_{sc},z_{sn}	Phase a, b, c and neutral source impedance
V_{dc}	DC link voltage
V_{dc}^{*}	Reference DC link voltage
C_{dc}	DC link capacitance
i_{Zn}	Zigzag transformer neutral current
i_{Zna}, i_{Znb}, i_{Znc}	Zigzag transformer output currents
ε	Damping constant
i_{sa}^{*}, i_{sb}^{*}, i_{sc}^{*}	Phase a, b, c supply reference currents
$i_{L\alpha}$, $i_{L\beta}$	Load current alpha-beta components
$v_{s\alpha}$, $v_{s\beta}$	Supply voltages alpha-beta components
I_{pa}, I_{pb}, I_{pc}	Phase a, b, c fundamental active power components
I_{pabc}	Fundamental active power component of load currents
I_{avg}	Average fundamental active power component
I_{loss}	Loss component due to IGBT switching
I_{eff}	Effective fundamental active power component
u_{ia}, u_{ib}, u_{ic}	Phase a, b, c in-phase unit templates
KG	Kalman gain
ξ	Error for Least Mean Square (LMS) technique
X_n	State vector of order Nx1

A	System matrix of order NxN
J	Process noise vector of order Nx1
Y_n	Measurement Vector of order Mx1
H	Constant Matrix of order Mx1
L	Measurement noise vector of order Mx1
$P_{n/n-1}$	State covariance matrix
P	Final state covariance matrix
Q	Process Noise covariance
H	Output Matrix
R	Measurement Noise Covariance
G	Gain constant
Γ(na)	Objective function for Hopfield Neural Network (HNN) technique
α_{am} ,β_{am}	Weighted components of the m^{th} harmonic load current extracted using HNN
K_p, K_I	Proportional and integral gain of PI controller
e_{dc}	Error between V_{dc} and V_{dc}^*
V_t	Amplitude of PCC voltages
$i_{L\alpha f}$, $i_{L\beta f}$	Filtered load current alpha-beta component
D	Constant gain
χ_m	Zero mean white noise
M_m	Peak magnitude of m^{th} harmonic load current
γ_m	Phase value of m^{th} harmonic load current
ρ(k)	Error at k^{th} instant between actual and calculated load current
ζ	Forgetting factor
$H(k)$	Hessian matrix

$\Upsilon(k)$	Gradient matrix
Z_1, Z_2, Z_3	Chebyshev polynomial
Z_{a1}, Z_{a2}, Z_{a3}	Weighted Chebyshev expansion for phase 'a'
w_{a1}, w_{a2}, w_{a3}	Weightes of Chebyshev Polynomial control algorithm for phase 'a'
ω_0	Fundamental frequency
ω_b	Bandwidth of Complex Coefficient Filter
$i_{L\alpha n}^{+}, i_{L\beta n}^{+}$	Positive sequence n^{th} harmonic alpha-beta load currents component
$i_{L\alpha n}^{-}, i_{L\beta n}^{-}$	Negative sequence fundamental alpha-beta component of load currents.
$v_{s\alpha f}, v_{s\beta f}$	Filtered PCC voltage alpha-beta components
$v_{saf}, v_{sbf}, v_{scf}$	Filtered phase a, b, c PCC voltages
W	Constant gain
i_{Laj}, i_{Lak}	SOGI phase 'a' in-phase and quadrature load current components
$u_{ia}^{+}, u_{ib}^{+}, u_{ic}^{+}$	Modified in-phase unit templates

LIST OF ABBREVIATIONS

ADC	Analog to Digital
ChANN	Chebyshev Polynomial based Artificial Neural Network
DAC	Digital to Analog
DSO	Digital Signal Oscilloscope
DSP	Digital Signal Processor
EAC	Electric Arc Furnace
HCC	Hysteresis Current Control
HNN	Hopfield Neural Network
IGBT	Insulated Gate Bipolar Transistors
IRPT	Instantaneous Reactive Power Theory
KF	Kalman Filter
KG	Kalman Gain
LMS	Least Mean Square
MCCF	Multiple Complex Coefficient Filter
MPPT	Maximum Power Point Tracking
MRGN	Modified Recursive Gauss Newton
NF	Notch Filter
PBT	Power Balance Theory
PCC	Point of Common Coupling
PF	Power Factor
PLL	Phase locked Loop
PQ	Power Quality
PV	Photo Voltaic
PWM	Pulse Width modulation

RES	Renewable Energy Sources
SAPF	Shunt Active Power Filter
SRFT	Synchronous Reference Frame Theory
SOGI	Second Order Generalized Integrator
STF	Self Tuning Filter
THD	Total Harmonic Distortion
TPFW	Three-Phase-Four-Wire
TPTW	Three-Phase-Three-Wire
UPF	Unity Power Factor
VSC	Voltage Source Converter

Chapter 1
INTRODUCTION

1.0 GENERAL

Power quality (PQ) refers to maintaining sufficiently high grade electricity at the generation, transmission and distribution level. The PQ is a concept to describe the quality of electrical power delivered. The quality of electricity may be described in terms of number of parameters, such as harmonic distortions in the supply voltage and current waveforms, continuity of electricity, variation in voltage level, transients in voltages and currents etc. Poor PQ may result in mal-operation or failure of customer's equipment and an electrical load (or device) may not able to operate or fail prematurely.

PQ problems in electric distribution systems have increased tremendously in the recent past [1-7]. Nonlinear loads such as Uninterrupted Power Supply (UPS), Electric Arc Furnaces (EAF), Switch Mode Power Supplies (SMPS), Variable Frequency Drives (VFD), computers and other electronic equipment installed at the distribution level are main causes of distortion in voltage and current. Various PQ problems such as current and voltage distortions, load unbalancing, excessive reactive power demand and voltage drop at Point of Common Coupling (PCC) cause detrimental effects to the electric power distribution system [8-9]. Mitigation of harmonics and other PQ issues [10-23] and maintaining reliable power supply to all consumers are main objectives of the electrical utilities. PQ estimation [24-39] focuses on techniques for easy measurement of PQ levels in a particular power system. PQ standards provide guidelines, limits and recommendations to help and ensure compatibility between power system and end user equipment [40]-[46]. Custom power devices, which use power electronic based controllers for distribution systems enhance the reliability and quality of power delivered by electric distribution

system. These devices can be series connected, shunt connected or be a combination of series and shunt connected at PCC. One acceptable solution for current related PQ problems at distribution level is an active shunt compensator which is also commonly named as Shunt Active Power Filter (SAPF). Various PQ issues such as harmonics distortion, poor Power Factor (PF), load unbalancing and neutral current compensation etc. [47-67] can be mitigated using SAPF. The SAPF has fast response time, eliminates specific harmonics and has a small size. Its implementation has also become cost effective because of tremendous progress in the area of power semiconductor devices and Digital Signal Processor (DSP). Developments in the area of converter topologies and control algorithms for operation and control of the shunt compensator are due to research in the area of SAPF. The current related PQ issues are mitigated using SAPF in small hydro power generation [68], air craft power system [69], distribution networks and electric ship supply system [70] etc. The performance of SAPF depends mainly upon the type of control algorithm used for extracting fundamental load current component. The fundamental active and reactive load current components are further utilized to estimate reference supply currents and switching pulses for voltage source converter (VSC) used as SAPF are generated using these reference supply currents. Today the practical implementation of SAPF has become feasible due to availability of efficient and fast switching power electronics devices, DSPs and voltage and current sensors. Fast and accurate algorithms need to be developed for SAPF which can be experimentally implemented for control.

1.1 POWER QUALITY ISSUES

There are numerous PQ issues present in power distribution system. These PQ issues can be classified into transient and steady state categories [1-4] which are explained below.

1.1.1 Transient PQ Issues

These PQ issues are transient in nature and last for few power cycles. These PQ issues are as follows.

1.1.1.1 Voltage Sag and Swell

Voltage sag is defined as decrease in Root Mean Square (rms) value between 0.1 and 0.9 pu in voltage at the power frequency level and voltage Swell is defined as increase in rms value between 1.1 and 1.8 pu at the power frequency level. The duration for voltage sag and swell ranges from 0.5 cycles to 1 min.

1.1.1.2 Short Voltage Interruption

Short duration voltage interruption is the complete loss of voltage (rms<0.1 pu) in an electrical power system. The duration of this interruption ranges from half cycle up to 3 s.

1.1.1.3 Voltage Fluctuations

The voltage fluctuation refers to transient variations in voltage magnitude. This variation is normally less than 0.1 pu.

1.1.1.4 Voltage Spikes

Sudden large variation of the voltage magnitude is termed as voltage spike. The duration of spikes ranges between several microseconds to few milliseconds.

1.1.2 Steady State PQ Issues

These PQ issues remains in the system for longer duration These PQ issues are classified as follows.

1.1.2.1 Long Voltage Interruption

Long voltage interruption refers to the complete absence of electrical supply for duration greater than 1 minute.

1.1.2.2 Voltage Flicker

Continuous oscillation in voltage magnitude of frequency less than power frequency is called voltage flicker.

1.1.2.3 Unbalanced Voltages and Currents

Voltage or current unbalance is defined as the ratio of the negative or zero sequence component to the positive sequence component. Unbalanced voltages are responsible for unbalanced operation of three phase equipment connected to the system. Unbalanced currents cause excess current in neutral wire of the system, which may result in malfunction of connected equipment.

1.1.2.4 Noise

Noise is the unwanted high frequency signal superimposed upon the power system fundamental frequency voltage or current signals. Noise produces distortion in the voltage and current waveforms.

1.1.2.5 Poor Power Factor

In power distribution system low PF on the supply side increases burden on supply system for equal real power transfer to load as compared to Unity Power Factor (UPF) conditions.

1.1.2.6 Harmonic Distortion in Voltage and Current

Harmonics are sinusoidal currents and voltages having frequencies that are integer multiples of the fundamental frequency which is 50 Hz for Indian power system. Harmonics signals distort the sinusoidal shape of voltage and current waveforms in the power system. The harmonic distortion is measured in terms of Total Harmonic Distortion (THD) is calculated using [1,4]

$$THD = \sqrt{\frac{1}{DF^2} - 1} \tag{1.1}$$

where DF is distortion factor and calculated using

$$DF = \frac{I_{orms}}{I_{rms}} \tag{1.2}$$

where I_{0rms} is fundamental rms value of current and I_{rms} is total rms value of current so if harmonic content is more, its THD will also be high,

1.2 STATE OF THE ART IN THE POWER QUALITY

The SAPF is one of the prominent area of power electronics. The research in SAPF during last few decades has seen enormous growth. Substantial literature is reported on the shunt compensators and their control techniques for PQ improvement at distribution level [71-206]. Shunt compensation provides several PQ improvement features such as reactive power compensation, harmonics elimination, PCC voltage regulation and load balancing. The building block of SAPF is Insulated Gate Bipolar Transistors (IGBTs) based VSC. Proper designing [71-76] of SAPF is necessary for the effective implementation of shunt compensator system. Different configurations of SAPF are possible which include two-leg, three-leg, four-leg and six-leg VSCs and different operating modes [77-93]. Effective control of SAPF is a prerequisite to generate gating pulses [94] of its VSC and to achieve desired performance under steady state as well as dynamic conditions.

Different techniques for extracting harmonics from distorted load current have been suggested by various authors [95-125]. It is desired that control algorithms should able to produce fast response and stable operation of SAPF in both steady state and dynamic conditions. The selection of a control algorithm depends on factors viz. low processing time and mathematical complexity, fast response, stable operation and easy implementation. Some conventional control algorithms [95-105] reported in the literature are Synchronous Reference Frame Theory (SRFT), Instantaneous Reactive Power Theory (IRPT), Power Balance Theory (PBT), Symmetrical Component Theory (SCT) and Fryze Current Minimization Theory (FCMT) etc. A comparison

of conventional algorithms based on SRFT, Adaline and IRPT is reported in [106], in which the Adaline based control technique is shown to be better.

Adaptive filtering [107] based adaptive Least Mean Square (LMS) control techniques with fixed and variable step have recently been reported in the literature, where variable step LMS has advantages in terms of reduced steady state error and fast convergence. The LMS techniques can be used to mitigate PQ problems using SAPF [108]. Many similar control techniques are available in literature such as Leaky Least Mean Square [109] and adaptive LMS [110], Variable Step LMS [111-112], Adaptive Neurofuzzy Inference System (ANFIS) LMS [113] and Hyperbolic Tangent based LMS [114] etc.

Several research papers have been reported on the use of fuzzy and neural techniques [115-116] for control of SAPF during the past few decades [117-120]. These control techniques are based on artificial neural network (ANN) [117-118], Recurrent Wavelet ANN [119] and Adaptive Neural Filtering (ANF) [120] etc. Various modern control techniques [121-128] are also reported in literature. These techniques includes Mixed and Stationary Frame Repetitive Control [123], second-order odd-harmonic repetitive control [124], frequency-adaptive fractional-order repetitive control [125], Extended Kalman Filter [126], Optimum Filtering Theory (OFT) [127], Back-Propagation Technique [128] etc.

Three-Phase-Three-Wire (TPTW) supply system suffers from several PQ problems such as harmonics, load unbalancing and poor PF etc. Single cycle control technique [129] is reported in the literature and the calculations are shown to be independent of phase and frequency of supply voltages. The predictive current control [130] is also used for active power filter for shunt compensation. Some other time domain control techniques [131-150] includes Lyapunov Square function based control, Power balance Control, Variable Forgetting Factor Recursive Least

Control Algorithm, Fryze Technique etc.

Three-Phase-Four-Wire (TPFW) distribution systems may have excessive neutral current due to unbalanced nature of load. This may cause damage to the neutral conductor because rating of neutral conductor is small. Also distribution transformer may get damaged which affect the safety of end consumers. Various control techniques [151-163] are reported for PQ improvement in TPFW system. The control algorithms include IcosΦ algorithm, Composite Observer-based Control, Wavelet Transform based Algorithm, Frequency Adaptive Disturbance Observer etc. The easiest way to implement SAPF for four wire system is to use an additional leg for control of neutral current. However, to avoid costly four leg structure of SAPF, T-connected transformer, zig-zag transformer [164-167] etc. are incorporated in combination with the conventional three leg SAPF.

Many research papers on PQ compensation using SAPF for distorted grid have been reported [168-177]. The grid voltage has significant source impedance, which causes voltage distortions due to harmonics injected from the loads. The conventional techniques developed for stiff grid are not applicable to distorted grid systems and new control techniques need to be explored for such applications. The distorted grid voltages need to be filtered before being utilized for synchronization and development of reference current signals.

The conventional energy sources such as coal, gas etc. are limited and depleting very fast, hence generation of electrical energy from renewable energy sources and their grid integration is necessary [178-180]. Various standards [181-186] are available in literature for design, installation and maintenance of standalone and grid connected Photo-Voltaic (PV) system. To increase the efficiency of PV system, Maximum Power Point Tracking (MPPT) algorithms [187-192] are available in literature. These techniques help to extract maximum power out of existing

PV system. N. Saxena et al. [193] have presented synchronization scheme of PV system to the grid. The excess power obtained from PV system is fed to the supply system. Both single phase standalone PV and grid connected PV is discussed in this paper. Proper synchronization techniques [194-197] are required for grid connected operation of PV system. B. Singh et. al. have presented a single stage Solar Photo-Voltaic (SPV) array connected to a three phase three wire power distribution system [198] using an improved second-order generalized integrator quadrature (ISOGI-Q) based control technique. Some other control techniques for grid connected PV system include [199-206] Adaptive Digital Control Technique, ANF-Based Control, LMF-based control etc.

1.3 OBJECTIVES OF THE PRESENT WORK

Based on the extensive literature review on the design and development of the shunt compensator and its control techniques, it is felt that new control techniques for PQ problems mitigation need to be developed for power distribution systems including those interfaced with PV generation.

The main objectives of the present research work are to mitigate PQ problems in an electrical power distribution network, namely TPTW as well as for TPFW systems. New control techniques are designed and developed which are robust, simple and easy to implement as compared to conventionally available control techniques. The PQ issues which are considered in the thesis include effect of distorted grid supply, presence of harmonics, linear and non-linear unbalanced load, poor PF in the power distribution system, reactive power compensation to load. Some of the designed control techniques can also be used for extraction of harmonics from the load current. The problem of neutral current compensation in TPFW system has also been addressed with a three leg SAPF by designing suitable control algorithms. PV based renewable

energy integration with SAPF has also been analyzed and demonstrated experimentally. This thesis includes following aspects of PQ issues and remedies.

1.3.1 Design and Development of Shunt Compensator for Distribution System

The design and rating selection of three-phase, three-leg SAPF depends on the required PQ features it is expected to mitigate. Design of SAPF for reactive power compensation, harmonics elimination and load balancing is carried out through simulation studies and experimental validation. Power circuit components of the SAPF are IGBT based VSC, DC bus capacitor, interfacing inductors and ripple filters. The zigzag transformer design for neutral current compensation is also discussed for TPFW system. Control algorithm for SAPF has been implemented on dSpace 1104 which requires appropriate sensor circuits for sensing the signals (load currents, supply currents, PCC and DC link voltages) in a developed prototype of SAPF. The sensed signals are used by the control algorithms through ADC channels of DSP. The generated switching signals from the DSP are fed to driver circuit of three phase VSC used as SAPF. Conventional control algorithms for control of SAPF such as IRPT, SRFT and PBT are first tested on the developed prototype system and experimental results are captured and compared to that of Simulation results, which shows good agreement among the two in implementation of prototype SAPF system.

1.3.2 Investigations on Mitigation of PQ Problems in TPTW Distribution System

A TPTW distribution system suffers from PQ issues such as voltage fluctuations, harmonics distortion, poor PF and load unbalancing due to inductive nature of loads. It is important and mandatory as per IEEE standards to mitigate the harmonics in the supply current and also ensure balanced and sinusoidal supply currents. Design and development of new control techniques for SAPF in TPTW prototype power system has emerged as an important area of research during last decade. In this thesis efforts have been made to implement new control algorithms for SAPF for distribution systems. The control

techniques developed include Notch Filter based, Kalman-LMS and Hopfield Neural Network (HNN) based control for VSC in SAPF. Extensive simulation studies and hardware implementation of SAPF are carried out for linear as well as non-linear load. The dynamic performance of SAPF and effectiveness of the proposed control techniques in mitigating of PQ problems under steady state as well as under dynamic load condition are described in detail.

1.3.3 Investigation on Mitigation of PQ Problems in TPFW Distribution System

In TPFW distribution system, the connected loads are normally mixed type of loads i.e. single phase/ three phase, linear and nonlinear balanced or unbalanced loads. These loads may include arc and induction furnaces, sugar mills, steel mills, VFD etc. In such diverse load situations it is difficult to implement the control techniques of SAPF for effective compensation. Mitigation of the PQ problems in TPFW system can be achieved using either a four leg SAPF or zig-zag, T-transformer etc. based three leg SAPF. The fourth leg or transformers are employed for compensation of neutral current. In the present work a three leg VSC along with a zig-zag transformer is used for implementation of SAPF in TPFW distribution system. New control techniques designed and developed for TPFW system include Self Tuning Filter (STF), Modified Recursive Gauss Newton (MRGN) and Chebyshev Polynomial based Artificial Neural Network (*ChANN*). Extensive simulation studies and hardware results have been shown for mitigation of PQ problems in TPFW systems.

1.3.4 Investigations on Mitigation of PQ Problems in Distorted Grid System

The PQ issues such as voltage distortion, voltage imbalance and low PF at the PCC due to significant increase of non-linear loads can impose adverse effect to other connected load in the distribution system. The conventional control techniques like PBT and SRFT etc. which employ PCC voltages for reference current generation do not work satisfactorily under distorted grid voltage. Hence, new compensation techniques for the distorted grid voltage were studied and implemented. The control

techniques developed for TPFW system under distorted supply mains include Second Order Generalized Integrator (SOGI) and Multiple Complex Coefficient Filter (MCCF). Both the algorithms are designed and implemented on three phase supply voltages to filter out positive sequence component of supply voltages and also for mitigating PQ problems with linear as well as non-linear loads.

1.3.5 Investigations on Grid Connected PV System

The conventional energy sources such as coal, gas are depleting fast and PV based generation has to catch up to meet the load requirement of the future. The installation and integration of renewable energy systems especially PV power plant is rapidly increasing due to availability of solar energy in abundance. There is a need for the development of suitable control techniques for integration of renewable energy sources to the grid.

Photovoltaic system has been designed, simulated and integrated to the grid. A DC-DC boost converter is being used for implementation of MPPT technique and Its interconnection to the grid through a H bridge VSC. Some new control techniques have been designed, developed and tested. These control techniques include SRFT, Notch filter and SOGI based controller. Design and comparative performance analysis of algorithms without/with PV are described.

1.4 OUTLINE OF THE THESIS

The content of the thesis have been divided into following chapters:

Chapter I presents a brief introduction to the various PQ issues and their solutions. One of the feasible solutions is to use a shunt compensator, which can be controlled to inject compensating currents into the system. Mitigation of PQ problems is important from utility as well as end user perspective.

Chapter II includes an extensive literature review on PQ problems in TPTW and TPFW and

distorted grid systems. Exhaustive literature survey on the configurations and control algorithms for the shunt compensator is given in this chapter. It also provides literature survey on the problems and issues in interconnections of renewable energy sources to the grid. Based on the exhaustive literature review, identified research areas are presented at the end of this chapter.

Chapter III presents system configuration of three phase SAPF. The design and selection of various components for SAPF such as VSC, DC link voltage, DC link capacitance are given in detail. Development of voltage sensor circuits, current sensor circuits, gating circuits for generation of pulses for control of VSC are discussed in this chapter. Parameter selection and design of interfacing filter inductors used in prototype hardware setup in the laboratory are also presented in this chapter. The design of zigzag transformer for neutral current compensation in TPFW system is described in detail.

Chapter IV presents the implementation of some modern control techniques in operation and control of SAPF system for TPTW distribution system. It also gives a deep mathematical analysis of the proposed control techniques such as Notch Filter, Kalman-LMS and Hopfield based neural network technique. The mathematical analysis is shown and simulation and experimental results of SAPF are presented for linear and non-linear loads.

Chapter V presents TPFW distribution system with three-leg SAPF. The control techniques such as STF, MRGN and *ChANN* are designed and developed and used for analysis and control of SAPF. Both linear and nonlinear loads are considered and performance of the shunt compensator is tested and demonstrated by presenting simulation and hardware results.

Chapter VI describes control techniques for SAPF when the PCC voltages are distorted. The distorted supply voltages in this system impose a major challenge in implementation of a suitable control technique. There is a need for two controllers, one for achieving load compensation

current and other for filtration of distorted supply. The control techniques developed are SOGI and MCCF. Both the control techniques are designed, developed and tested and extensive simulation and hardware results are presented.

Chapter VII proposes control techniques for integration of renewable energy sources to the grid. A boost converter is used in between PV system and DC link of the VSC to enable active power flow to the load/grid. The control techniques considered in this chapter are SRFT, Notch Filter and SOGI. Integration of PV system into distribution system through a single phase VSC is demonstrated and necessary changes in control algorithm is discussed. The performance of analysis of PV system and mitigation of PQ issues with and without PV system is also analyzed and discussed.

C**hapter VIII** summarizes the performance of different control algorithms presented for SAPF and highlights the main conclusions of the present work. The scope of future work in the area of SAPF is also listed at the end of this chapter.

Chapter 2
LITERATURE SURVEY

2.0 GENERAL

PQ problems have posed new challenges in distribution system. One commonly used shunt device for mitigation of PQ problem is SAPF. The SAPF is a custom power device utilized for overcoming PQ issues within power distribution networks. During last three decades, Distributed Generation (DG) involving renewable sources has a substantial impact in worldwide energy contribution. An electric power system is highly complex, huge and dynamic network, which involves generation, transmission and distribution of electrical power. The electric power distribution systems are usually over-stressed and have low voltage problems due to excess reactive power demand and harmonic pollution, causing them to operate less efficiently. New solutions are being researched by power engineers worldwide. Installation of SAPF in distribution system opens up ample opportunities to achieve load compensation. The conventional SAPF is realized as a three leg VSC and is controlled to deliver leading/Lagging reactive power, reduce harmonic currents in grid and provide load balancing features. Insulated Gate Bipolar Transistor (IGBT) based VSC is the fundamental building block along with a DC link capacitor. A critical review of literature on SAPF is carried out and summarized in different classes.

2.1 LITERATURE SURVEY

An exhaustive survey of the available literature related to PQ improvement in power distribution system is studied and analyzed in this chapter. Various PQ problems related to distribution system are first summarized. International standards related to various PQ problems are mentioned. Then PQ problems in TPTW, TPFW and distorted grid systems are

listed. The possibility of PQ issues in grid connected PV system is also considered and analyzed in details.

2.1.1 General PQ Problems

Power quality problems make the distribution system inefficient and unreliable. The electrical equipment may malfunction, fail permanently or not operate at all due to PQ problems. The general PQ problems include voltage sag, swell, voltage and current harmonics, load unbalancing, voltage interruption etc. Mark F. McGranaghan et al. describe [10] the causes of voltage sags in industrial plants. The paper highlights system faults as a major concern for voltage sags. P. Wang et al. focused on the study of voltage sags and phase angle jump associated with this problem [11]. An Advanced Static Var Compensator (ASVC) is described and its effect on voltage sags of different magnitude is shown. R. T. Ugale et al., explained the deteriorating effect of short power interruptions and voltage sag on synchronous motor [12]. Short power interruption for a duration of 300 ms, severely affect the post interruption synchronization of the machine under loaded condition. P.G. Therond et al., emphasized on short power interruption problems in industrial plants [13]. The authors have proposed use of superconducting coil for mitigating industrial PQ problems. Pui Ying Or et al., described problems associated with voltage spikes [14]. An output-capacitor less low-dropout regulator (LDO) with a direct voltage-spike detection circuit is also described in the paper. In papers [15-22] PQ problems introduced by Electric Arc Furnace (EAF) are analyzed in detail. Different models [15-20] to predict the behavior of EAF have been developed to study its effect on power system. Various PQ problems such as voltage flickering, harmonics injection, voltage fluctuations, large transients in current [21] etc. are introduced by EAF. G. C. Montanari et al. [1994], introduced installation of series inductors at the EAF supply side [22], which reduces flicker at PCC. Philip P. Barker et al. conducted

studies on PQ of two distribution feeders in the Buffalo, New York region [23] and performed various steady state and dynamic measurements on the system.

2.1.2 General PQ Estimations

Power quality estimation enables us to detect and analyze PQ of electrical supply system. Various PQ indices such as THD, PF of supply, phase difference between voltage and current, frequency etc. measurement have become necessary for PQ estimation. By knowing the PQ problems of power system network, suitable compensation techniques can be implemented to mitigate these problems easily and effectively. V. Terzija et al. presented two-stage, Self Tuning Least Square (STSL) control technique for estimation of PQ indices [24]. M. Biswal et al. introduced adaptive window-based fast generalised S-transform for estimation of time-varying PQ indices [25]. P.S. Wright et al. studied Sweden–Poland HVDC Link and conducted onsite measurements for PQ estimation [26]. V. Terzija et al. presented a two-stage improved recursive Newton type control technique for measurement of PQ indices according to the IEEE Standard 1459-2000 [27]. A. Bagheri et al. used Kalman Filtering (KF) technique in combination with Generalized Averaging Method (GAM) approach for calculation of fundamental and harmonics components of grid voltage [28]. R. Cisneros-Magaña et al. used KF approach [29] to estimate PQ of system. A. A. Girgis et al. emphasized on power system harmonics [30] and this paper proposes a digital recursive measurement scheme for direct estimation of system harmonics. M. Mojiri et al. proposed use of adaptive notch filter [31] for extraction of harmonics. K. B. Nazirov et al. studied a 400 V (L-L) power distribution networks, in Dushanbe city of the Republic of Tajikistan for PQ estimation [32]. N. Anandh et al. performed a comprehensive study in [33] on PQ estimation for uninterrupted power supply. P. V. Morozov et al. presented statistical methods for PQ estimation [34] in power transmission system by assuming the load to be dynamic in nature. S. Ali et al. proposed PQ estimation for smart grid [35] system. Q. Ai et al. introduced

ADALINE control technique [36] application in PQ disturbances detection. The frequency tracking is also considered in this paper. I.S. Ilie et al. developed theoretical interruption model for reliability study of power supply system [37]. D. Andrews et al. have shown study of steel manufacturing plant for measurement of harmonics [38] and performed PF correction in the system. A Variable Least Mean Square (VLMS) method for estimation of power system harmonics is shown in [39] by S.K. Singh et al.

2.1.3 Power Quality Standards

International standards have been formulated to ensure the quality of power across the world. Institute of Electrical & Electronics Engineers (IEEE) and International Electro-technical Commission (IEC), have formulated, updated and revised international standards related to PQ from time to time. IEEE standard 519 [40], tabulates the specified THD for a general power system in presence of nonlinear loads and recommends the supply voltage and current should have THD level below 5%. W. E. Reid also mentioned about PQ issues such as transient overvoltage, under-voltage, outage, harmonics distortion etc. and provided industry specified standards [41]. IEEE standard 1159 provides standard routine practice for monitoring PQ in single and poly phase power transmission and distribution system [42]. It enlists various PQ problems and their typical spectral content and duration. The allowable voltage magnitude for different system transients such as sag, swell, outage etc. are also defined. IEEE standard 1100 [43], presents recommended design, installation, and maintenance practices for electrical power and grounding (including both safety and noise control) and protection of electronic loads such as computers, industrial controllers etc. The protection of electronic equipment and their performance analysis is also discussed. The IEEE standard 1459 [44], presents standard definitions and formulas to calculate active, reactive, apparent power, PF, THD etc. in single and three phase system. Positive, negative and zero sequence components and their analysis is also discussed. IEC standard 61000, 3-2

[45] presents the limitation on harmonic currents to be injected into the grid. This standard applies to all electronic and electrical equipment having 16 A/phase rated input current. For this standard, a low voltage distribution system is considered. IEC standard 61000-4-15 [46] presents an analogue or digital flicker measuring apparatus functional and design specifications. The flicker meter specifications are applicable for 120 V and 230 V, 50 Hz and 60 Hz inputs. All standards related to PQ ensure proper operation of power system across the globe.

2.1.4 Power Quality Issues and Mitigation Techniques

Power quality imposes serious concerns to the power system network. So mitigation becomes necessary for safe and reliable operation of power system. Several techniques are reported in literature for mitigation of various PQ problems. J. Miret et al., proposed a reactive current injection technique for mitigation of voltage swell [47]. They have shown that the maximum rated reactive current is injected during the voltage sag. S. S. Choi et al. introduced a voltage-injection technique for dynamic restoration of load voltage in case of voltage sag as well as voltage swell conditions [48]. H. Ghosh et al. compared the performance of Distribution Static Compensator (DSTATCOM) and Dynamic Voltage Restorer (DVR) for load voltage control in a power distribution network [49]. A. Elnady et al. used DSTATCOM for mitigating voltage flicker and sag [50]. B. singh et al. reported PQ improvement in standalone permanent magnet synchronous generator based supply system [51] using DSTATCOM and Battery Energy Storage System (BESS). V. Virulkar et. al. used DSTATCOM with BESS [52] for mitigation of voltage flicker. X. Yu et. al. have shown the use of power converters for generation of electrical energy from fuel cells [53]. T. L. Baldwin et al. focused study on reactive-power demand of resistance welders for voltage level control [54]. Various control techniques and system configuration for PQ improvement for EAF connected system are available in literature [55-61]. H. Samet et al. used Grey–Markov

prediction method for proper reactive power compensation in EAF connected system [55]. Various hardware configurations such as thyristor-controlled reactors and voltage-source inverters [56], D-STATCOM [57-58], nonlinear STATCOM [59], Unified Power Flow Controller (UPFC) [60] have been used for PQ improvement in EAF connected system. T. S. Saggu et. al. used 11 level cascaded DSTATCOM for harmonic mitigation in steel plant [61]. J. Kanieski et al. shows the application of Kalman Filter for PQ improvement [62]. Leon H. Beverly et. al. developed method and apparatus for reducing the harmonic currents in power distribution networks [63]. G. Karmiris et. al. presented a control scheme for voltage sag mitigation and current harmonic elimination using a flying capacitor inverter circuit [64]. Literature review [65-67] discuss mitigation techniques in single phase systems. Here, the PQ has been improved by use of zigzag transformer [65], and control techniques such as composite observer [66] and SRFT [67] etc. V. Rajagopal et al. proposed PQ improvement for small hydro power generation using electronic load controller [68]. H. Hu et al. focused on design for DSP controlled 400 Hz SAPF in an aircraft power system [69]. P. Mitra et. al. proposed an adaptive control scheme for electric ship power system using DSTATCOM [70].

2.1.5 Design and Configurations of SAPF

SAPF has played an important role in operation and control of modern power system. The recent research efforts and solutions are aimed at designing of appropriate compensator for fast and effective compensation. Designing of system involves mathematical modeling and analyzing before implementation of hardware setup. B. Singh et al. presented suitable design of DSTATCOM for TPTW system using the cross correlation function approach for PQ improvement [71]. S. K. Khadem et al. described harmonic power compensation capacity of SAPF with its system parameters [72]. G. Zhao et al. analyzed the influence of interfacing inductor to the performance of STATCOM [73]. D. Kumar and Rajesh have shown the modeling and performance analysis of a shunt compensated system [74]. In this analysis,

unbalanced linear/non-linear loads were considered. T. Tian-yuan et al. compared the performance of DSTATCOM under direct and indirect current control scheme in [75]. Both techniques were tested for voltage source un-balance, sudden voltage amplitude and phase change and presence of current harmonics in system. It is reported that with the direct current control, the system performance is found to be better than indirect current control. R. Panigrahi et al. presented the comparison between the performances of Hysteresis Current Control (HCC) and dead beat controllers for SAPF [76]. It is reported that the HCC performs better than dead beat controller. Moreover, the HCC control is simple and transients die out faster. C. Kumar and M.K. Mishra presented a PQ improvement control technique for DSTATCOM in voltage and current control mode [77]. The same authors have implemented a voltage-controlled DSTATCOM for PQ problem mitigation [78]. C. A. Sepulveda et al. compared FPGA and DSP performance for VSC-based STATCOM control [79]. It is reported that FPGA has best computation speed due to availability of high degree of parallelism on the device. S. Srikanthan and M. K. Mishra performed voltage equalization of DC link in neutral clamped SAPF [80]. C. A. Sepulveda et. al. implemented d-q-frame based SAPF control technique using low-cost FPGA [81]. R. Tadeu et al. discussed minimum power point tracker based voltage regulator scheme for VSC based DSTATCOM [82]. N. Voraphonpiput et al. designed a control System for a STATCOM using Complex Transfer Function [83]. B. Singh et al. implemented an isolated H-bridge VSC based TPFW SAPF for PQ problem mitigation [84]. S. Kumar et al. presented Modified Instantaneous Symmetrical Component Theory (MISCT) for three leg and four leg SAPF [85-86]. A. Dheepanchakkravarthy et al. introduced TPTW VSC integrated with T connected transformer as DSTATCOM [87] which is able to perform all the compensation required for TPFW system. A T-connected transformer is also implemented in [88] for TPFW distribution system. P. Jayaprakash et al. implemented TPTW VSC with Star/Hexagon transformer for

TPFW distribution system [89]. J. Kanieski et al. applied Kalman Filtering (KF) approach to PQ conditioning devices [90]. In [91] the concept of smart DSTATCOM is introduced, which is able to mitigate PQ problems easily. Papers [92-94] presented comprehensive information about DSTATCOM configurations and different applications for PQ improvement.

2.1.6 SAPF Control Techniques

The SAPF is useful device to mitigate PQ problems in distribution system. The control algorithms are key element in effective operation of SAPF. This section discusses the various control techniques required to improve the operation and control of SAPF.

2.1.6.1 Conventional Control Algorithms

These techniques are based on conventional control algorithms. Many conventional techniques are available in literature [95-106]. H. Akagi et al. introduced a new instantaneous reactive power (IRP) [95] compensator without any energy storage devices. F. Z. Peng et al. proposed IRP theory for PQ improvement in TPFW supply system [96]. A synchronous reference frame based control technique for PQ problem mitigation has been applied in [97-98]. Many new control techniques have been developed for DSTATCOM connected system for PQ improvement such as Adaline [99], Instantaneous Symmetrical Component theory (ISCT) [100], Power Balance Theory [101] etc. A comparison of conventional control techniques [102-103] for PQ improvement using DSTATCOM has been described. The DC link of DSTATCOM needs to be regulated to ensure satisfactory performance. Z. Yuan and X. Mingchao, proposed use of two-way inverter bridge along with isolation transformer for making DC link stiff [104]. Papers [105-106] proposed use of split capacitor etc. for making DC link of DSTATCOM robust.

2.1.6.2 Adaptive Control Algorithms

Adaptive control algorithms [107] have advantages to adapt to any control system in real time and provide higher system performance. Unlike neural networks, it is not trained offline. It

process real time signals to reduce steady state error. These algorithms output the required signal and data adaptively. Least mean square (LMS) algorithms are also adaptive control techniques. The LMS and Variable LMS techniques have been developed, analyzed through simulation studies and verified by hardware prototype in [108]. Various Least Mean Square (LMS) control techniques such as leaky LMS [109], Adaptive LMS [110], Variable LMS [111], Lorentzian Function based LMS [112], Adaptive Neurofuzzy Inference System LMS [113] etc. have been developed for PQ improvement using DSTATCOM as a compensator. A hyperbolic tangent based LMS control algorithm has developed [114]. The adaptive control techniques have disadvantages of being parameter dependent so proper designing is necessary before implementing these techniques.

2.1.6.3 Neural Network Based Control Techniques

Artificial Neural Network (ANN) techniques [115-116] uses set of hidden layers based on certain rules to imitate a physical system. These networks are trained offline so that they can work effectively on any other system. Real time control techniques for training of ANN is also available in literature [117]. R. Waswani et al. implemented ANN for PQ improvement electric ship using DSTATCOM [118]. L.T. Teng et. al. have shown recurrent wavelet neural network (RWNN) for shunt compensation [119]. Improved particle swarm optimization has been used for RWNN. M. Cirrincione et. al. presented current harmonic compensation using single-phase SAPF. The control has been developed using adaptive neural filtering [120].

2.1.6.4 Modern Control Techniques

Power quality improvement is an interesting area of research in the field of power electronic system. Various modern control algorithms are being developed for mitigation of PQ problems in power system network. R. Panigrahi et al. developed a new technique for generation of reference currents for SAPF under distorted grid [121]. R.L. de Araujo Ribeiro et. al. developed a new adaptive control scheme for SAPF for Power-Factor correction,

unbalancing and harmonic reduction [122]. P. C. Loh et. al. presented mixed-frame and stationary-frame repetitive control schemes. This scheme provide compensation for load and grid harmonics [123]. Z. Xiang Zou et al. proposed frequency-adaptive fractional-order repetitive control [124] of SAPF. Power system harmonic elimination under grid frequency variations has been effectively shown in this paper. G.A. Ramos and R. Costa-Castelló implemented second-order, odd-harmonic repetitive control for reduction of PQ problem [125]. N. Hoffmann and F. W. Fuchs used Kalman filter approach for grid impedance estimation [126]. Using grid impedance, a control scheme has been developed to control SAPF for PQ improvement in distributed power-networks. Some other modern control techniques developed are Optimum Filtering Theory [127], Back Propagation [128] etc. Several new simple, easy to implement and less complex control techniques are being developed for PQ improvement during last few decades.

2.1.7 SAPF Applications to TPTW Distribution System

TPTW distribution system suffers from many PQ problems such as low voltage level, harmonics in load, load unbalancing, poor PF etc. Mitigation of these problems using SAPF requires appropriate control techniques to be developed. Several control techniques [129-150] have been developed for TPTW distribution system using SAPF. T. Jin et al. presented one-cycle controlled three phase SAPF for PQ improvement [129]. S. A. Verne and M. I. Valla applied predictive current control technique for TPTW power system network [130]. A Lyapunov-function-based control scheme [131] has been developed for TPTW shunt hybrid active filter. B. Singh and S. R. Arya implemented single-phase enhanced phase-locked loop (EPLL) based control technique for TPTW SAPF [132]. N. Dhyani et al. shown application of power balance theory to control shunt compensator [133]. S. K. Kesharvani et al. proposed conductance based Fryze control scheme for reducing PQ problems in the presence of non-linear loads [134]. General use of Neural Network (NN) based control of SAPF has been

shown in [135-137]. S. R. Arya et al. proposed learning-Based Anti-Hebbian control technique for SAPF [135]. M. T. Ahmad et al. implemented fast multilayer perceptron NN based technique for SAPF [136]. A. Panda Kumar and M. Mangaraj have controlled SAPF employing hybrid NN control scheme [137]. B. Singh et al. used Self Tuning Filter (STF) based IRPT control technique for control of shunt compensator for PQ improvement [138]. M. Badoni et al. implemented Variable Forgetting Factor Recursive Least Square (VFFRLS) control scheme for TPTW SAPF [139]. R. B. Roy et al. proposed Super Capacitor Energy Storage System (SCESS) based SAPF developed, which has been used for both real and reactive power compensation [140]. Some other recently developed control techniques for PQ improvement in TPTW distribution system include discrete derivative control [141], immune feedback algorithm [142], amplitude adaptive filter [143], Echo-State Network [144], PI and Fuzzy Logic Controller [145], Demodulation-Second Order Generalized Integrator (D-SOGI) control [146], deadbeat predictive controller [147], Adaptive Volterra Second-Order Filter (AVSF) [148], Naive Back Propagation (NBP) based *icosϕ* control [149], Generalised neural network-based control algorithm [150]. Different controls are being developed to generate reference currents for shunt compensator. Fast tracking good convergence, stability, and simplicity are some desired objectives for designing any new control technique.

2.1.8 SAPF Applications to TPFW Distribution System

TPFW suffers additionally from excessive neutral current problems due to unbalanced load. The three phase loads are practically unpredictable in power distribution network. So there is need of suitable control techniques for TPFW systems. P. Jayaprakash et al. presented implementation of a TPFW SAPF in TPFW distribution system for PQ improvement using d-q control algorithm [151] and a star/delta transformer. B. Singh and S. Kumar developed IcosΦ control technique for implementation on SAPF to mitigate various PQ problems [152].

V. George and M.K. Mishra presented design of constant switching frequency current controlled TPFW SAPF [153]. A detailed system analysis is also presented in this paper. T. Zaveri et al. compared the performance of control techniques for SAPF in TPFW distribution system [154]. The control techniques considered include Instantaneous Reactive Power (IRP) theory, an improved Instantaneous Active and Reactive Current Component (IARCC) theory and Symmetrical Component (SC) theory. The IARCC control algorithm has been found to be better than other two control techniques. B. Singh and S. R. Arya applied composite observer based control technique for SAPF in TPFW supply system [155]. M. Kumar et al. presented a detailed analysis of SAPF operated in voltage control mode to improve PQ [156] in power system. By using deadbeat voltage control technique, fast voltage regulation at load terminal is achieved with UPF of system. M. Mangaraj et al. shown PQ improvement by a TPFW SAPF along with super-capacitor [157]. The super-capacitor has the capacity to store energy for the long time and has advantages over the normal capacitor. D. Suresh et al. implemented reduced rating hybrid SAPF for TPFW distribution system [158]. AC power capacitors have been used at the DC link of TPTW, which reduces the rating of SAPF. H. Myneni et al. proposed adaptive dc-link voltage regulation for SAPF, in which DC link voltage is not set fixed but is changing as per the loading conditions [159]. SRFT control technique is implemented for TPFW [160] using Pulse Width Modulation (PWM) controller in place of HCC for generation of SAPF gating pulses. Some recently developed control techniques for TPFW distribution system include Wavelet transform [161], Notch filter [162], Frequency Adaptive Disturbance Observer [163] etc. S. Singhai et al. used isolated zig-zag/star transformer along with TPTW VSC for PQ improvement [164]. Y. Rohilla and Y. Pal proposed the use of T-connected transformer used in TPFW distribution system [165] using a three leg conventional VSC. The use of TPTW VSC for TPFW distribution system results in huge cost saving. B. Singh et al. also implemented neural network control

techniques using zigzag transformer [167] and four leg DSTATCOM [168] on TPFW distribution system. TPFW system is more complex than TPTW system due to extra neutral wire. Hence, fast and easy control techniques need to be developed for PQ improvement for TPFW system.

2.1.9 SAPF Application to Distorted Grid Supply Systems

Modern power electronic systems such as Switch Mode Power Supply (SMPS), Uninterrupted Power Supply (UPS), Variable Frequency Drives, Inverter Air conditioner etc. introduce distortion in the supply current and voltages. The performance of SAPF needs to be observed under non-ideal supply condition also. G. D. Marques presented a comparative performance analysis of IRPT, the modified IRPT, the SRFT and the modified SRFT control technique for PQ improvement under unbalanced and non-sinusoidal supply conditions [168]. It is reported that the SRFT algorithm is found to be working best among the considered techniques. U. K. Rao et al. described the ISCT control technique [169] under a variety of supply voltage conditions including distortions. N. Gupta et al. presented a control scheme for reactive power compensation, harmonic elimination and balancing of non-linear loads under non-ideal supply voltage conditions [170]. Harmonic tuned filter and positive sequence extractor has been used for this purpose. N. S. Pande et al. implemented Synchronous Detection method for the control of SAPF under unbalanced and distorted supply voltages [171]. K. Srinivas and S. S. Tulasi Ram extracted positive sequence component of grid voltage using symmetrical component theory [172] for compensator in distorted grid. The control algorithm developed for the generation of reference currents utilizes the extracted positive sequence components of supply voltages. N. Beniwal et al. presented an improved proportionate normalized least mean square (i-PNLMS) control scheme under distorted grid conditions [173]. S. Mishra et al. used photovoltaic fed distributed static compensator (PV-DSTATCOM) to reduce the PQ problems and tested the system under non-ideal supply

conditions including distorted grid voltages [174]. N. Beniwal et al. presented hybrid variable step size-least mean square-least mean fourth (VSS-LMS-LMF) control scheme under distorted grid conditions for PQ improvement studies [175]. I. Hussain et al. focused their study on weak grid system and developed multilayer perceptron (MLP) neural network control scheme to improve the overall PQ [176]. R. K. Agarwal et al. implemented LMS-Based NN control scheme for PQ improvement under abnormal supply conditions [177]. Some literature is available for PQ improvement in distorted grid and it is one of the prominent area in the field of PQ research.

2.1.10 SAPF Applications to Renewable Energy System

The use of renewable sources is growing now days [178] and the integration of SAPF with these resources is a major challenge [179-180]. International organizations such as IEEE and IEC have also formed standards regarding solar PV system [181-186]. IEC standard 61853 [181] focuses on calculation of maximum power (P_{max}) matrix at various irradiance and temperatures levels. The P_{max} matrix can be generated using an outdoor natural sunlight method or indoor solar simulator method. The outdoor test method is less expensive, but it is a time consuming process. There is no mismatch error. The indoor test method is expensive because it requires expensive solar simulators. IEC 62446 standard [182] provides information regarding grid connected PV system. The installation guidelines are provided in this standard. The commissioning tests, inspection criteria and documentation required for verification of proper operation of the system is also provided. IEC TS 61724 part 1 [183] provides systematic planning for photovoltaic system performance monitoring. The scope is to define the measuring system components and procedures. This standard also focuses to keep measurement errors within specified limits. The standard also lays emphasis on proper measurement of solar irradiance, module and air temperature, soiling ratio, (AC and DC) current and voltage, wind speed and direction. IEC TS 61724 part 2 [184] provides a method

for measuring and analyzing the energy produced by PV system for the quality of the PV system performance. This standard basically provides quality of PV outcome against the expected power from a PV system on sunny days. The IEC TS 61724 part 3 [185] provides a method for measuring and analyzing the energy produced by PV system relative to expected electrical energy production. The actual weather conditions are taken for estimating the expected electrical energy production. IEEE standard 1547 [186] is used for interconnection of distributed energy sources to the GRID.

The Photo-Voltaic energy source has the advantage of having free of cost fuel. To extract maximum power from PV system, MPPT control techniques [187-192] are available in literature. N. Saxena et al. presented solar battery energy storage connected to PV system [193]. The PV may be operated in standalone and grid connected mode. A simple PI controller has been used in the proposed control techniques. The integration of PV system to the grid requires synchronizing techniques to be developed. M. S. Padua et al. discussed different synchronizing methods such as Phase Locked Loop (PLL), Recursive Discrete Fourier Transform (RDFT) and Kalman Filter [194] based techniques. A synchronizing scheme based on conventional p-q theory has been developed in [195] by L. G. Barbosa Rolim et al. S. Deo et al. introduced a PLL less scheme for grid interfaced solar PV system [196] by using a simple Notch Filter (NF) to improve the system performance. S. Kumar et al. implemented Improved Enhanced Phase-Locked Loop (EPLL) for control under variable irradiance [197]. Grid integration of PV system can be used so that PV can supply the peak load demand of power system. Some good control techniques for grid integration of PV system include ISOGI-Q [198], Adaptive Digital Control [199], Adaptive Notch Filter [200], Least Mean Fourth (LMF) [201], ANFIS Control [202] etc. Y. Liu et al. presented single-phase quasi-Z-source grid-tie PV modulated with Hybrid Pulse Width Modulation (HPWM) [203]. T.F. Wu et al. compared the power loss for single stage and two stage PV system

[204]. F. Wu et al. implemented multilevel inverter to connect PV system to the grid [205]. The integrated system has low grid current THD and high efficiency. M. Mahdianpoor et al. discussed Quantitative Feedback Theory (QFT) for the DSTATCOM for grid integration of wind energy [206]. The DSTATCOM is connected in parallel with the wind turbine with a bridge-type-fault-current-limiter in series so as to improve Fault Ride Through (FRT) capability of the wind turbine.

The solar is infinite source of energy. The development of fast and reliable synchronization techniques for solar PV system, which can practically be implemented must be explored.

2.2 IDENTIFIED RESEARCH GAPS

Based upon exhaustive literature survey discussed above, following research gaps were identified

1. Development of simple and effective control techniques for shunt compensators in TPTW and TPFW distribution systems.
2. Investigations on applications of frequency domain techniques such as Kalman filter for power quality monitoring/mitigation.
3. Power quality issues and remedies through static compensator in distorted grid distribution systems.
4. Development of efficient control algorithms for integrating renewable energy sources to grid.

2.3 OBJECTIVES OF CURRENT RESEARCH

1. Analysis of power quality issues due to different types of loads such as linear, nonlinear and dynamic load in TPTW and TPFW distribution systems.
2. Development of simple and effective control techniques for mitigation of power quality issues using shunt compensators in TPTW and TPFW distribution systems.

3. Investigations on applications of nonlinear/frequency domain techniques for power quality monitoring/mitigation.
4. To study and mitigate PQ problems in a distorted distribution system.
5. Integration of Photo-Voltaic (PV) system into grid and mitigation of PQ issues.

2.4 CONCLUSIONS

In this chapter an extensive literature on SAPF for compensation in TPTW and TPFW distribution system is discussed and different control techniques are classified.

Chapter 3
DESIGN AND DEVELOPMENT OF SHUNT COMPENSATOR SYSTEM

3.0 GENERAL

In this chapter, designing of a SAPF as compensator for TPTW and TPFW is discussed in detail. Design of the SAPF systems is carried out to ensure effective implementation of new control techniques and study performance of the prototype system under different system conditions. The main components of the developed system are viz. grid supply, current and voltage sensors, a DSP, a SAPF and linear-nonlinear loads. In the following sections, design of each part is discussed in detail.

3.1 THE PROPOSED SHUNT COMPENSATOR SYSTEM

Fig. 3.1 and 3.2 show the proposed TPTW and TPFW systems respectively. It consists of three phase, 50 Hz grid supply which is supplied through a three phase auto transformer. At the PCC the supply, compensator and load are connected. Voltages and currents in the system are measured with the help of LEM make sensors. A DSP, dSPACE1104 is used for processing input signals and producing proper gating pulses for the operation of SAPF. The SAPF is modeled using TPTW VSC connected in shunt with a DC link capacitor. Six gating pulses are required for operating VSC. The interfacing inductors are designed and appropriate value is chosen to connect VSC to the PCC. The type of loads considered in the present analysis are linear and nonlinear loads. The performance/system variables are recorded through Digital Storage Oscilloscope (DSO).

The basic difference between TPTW and TPFW system lies in neural current compensation. In TPFW distribution system, a path to neutral is provided so that the unbalanced load current

passes through it, which is not the case in the TPTW distribution system. Hence, an additional control on the neutral current is necessary for which a zig-zag transformer is suitably connected as shown in Fig. 3.2.

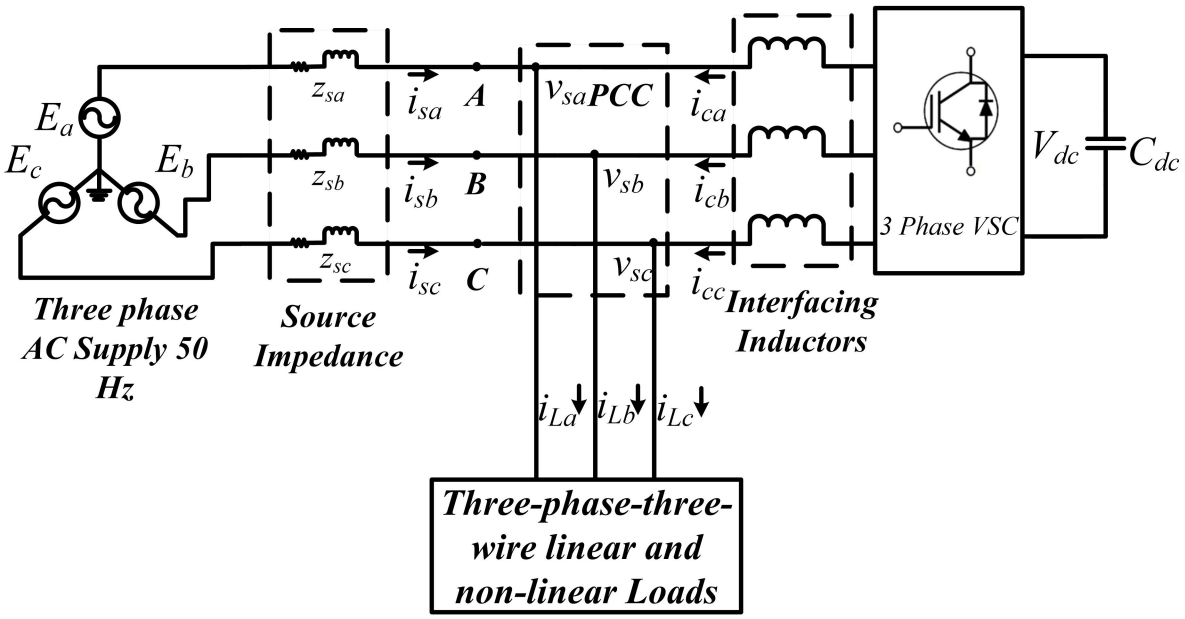

Fig. 3.1 TPTW system under consideration

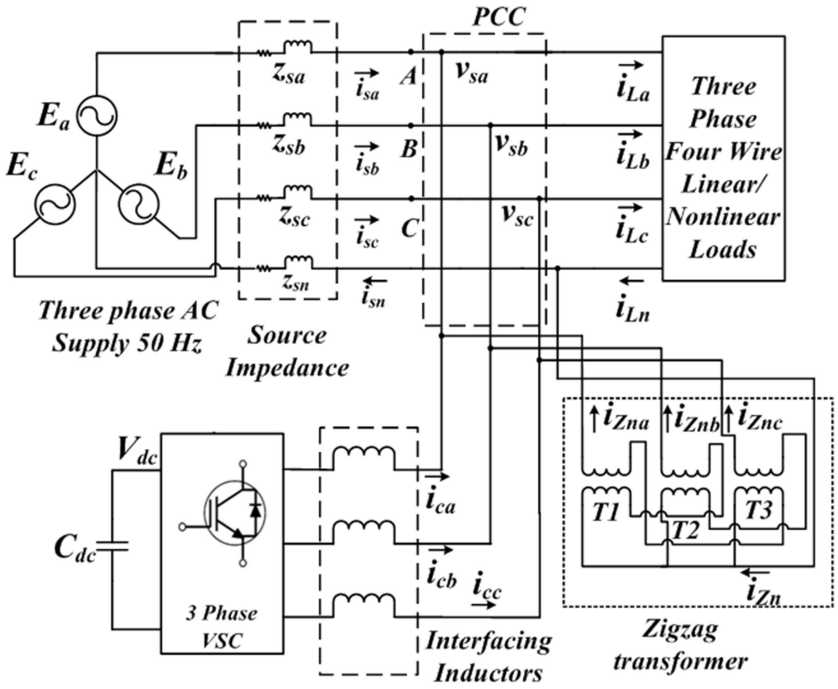

Fig. 3.2 TPFW system under consideration

3.2 DESIGN OF SHUNT COMPENSATOR

A TPTW VSC is realized as SAPF. It consists of DC link capacitor which is also responsible for generating proper compensating currents. The detailed formulas and calculations involved for its design are as follows.

3.2.1 DC Link Voltage Calculation

The voltage of DC link should be sufficient enough to inject switching losses of IGBT switches. For proper PWM control, the system the voltage of DC link voltage must be greater than the peak value of the supply line-to-line voltage in three phase system. The peak value is calculated as

$$V_m = \frac{\sqrt{2}V_{LL}}{\sqrt{3}} \tag{3.1}$$

where V_m= peak value of AC phase voltage, V_{LL}=line to line rms AC voltage.

So the voltage of DC link is obtained as [71]

$$V_{dc} = \frac{2\sqrt{2}V_{LL}}{\sqrt{3}m} \tag{3.2}$$

where V_{dc} is voltage of DC link, m is modulation index and chosen as one. The line voltage for the proposed system is chosen as 110 V. So on solving Eq. (3.2)

$$V_{dc} = \frac{2*\sqrt{2}*110}{\sqrt{3}*1} = 179.60V \tag{3.3}$$

The DC link voltage (V_{dc}) calculated is 179.60V and the reference is chosen as 200 V.

3.2.2 Calculation of Capacitance of DC Link

The capacitance of DC link should be large enough to absorb any dynamic changes in the system. The DC link voltage should be insensitive to small load increase or decrease. By applying energy conservation theorem on AC and DC side, which is [71]

$$g[3*V_{ph}(oI_{ph})t] = \frac{1}{2}[V_{dc}^2 - V_{dc1}^2]C_{dc} \quad (3.4)$$

where g is gain constant, V_{ph} is phase voltage of VSC, 'o' is the overloading factor, I_{ph} is the phase current of VSC, t is time, V_{dc1} is minimum voltage level of DC link voltage and C_{dc} is DC link capacitor.

Choosing 'g' as 0.05, V_{ph}=63.5 V, 'o' as 1.2, I_{ph} as 25 A, t=0.02s, V_{dc} = 200 V, V_{dc1} = 179.60V

From Eq. (3.4) C_{dc} is computed to be 1476.01 μF and chosen as 1500 μF.

3.2.3 Rating of AC Interfacing Inductors

The interfacing inductor filter out ripple current from the compensating current of SAPF. The voltage drop across filter inductors should be minimum so as to ensure proper operation of SAPF. The AC interfacing inductor is calculated using [71]

$$L_i = \frac{\sqrt{3}*m*V_{dc}}{12*o*f_s*i_{rcpp}} \quad (3.5)$$

where L_i is value of interfacing inductor, f_s is switching frequency and i_{crpp} is peak to peak ripple current.

Taking 'm' as 1, V_{dc} as 200 V, 'o' as 1.2, f_s as 10 kHz and i_{rcpp} to be 2.5 A.

$$L_i = \frac{\sqrt{3}*1*200}{12*1.2*10000*2.5} = 0.962\,mH \quad (3.6)$$

The value used for experimental setup is 1 mH.

3.2.4 Rating of Switches of SAPF

IGBT is used as switch for SAPF. The IGBTs have high voltage capability and low on-state voltage drop. Smoother turn-on/-off waveforms are obtained Using IGBT. Other useful parameters include ease of drive and almost zero gate drive current. The rating of switches depends mainly upon the current limit and switching speed. Considering switching speed to be 10 kHz, and I_{VSC} to be 25 A, The IGBT selected module is SKM150GB12V. Fig. 3.3 shows the

internal connection diagram of IGBT switches used. A total of three such modules are used for three phase SAPF. The specification of IGBT are V_{CE}=1200V, I_C=150A, f_s =20kHz, V_{GE}= 15V, T_{op}= -40°C to 150°C.

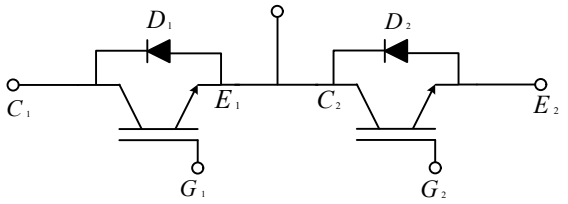

Fig. 3.3 Internal connection diagram for IGBT module SKM150GB12V

3.3 DESIGN OF CURRENT AND VOLTAGE SENSING CIRCUITS

The sensing circuits are essential for implementing control function in SAPF system. It provides the necessary input signals to DSP. The circuit diagrams for current and voltage sensing circuits are as shown in Fig. 3.4. For current sensing circuit, LEM make LA25-NP model is used, which has current range of 0-25 A (rms). The output of current sensor is in the ratio of 1:1000. For a input current of 25 A, output current is 25 mA. This current signal is converted to voltage signal by connecting a shunt resistor of 330Ω. Hence, maximum voltage at OP-Amp input is 8.25 V. This signal is passed through a negative feedback Operational amplifier (Op-Amp) circuit, which is basically used for gain adjustment of output signal by variable resistor pot used in feedback path. The gain range of Op-Amp circuit is from 1/5 to 6/5. The various resistors value used are as shown in Fig 3.4(a). The output signal is fed to Analog to Digital (ADC) port of dSPACE 1104.

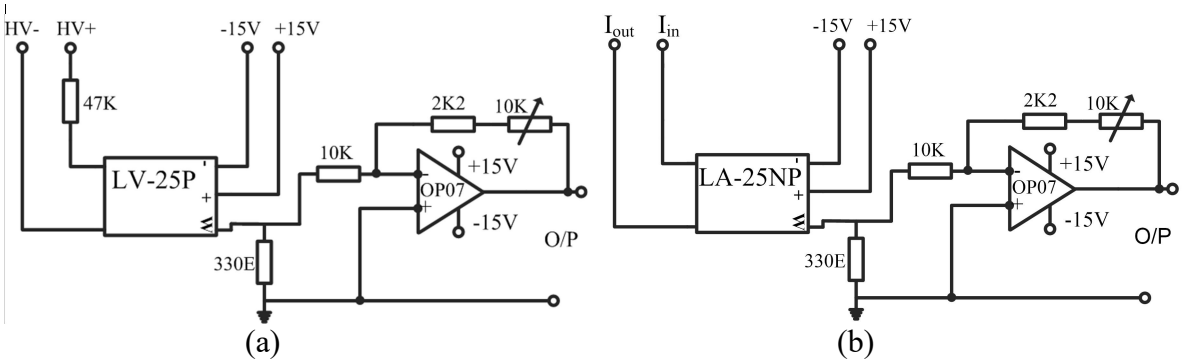

Fig. 3.4 (a) Voltage sensing circuit using LV-25 P and (b) Current sensing circuit using LA25-NP.

Voltage sensor of LEM make LV25-P is used, which has input voltage range of 0-500 V. For DC link voltage sensor LV25-P/sp2 is used, which has higher input voltage range of 1500 V. The maximum current at voltage sensor (LV25-P and LV25-P/sp2) input should not exceed 10 mA. So for measuring voltage of 110 V, the value of input side resistance is chosen to be

$$R_{in} = \frac{V_{in}}{I_{in}} = \frac{110}{10*10^{-3}} = 11k\Omega \tag{3.7}$$

The minimum wattage of input side resistance should be

$$P_{in} = V_{in} * I_{in} = 110*10*10^{-3} = 1.1\,watt \tag{3.8}$$

For measuring 200 V (for DC bus) the R_{indc}, P_{indc} are calculated using (3.9) and (3.10)

$$R_{indc} = \frac{V_{dc}}{I_{in}} = \frac{200}{10*10^{-3}} = 20k\Omega \tag{3.9}$$

$$P_{indc} = V_{dc} * I_{in} = 200*10*10^{-3} = 2\,watt \tag{3.10}$$

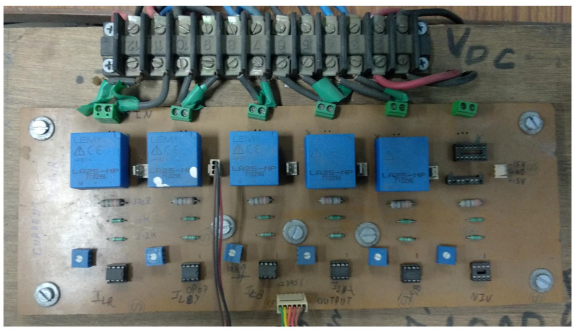

(a)

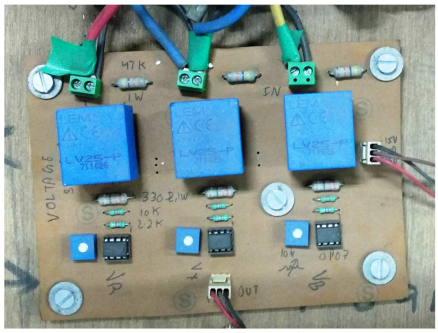

(b)

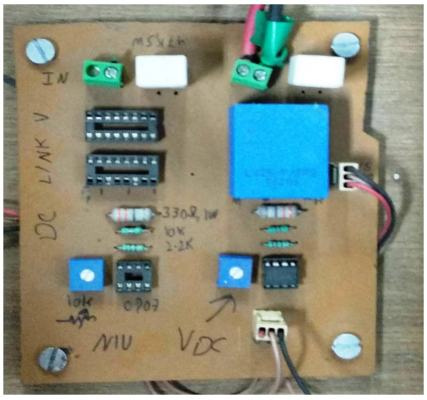

(c)

Fig. 3.5 Hardware developed (a) Current sensors (b) Voltage sensors (c) DC link voltage sensor

The selected value of input resistor for 110 V and 200 V is chosen as 47 kΩ. The power rating of resistance for 110V is taken as 2 W and for 200 V is taken as 5 W. The Op-Amp circuit is same as that of current sensor circuit. The output signals from sensors are fed to dSPACE1104 through the ADC port. The hardware circuits of voltage and current sensors are shown in Fig. 3.5(a) and Fig 3.5(b). The DC link voltage sensor is as shown in Fig. 3.5(c).

3.4 DESIGN OF VOLTAGE AMPLIFIER CIRCUIT FOR GATING SIGNALS

The output signals generated from dSPACE1104 are of the order 5 V, and to drive IGBT switches of SAPF a minimum of 15 V gating pulses are required. To amplify the gating signal without introduction of any phase shift, a voltage amplifier circuit is used as shown in Fig. 3.6(a). It consists of signal inverting circuit using IC7406. The inverting circuit is used to counter effect the 180˚ phase shift of common emitter amplifier circuit. The output of inverting circuit is fed to common emitter amplifier transistor circuit in which a Bipolar Junction Transistor (BJT) 2222N is used. The IC7406 require 5V DC supply and 2222N require 15 V DC supply, which are provided by DC supply. The hardware circuit for voltage amplifier is shown in Fig. 3.6(b).

3.5 DESIGN OF ZIGZAG TRANSFORMER

Zigzag transformer is a special purpose transformer and used in the hardware to compensate for

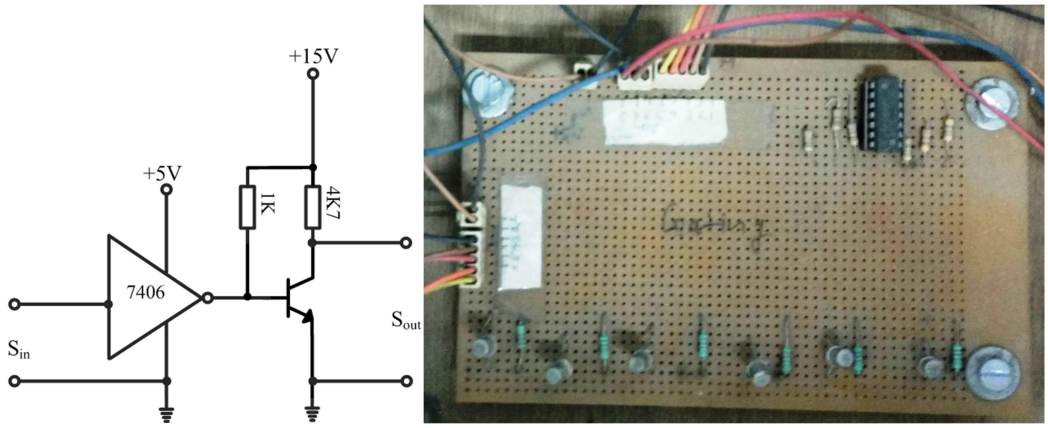

Fig. 3.6 Voltage level shifter circuit (a) connection diagram (b) hardware implementation

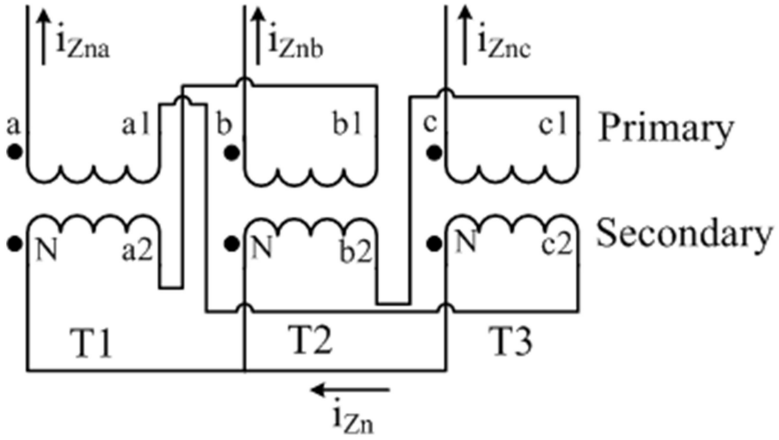

Fig. 3.7 Zigzag transformer connection diagram

neutral current in TPFW system in case of unbalanced load. For zigzag transformer connection three single phase transformers (T1, T2, T3) are interconnected as shown in Fig 3.7. The primary winding of T1 is connected in phase opposition to secondary winding of T3. Similarly primary winding of T2 is connected in phase opposition to secondary winding of T1 and primary winding of T3 is connected in phase opposition to secondary winding of T2.

Assuming the maximum neutral current to be compensated is 20 A and equal primary and secondary voltage of 110 V, the kVA rating of each zigzag transformer is

$$\boldsymbol{Z_{kVA} = V_Z * I_N} \tag{3.11}$$

where Z_{kVA} is the kVA rating of single transformer, V_Z, I_N is the voltage and current of each transformer. The Z_{kVA} calculated using Eq. 3.11 is 2.2 kVA and selected as 2.5 kVA.

3.6 SELECTION OF RATING OF LINEAR, NONLINEAR LOADS

The developed hardware setup of SAPF is tested with linear as well as non-linear loads in TPTW and TPFW system. A linear load is a series combination of resistor and inductor for each phase. In TPFW system the load is star connected so that neutral point is available from the load. By varying the load impedance the load current and PF of the system can be changed as per requirement.

For TPTW nonlinear load, a three phase diode bridge rectifier using 25D40N diodes is used. On the DC side of rectifier, a variable resistor (20-120 ohm) and an inductor (80 mH) are connected in series. For TPFW nonlinear system, three single phase diode bridge rectifiers are connected. The DC side of each rectifier has a variable resistor (20-120 ohm) and a fixed inductor (80 mH). The specifications of TPTW and TPFW linear/nonlinear system are given in APPENDIX.

3.7 EXPERIMENTAL HARDWARE SET-UP OF SAPF

A complete block diagram of SAPF including sensors, dSPACE 1104 controller, VSC, filter inductors, zig-zag transformer and three phase AC supply is shown in Fig. 3.8 (a). A prototype hardware is assembled as shown in Fig. 3.8 (b) after testing of individual building blocks such as VSC, voltage and current sensors, ADC/DAC units on dSPACE 1104 controller etc. The supply for TPTW and TPFW systems is taken from three phase variac. The output of three phase variac and TPTW SAPF is connected at PCC and load terminals. A single phase isolator switch as shown in Fig. 3.8 (b), is used to create unbalanced condition in loads. The SAPF is connected to the three phase supply through interfacing inductors. A zigzag transformer is connected to PCC as shown in Fig. 3.8 (a) in TPFW system. For TPFW, small impedance is connected in AC supply neutral wire to restrict high neutral current.

The supply voltages (v_{sa}, v_{sb}, v_{sc}), supply currents (i_{sa}, i_{sb}, i_{sc}), non-linear load currents (i_{La},i_{Lb}, i_{Lc}) and DC link voltage (V_{dc}) of SAPF are sensed and applied to ADC ports of dSPACE 1104. After processing signals using appropriate control algorithms, the output gating pulses are generated from digital I/O ports of dSPACE 1104. These signals are amplified by voltage level amplifier circuit and fed to the IGBT switches of SAPF. Two separate DC supplies for operation of sensors circuit (-15 to +15 V) and voltage amplifier circuit and IGBT switches (0-30 V) are required.

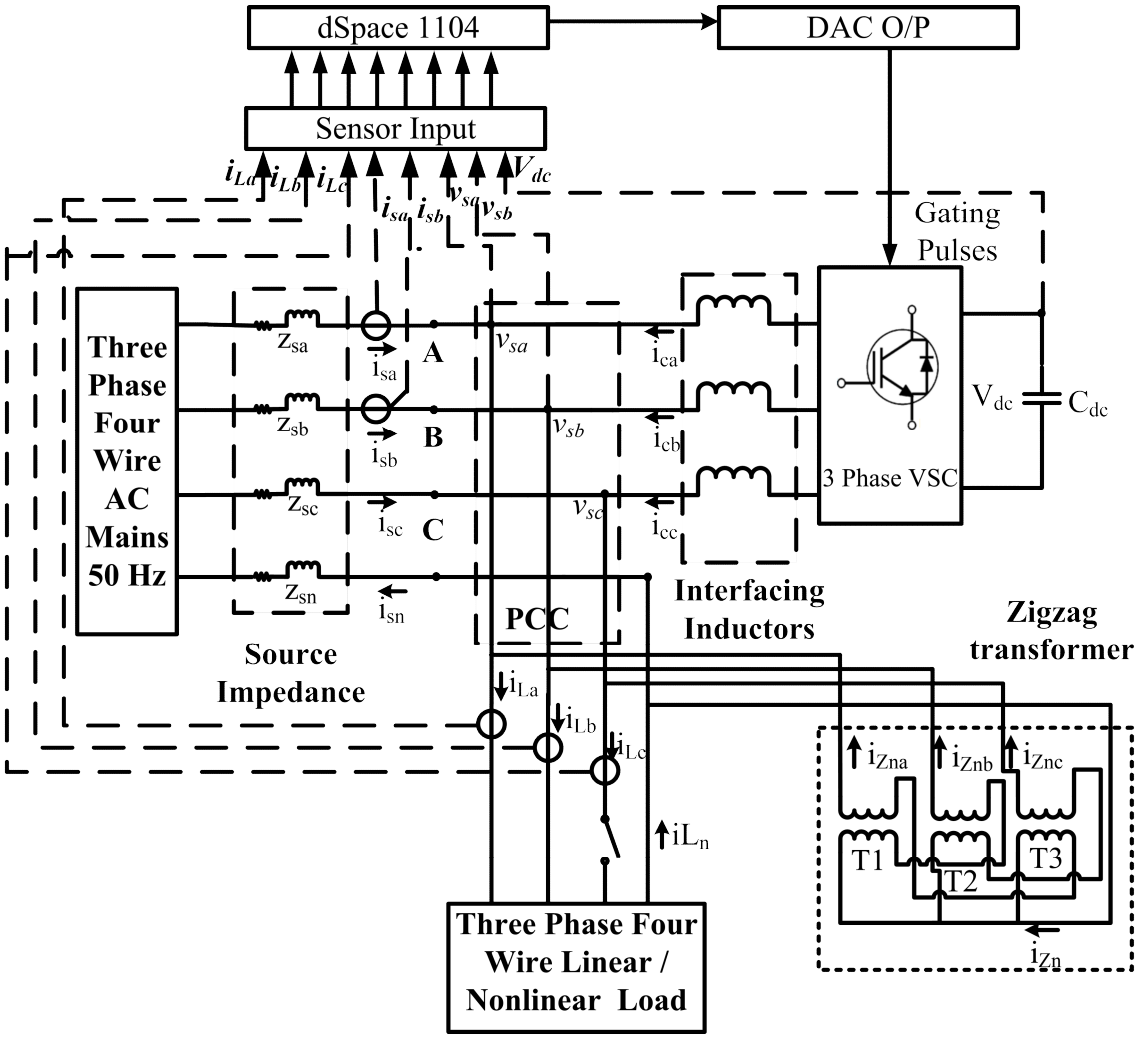

Fig. 3.8 (a) Block Diagram of TPFW system

The THD of the supply and load currents/voltages are measured using power analyzer Fluke 43B. The DC link of SAPF is monitored using a multi-meter.

3.8 MATHEMATICAL ANALYSIS OF CONVENTIONAL CONTROL ALGORITHMS FOR CONTROL OF SAPF

This section deals with mathematical analysis for control of SAPF using three conventional control algorithms as SRFT, PBT and IRPT in TPTW distribution system.

3.8.1 Switching Losses in SAPF

A TPTW VSC with DC link capacitor is used as SAPF. The switching losses in IGBT switches

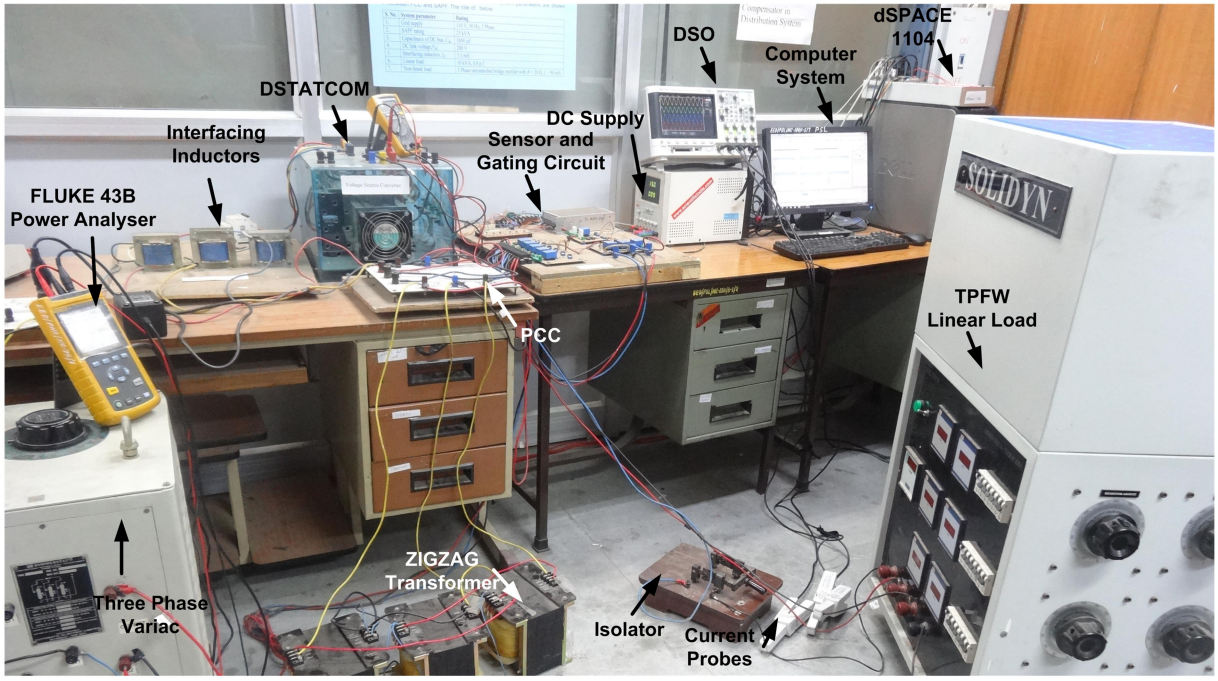

Fig. 3.8 (b) TPFW system experimental setup developed in the laboratory

of SAPF in HCC mode are significant and should be considered in modeling of the SAPF. A method to estimate switching losses in VSC is given by the following Eq. 3.12

$$I_{loss}(k) = I_{loss}(k-1) + K_p\{(e_{dc}(k) - e_{dc}(k-1)\} + K_I[e_{dc}(k)] \tag{3.12}$$

where $e_{dc}(k) = V_{dc}^{*}(k) - V_{dc}(k)$ (3.13)

V_{dc}^{*} is the reference voltage of DC link, K_p, K_I are the proportional and integral gain constant of the P-I controller block and e_{dc} is the error between actual DC link voltage V_{dc} and reference DC link voltage V_{dc}^{*}. The I_{loss} component corresponds to active power required by SAPF and added to fundamental active power component of load current extracted using control techniques under consideration.

3.8.2 Brief Theory of Conventional Control Algorithms

A brief theory of three conventional control techniques is presented in this sub-section. It includes basic formulas involved and generation of reference currents for SAPF.

3.8.2.1 Synchronous Reference Frame Theory (SRFT)

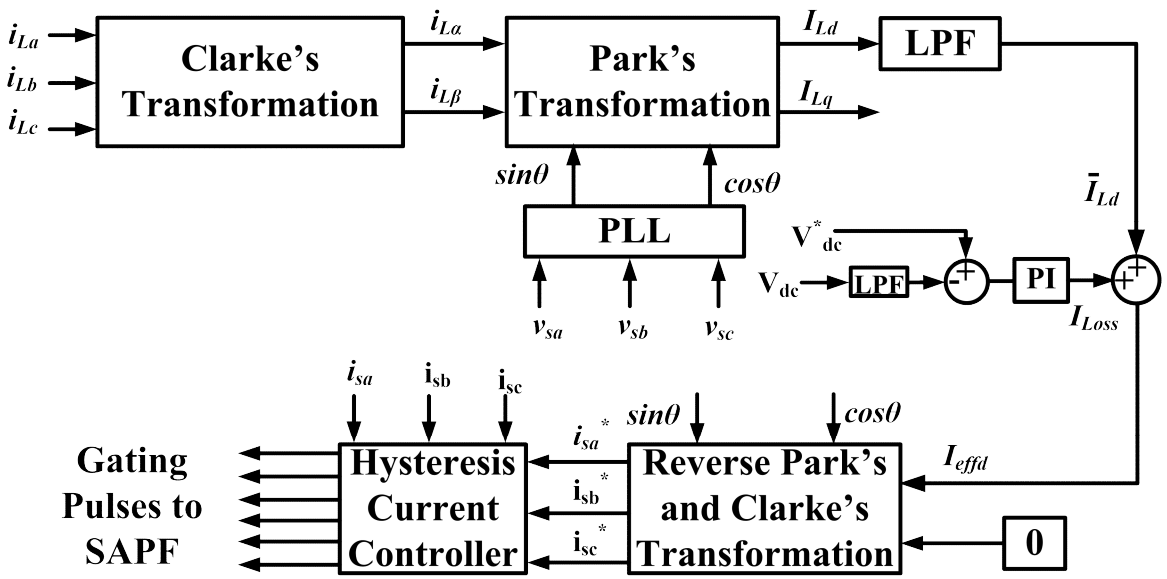

Fig. 3.9 Block diagram of SRFT control algorithm implementation

In this section the fundamental active power component of the load current is extracted using SRFT technique [99]. SRFT is based on the Clarke's and Park's transformations of load currents to obtain stationary load current components. The various transformations involved are

a. Clarke's transformation

$$\begin{bmatrix} i_{L\alpha} \\ i_{L\beta} \end{bmatrix} = \sqrt{\frac{2}{3}} \begin{bmatrix} 1 & -1/2 & -1/2 \\ 0 & \sqrt{3}/2 & -\sqrt{3}/2 \end{bmatrix} \begin{bmatrix} i_{La} \\ i_{Lb} \\ i_{Lc} \end{bmatrix} \tag{3.14}$$

b. Park's transformation

$$\begin{bmatrix} I_{Ld} \\ I_{Lq} \end{bmatrix} = \sqrt{\frac{2}{3}} \begin{bmatrix} \cos\theta & \sin\theta \\ -\sin\theta & \cos\theta \end{bmatrix} \begin{bmatrix} i_{L\alpha} \\ i_{L\beta} \end{bmatrix} \tag{3.15}$$

Fig. 3.9 shows the complete block diagram of SRFT control techniques for SAPF. The load currents after Clarke's and Park's transformation provide I_{Ld} and I_{Lq}. The component I_{Ld} is passed through a low pass filter (LPF). The DC bus loss component I_{loss} calculated using Eq. 3.12, is added to filtered I_{Ld} so as to obtain I_{effd}. Thereafter, inverse Park's and Clarke's

transformation is used as per Eq. (3.16-3.17) on I_{effd}, which gives the required reference currents (i_{sa}^*, i_{sb}^*, i_{sc}^*).

$$\begin{bmatrix} i_{s\alpha}^* \\ i_{s\beta}^* \end{bmatrix} = \sqrt{\frac{2}{3}} \begin{bmatrix} \cos & -\sin \\ \sin & \cos \end{bmatrix} \begin{bmatrix} I_{effd} \\ 0 \end{bmatrix} \tag{3.16}$$

$$\begin{bmatrix} i_{sa}^* \\ i_{sb}^* \\ i_{sc}^* \end{bmatrix} = \sqrt{\frac{2}{3}} \begin{bmatrix} 1 & 0 \\ -1/2 & \sqrt{3}/2 \\ -1/2 & -\sqrt{3}/2 \end{bmatrix} \begin{bmatrix} i_{s\alpha}^* \\ i_{s\beta}^* \end{bmatrix} \tag{3.17}$$

The reference currents (i_{sa}^*, i_{sb}^*, i_{sc}^*) are compared with actual supply currents (i_{sa}, i_{sb}, i_{sc}) using HCC and six gating pulses for SAPF are generated.

3.8.2.2 Power Balance Theory (PBT)

Fig. 3.10 shows the block diagram of PBT. The unit templates of supply voltage u_{ia}, u_{ib}, u_{ic} are used for generating reference currents, which are calculated using Eq. (3.18)

$$u_{ia} = \frac{v_{sa}}{V_t}; u_{ib} = \frac{v_{sb}}{V_t}; u_{ic} = \frac{v_{sc}}{V_t} \tag{3.18}$$

where v_{sa}, v_{sb}, v_{sc} are three phase PCC voltages, V_t is peak value of supply voltage and calculated using Eq. (3.19)

$$V_t = \sqrt{\frac{2}{3}(v_{sa}^2 + v_{sb}^2 + v_{sc}^2)} \tag{3.19}$$

The active power required by load is calculated as follows [101]

$$p = V_t(u_{ia} i_{La} + u_{ib} i_{Lb} + u_{ic} i_{Lc}) \tag{3.20}$$

It is filtered and DC link loss p_{loss} is added to it to obtain $\bar{p}_{eff}$. Fundamental active power component of load current I_{eff} is calculated using Eq. (3.21)

$$I_{eff} = \left(\frac{2}{3}\right) \frac{\bar{p}_{eff}}{V_t} \tag{3.21}$$

Now the reference currents are generated using Eq. (3.22)

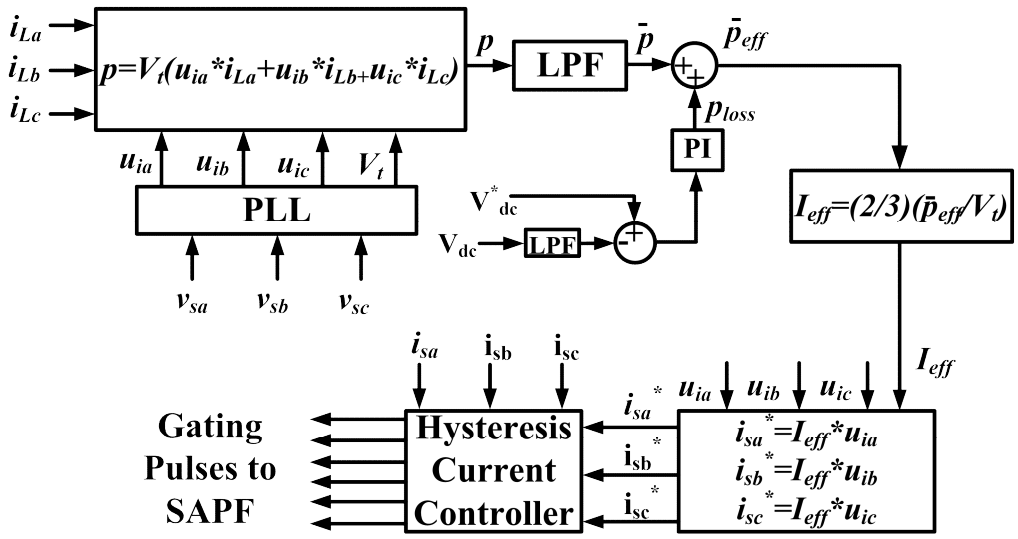

Fig. 3.10 Block diagram of PBT control algorithm implementation

$$i_{sa}^* = I_{eff} * u_{ia}; i_{sb}^* = I_{eff} * u_{ib}; i_{sc}^* = I_{eff} * u_{ic} \tag{3.22}$$

The reference source currents are compared to actual source currents using HCC and six gating pulses are generated.

3.8.2.3 Instantaneous Reactive Power Theory (IRPT)

Fig. 3.11 shows the block diagram of conventional IRPT [95-96] based algorithm. The α-β components of load currents and PCC voltages are calculated as per Eq. (3.14). Now the instantaneous active power component (p) is calculated using following Eq.

$$p = v_\alpha i_\alpha + v_\beta i_\beta \tag{3.23}$$

The active power p is passed through a LPF and DC bus loss component p_{loss} is added to it. Now the fundamental α-β component of reference currents are calculated using Eq. (3.24-3.25)

$$i_\alpha^* = \frac{1}{\sqrt{v_\alpha^2 + v_\beta^2}}\left(v_\alpha \bar{p}_{eff} - v_\beta \bar{q}_{eff}\right) \tag{3.24}$$

$$i_\beta^* = \frac{1}{\sqrt{v_\alpha^2 + v_\beta^2}}\left(v_\alpha \bar{q}_{eff} + v_\beta \bar{p}_{eff}\right) \tag{3.25}$$

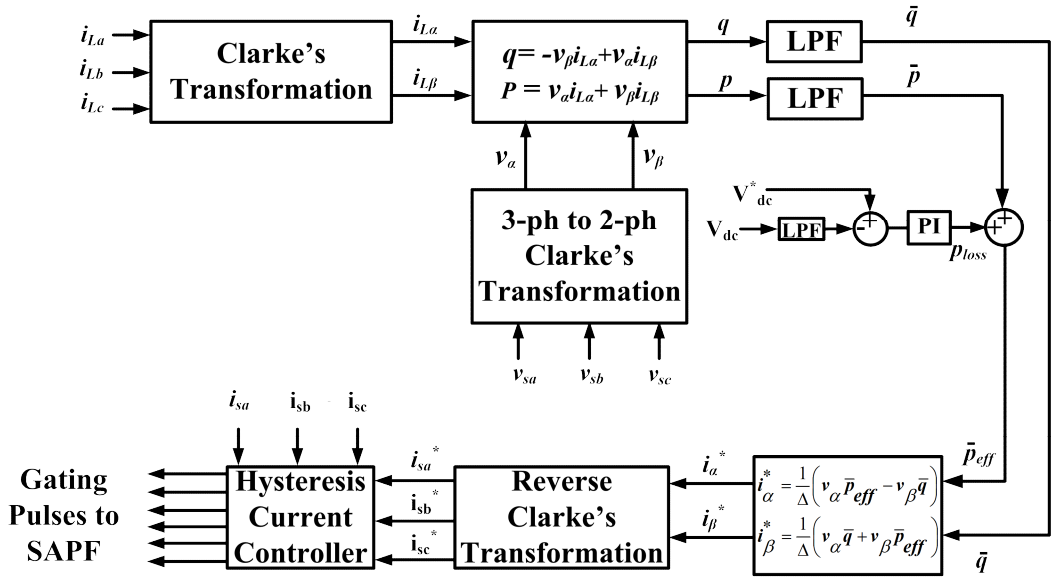

Fig. 3.11 Block diagram of IRPT control algorithm implementation

The supply reference currents are obtained using reverse Clarke's transformation as per Eq. (3.17), which on processing by HCC generates six gating pulses.

3.9 SIMULATION RESULTS

A MATLAB/SIMULINK model of SAPF for TPTW system is developed and SRFT, PBT and IRPT conventional control techniques are implemented for effective operation and control of SAPF. The simulation results obtained are analyzed in following subsections.

3.9.1 Synchronous Reference Frame Theory (SRFT)

Fig. 3.12 shows the simulation results for compensating PQ problems using SRFT based control of SAPF in MATLAB environment. Fig. 3.12 shows the waveforms of three phase supply voltages (v_{sa}, v_{sb}, v_{sc}), three phase supply currents (i_{sa}, i_{sb}, i_{sc}), three phase non-linear load currents (i_{La}, i_{Lb}, i_{Lc}), three phase compensating currents (i_{ca}, i_{cb}, i_{cc}), and DC link voltage (V_{dc}) of SAPF. A load unbalancing is introduced in the system at t=0.3 sec. The unbalancing is introduced by sudden disconnection of phase 'c' of the load, which results in i_{Lc} to be zero after t=0.3 sec. The supply currents are observed to be balanced and sinusoidal during t=0.3 to 0.4 sec

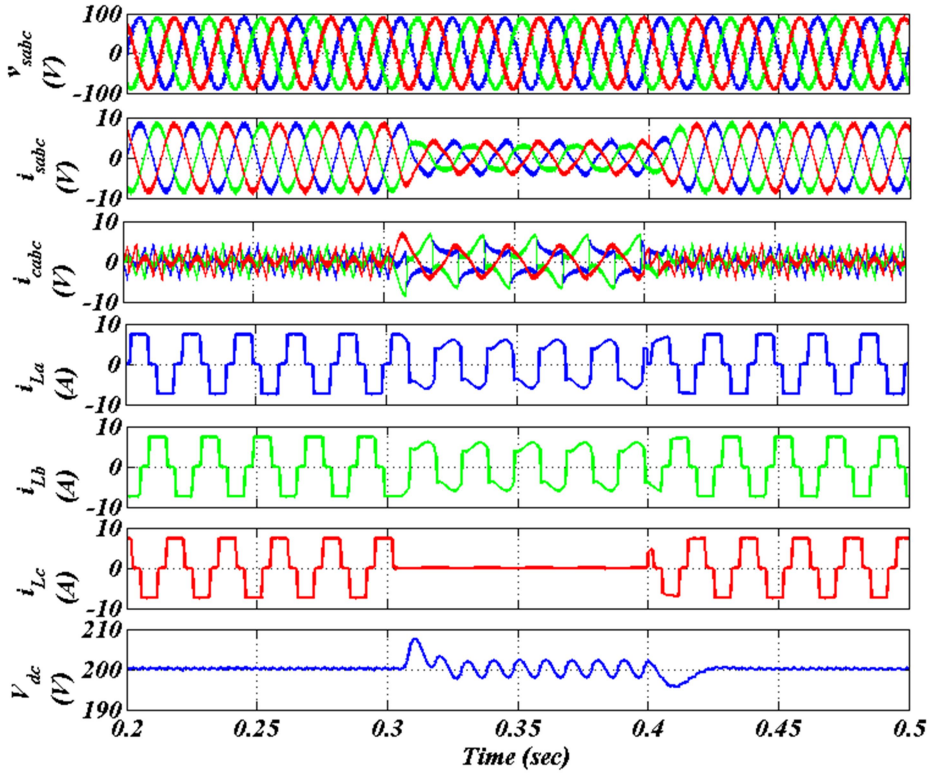

Fig. 3.12 Simulation results using SRFT control algorithm for non-linear load

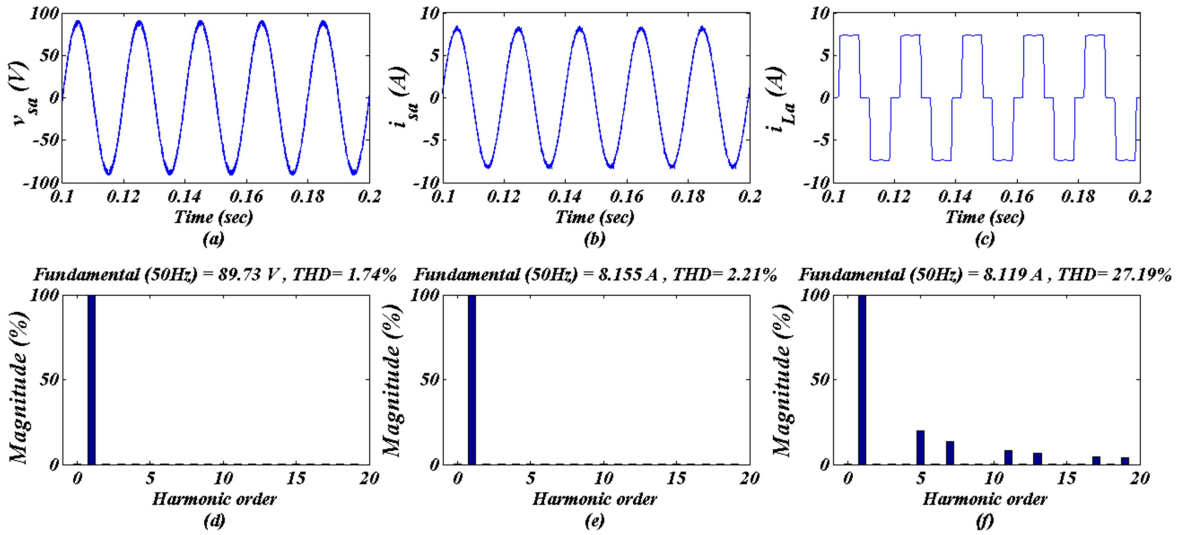

Fig. 3.13 Harmonic analysis using SRFT based control algorithm (a-c) waveforms of v_{sa}, i_{sa}, i_{La} (d-f) THD of v_{sa}, i_{sa}, i_{La} for non-linear load

due to suitable compensation currents supplied by SAPF. The DC link voltage is also maintained to reference value of 200 V. Figs. 3.13 (a)-(c) show the waveforms and Figs. 3.13 (d)-(f) show the THD content of phase 'a' supply voltage v_{sa}, phase 'a' supply current i_{sa} and phase 'a' load

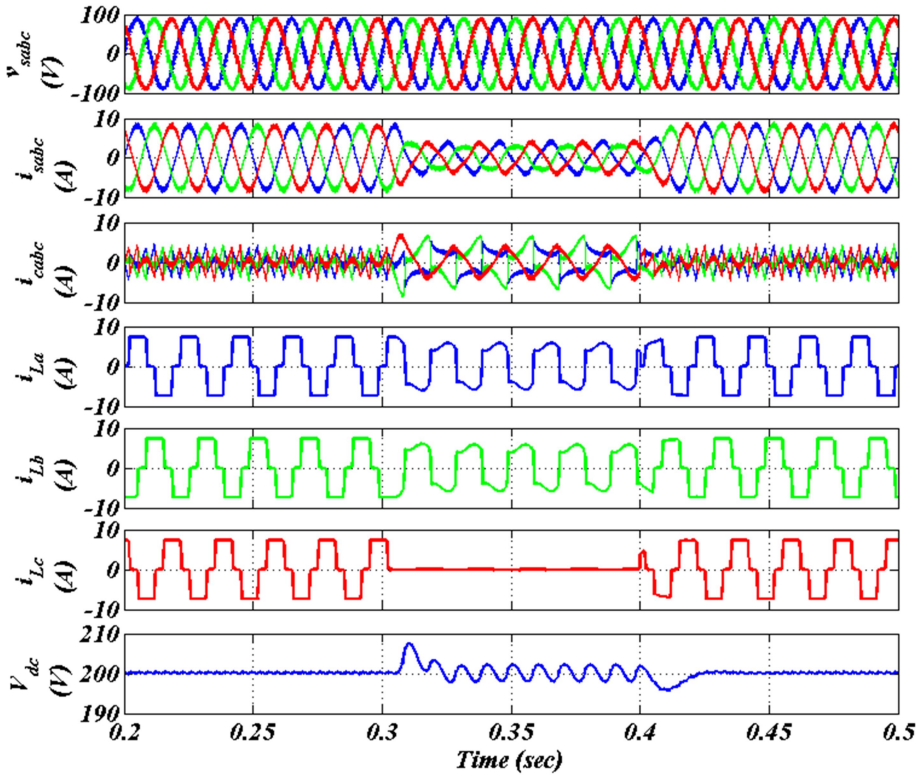

Fig. 3.14 Simulation results using PBT control algorithm for non-linear load

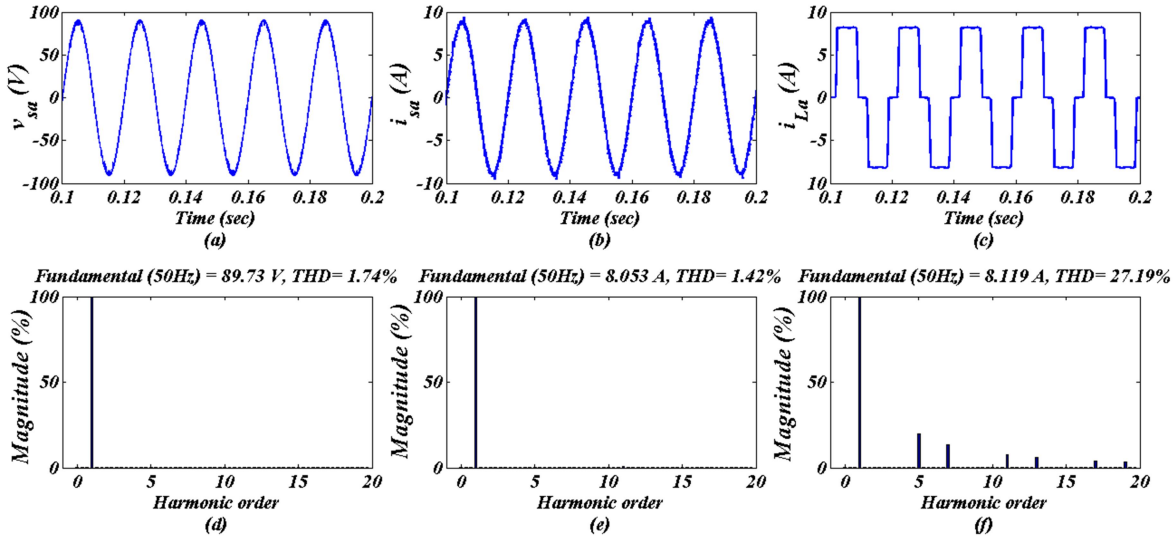

Fig. 3.15 Harmonic analysis using PBT based control algorithm (a-c) waveforms of v_{sa}, i_{sa}, i_{La} (d-f) THD of v_{sa}, i_{sa}, i_{La} for non-linear load

current i_{La} respectively. It is noted that despite the load being highly nonlinear and having a current THD as high as 27.19%, however with SAPF the supply current is balanced and sinusoidal. The supply current has a low THD of 2.21%, which is acceptable as per IEEE 519.

3.9.2 Power Balance Theory (PBT)

Fig. 3.14 shows the simulation results of SAPF implementation using PBT control technique. Fig. 3.14 shows the waveforms of three phase supply voltages (v_{sa}, v_{sb}, v_{sc}), three phase supply currents (i_{sa}, i_{sb}, i_{sc}), three phase non-sinusoidal load currents (i_{La}, i_{Lb}, i_{Lc}), three phase compensating currents (i_{ca}, i_{cb}, i_{cc}), and DC link voltage (V_{dc}) of SAPF feeding non-linear load. It is seen that the supply currents are balanced and sinusoidal under all operating conditions with PBT also. Appropriate compensating currents are injected by SAPF in supply system. Figs. 3.15(a)-(c) show the waveforms and Figs. 3.15(d)-(f) show the harmonic spectra of phase 'a' supply voltage v_{sa}, phase 'a' supply current i_{sa} and phase 'a' load current i_{La} respectively. The load current is non-sinusoidal and has a THD of 27.19%, however supply current THD is reduced to 1.42% with the application of SAPF. The three phase supply currents (i_{sa}, i_{sb}, i_{sc}) are balanced and sinusoidal. The grid voltage has a THD of 1.74%.

3.9.3 Instantaneous Reactive Power Theory (IRPT)

Fig. 3.16 shows the simulation results using SAPF with IRPT implemented in MATLAB-SIMULINK. Fig. 3.16 shows the waveforms of three phase PCC voltages (v_{sa}, v_{sb}, v_{sc}), three phase supply currents (i_{sa}, i_{sb}, i_{sc}), three phase non-sinusoidal load currents (i_{La}, i_{Lb}, i_{Lc}), three phase compensating currents (i_{ca}, i_{cb}, i_{cc}), and DC link voltage (V_{dc}) of SAPF. In this case phase 'c' of load is removed at t=0.4 sec and waveforms are captured. It is observed that the DC link has small transients but attains its steady state value of 200 V rapidly. Further, the phase 'c' of load is reconnected at t=0.6 sec which enables the supply currents to be balanced. With SAPF the supply currents are sinusoidal and balanced under different loading condition. The compensating currents also change in magnitude during t=0.4 sec to 0.6 sec. Figs. 3.17(a)-(c) show the waveforms and Figs. 3.17(d)-(f) show the harmonic spectra of phase 'a' supply voltage v_{sa},phase

'a' supply current i_{sa} and non-sinusoidal phase 'a' load current i_{La}. The load current is non-sinusoidal and has a THD of 27.19% in absence of SAPF, whereas with SAPF-IRPT control, the supply current has reduced THD of 4.91%.

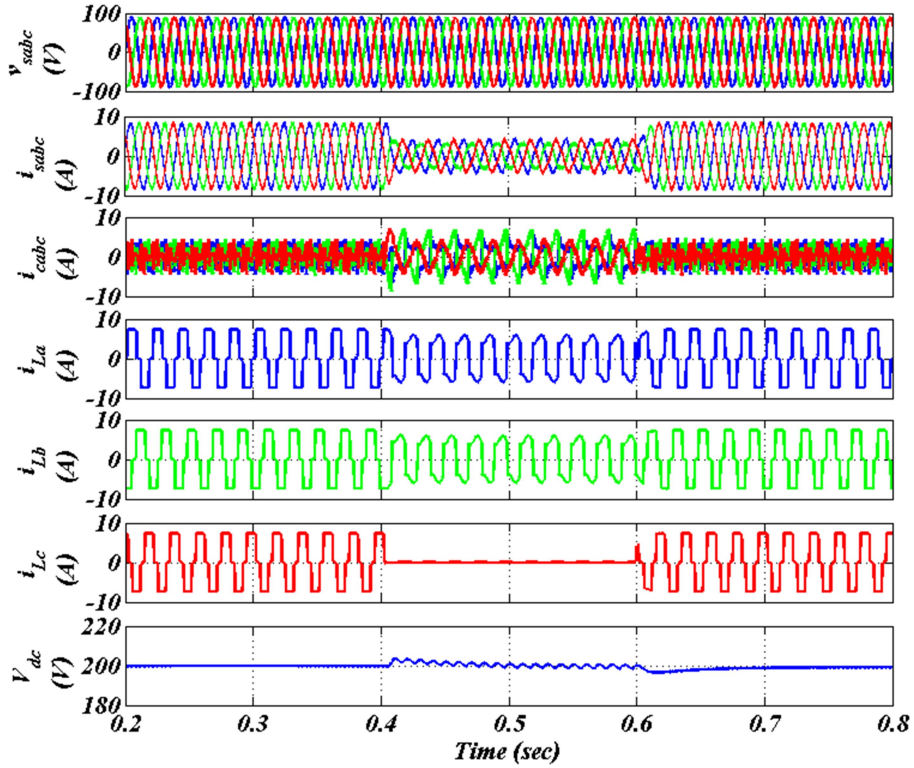

Fig. 3.16 Simulation results using IRPT control algorithm for non-linear load.

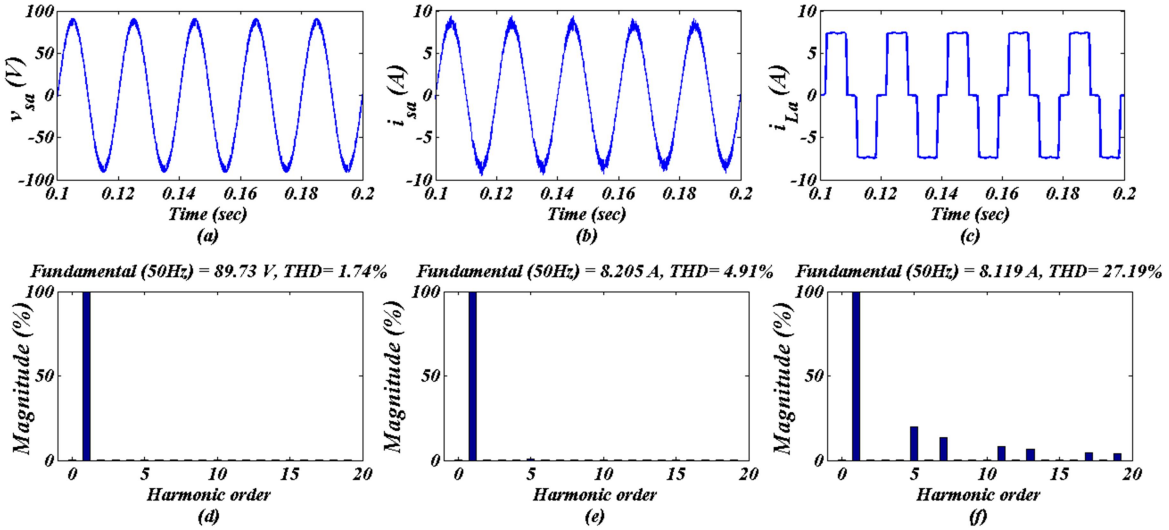

Fig. 3.17 Harmonic Analysis using IRPT control algorithm (a-c) waveforms of v_{sa}, i_{sa}, i_{La} (d-f) THD of v_{sa}, i_{sa}, i_{La}

3.10 EXPERIMENTAL RESULTS

The conventional control techniques of SAPF are also tested on the developed prototype hardware system. Experimental results obtained using SRFT, PBT and IRPT are discussed.

3.10.1 Synchronous Reference Frame Theory (SRFT)

Fig. 3.18 presents the steady state results for TPTW distribution system compensated with SAPF. Figs. 3.18(a)-(c) show the waveforms of phase 'a' supply current (i_{sa}), phase 'a' load current (i_{La}) and phase 'a' compensator current (i_{ca}) along with phase 'a' supply voltage (v_{sa}). Figs. 3.18(d)-(f) show the THD of phase 'a' supply voltage (v_{sa}), phase 'a' supply current (i_{sa}) and phase 'a' load current (i_{La}) respectively. It is concluded that despite the load being highly nonlinear and having a high THD of 22.7%, the supply currents are sinusoidal and having a low THD of 2.3%. The phase 'a' supply voltage (v_{sa}) has a THD of 4.2%.

Fig. 3.19-3.20 show the dynamic performance of SAPF. An unbalancing in load current with the help of single phase isolator is introduced in phase 'c' of the system. Fig. 3.19(a) shows the phase 'a' supply voltage (v_{sa}) with three phase SAPF compensated supply currents (i_{sa}, i_{sb}, i_{sc}). The supply currents are balanced and sinusoidal. Fig 3.19(b) shows the phase 'a' supply voltage (v_{sa}), and non-sinusoidal load currents (i_{La}, i_{Lb}, i_{Lc}). The phase 'c' load current is absent during unbalancing. Fig. 3.19(c) shows phase 'a'supply voltage (v_{sa}) and SAPF injected compensating currents (i_{ca}, i_{cb}, i_{cc}). The phase 'c' compensating current is observed to be large during unbalancing. Fig. 3.19(d) shows DC link voltage (V_{dc}) and phase 'c' supply, load and compensating currents. It is observed from the Fig. 3.19 that SAPF operates effectively during dynamics changes in loads. The DC link voltage is regulated to reference value of 200 V by PI controller.

Fig. 3.20 presents the intermediate results for the proposed system. Fig 3.20(a) shows phase 'a'

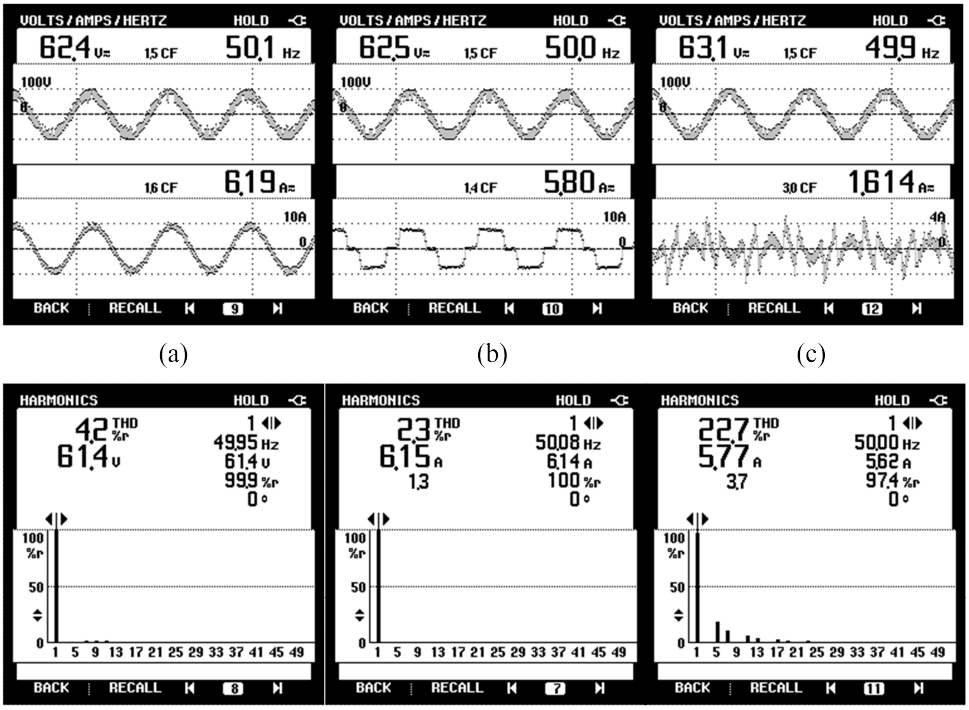

Fig. 3.18 Steady state waveforms for TPTW system using SRFT control algorithm (a) v_{sa}-i_{sa} (b) v_{sa}-i_{La} (c) v_{sa}-i_{ca} and (d-f) THD of (d) v_{sa} (e) i_{sa} (f) i_{La} for non-linear load

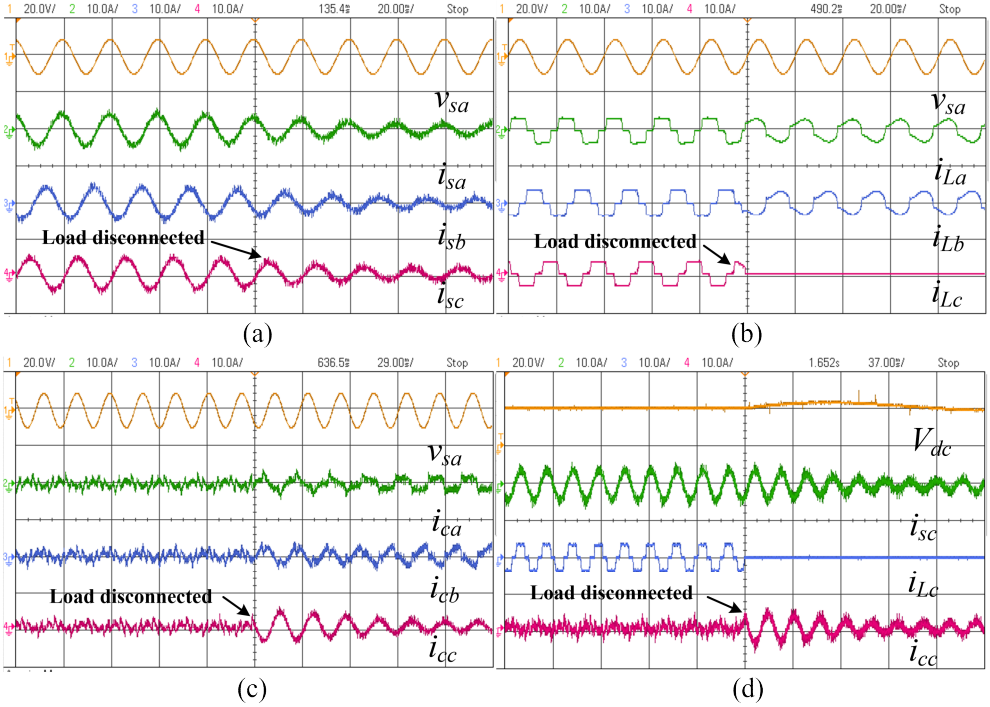

Fig. 3.19 Results showing dynamics for load disconnected in phase 'c' using SRFT control algorithm (a) v_{sa}, i_{sa}, i_{sb}, i_{sc} (b) v_{sa}, i_{La}, i_{Lb}, i_{Lc} (c) v_{sa}, i_{ca}, i_{cb}, i_{cc} (d) V_{dc}, i_{sc}, i_{Lc}, i_{cc} for non-linear load

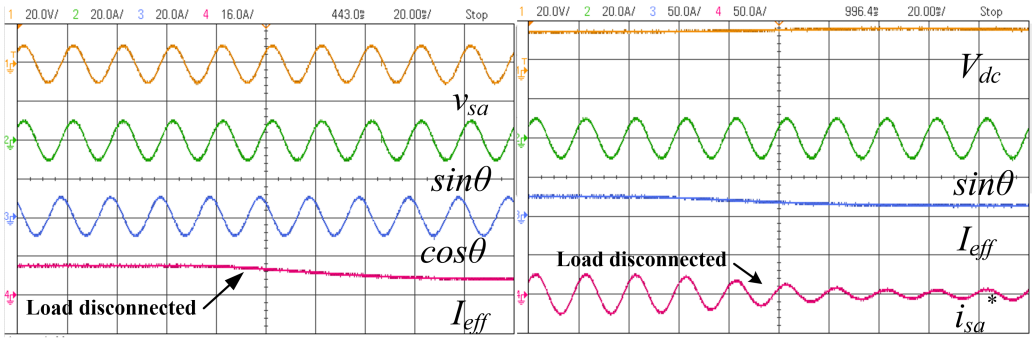

(a) (b)

Fig. 3.20 Intermediate results using SRFT control algorithm (a) v_{sa}, $sin\theta$, $cos\theta$, I_{eff} (b) V_{dc}, $sin\theta$, I_{eff}, i_{sa}^* for non-linear load

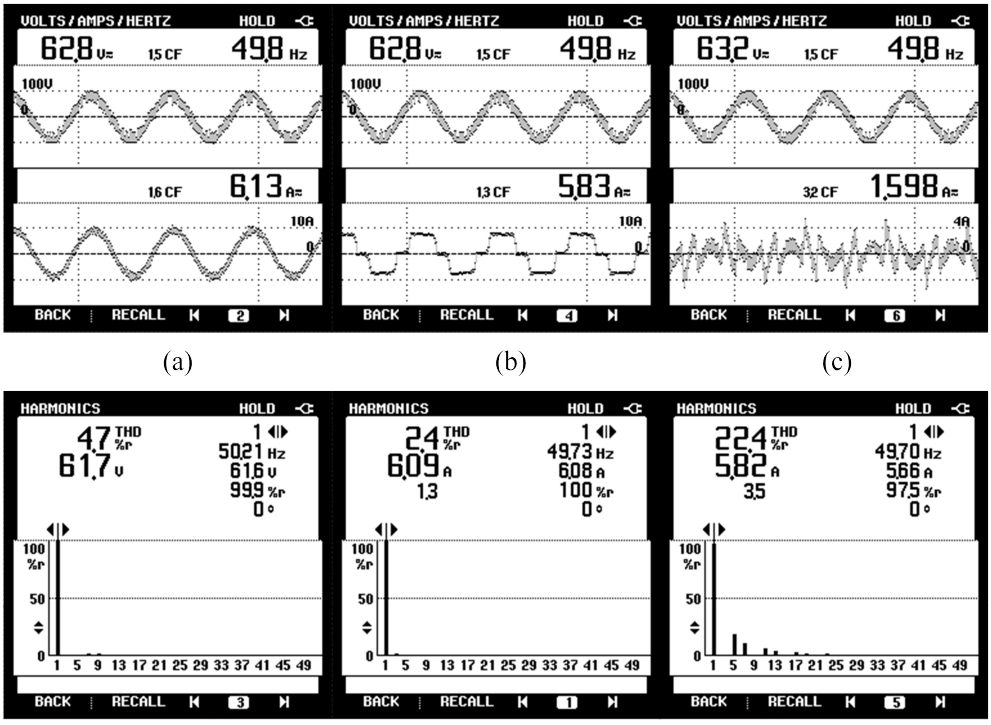

(a) (b) (c)

(d) (e) (f)

Fig. 3.21 Steady state waveforms for TPTW system using PBT control algorithm (a) v_{sa}-i_{sa} (b) v_{sa}-i_{La} (c) v_{sa}-i_{ca} and (d-f) THD of (d) v_{sa} (e) i_{sa} (f) i_{La} for non-linear load

supply voltage (v_{sa}), synchronizing templates ($sin\theta$, $cos\theta$), and fundamental active power component of current (I_{effd}). The magnitude of I_{effd} changes according to the loading condition. However, the synchronizing templates are not affected due to load unbalancing. Fig 3.20(b) shows DC link voltage (V_{dc}), synchronizing template ($sin\theta$), and effective weight (I_{effd}) and phase 'a' reference current (i_{sa}^*). The reference currents vary during load unbalancing period to enable

the supply currents remain balanced and sinusoidal.

It is demonstrated that the conventional algorithm SRFT is effective in harmonic elimination and balancing of supply currents under unbalanced non-sinusoidal load.

3.10.2 Power Balance Theory (PBT)

Fig. 3.21 shows the steady state performance of a TPTW distribution system with SAPF using PBT. It is observed from Figs. 3.21(a)-(b) that the supply current (i_{sa}) is sinusoidal despite the load being highly non-linear. The SAPF compensating current is necessary for making sinusoidal AC supply currents. Figs. 3.21(d)-(f) show the THD of phase 'a' supply voltage (v_{sa}), phase 'a' supply current (i_{sa}) and phase 'a' load current (i_{La}) respectively. The load current THD is as high as 22.4% and the supply current has a THD of 2.4%. The supply voltage has a THD of 4.7%. With application of SAPF the supply current and voltage THD is within acceptable limit as

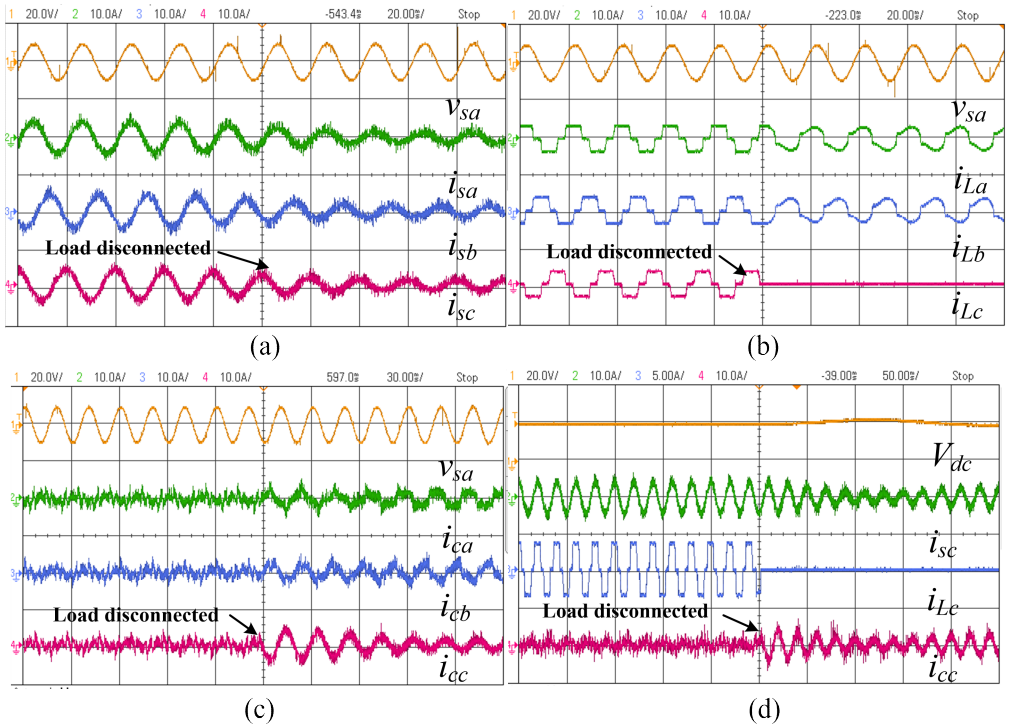

Fig. 3.22 Results showing dynamics for load disconnected in phase 'c' using PBT control algorithm (a) v_{sa}, i_{sa}, i_{sb}, i_{sc} (b) v_{sa}, i_{La}, i_{Lb}, i_{Lc} (c) v_{sa}, i_{ca}, i_{cb}, i_{cc} (d) V_{dc}, i_{sc}, i_{Lc}, i_{cc} for non-linear load

permissible in IEEE 519 [40].

Fig. 3.22 and Fig. 3.23 present the dynamic performance of SAPF implemented using PBT. The isolator switch connected in phase 'c' is opened so that system load becomes unbalanced. The system performance is captured on DSO during unbalancing. Fig. 3.22(a) presents phase 'a' supply voltage (v_{sa}) and SAPF compensated supply currents (i_{sa}, i_{sb}, i_{sc}). The supply currents have lower magnitude during unbalancing but are sinusoidal and balanced. Fig. 3.22(b) presents phase 'a' supply voltage (v_{sa}) and non-sinusoidal load currents (i_{La}, i_{Lb}, i_{Lc}). Fig. 3.22(c) shows phase 'a' supply voltage (v_{sa}) and SAPF injected compensating currents (i_{ca}, i_{cb}, i_{cc}). The compensating currents provide necessary currents to be injected during different load conditions. Fig. 3.22(d) shows DC link voltage (V_{dc}), phase 'c' supply current (i_{sc}), phase 'c' load current (i_{Lc}) and phase 'c' compensating currents (i_{cc}). The supply currents are balanced and the DC link voltage also settles rapidly to set value of 200 V.

Fig. 3.23 shows the intermediate results in the implementation of PBT technique. Fig. 3.23(a) shows phase 'a' supply voltage (v_{sa}), synchronizing template ($sin\theta$), active power component of load current (I_{eff}), phase 'a' reference current (i_{sa}^*). Both the active component and synchronizing templates are responsible for generation of reference currents. Fig. 3.23(b) shows the DC link voltage (V_{dc}), effective power component (p_{eff}), active power component of load current (I_{eff}) and

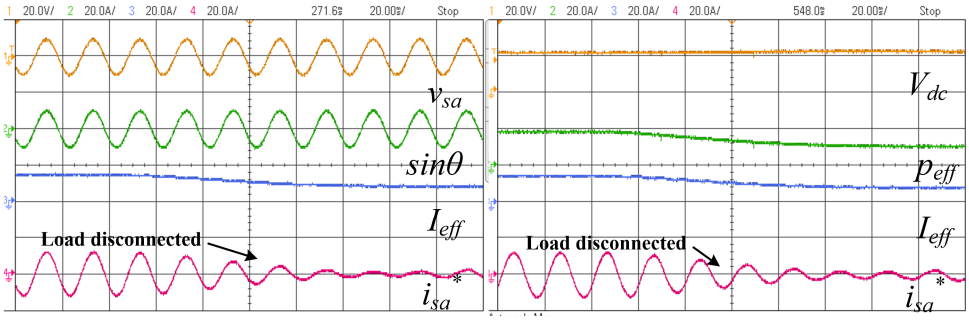

(a) (b)

Fig. 3.23 Intermediate results using PBT control technique (a) v_{sa}, $sin\theta$, I_{eff}, i_{sa}^* (b) V_{dc}, p_{eff}, I_{eff}, i_{sa}^* for non-linear load

phase ‘a’ reference supply current (i_{sa}^{*}).

It is observed that PBT can be implemented for effective PQ improvement of TPTW distribution system.

3.10.3 Instantaneous Reactive Power Theory (IRPT)

Fig. 3.24 shows the steady state performance of a TPTW distribution system with SAPF implemented using IRPT control algorithm. It is observed from Fig. 3.24 that the supply current (i_{sa}) is sinusoidal and have low THD of 3.1%. The load current (i_{La}) and supply voltage (v_{sa}) have a THD of 22.5% and 4.4% respectively. The THD of supply current obtained using IRPT is high as compared to THD obtained using SRFT (2.3%) and PBT (2.4%). So IRPT control technique is observed to be comparatively less effective as compared to SRFT and PBT for harmonic elimination using SAPF.

Fig. 3.25 and Fig. 3.26 show the dynamic performance of SAPF implemented with PBT. In Fig.

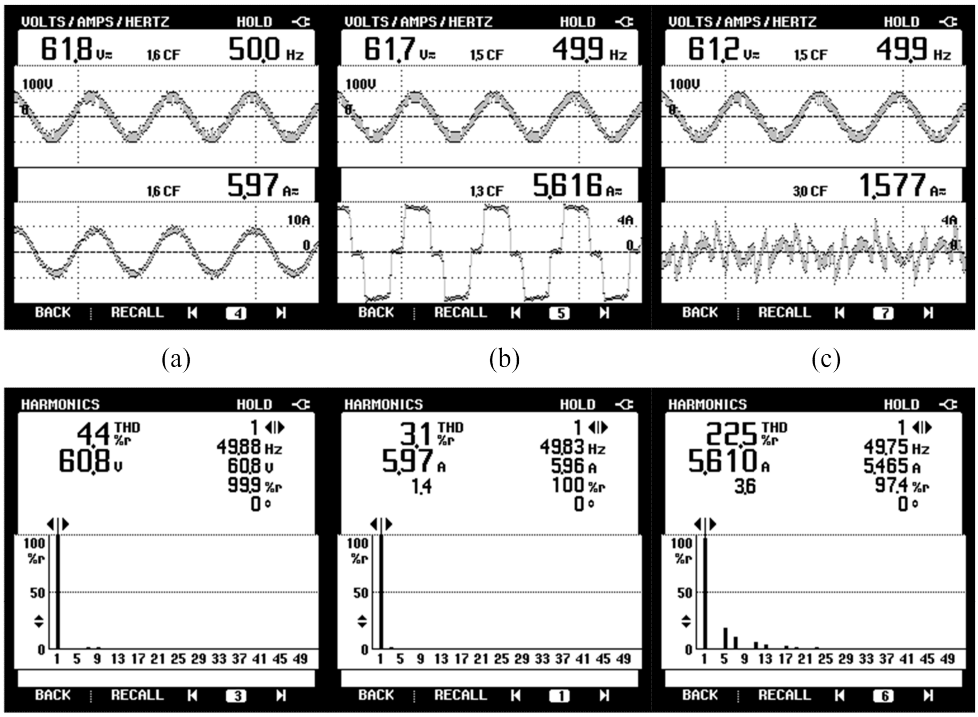

Fig. 3.24 Steady state waveforms for TPTW system using IRPT control algorithm (a) v_{sa}-i_{sa} (b) v_{sa}-i_{La} (c) v_{sa}-i_{ca} and (d-f) THD of (d) v_{sa} (e) i_{sa} (f) i_{La} for non-linear load

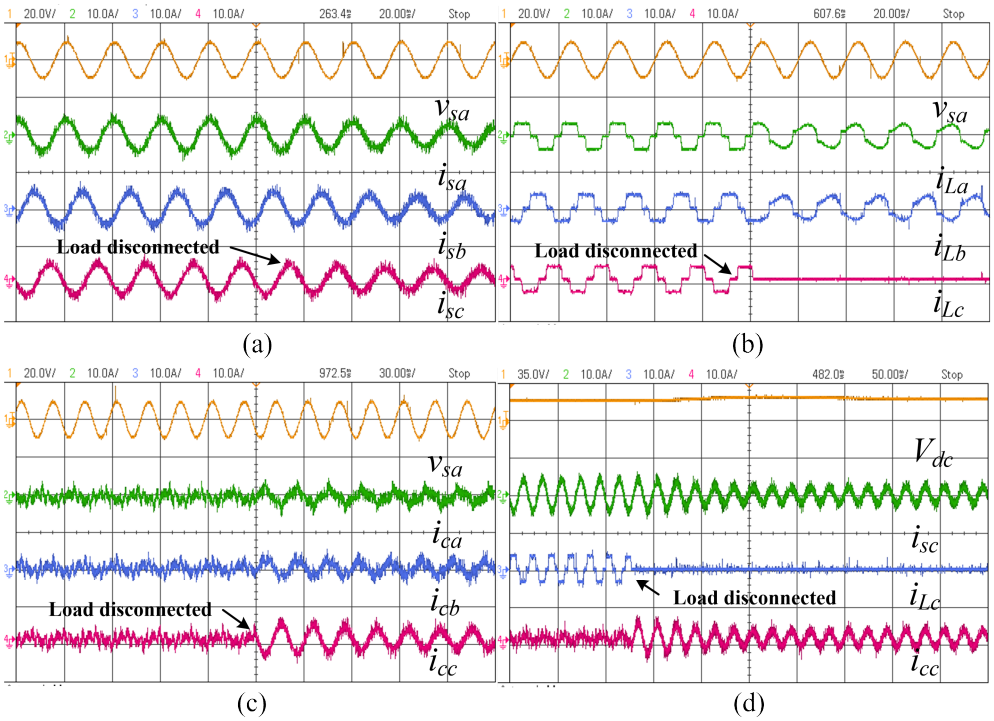

Fig. 3.25 Results showing dynamics for load disconnected in phase 'c' using IRPT control algorithm (a) v_{sa}, i_{sa}, i_{sb}, i_{sc} (b) v_{sa}, i_{La}, i_{Lb}, i_{Lc} (c) v_{sa}, i_{ca}, i_{cb}, i_{cc} (d) V_{dc}, i_{sc}, i_{Lc}, i_{cc} for nonlinear load

3.25(a), phase 'a' supply voltage (v_{sa}) and SAPF compensated supply currents (i_{sa}, i_{sb}, i_{sc}) are shown. The supply currents are balanced and sinusoidal during different load conditions. In Fig. 3.25(b) phase 'a' supply voltage (v_{sa}), and non-sinusoidal load currents (i_{La}, i_{Lb}, i_{Lc}) are shown. An unbalancing in the load is created by isolating phase 'c'. Fig. 3.25(c) shows phase 'a' supply voltage (v_{sa}), and SAPF injected compensating currents (i_{ca}, i_{cb}, i_{cc}). The compensating currents have some switching transients. Fig. 3.25(d) shows DC link voltage (V_{dc}), phase 'c' supply current (i_{sc}), phase 'c' load current (i_{Lc}) and phase 'c' compensating (i_{cc}) current. During unbalancing the phase 'c' supply current is provided by SAPF and supply currents remain balanced.

Fig. 3.26 shows the intermediate waveforms in implementation of IRPT control technique. Fig. 3.26(a) shows phase 'a' supply voltage (v_{sa}), synchronizing template ($sin\theta$), effective power component (p_{eff}) and phase 'a' reference supply current (i_{sa}^{*}). The active current component

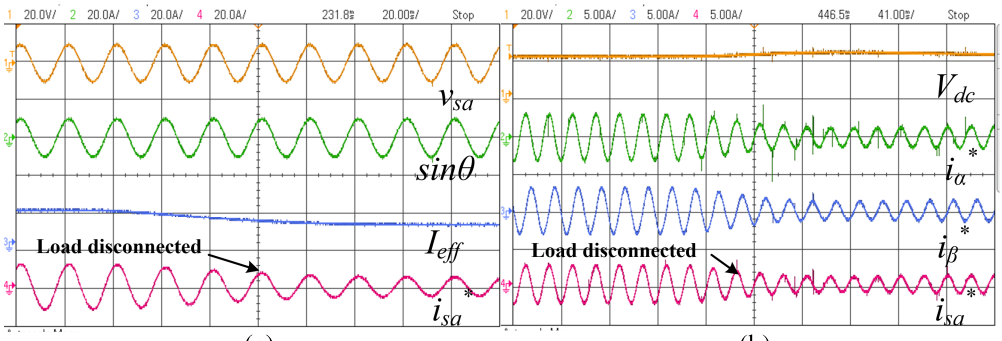

Fig. 3.26 Intermediate results using IRPT control technique (a) v_{sa}, $sin\theta$, I_{eff}, i_{sa}^* (b) V_{dc}, i_α^*, i_β^*, i_{sa}^* for non-linear load

magnitude is lowered due to reduction in the load current. Fig. 3.26(b) shows DC link voltage (V_{dc}), alpha component (I_α^*) and beta component (I_β^*) of reference supply current, and phase 'a' reference supply current (i_{sa}^*). The alpha-beta components of reference supply currents are extracted using IRPT and are in quadrature with each other.

It is observed that IRPT can be implemented for PQ improvement of TPTW distribution system but its performance is inferior as compared to that of SRFT and PBT.

3.11 CONCLUSIONS

In this chapter a detailed design and development of prototype SAPF for TPTW and TPFW power distribution system is discussed. The TPTW proposed system is tested for PQ improvement using three conventional control techniques viz SRFT, PBT and IRPT. The simula-

TABLE 3.1 COMPARISON OF CONVENTIONAL CONTROL ALGORITHMS

S.No.	Quantity	SRFT	PBT	IRPT
1.	Supply Voltage (v_{sa})	61.4 V, 4.2% THD	61.7 V, 4.7% THD	60.8 V, 4.4% THD
2.	Load Current (i_{La})	5.77 A, 22.7% THD	5.82, 22.4% THD	5.610 A, 22.5% THD
3.	Supply Current (i_{sa})	6.15 A, 2.3% THD	6.09 A, 2.4% THD	5.97 A, 3.1% THD

tion results are validated through experimental results on prototype SAPF developed in the laboratory. Table 3.1 shows the comparative analysis of performance of three conventional control algorithms in presence of non-linear load. The non-linear load considered has high THD in current i.e. 22.5%, which has been reduced to 2.3%, 2.4% and 3.1% on the supply side using SAPF implemented with SRFT, PBT and IRPT respectively. The THD of the supply voltage is almost same in all three cases, and is around 4.5%. The hardware results with all three algorithms implemented on the SAPF system regulate the supply current THD to less than 5%. It has been observed that SRFT control algorithm give the lowest THD of 2.3% in supply current. The successful implementation of conventional algorithms indicate that the developed prototype hardware can be used to test new and advanced control techniques on SAPF.

Chapter 4
POWER QUALITY IMPROVEMENT IN THREE PHASE THREE WIRE DISTRIBUTION SYSTEM

4.0 INTRODUCTION

In this chapter PQ problems in TPTW distribution system are discussed in detail. Linear as well as nonlinear loads are considered for analysis of PQ issues in distribution system. Many advanced control techniques are developed for control of SAPF for mitigation of PQ problems under varying load conditions. These techniques are simulated in a MATLAB/SIMULINK environment and experimentally validated.

4.1 POWER QUALITY ISSUES IN TPTW DISTRIBUTION SYSTEM

TPTW distribution systems are prone to many PQ problems such as unbalanced load, poor PF, harmonics injection, reactive power demand etc. Persistence of such PQ problems affects the distribution system and reduces the life of various electrical equipment. PQ problems over a prolonged period may even damage the equipment and which could result in financial loss or even could lead to human loss in some cases.

Power distribution system is a large, complicated networks comprising of dynamic loads. It is a major challenge for power engineers to equally distribute the load under all loading conditions. Proper shunt compensation can be a feasible solution to tackle load unbalancing. Moreover, the connected load in distribution system in largely resistive-inductive type has a PF less than unity. In some cases, when the load is highly inductive, poor PF causes lower active power transfer as compared to power transfer at nearly UPF. Also lower value of PF increases reactive power burden on the distribution transformer and transmission feeder. Shunt compensation is extensively used to maintain PF of supply current close to unity.

There are varieties of loads connected in distribution system such as EAF, electric arc welding, high power LED lights etc. These are nonlinear loads and introduce harmonics in

the distribution system. Compensation devices are provided for PQ improvement for this type of loads. The reactive power demand of load is provided locally so as to reduce the burden on the grid. Mitigation of PQ problems is essential for smooth operation of distribution system. Suitable mitigation techniques and control algorithms are developed for real time implementation and study of their impact for PQ of the distribution system is performed.

4.2 DEVELOPMENT AND ANALYSIS OF MODERN CONTROL ALGORITHMS IN TPTW DISTRIBUTION SYSTEM

In this section Notch Filter (NF), Kalman LMS and Hopfield NN based control techniques are developed for SAPF control and tested in linear as well as non-linear loads conditions. Various aspects of PQ problems are analyzed using these control techniques. The details of control techniques being developed are presented in this section.

4.2.1 Extraction of Fundamental Active Power Components

The extraction of average fundamental active power component of load current (I_{avg}) using different advance control algorithms are described below.

4.2.1.1 Notch Filter Based Control Algorithm

Notch filter is a special type of filter which is tuned to a particular frequency and estimates the magnitude of tuned frequency component [162]. It allows only a particular frequency component signal to pass and block all other frequency component signal. This NF can be used to extract fundamental frequency (50 Hz) component of supply system and thus it is used in controlling SAPF for PQ improvement in TPTW distribution system having linear and non-linear loads. Fig. 4.1 shows the NF block. It is used to calculate in-phase (α-component) and quadrature phase (β-component) component of the given signal. The NF overall transfer function is given by

$$N(s) = \frac{s^2 + \phi^2}{s^2 + 2\varepsilon\phi s + \phi^2} \tag{4.1}$$

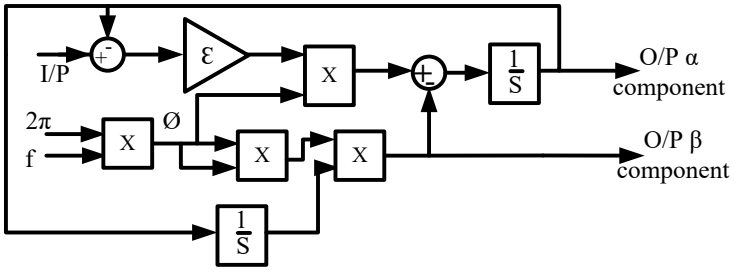

Fig. 4.1 Notch Filter block

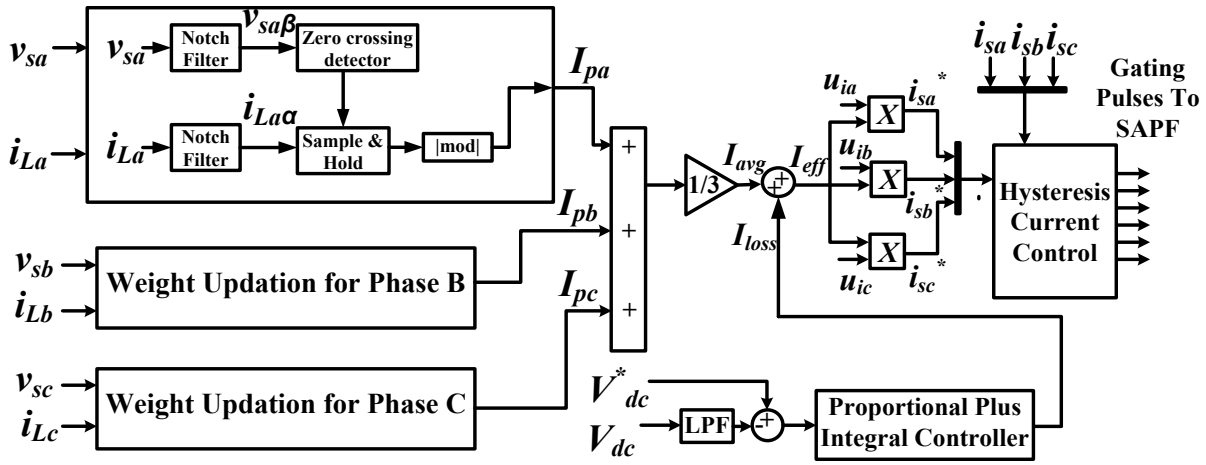

Fig. 4.2 Block diagram of Notch Filter based control algorithm implementation

where ϕ is phase angle of input signal, ε is damping constant of system,

The damping constant 'ε' is selected using following Equations.

$$Q = \frac{1}{2 * \varepsilon} \tag{4.2}$$

$$T_{st} = -\frac{\ln(\vartheta)}{\varepsilon * \omega_n} \tag{4.3}$$

where Q is quality factor of N(s), T_{st} is settling time of NF output, ϑ is the tolerance fraction chosen as 2%, ω_n is natural frequency of oscillation. Eqs. (4.2-4.3) show that for high quality factor, the value of ε must be small, but at the same time small ε results in larger settling time, so value of ε is selected keeping in mind both the constraints. The selected value of ε is 0.45.

Fig. 4.2 shows a block diagram of control technique using NF. Two NFs are used for each phase. The first NF is operated on voltage to obtain β-component of supply voltage '$v_{sa\beta}$' and

second NF is used to extract α-component of load current '$i_{La\alpha}$'. Sample and hold circuit along with zero order hold circuits are used to calculate fundamental active power component 'I_{pa}' of phase 'a' load current. Similar technique is used to calculate phase 'b' and phase 'c' fundamental active power component 'I_{pb}', 'I_{pc}' respectively. Now all the three fundamental active power components (I_{pa}, I_{pb}, I_{pc}) are averaged so as to obtain I_{avg}.

$$I_{avg} = \frac{I_{pa} + I_{pb} + I_{pc}}{3} \tag{4.4}$$

This average active power component 'I_{avg}' is used further for calculation of magnitude of reference currents for SAPF and discussed in section 4.2.2.

4.2.1.2 Kalman Least Mean Square Control Algorithm

Kalman Filter (KF) is a method to estimate the parameters of unknown system iteratively. It consists of set of equations which are updated at each instance. These equations include statistical noise and inaccuracies [28-29]. KF in an iterative process so unknown system parameters are identified iteratively and more precisely as compared to non-iterative

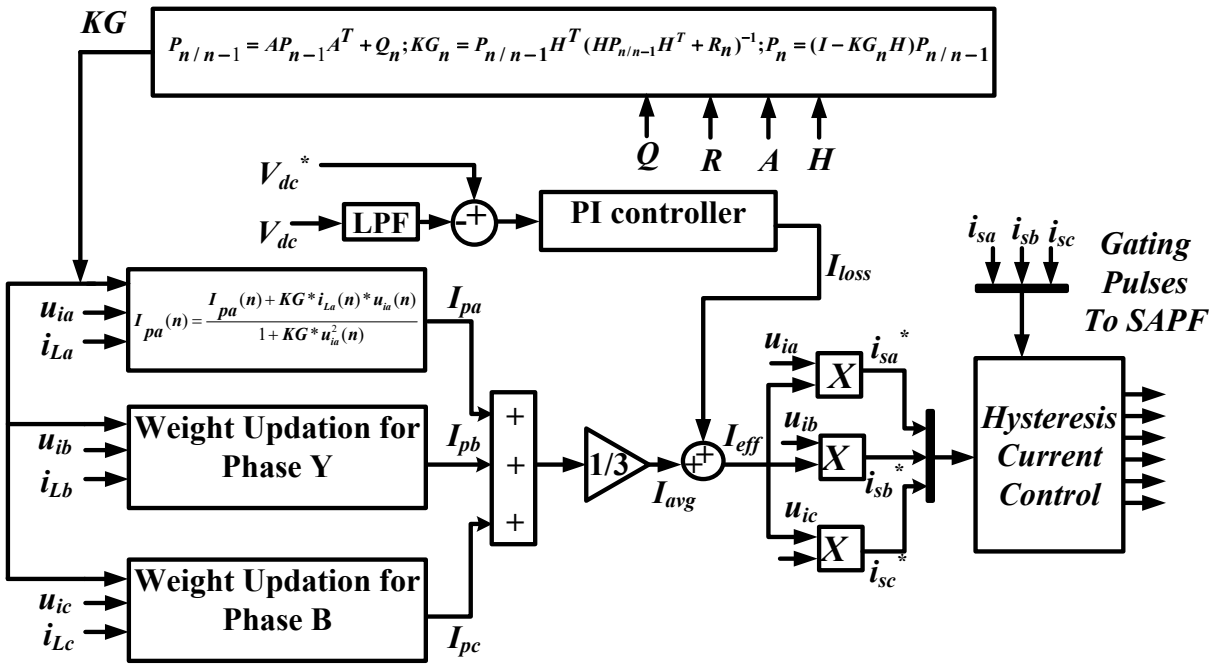

Fig. 4.3 Block diagram of Kalman-LMS based control algorithm implementation

methods. The Least Mean Square (LMS) algorithms are popular in control of SAPF. It suffers majorly from parameter dependent problems. A basic LMS equation is described by

$$W(n) = W(n-1) + G\xi \sin(\theta) \tag{4.5}$$

Where *W(n)* and *W(n-1)* are the final and previous state weight. G is learning rate of LMS technique and 'ξ' is error between actual and estimated signal. The learning rate must be chosen wisely for fast convergence of the control algorithm, A KF is used in conjunction with LMS technique, and the Kalman Gain (KG) is used as learning rate for LMS technique for proper operation of SAPF.

Fig. 4.3 presents KF based control algorithm block diagram for SAPF. First KG is calculated using the standard KF approach. Following state space equations represent the basic equations in KF:

$$X_n = AX_{n-1} + J_n \tag{4.6}$$

$$Y_n = HX_{n-1} + L_n \tag{4.7}$$

where, X_n = state vector (Nx1), A= system matrix (NxN), J = process noise vector (Nx1), Y_n = measurement vector (Mx1), H = constant matrix (Mx1), L = measurement noise vector (Mx1).

The KG is computed using the following equations

$$P_{n/n-1} = AP_{n-1}A^T + Q_n \tag{4.8}$$

$$KG_n = P_{n/n-1}H^T(HP_{n/n-1}H^T + R_n)^{-1} \tag{4.9}$$

$$P_n = (I - KG_nH)P_{n/n-1} \tag{4.10}$$

where $P_{n/n-1}$ = State covariance matrix, Q = Process Noise covariance, P = Final state covariance matrix, R= Measurement Noise Covariance and H = output Matrix.

Once the value of KG is computed, it is used in conventional LMS technique as learning rate

as shown in Fig. 4.3. The fundamental active power component of phase 'a' (I_{pa}) is calculated using LMS technique as follows

$$I_{pa}(n) = I_{pa}(n-1) + KG\xi u_{ia}(n) \tag{4.11}$$

where ξ error, and calculated as

$$\xi = i_{La}(n) - i_{La}^{*}(n) \tag{4.12}$$

where $i_{La}^{*}(n)$ is reference current for error calculation and given by

$$i_{La}^{*}(n) = I_{pa}(n) * KG * u_{ia}(n) \tag{4.13}$$

Eq. (4.10) is modified using Eq. (4.11) and (4.12)

$$I_{pa}(n) = I_{pa}(n-1) + KG\left\{i_{La}(n) - I_{pa}(n) * KG * u_{ia}(n)\right\} u_{ia}(n) \tag{4.14}$$

Further, I_{pa} is rewritten as

$$I_{pa}(n) = \frac{I_{pa}(n-1) + KG * i_{La}(n) u_{ia}(n)}{1 + KG * u_{ia}^{2}(n)} \tag{4.15}$$

Similarly phase 'b' and phase 'c' fundamental active power components 'I_{pb}', 'I_{pc}' are calculated and average of three components are determined

$$I_{avg} = \frac{I_{pa} + I_{pb} + I_{pc}}{3} \tag{4.16}$$

The average fundamental active power component (I_{avg}) used to calculate reference currents for SAPF and discussed in later sections.

4.2.1.3 Hopfield Neural Network Based Control Algorithm

Hopfield Neural Network (HNN) is a recurrent neural network [115], in which the outputs are updated iteratively based upon desired objective function. The objective function should be defined clearly so that convergence is achieved easily. The Hopfield Neural Network (HNN) is a network of '2n' neurons. It is a multiple loop feedback system consisting in-phase 'α' and quadrature 'β' components extraction block for fundamental and harmonic frequency

input signal. This HNN can also be tuned to particular frequency and it enables to extract harmonics from non-linear signals having multiple frequency components.

In general the non-linear load current can be expressed as

$$\boldsymbol{i_L(t)} = \sum_{\boldsymbol{m}=1}^{\boldsymbol{N}} \boldsymbol{I_m} \sin(\boldsymbol{m\omega t} + \theta_{\boldsymbol{m}}) \tag{4.17}$$

where I_m is peak magnitude of m^{th} harmonic component of load current and θ_m is the phase shift of m^{th} harmonic component of load current. The Eq. 4.22 can also be written as

$$\boldsymbol{i_L(t)} = \sum_{\boldsymbol{m}=1}^{\boldsymbol{N}} \alpha_{\boldsymbol{m}} \sin(\boldsymbol{m\omega t}) + \beta_{\boldsymbol{n}} \cos(\boldsymbol{m\omega t}) \tag{4.18}$$

where α_m and β_m are the in-phase and quadrature components.

The objective function for HNN technique Γ(na) is developed using the error between actual (i_{La}) and estimated load current (i_{La}^*) as

$$\Gamma_a = 0.5\left[i_{La}^*(t) - i_{La}\right]^2 \tag{4.19}$$

From Eq. (4.17) and (4.19)

$$\Gamma_a = 0.5[\sum_{\boldsymbol{m}=1}^{\boldsymbol{N}} (\alpha_{\boldsymbol{am}} \sin(\boldsymbol{m\omega t}) + \beta_{\boldsymbol{am}} \cos(\boldsymbol{m\omega t})) - \boldsymbol{i_{La}}]^2 \tag{4.20}$$

Defining two matrix, A_{am} and B_{am} as

$A_{am} = [\alpha_{a1}\ \beta_{a1}\ \alpha_{a2}\ \beta_{a2}$ ..... $\alpha_{aN}\ \beta_{aN}]$ and

$B_{am} = [\sin(\omega t)\ \cos(\omega t)\ \sin(2\omega t)\ \cos(2\omega t)$ .....$\sin(N\omega t)\ \cos(N\omega t)]$

Eq. (4.19) is re-written for phase 'a' as

$$\Gamma_a = 0.5\left[\sum_{\boldsymbol{m}=1}^{\boldsymbol{N}} \boldsymbol{A_{am}} \boldsymbol{B_{am}^T} - \boldsymbol{i_{La}}\right]^2 \tag{4.21}$$

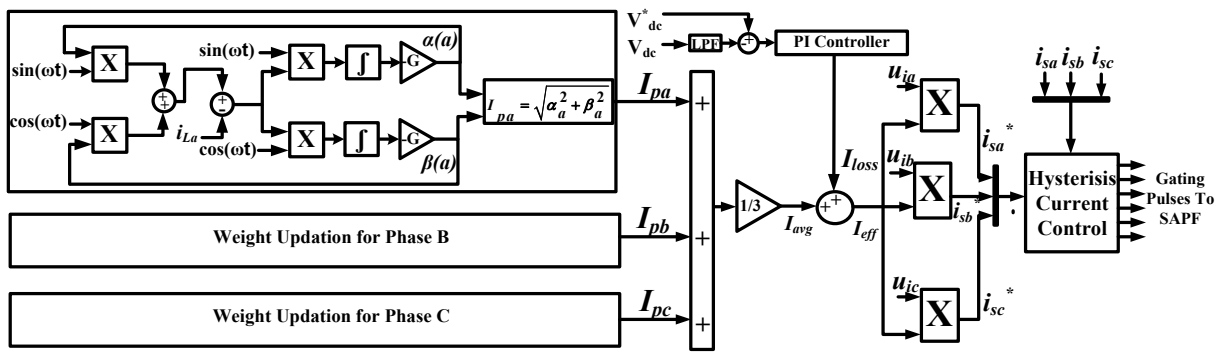

Fig. 4.4 Block diagram of Hopfield NN based control algorithm implementation

To obtain the minimum value of Γ_a,

$$\frac{d\Gamma_a}{dt} = 0 \tag{4.22}$$

and

$$\frac{\partial A_{am}}{\partial t} = -G\frac{\partial \Gamma_a}{\partial A_{am}} \tag{4.23}$$

where G is a gain constant. Rewriting matrix A_{am} in terms of component gives,

$$\frac{\partial[\alpha_{a1}\beta_{a1}.....\alpha_{an}\beta_{an}]}{\partial t} = -K\frac{\partial \Gamma_a}{\partial A_{am}} \tag{4.24}$$

From Eq. (4.23), it can be written

$$\sum_{m=1}^{N}\frac{\partial \alpha_{am}}{\partial t} = -G\sum_{m=1}^{N}\frac{\partial \Gamma_a}{\partial \alpha_{am}} \tag{4.25}$$

$$\sum_{m=1}^{N}\frac{\partial \beta_{am}}{\partial t} = -G\sum_{m=1}^{N}\frac{\partial \Gamma_a}{\partial \beta_{am}} \tag{4.26}$$

The right hand side of Eq. (4.24) is calculated using Eq. (4.19)

$$-G\sum_{m=1}^{N}\frac{\partial \Gamma_a}{\partial \alpha_{am}} = -G\sum_{m=1}^{N}\{\alpha_{am}\sin(m\omega t) + \beta_{am}\cos(m\omega t) - i_{La}\}\sin(m\omega t) \tag{4.27}$$

And the right hand side of Eq. (4.25) is also calculated using Eq. (4.19)

$$-G\sum_{m=1}^{N}\frac{\partial \Gamma_a}{\partial \alpha_{am}} = -G\sum_{m=1}^{N}\{\alpha_{am}\sin(m\omega t) + \beta_{am}\cos(m\omega t) - i_{La}\}\cos(m\omega t) \tag{4.28}$$

So, α_{am} component of A_{am} is estimated from eq. (4.24) and (4.26) as

$$\frac{\partial \alpha_{am}}{\partial t} = -G\left[\{\alpha_{am}\sin(m\omega t) + \beta_{am}\cos(m\omega t) - i_{La}\}\sin(m\omega t)\right] \tag{4.29}$$

Hence, α_{am} is calculated using

$$\alpha_{am} = -G\int\{\alpha_{am}\sin(m\omega t) + \beta_{am}\cos(m\omega t) - i_{La}\}\sin(m\omega t)dt \tag{4.30}$$

Similarly β_{am} is calculated using

$$\beta_{am} = -G\int\{\alpha_{am}\sin(m\omega t) + \beta_{am}\cos(m\omega t) - i_{La}\}\cos(m\omega t)dt \tag{4.31}$$

Here α_{am} ,β_{am} are the weighted components of the m^{th} harmonic current.

The I_{pa} is obtained from Eq. (4.30) and (4.31) by putting m=1 and calculating α_a, β_a and given by

$$I_{pa} = \sqrt{\alpha_a^2 + \beta_a^2} \tag{4.32}$$

Similarly 'I_{pb}' and 'I_{pc}'for phase 'b' and phase 'c' are determined and averaged. The average fundamental active power component I_{avg} is given as:

$$I_{avg} = \frac{I_{pa} + I_{pb} + I_{pc}}{3} \tag{4.33}$$

4.2.2 Generation of Reference Currents for Control of SAPF

As discussed in Section 3.8.1, the switching losses in the IGBT switches of SAPF can be determined using the Eq. (3.12), (3.13) as:

$$I_{loss}(k) = I_{loss}(k-1) + K_p\{(e_{dc}(k) - e_{dc}(k-1)\} + K_I[e_{dc}(k)] \tag{3.12}$$

where $e_{dc}(k) = V_{dc}^{*}(k) - V_{dc}(k)$ (3.13)

Now the switching loss component I_{loss} is added to average fundamental active power component (I_{avg}) to get effective active power component I_{eff}

$$I_{eff} = I_{avg} + I_{loss} \tag{4.34}$$

The unit templates are necessary for reference current generation. Unit templates ensure generation of in phase reference currents. As discussed in chapter 3, in phase unit templates are calculated using following Eq.

$$u_{ia} = \frac{v_{sa}}{V_t}; u_{ib} = \frac{v_{sb}}{V_t}; u_{ic} = \frac{v_{sc}}{V_t} \tag{3.18}$$

where v_{sa}, v_{sb}, v_{sc} are three phase supply phase voltages, and peak value of supply phase voltage (V_t) is the calculated using

$$V_t = \sqrt{\frac{2}{3}(v_{sa}^2 + v_{sb}^2 + v_{sc}^2)} \tag{3.19}$$

Finally I_{eff} is multiplied by unit templates u_{ia}, u_{ib}, u_{ic} to obtain reference currents i_{sa}^{*}, i_{sb}^{*}, i_{sc}^{*}.

$$i_{sa}^{*} = u_{ia} * I_{eff}; i_{sb}^{*} = u_{ib} * I_{eff}; i_{sc}^{*} = u_{ic} * I_{eff} \tag{4.35}$$

These reference currents and actual supply currents (i_{sa}, i_{sb}, i_{sc}) are compared using HCC block and six gating pulses are generated for proper operation of SAPF. The reference currents generated are in phase with the grid supply, sinusoidal and magnitude is proportional to active power demand by load.

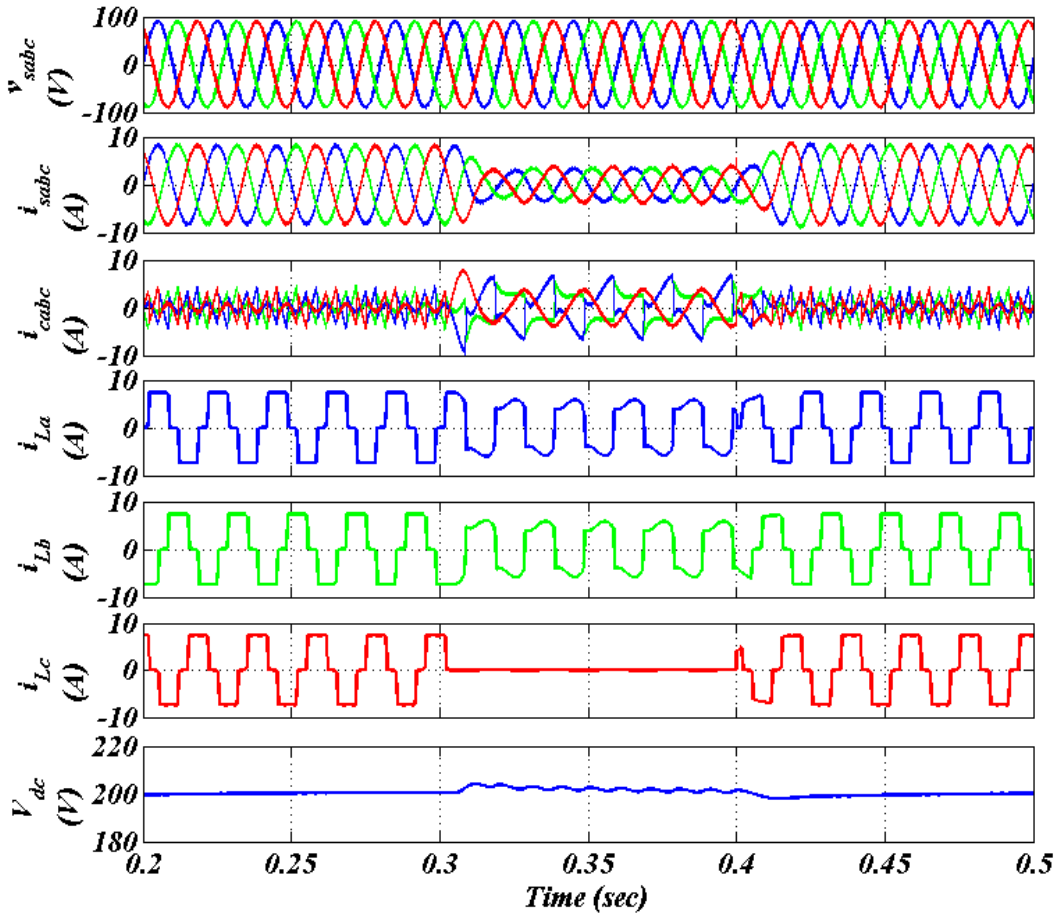

Fig. 4.5 Simulation results using Notch Filter based control algorithm for non-linear load.

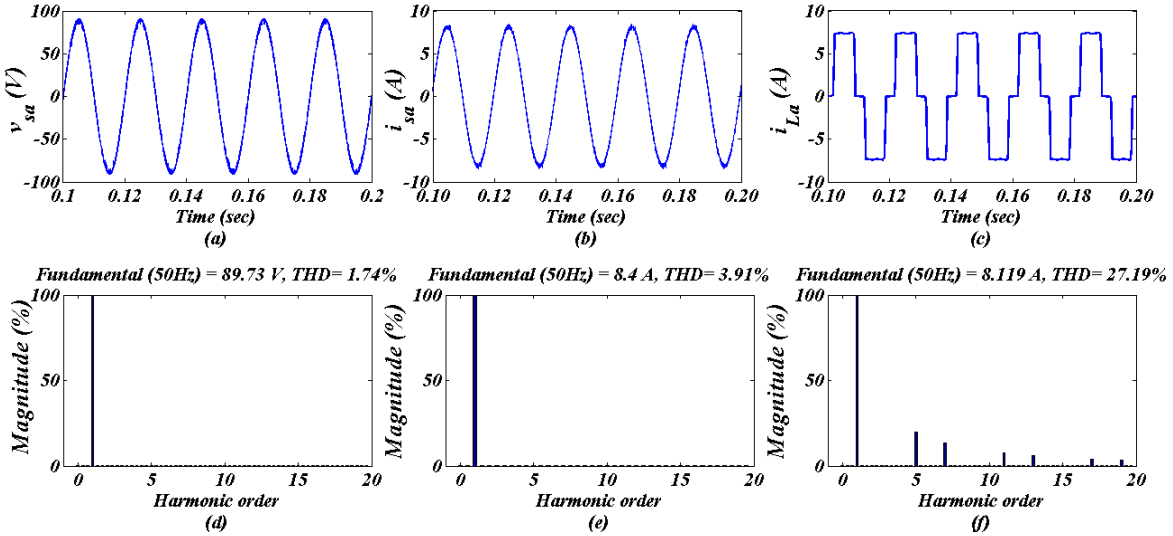

Fig. 4.6 Harmonic analysis using Notch Filter based control algorithm (a-c) waveforms of v_{sa}, i_{sa}, i_{La} (d-f) THD of v_{sa}, i_{sa}, i_{La} for non-linear load

4.3 SIMULATIONS RESULTS

Modeling and simulation of SAPF using NF, Kalman-LMS and Hopfield NN control technique was carried out and TPTW distribution system was discussed. The simulation results with linear and non-linear loads are considered in the present analysis.

4.3.1 Notch Filter Based Control Algorithm

A NF based control scheme for SAPF in TPTW distribution system was simulated in MATLAB/SIMULINK and simulation results are described in this section. Fig 4.5 shows the waveforms of three phase supply voltages (v_{sa}, v_{sb}, v_{sc}), three phase supply currents (i_{sa}, i_{sb}, i_{sc}), three phase non-sinusoidal load currents (i_{La}, i_{Lb}, i_{Lc}), three phase compensating currents (i_{ca}, i_{cb}, i_{cc}) and DC link voltage (V_{dc}) of SAPF with non-linear loads. The load currents have harmonic components. At t=0.3 sec, phase 'c' is suddenly discontinued till t=0.4 sec. The phase 'c' load current is absent during this time interval. However, SAPF provides necessary compensation and supply currents have become sinusoidal and balanced. The DC link voltage has slight fluctuations around set value of 200 V. The SAPF operation is critical for injecting proper compensating currents with appropriate phase and magnitude to be injected through interfacing inductors.

Figs. 4.6(a)-(c) show waveforms and Figs. 4.6(d)-(f) show harmonic content of phase 'a' supply voltage (v_{sa}), phase 'a' supply current (i_{sa}) and phase 'a' load current (i_{La}) respectively. The load current has a THD of 27.19%, however, the supply current (i_{sa}) has a low THD of 3.91%. The grid supply almost sinusoidal supply with acceptable THD of 1.74%. The supply current and voltage have low THD and it satisfies the standard prescribed in IEEE 519 [40].

Fig 4.7 shows three phase supply voltages (v_{sabc}), three phase supply currents (i_{sabc}), three phase compensating currents (i_{ca}, i_{cb}, i_{cc}), three phase lagging load currents (i_{La}, i_{Lb}, i_{Lc}) and DC link voltage (V_{dc}) of SAPF in the case of linear load. The load considered is three phase delta connected load with real and reactive power demand of 2000 W and 550 VARs. The

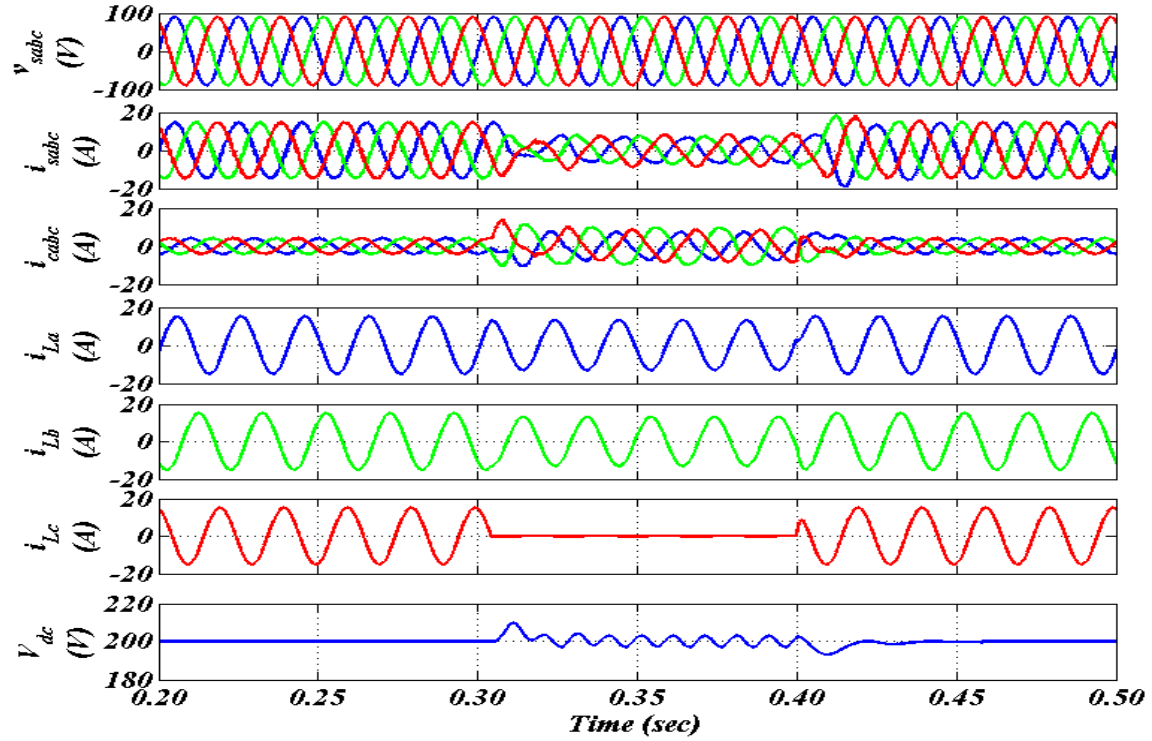

Fig. 4.7 Simulation results using Notch Filter based control algorithm for linear load.

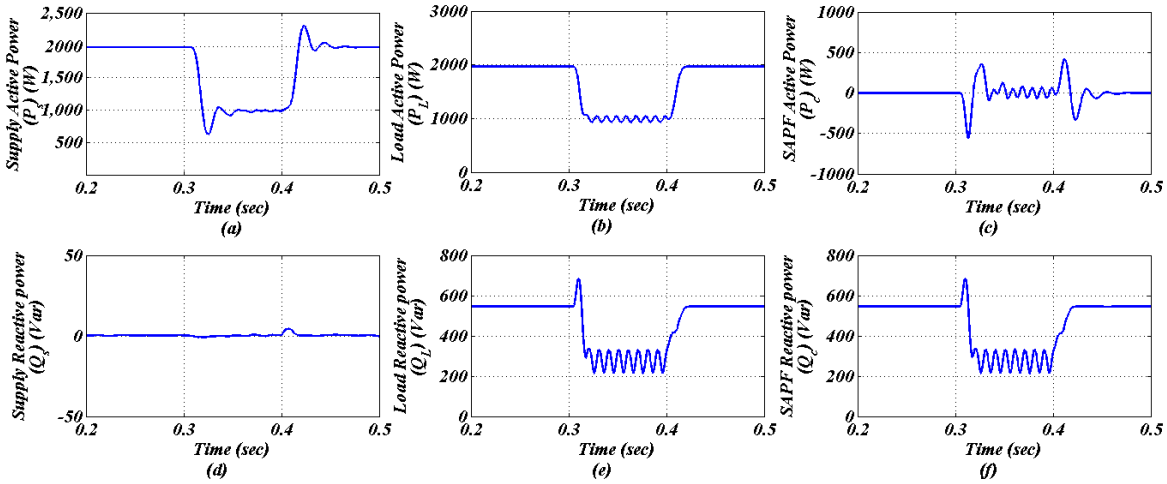

Fig. 4.8 Power flow in TPTW distribution system using Notch Filter based control algorithm (a-c) Active power P_s, P_L, P_c (d-f) Reactive Power Q_s, Q_L, Q_c for linear load

load is inductive in nature and load current lags w.r.t. the supply voltages. An unbalancing at t=0.3 is introduced by sudden removal of phase 'c' till t=0.4 sec. The supply currents are balanced and in-phase with the supply voltages in this load unbalancing condition, which demonstrates the effectiveness of control technique of SAPF with linear and unbalanced loads. The DC link is regulated and has minor fluctuations only during load unbalancing. The compensating currents are adequate in phase and magnitude to provide necessary compensation at PCC by the SAPF. Figs. 4.8(a)-(f) show the power balance waveforms

between supply, load and compensator side respectively. The load side has a demand of 2000 W active power and 550 VAR of reactive power under steady state. The active power is supplied by AC supply and SAPF compensator provides total reactive power. The real power consumed by compensator is zero and the reactive power drawn from supply is nearly zero. This power balance is valid when load is unbalanced during time t=0.3 sec to t=0.4 sec also.

4.3.2 Kalman Least Mean Square Control Algorithm

Kalman LMS control algorithm is implemented for SAPF supported TPTW distribution system. A 110 V, 50 Hz distribution system with nonlinear load and SAPF is considered for present analysis. Fig 4.9 shows the waveforms of three phase supply voltages (v_{sa}, v_{sb}, v_{sc}), three phase supply currents (i_{sa}, i_{sb}, i_{sc}), three phase compensating currents (i_{ca}, i_{cb}, i_{cc}), three phase non-sinusoidal load currents (i_{La}, i_{Lb}, i_{Lc}) and DC link voltage (V_{dc}) of SAPF in the case of non-linear loads. The nonlinearity present in the load is due to three phase diode bridge rectifier connected at the load end. The Kalman LMS algorithm provides needed compensation through SAPF. The supply currents are sinusoidal and in-phase with the supply voltages and reactive power demand of load is supported by SAPF. The TPTW system is also subjected load unbalancing by sudden removal of load in phase 'c' at t=0.3 sec till t=0.4 sec. The Kalman LMS control algorithm generates adequate reference currents to enable through PI controller at voltage level of 200 V. Figs. 4.10(a)-(c) show waveforms and Figs. 4.10(d)-(f) show harmonic spectra of phase 'a' supply voltage (v_{sa}), phase 'a' supply current (i_{sa}) and phase 'a' load current (i_{La}) respectively. The PCC voltage has a THD of 1.74%. The non-sinusoidal load current has a high THD of 27.19%. However, the SAPF is able to inject needed compensation to the supply current. The phase 'a' AC supply current has THD of 3.08%. The voltage and current satisfies the THD level as provided in IEEE 519 [40]. Fig 4.11 presents the waveforms of three phase supply voltages (v_{sa}, v_{sb}, v_{sc}), three phase supply currents (i_{sa}, i_b, i_{sc}), three phase compensating currents (i_{ca}, i_{cb}, i_{cc}), three phase lagging PF

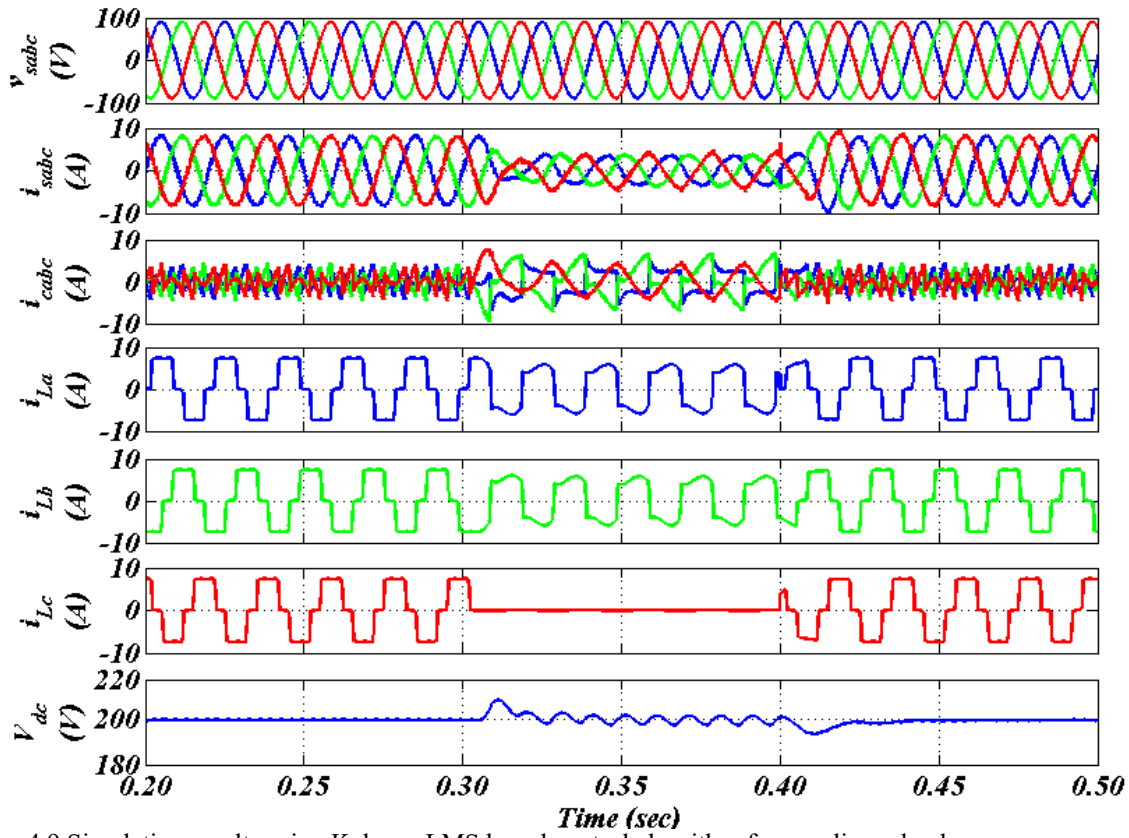

Fig. 4.9 Simulation results using Kalman-LMS based control algorithm for non-linear load.

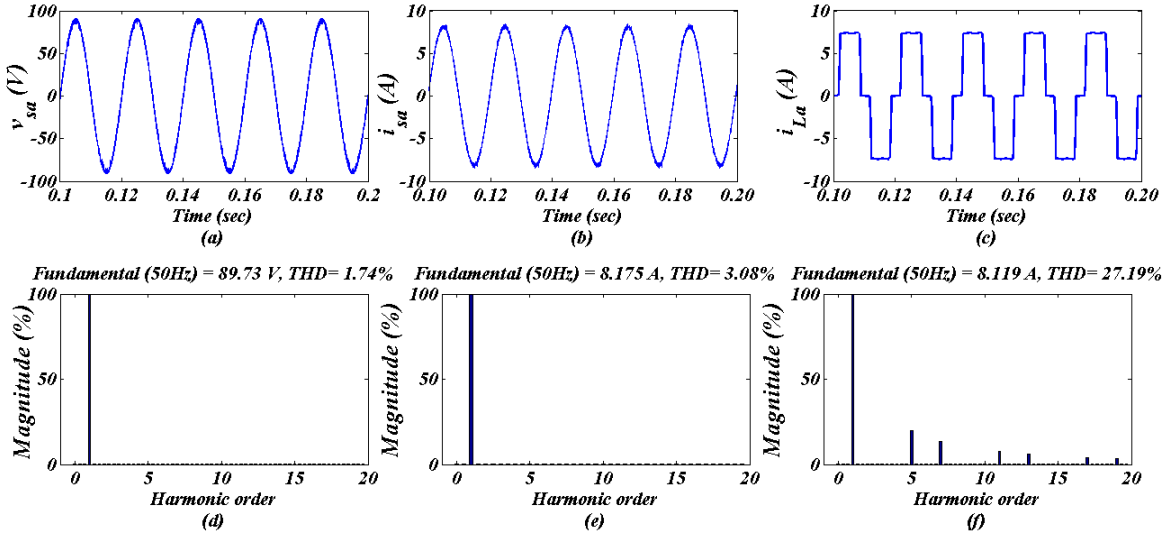

Fig. 4.10 Harmonic analysis using Kalman-LMS based control algorithm (a-c) waveforms of v_{sa}, i_{sa}, i_{La} (d-f) THD of v_{sa}, i_{sa}, i_{La} for non-linear load

load currents (i_{La}, i_{Lb}, i_{Lc}) and DC link voltage (V_{dc}) of SAPF with linear load. A linear load with 2 kW active power and 550 VARs reactive power demand is connected as load in TPTW distribution system. Since the load is lagging in nature so the reference currents generated are leading the load currents. The reference currents are also in-phase with the grid

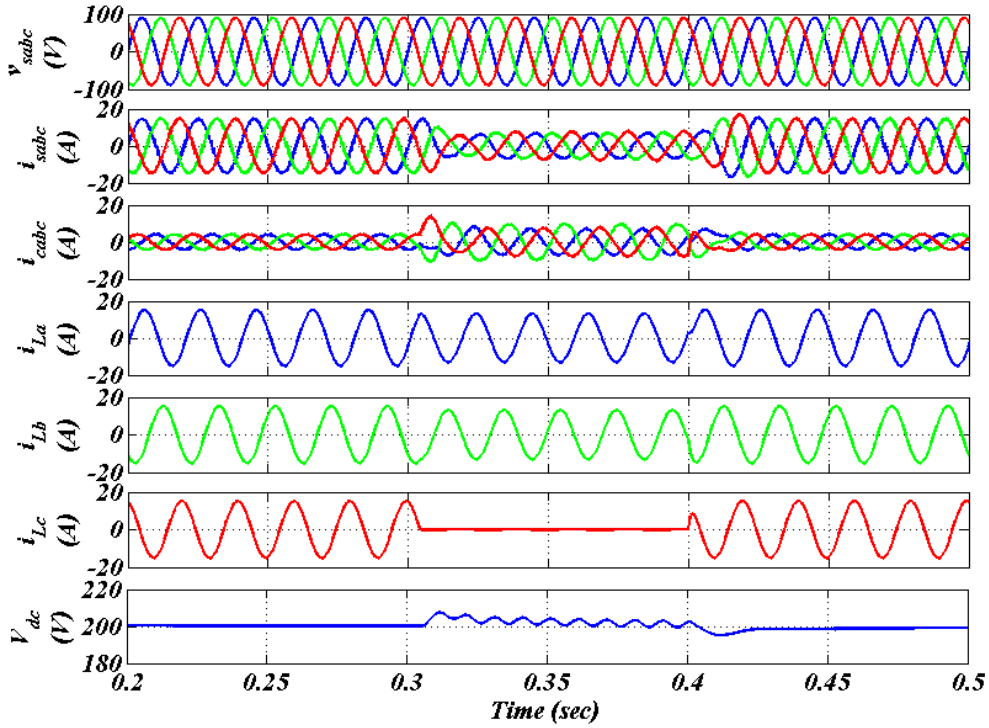

Fig. 4.11 Simulation results using Kalman-LMS based control algorithm for linear load.

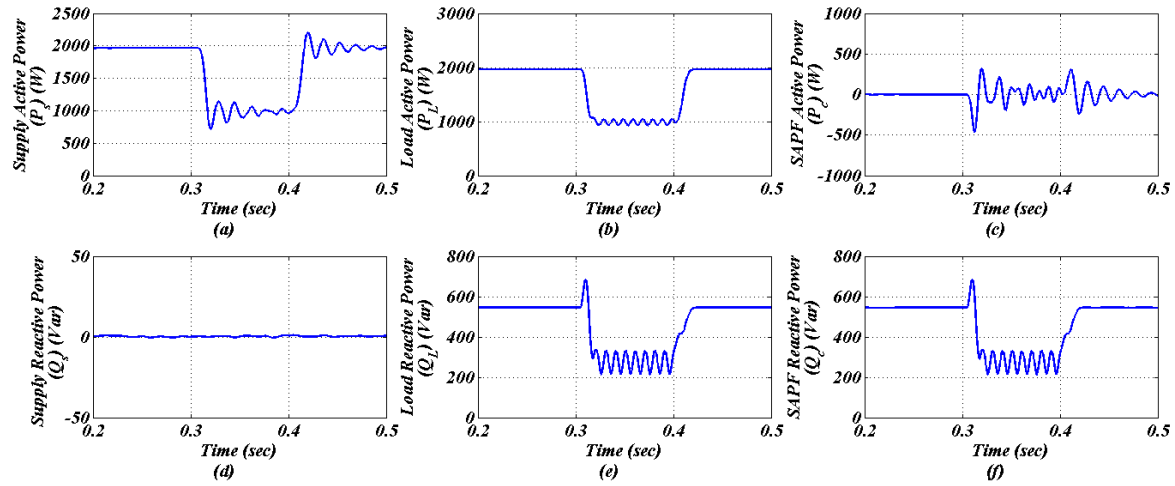

Fig. 4.12 Power flow in TPTW distribution system using Kalman-LMS based control algorithm (a-c) Active power P_s, P_L, P_c (d-f) Reactive Power Q_s, Q_L, Q_c for linear load

voltages. A load unbalancing is introduced from t=0.3 to t=0.4 sec by sudden removal of phase 'c' of three phase supply. The supply currents are balanced and in-phase with the respective grid voltages. The DC link has small fluctuations during unbalanced load condition. The compensating currents generated by SAPF using Kalman LMS control technique improve PQ of the TPTW grid. Figs. 4.12(a)-(f) present the power flow between supply, load and SAPF respectively in TPTW system. The three phase linear load demands 2000 W active power and 550 VARs of reactive power under steady state. The AC supply

delivers the real power demand of 2000 W and also losses of SAPF. Whereas the SAPF supplies only reactive power burden of the load. The SAPF real power losses are small, and supplied by the grid. From time t=0.3 sec to 0.4 sec, when unbalanced load is connected to the supply, SAPF feed the necessary reactive power demand to keep source current balanced.

4.3.3 Hopfield Neural Network Based Control Algorithm

In this Section, simulation results using Hopfield NN control technique are discussed. The operation of SAPF in a three phase 110 V, 50 Hz distribution system feeding non-linear load is demonstrated. Fig 4.13 show the three phase supply voltages (v_{sabc}), three phase supply currents (i_{sabc}), three phase compensating currents (i_{ca}, i_{cb}, i_{cc}), three phase load currents (i_{La}, i_{Lb}, i_{Lc}) and DC link voltage (V_{dc}) of SAPF with non-linear load. The grid supply is balanced and sinusoidal voltage. The supply currents with SAPF compensation are also observed in-phase and distortion free. The Hopfield NN based SAPF control is effective in generating appropriate gating pulses for SAPF and improving PQ problems. The load currents are non-sinusoidal due to nonlinear load. The unbalancing in phase 'c' is introduced by sudden removal of phase 'c' supply voltage at t=0.3 sec. The DC link voltage is effectively regulated through PI controller at voltage level of 200 V. Figs. 4.14(a)-(c) show the waveforms of phase 'a' supply voltage (v_{sa}), phase 'a' supply current (i_{sa}) and phase 'a' load current (i_{La}) and Figs. 4.14(d)-(f) show their harmonic spectra in presence of SAPF compensation. The supply voltage, supply current and load current have a THD of 1.74%, 4.05 and 27.19% respectively. The voltage and current THD are within the limit prescribed in harmonic standard IEEE 519 [40].

Fig 4.15 show three phase supply voltages (v_{sabc}), three phase supply currents (i_{sabc}), three phase compensating currents (i_{cabc}), three phase load currents (i_{Labc}) and DC link voltage (V_{dc}) of SAPF in the case of linear load. The load is inductive in nature and demands reactive power of 550 VARs. The supply currents and voltage are observed to be in-phase and SAPF

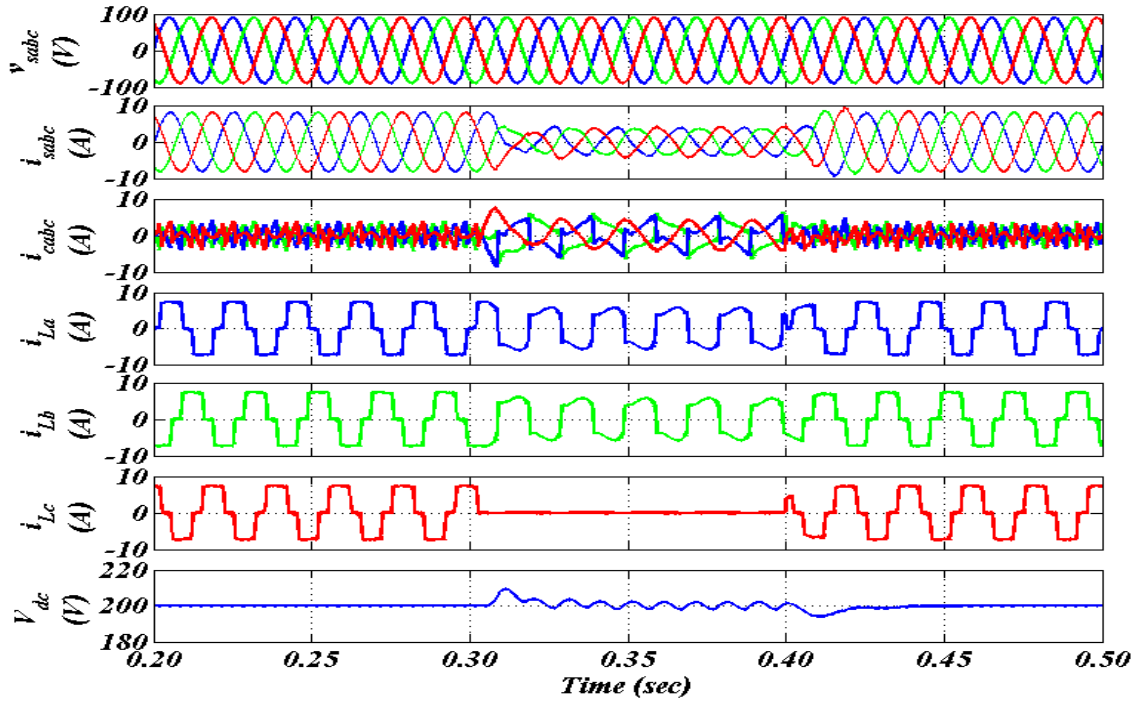

Fig. 4.13 Simulation results using Hopfield NN based control algorithm for non-linear load.

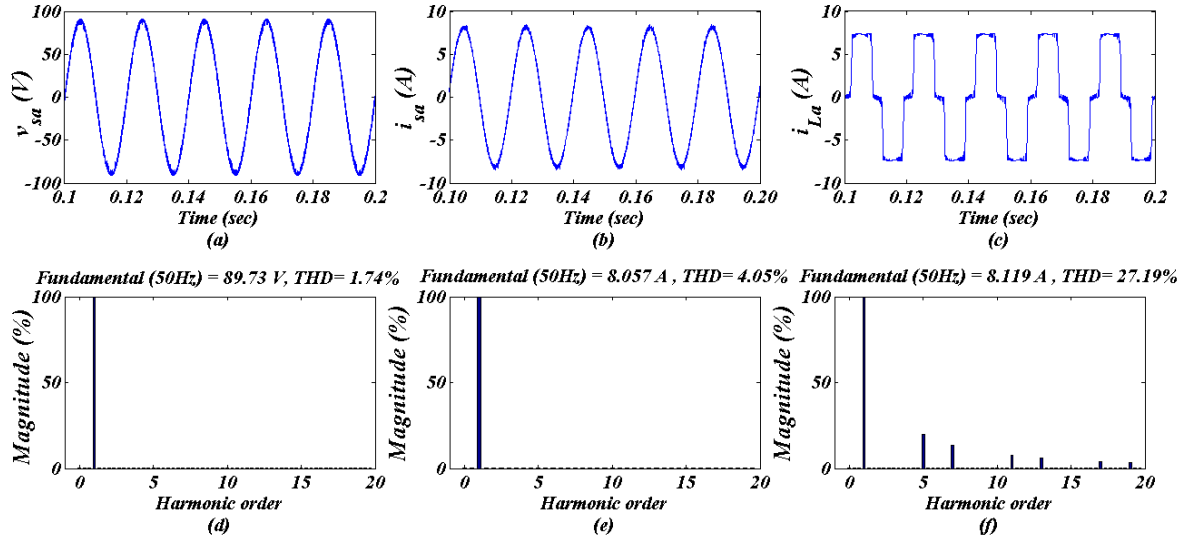

Fig. 4.14 Harmonic analysis using Hopfield NN based control algorithm (a-c) waveforms of v_{sa}, i_{sa}, i_{La} (d-f) THD of v_{sa}, i_{sa}, i_{La} for non-linear load

operates satisfactorily and provide required compensation. Figs. 4.16(a)-(f) show supply active power (P_s), reactive power (Q_s), load active power (P_L), reactive power (Q_L) demand and compensator active power (P_c), reactive power (Q_c) requirements. The supply active power includes the load active power demand and SAPF switching loss demand. The reactive power given by compensator meets the load reactive power demand. The reactive power burden on the grid side is reduced and the PF of TPTW distribution system is improved on

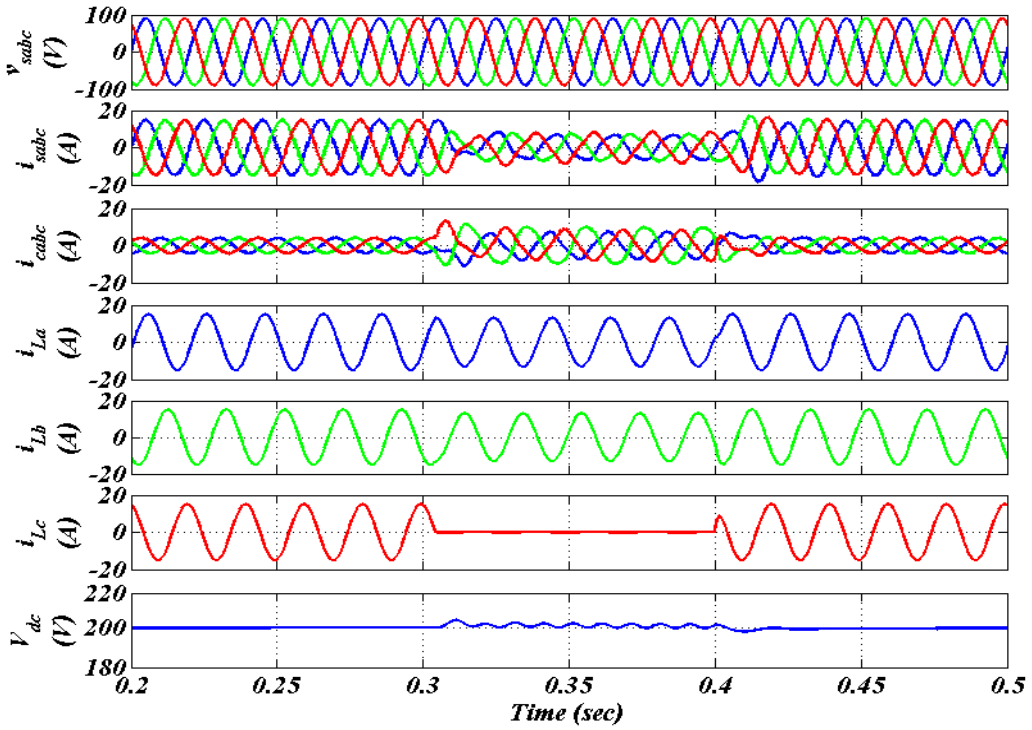

Fig. 4.15 Simulation results using Hopfield NN based control algorithm for linear load.

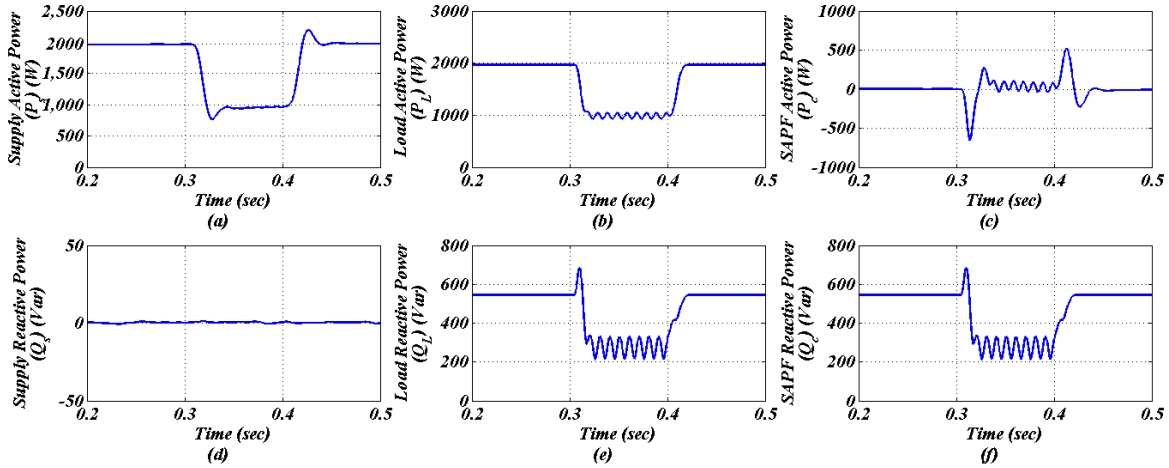

Fig. 4.16 Power flow in TPTW distribution system using Hopfield NN based control algorithm (a-c) Active power P_s, P_L, P_c (d-f) Reactive Power Q_s, Q_L, Q_c for linear load

the supply side.

4.4 EXPERIMENTAL RESULTS

A prototype hardware was developed to test the effectiveness of NF, Kalman LMS and Hopfield NN algorithms for the control of SAPF in TPTW distribution system. The dSPACE 1104 controller board is used as DSP, which provides necessary gating signals to SAPF as per the developed control algorithm. The experimental results for all the three algorithms to SAPF are discussed in this section.

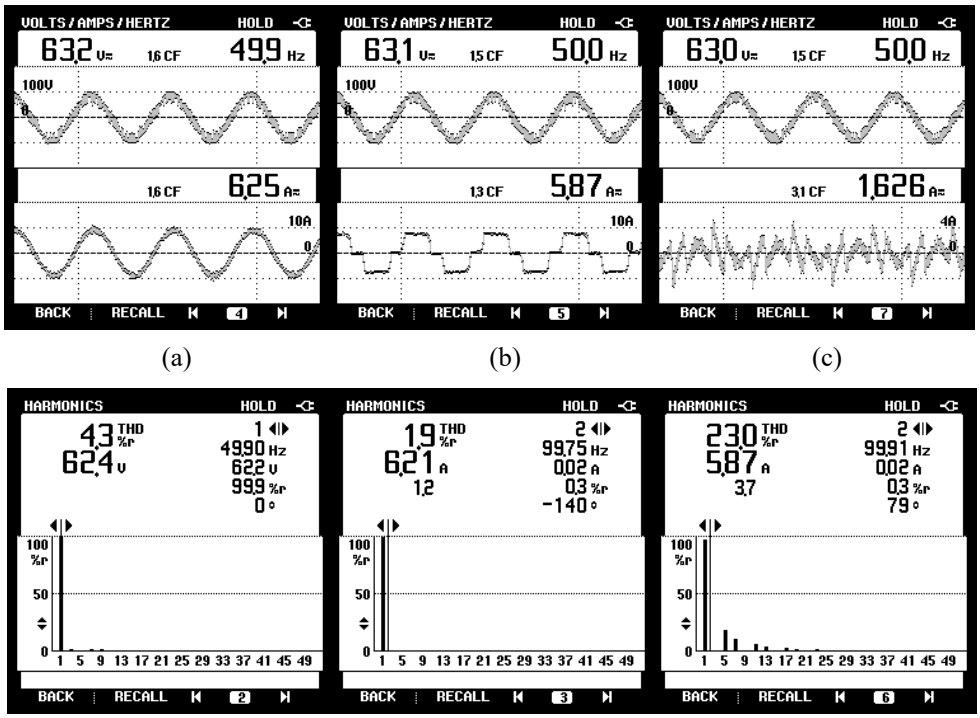

Fig. 4.17 Steady state waveforms for TPTW distribution system using Notch Filter based control algorithm (a) v_{sa}-i_{sa} (b) v_{sa}-i_{La} (c) v_{sa}-i_{ca} and (d-f) THD of (d) v_{sa} (e) i_{sa} (f) i_{La} for non-linear load

4.4.1 Notch Filter Based Control Algorithm

A NF based control scheme for extraction of load current average fundamental active power component (I_{avg}) was implemented on the hardware setup of 110 V, 50 Hz, three phase distribution system feeding non-linear load. Fig. 4.17 shows the steady state performance of SAPF with non-linear load. Figs. 4.17(a)-(c) show phase 'a' supply current (i_{sa}), phase 'a' load current (i_{La}) and phase 'a' compensator current (i_{ca}) along with phase 'a' supply voltage (v_{sa}). The supply current and supply voltage is observed to be in phase. Figs. 4.17(d)-(f) show THD analysis of the system. Figs. 4.17(d)-(f) show THD of phase 'a' supply voltage (v_{sa}), phase 'a' supply current (i_{sa}) and phase 'a' load current (i_{La}) respectively. The load current has a THD of 23.0% due to non-linear load. However, the NF scheme is able to extract fundamental active power component of load current and control SAPF to provide necessary compensation. The supply current THD is reduced to 1.90% and supply voltage has THD of 4.3%. Fig. 4.18, Fig. 4.19 shows the dynamic performance of SAPF for non-

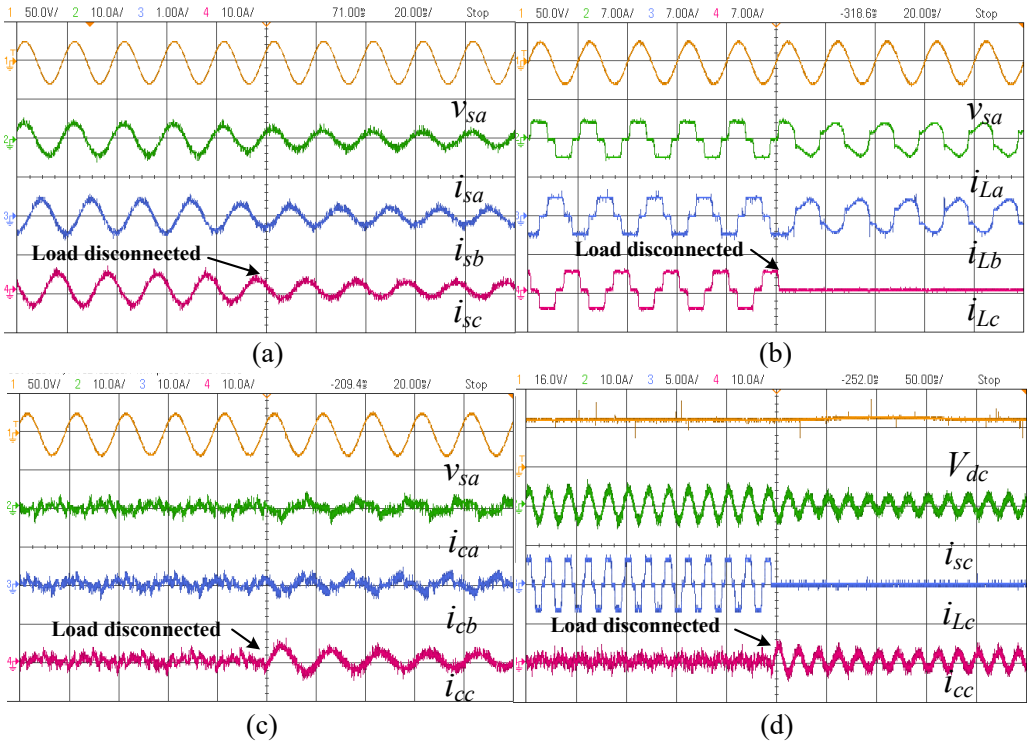

Fig. 4.18 Results showing dynamics for load disconnected in phase 'c' using Notch Filter based control algorithm (a) v_{sa}, i_{sa}, i_{sb}, i_{sc} (b) v_{sa}, i_{La}, i_{Lb}, i_{Lc} (c) v_{sa}, i_{ca}, i_{cb}, i_{cc} (d) V_{dc}, i_{sc}, i_{Lc}, i_{cc} for nonlinear load

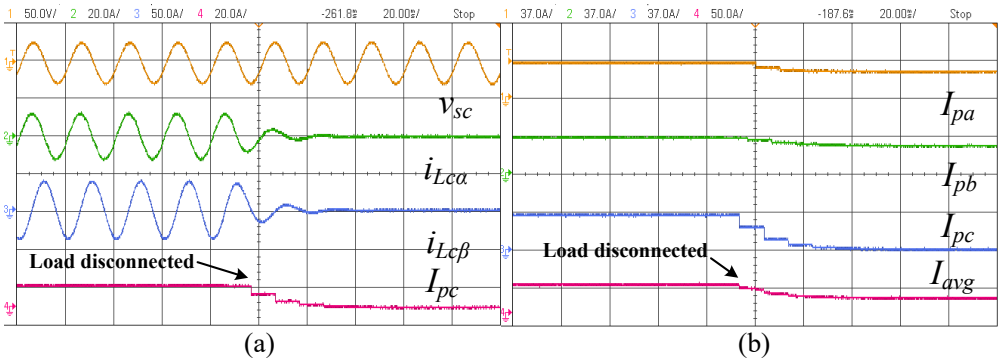

Fig. 4.19 Intermediate results using Notch Filter based control algorithm (a) v_{sc}, i_{Lca}, $i_{Lc\beta}$, I_{pc} (b) I_{pa}, I_{pb}, I_{pc}, I_{avg} for non-linear load

linear load. Fig. 4.18(a) shows phase 'a' supply voltage (v_{sa}) and SAPF compensated supply currents (i_{sa}, i_{sb}, i_{sc}). The supply currents are balanced and sinusoidal. The dynamic change introduced is disconnection of phase 'c' load. Fig. 4.18(b) shows phase 'a' supply voltage (v_{sa}) and non-sinusoidal load currents (i_{La}, i_{Lb}, i_{Lc}). Fig. 4.18(c) shows phase 'a' supply voltage (v_{sa}) and SAPF injected compensator currents (i_{ca}, i_{cb}, i_{cc}). The compensator currents are computed accurately by using developed control algorithm so as to make supply currents sinusoidal, balanced and distortion free. Fig. 4.18(d) shows DC link voltage (V_{dc}) and phase

'c' supply, load and compensator currents (i_{sc}, i_{Lc}, i_{cc}). The DC link is maintained at the level of 200 V through PI controller at DC link.

Fig. 4.19 shows the intermediate signals obtained in NF control technique for SAPF. Fig 4.19 (a) shows phase 'c' supply voltage (v_{sc}), alpha and beta component of phase 'c' load currents ($i_{Lc\alpha}$, $i_{Lc\beta}$) and fundamental active power component of phase 'c' (I_{pc}). The phase 'c' fundamental active power component is tracked continuously to generate proper reference currents for SAPF. Fig 4.19(b) shows fundamental active power components (I_{pa}, I_{pb}, I_{pc}) of phase 'a', 'b' and 'c' and average active power component (I_{avg}). The I_{avg} changed according to load change and is responsible for generation of suitable gating pulses.

Fig. 4.20 shows the steady state power in TPTW distribution system with SAPF using NF based control technique. Figs. 4.20(a)-(c) show supply, load and compensator steady state power along with PF. It is observed from Fig. 4.20 that the AC supply delivers all the active power requirement 700 W. The load active power demand is 630 W and SAPF losses are 70 W. The reference currents are generated which enables SAPF to feed reactive power burden of 190 VARs out of the load reactive power demand of 370 VARs. The supply feeds remaining reactive power burden 170 VARs of the load. The PF of AC supply is improved to 0.95. The experimental results validate the effectiveness of NF control technique in load balancing and harmonic elimination under non-linear load condition.

Fig 4.21 shows the dynamic performance analysis of SAPF for linear load with NF based

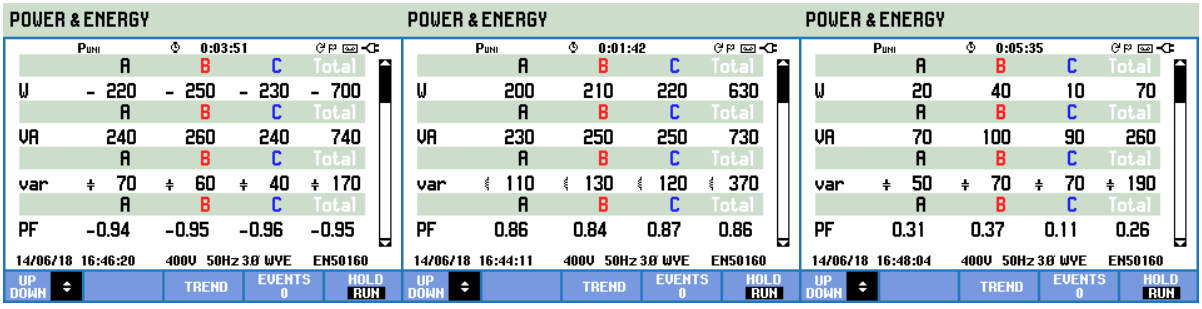

(a) (b) (c)

Fig. 4.20 Steady state power in TPTW distribution system using Notch Filter based control algorithm for (a) Supply (b) Load (c) Compensator in presence of linear load

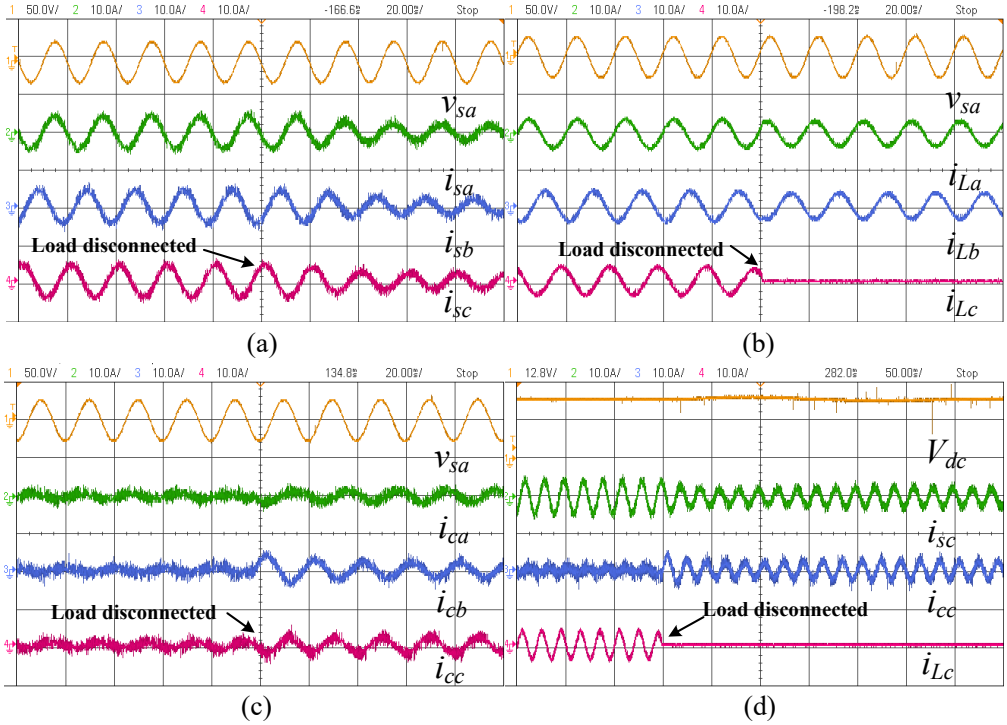

Fig. 4.21 Results showing dynamics for load disconnected in phase 'c' using Notch Filter based control algorithm (a) v_{sa}, i_{sa}, i_{sb}, i_{sc} (b) v_{sa}, i_{La}, i_{Lb}, i_{Lc} (c) v_{sa}, i_{ca}, i_{cb}, i_{cc} (d) V_{dc}, i_{sc}, i_{cc}, i_{Lc} for linear load

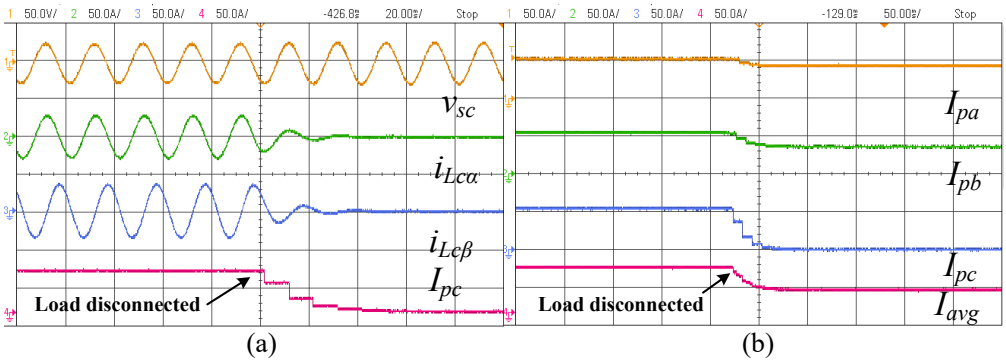

Fig. 4.22 Intermediate results using Notch Filter based control algorithm (a) v_{sc}, $i_{Lc\alpha}$, $i_{Lc\beta}$, I_{pc} (b) I_{pa}, I_{pb}, I_{pc}, I_{avg} for linear load

control algorithm for SAPF. Fig. 4.21(a) shows the phase 'a' supply voltage (v_{sa}) and SAPF compensated supply currents (i_{sa}, i_{sb}, i_{sc}). In this case also the supply currents are observed to be sinusoidal and balanced. In Fig. 4.21(b) phase 'a' supply voltage (v_{sa}) and load currents (i_{La}, i_{Lb}, i_{Lc}) are depicted. The phase 'c' of the load is removed to introduce unbalancing in the load. Fig. 4.21(c) presents phase 'a' supply voltage (v_{sa}) and compensator currents (i_{ca}, i_{cb}, i_{cc}). The compensating currents are observed to be sinusoidal in nature. After removal of phase 'c', the magnitude of all three compensating currents are increased in order to make supply currents balanced and in phase with supply voltages. Fig. 4.21(d) shows DC link

voltage (V_{dc}) and phase 'c' supply, load and compensator current (i_{sc}, i_{Lc}, i_{cc}). It is observed that the currents attain their steady state value within 2-3 cycles, which shows fast compensation. Fig. 4.22 shows the intermediate signals for NF technique for linear loads. Fig 4.22 (a) shows phase 'c' supply voltage (v_{sc}), phase 'c' alpha and beta components of load current ($i_{Lc\alpha}$, $i_{Lc\beta}$) and fundamental active power component of phase 'c' (I_{pc}). Fig 4.22(b) shows all three phase fundamental active power components (I_{pa}, I_{pb}, I_{pc}) and average active power component (I_{avg}). The performance of the NF technique is satisfactory in linear and non-linear loads and can be used to improve the PQ of the distribution system.

4.4.2 Kalman-LMS Based Control Algorithm

In this section, steady state and dynamic performance analysis of SAPF for TPTW system using Kalman-LMS based control technique are described. A SAPF as compensator is developed for 110 V, 50 Hz, TPTW distribution system feeding linear and non-linear loads.

Fig. 4.23 presents SAPF steady state performance with non-linear load. Figs. 4.23(a)-(c)

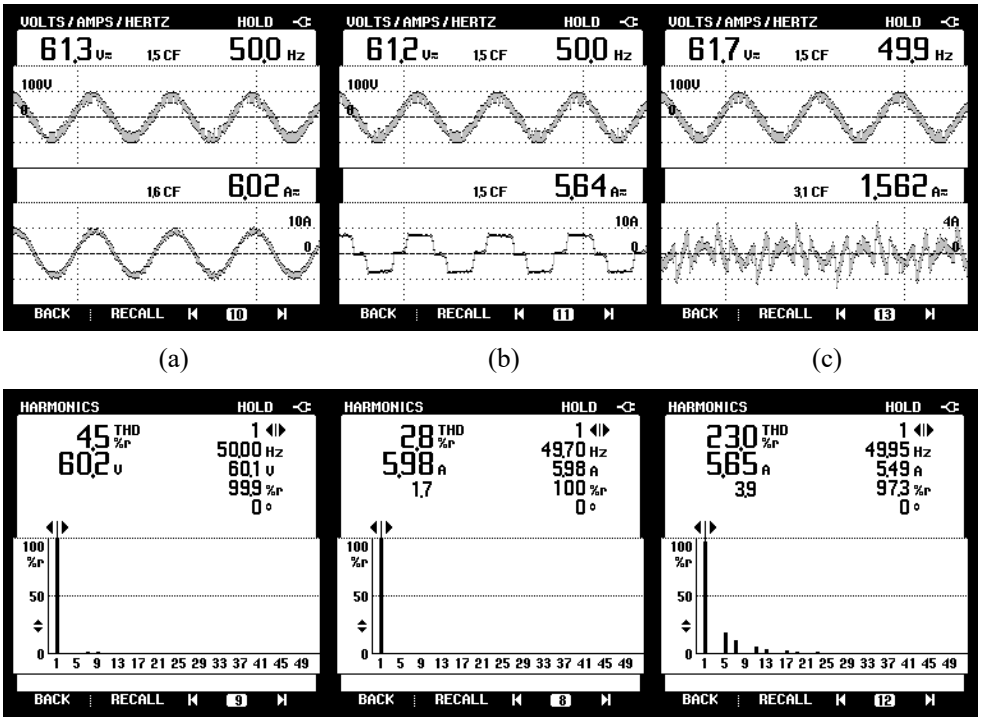

Fig. 4.23 Steady state waveforms for TPTW distribution system using Kalman-LMS based control algorithm (a) v_{sa}-i_{sa} (b) v_{sa}-i_{La} (c) v_{sa}-i_{ca} and (d-f) THD of (d) v_{sa} (e) i_{sa} (f) i_{La} for non-linear load

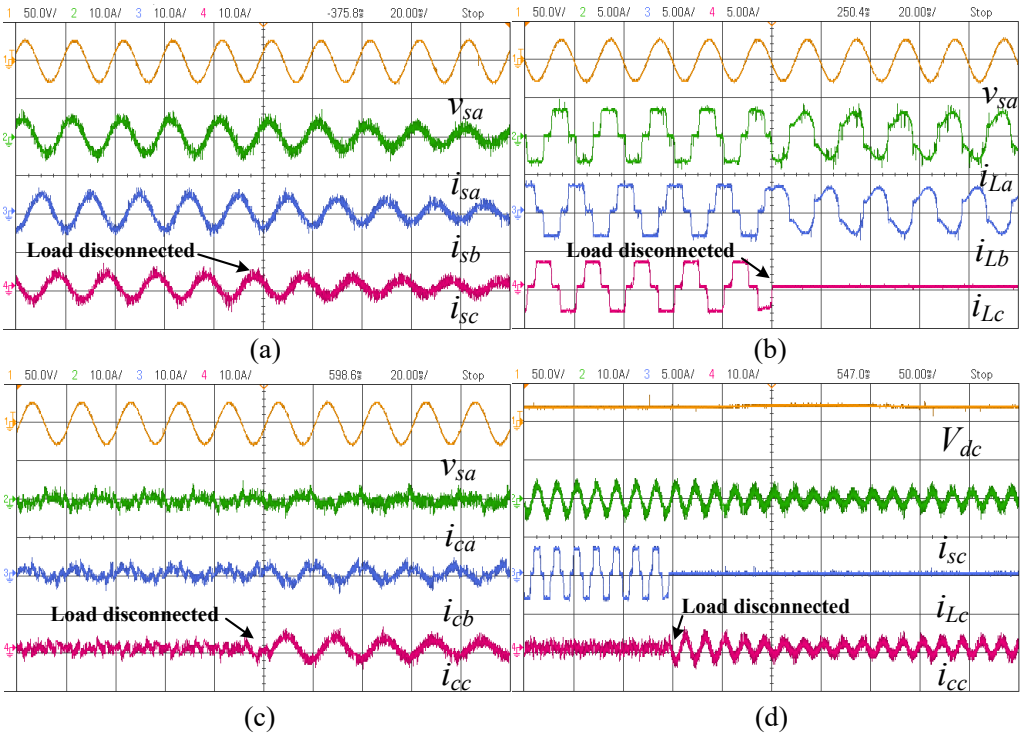

Fig. 4.24 Results showing dynamics for load disconnected in phase 'c' using Kalman-LMS based control algorithm (a) v_{sa}, i_{sa}, i_{sb}, i_{sc} (b) v_{sa}, i_{La}, i_{Lb}, i_{Lc} (c) v_{sa}, i_{ca}, i_{cb}, i_{cc} (d) V_{dc}, i_{sc}, i_{Lc}, i_{cc} for non-linear load

show the phase 'a' supply current (v_{sa}), phase 'a' load current (i_{La}) and phase 'a' compensator current (i_{ca}) along with phase 'a' supply voltage (v_{sa}). Figs. 4.23(d)-(f) show harmonic content for supply and load side. Figs. 4.23(d)-(f) show THD of 4.5% in supply voltage (v_{sa}), 2.8% in supply current (i_{sa}), and 23.0% in load current (i_{La}). A R-L load at the output three phase diode bridge rectifier is modeled in the form of a non-linear load. The Kalman-LMS controller is designed such that all the load harmonics are being supplied locally by SAPF and supply current is sinusoidal.

Fig 4.24 shows the dynamic performance of TPTW system feeding non-linear loads. Fig. 4.24(a) shows phase 'a' supply voltage (v_{sa}) and three phase shunt compensated supply currents (i_{sa}, i_{sb}, i_{sc}). The Kalman-LMS technique makes supply currents sinusoidal and balanced even under unbalanced load condition. Fig. 4.24(b) shows phase 'a' supply voltage (v_{sa}) and three phase non-sinusoidal load currents (i_{La}, i_{Lb}, i_{Lc}). A isolator in phase 'c' removes the load in phase 'c' and the currents in phase 'a' and 'b' also change due to this unbalancing. Fig. 4.24(c) shows phase 'a' supply voltage (v_{sa}) and three phase SAPF injected compensator

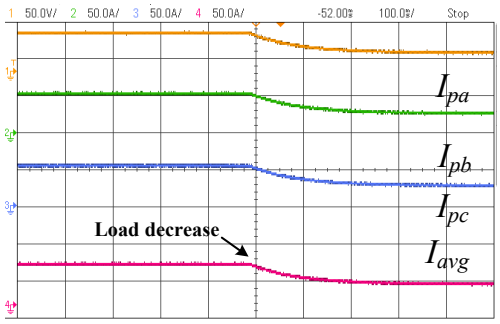

(a)

Fig. 4.25 Intermediate result using Kalman-LMS based control algorithm (a) I_{pa}, I_{pb}, I_{pc}, I_{avg} for non-linear load

currents (i_{ca}, i_{cb}, i_{cc}). Fig. 4.24(d) shows DC link voltage (V_{dc}) and phase 'c' supply, load and compensator currents (i_{sc}, i_{Lc}, i_{cc}). The supply current in phase 'c' is present due to compensator current 'i_{cc}' even though load current 'i_{Lc}' is absent and results in balanced and sinusoidal three phase supply currents.

Fig. 4.25 shows the intermediate signals in Kalman-LMS control technique for SAPF with non-linear load. Fig 4.25 shows the magnitude of three phase fundamental active power components (I_{pa}, I_{pb}, I_{pc}) along with average fundamental active power component (I_{avg}). The active power demand of three phase load is decreased to observe its effect on the fundamental component of load current. It is seen that all the three phases, fundamental active power components decrease in magnitude due to reduction in load power. Hence, the average active power component is also reduced by Kalman-LMS algorithm which is responsible for reducing the magnitude of reference signals during this period.

Fig. 4.26 shows the steady state performance of SAPF compensator with linear load. Figs. 4.26(a)-(c) show the steady state power requirement for supply, load and compensator respectively. The PF of load is observed to be 0.86 and that of AC supply is 0.95. The active power requirement of load is 620 W and reactive power demand of 360 VARs. The supply has active power supply of 700 W, reactive power supply of 180 VARs. The compensator has active power demand of 70 W and capacitive var supply of 180 VARs. So, the Kalman-LMS control algorithm is able to improve system PF with adequate control of power flow in the

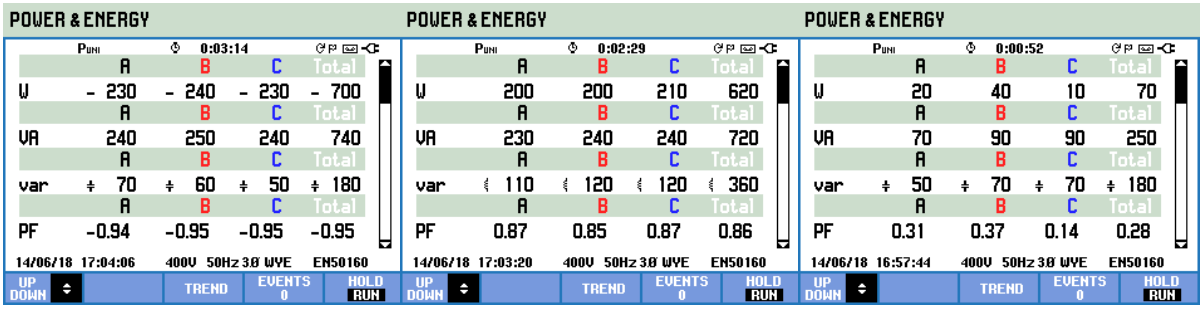

(a) (b) (c)

Fig. 4.26 Steady state power in TPTW distribution system using Kalman-LMS based control algorithm for (a) Supply (b) Load (c) Compensator in presence of linear load

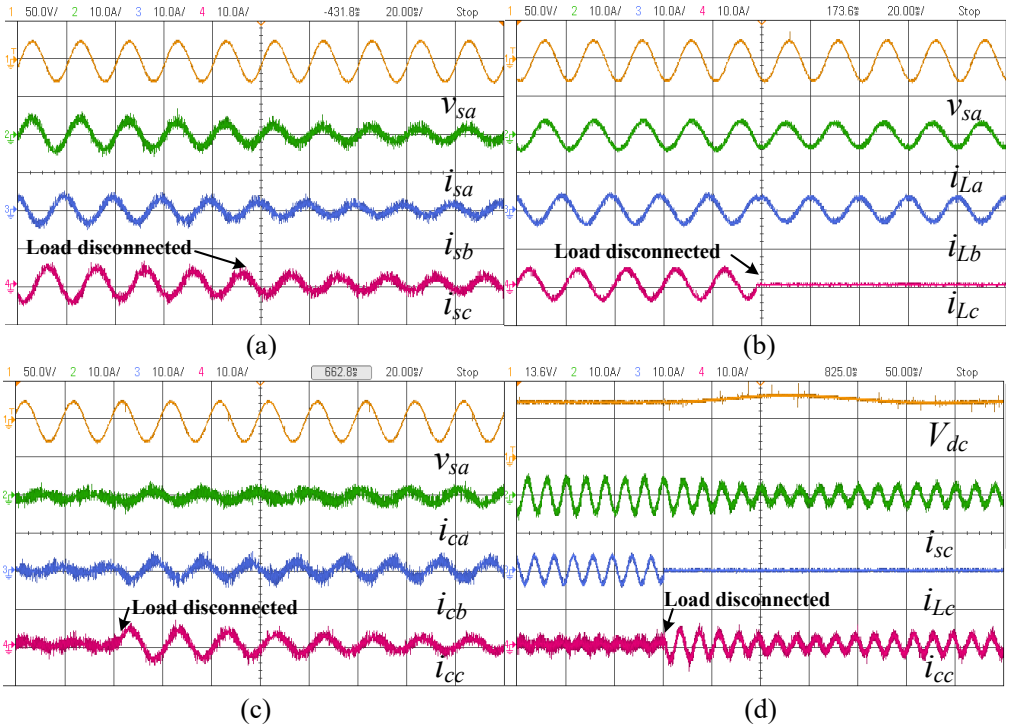

(a) (b)

(c) (d)

Fig. 4.27 Results showing dynamics for load disconnected in phase 'c' using Kalman-LMS based control algorithm (a) v_{sa}, i_{sa}, i_{sb}, i_{sc} (b) v_{sa}, i_{La}, i_{Lb}, i_{Lc} (c) v_{sa}, i_{ca}, i_{cb}, i_{cc} (d) V_{dc}, i_{sc}, i_{Lc}, i_{cc} for linear load system.

Fig 4.27 presents the results for linear load case under sudden change in load conditions. Fig. 4.27(a) shows phase 'a' supply voltage (v_{sa}) and SAPF compensated three phase supply currents (i_{sa}, i_{sb}, i_{sc}). In Fig. 4.27(b) phase 'a' supply voltage (v_{sa}) and three phase lagging PF load currents (i_{La}, i_{Lb}, i_{Lc}) are shown. Fig. 4.27(c) presents phase 'a' supply voltage (v_{sa}) and SAPF injected compensator currents (i_{ca}, i_{cb}, i_{cc}). Fig. 4.27(d) shows DC link voltage (V_{dc}) and phase 'c' supply (i_{sc}), phase 'c' load current (i_{Lc}) and phase 'c' compensator current (i_{cc}).

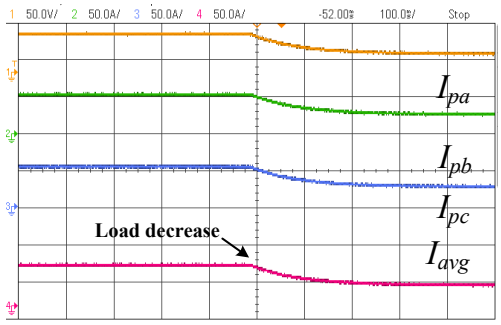

(a)

Fig. 4.28 Intermediate result using Kalman-LMS based control algorithm (a) I_{pa}, I_{pb}, I_{pc}, I_{avg} for linear load

The Kalman LMS technique is implemented successfully for compensation in linear and non-linear loads.

In Fig. 4.28, the intermediate signals of Kalman-LMS technique for SAPF with linear load are shown. Fig 4.28 shows three phase fundamental active power components (I_{pa}, I_{pb}, I_{pc}) along with average active power component (I_{avg}). A decrease in load is introduced and waveforms are recorded. Kalman-LMS control algorithm provides accurate estimation of fundamental components of three phase load currents and generation of control signals for SAPF in TPTW distribution system.

4.4.3 Hopfield NN Based Control Algorithm

The experimental results for Hopfield based control technique for 110 V, 50 Hz, three phase distribution system feeding linear and non-linear loads are shown in this section. Fig. 4.29 shows the steady state performance of SAPF with non-linear load. Figs. 4.29(a)-(c) show phase 'a' supply current (v_{sa}), phase 'a' load current (i_{La}) and phase 'a' compensator current (i_{ca}) along with phase 'a' supply voltage (v_{sa}). Figs. 4.29(d)-(f) show harmonic analysis for supply and load side. Figs. 4.29(d)-(f) shows THD of 4.2% in supply voltage (v_{sa}), 3.4% in supply current (i_{sa}), and 23.1% in load current (i_{La}). The supply current THD has been reduced to an adequate level by proper design and execution of Hopfield NN control technique.

In Fig 4.30 the dynamic results of TPTW system with non-linear loads are shown. Fig. 4.30

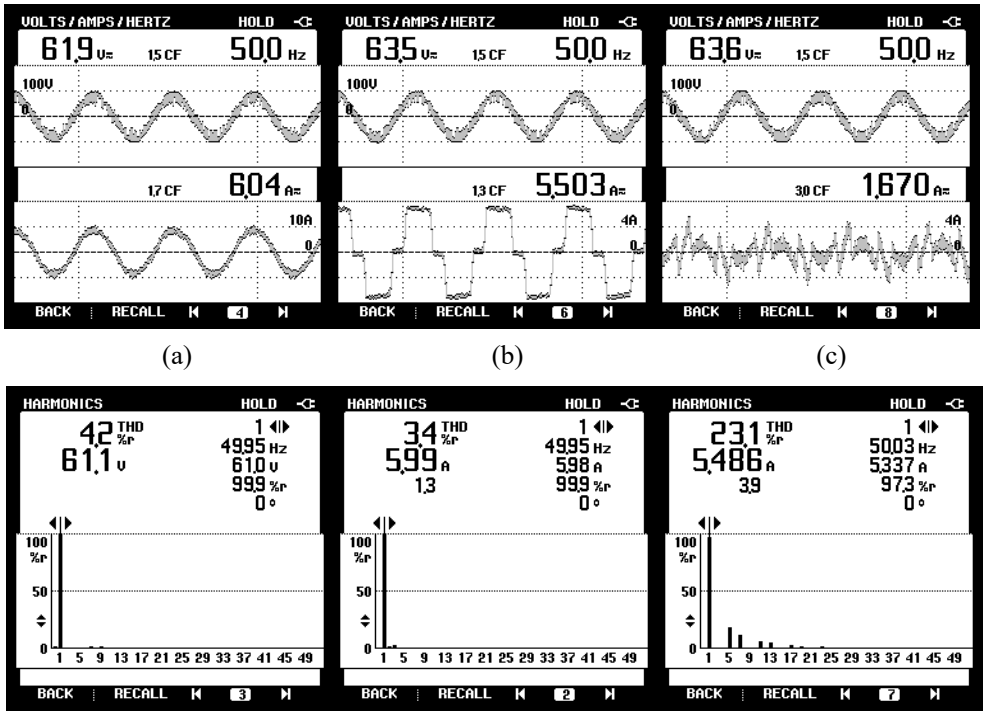

Fig. 4.29 Steady state waveforms for TPTW distribution system using Hopfield NN based control algorithm (a) v_{sa}-i_{sa} (b) v_{sa}-i_{La} (c) v_{sa}-i_{ca} and (d-f) THD of (d) v_{sa} (e) i_{sa} (f) i_{La} for nonlinear load

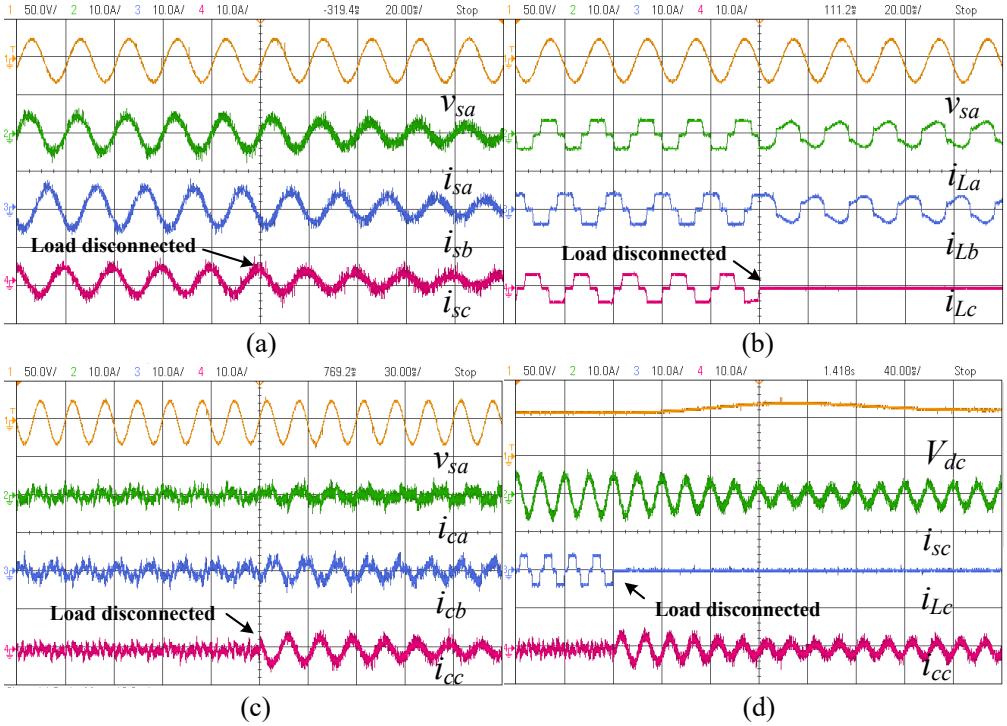

Fig. 4.30 Results showing dynamics for load disconnected in phase 'c' using Hopfield NN based control algorithm (a) v_{sa}, i_{sa}, i_{sb}, i_{sc} (b) v_{sa}, i_{La}, i_{Lb}, i_{Lc} (c) v_{sa}, i_{ca}, i_{cb}, i_{cc} (d) V_{dc}, i_{sc}, i_{Lc}, i_{cc} for non-linear load

(a) shows phase 'a' supply voltage (v_{sa}) and shunt compensated three phase supply currents (i_{sa}, i_{sb}, i_{sc}). The supply currents are observed to be sinusoidal and balanced. In Fig. 4.30 (b)

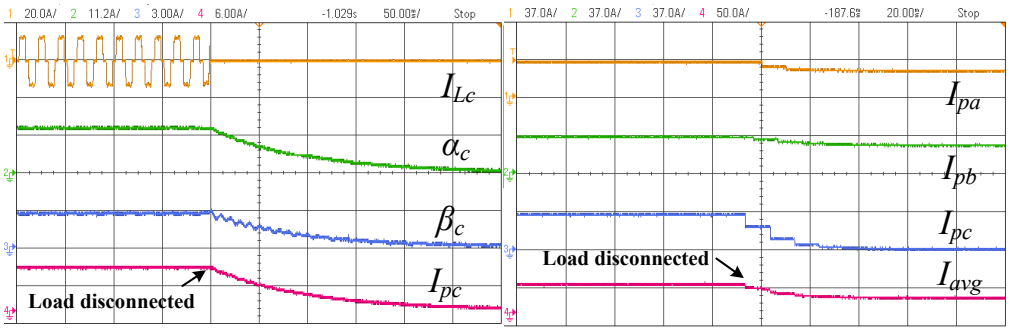

(a) (b)

Fig. 4.31 Intermediate results using Hopfield NN based control algorithm (a) I_{Lc}, α_c, β_c, I_{pc} (b) I_{pa}, I_{pb}, I_{pc}, I_{avg} for non-linear load

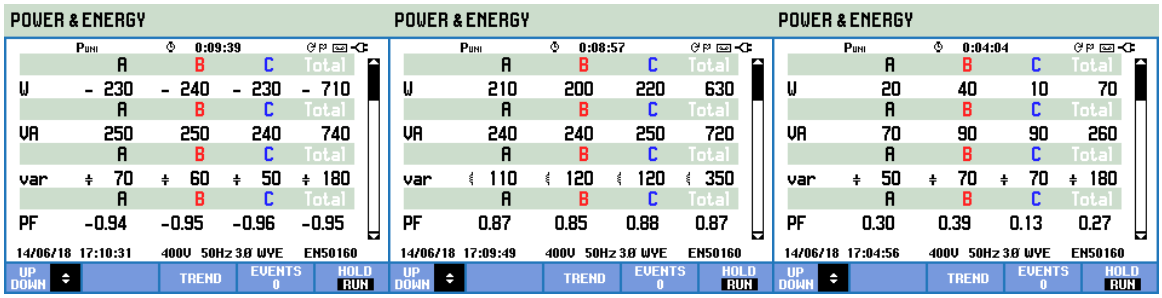

(a) (b) (c)

Fig. 4.32 Steady state power in TPTW distribution system using Hopfield NN based control algorithm for (a) Supply (b) Load (c) Compensator in presence of linear load

phase 'a' supply voltage (v_{sa}) and three phase non-sinusoidal load currents (i_{La}, i_{Lb}, i_{Lc}) are shown. Fig. 4.30(c) shows phase 'a' supply voltage (v_{sa}) and three phase compensator currents (i_{ca}, i_{cb}, i_{cc}). The Hopfield NN control technique generates appropriate compensating currents and injects at PCC of the TPTW power distribution system via the SAPF. In Fig. 4.30(d) DC link voltage (V_{dc}) and phase 'c' supply, load and compensator currents (i_{sc}, i_{Lc}, i_{cc}) are shown. The ability of Hopfield control technique to maintain AC supply currents sinusoidal and balanced under varying load conditions is demonstrated.

Fig. 4.31 shows the intermediate signals in Hopfield control technique for SAPF feeding non-linear load. Fig. 4.31(a) presents phase 'c' load current (i_{Lc}), phase 'c' alpha extracted component of load current (α_c), phase 'c' beta extracted component of load current (β_c) and fundamental active power component of phase 'c' (I_{pc}). Fig 4.31(b) shows three phase fundamental active power components (I_{pa}, I_{pb}, I_{pc}) and average fundamental active power component (I_{avg}). The changes in phase 'c' load current results in changes in the fundamental

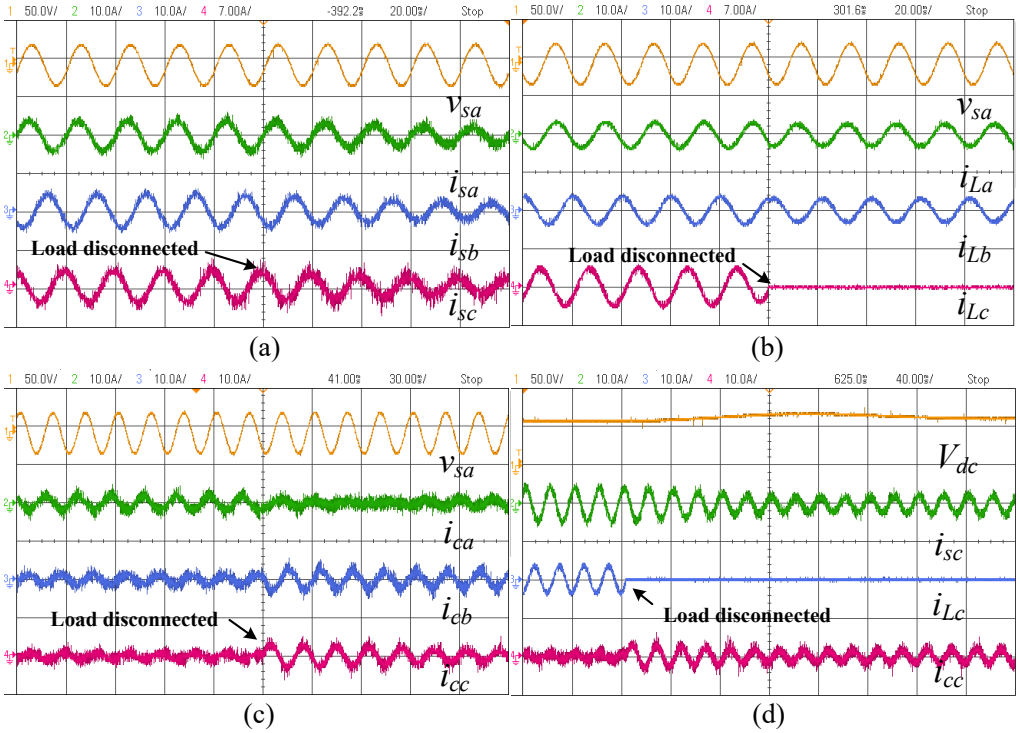

Fig. 4.33 Results showing dynamics for load disconnected in phase 'c' using Hopfield NN based control algorithm (a) v_{sa}, i_{sa}, i_{sb}, i_{sc} (b) v_{sa}, i_{La}, i_{Lb}, i_{Lc} (c) v_{sa}, i_{ca}, i_{cb}, i_{cc} (d) V_{dc}, i_{sc}, i_{Lc}, i_{cc} for linear load

active power component in all three phases.

Fig. 4.32 presents the steady state power flow in TPTW distribution system with SAPF controlled using Hopfield NN scheme in presence of linear load. Figs. 4.32(a)-(c) show steady state power of supply, load and compensator respectively. The PF of load is 0.87 and AC supply PF is 0.95. Load has active power requirement of 630 W and reactive power demand of 350 VARs. The AC supply delivers active power of 710 W and reactive power of 180 VARs. The compensator has active power requirement of 70 W and capacitive var delivered of 180 VARs. Thus the reactive power burden on the AC supply is reduced.

Fig 4.33 shows the dynamic performance of SAPF in presence of linear load using Hopfield NN based control algorithm in SAPF. Fig. 4.33(a) shows the phase 'a' supply voltage (v_{sa}) and three phase shunt compensated supply currents (i_{sa}, i_{sb}, i_{sc}). The three phase supply currents are balanced and sinusoidal. In Fig. 4.33(b) phase 'a' supply voltage (v_{sa}) and three phase load currents (i_{La}, i_{Lb}, i_{Lc}) are depicted. The phase 'c' of the load is suddenly removed and dynamic performance of SAPF is captured. Fig. 4.33(c) presents phase 'a' supply voltage

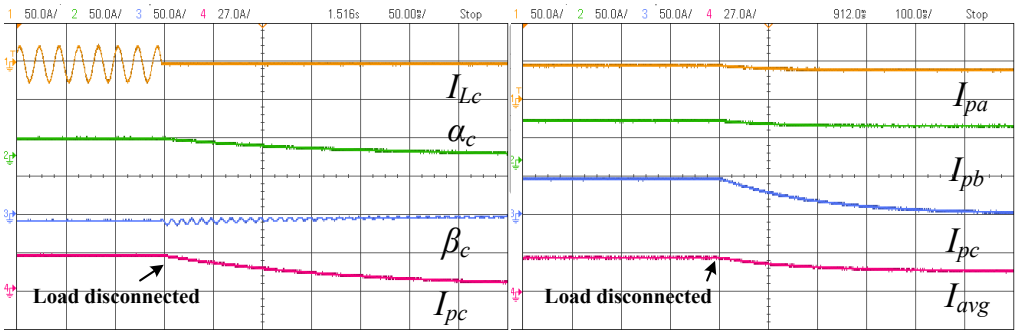

(a) (b)

Fig. 4.34 Intermediate results using Hopfield NN based control algorithm (a) I_{Lc}, α_c, β_c, I_{pc} (b) I_{pa}, I_{pb}, I_{pc}, I_{avg} for linear load

(v_{sa}) and three phase shunt injected compensator currents (i_{ca}, i_{cb}, i_{cc}). Fig. 4.33(d) shows DC link voltage (V_{dc}) and phase 'c' supply, load and compensator current (i_{sc}, i_{Lc}, i_{cc}). Figs. 4.33 (a)-(d) show the effectiveness of Hopfield NN control algorithm for PQ improvement in TPTW distribution system.

Fig. 4.34(a) shows phase 'c' load current (i_{Lc}), HNN extracted 'α' component of phase 'c' load current (α_c), HNN extracted 'β' component of phase 'c' load current (β_c) and fundamental active power component of phase 'c' (I_{pc}). The fundamental active power component of phase 'c' reduced to zero in absence of phase 'c'. Fig. 4.34(b) presents three phase fundamental active power components (I_{pa}, I_{pb}, I_{pc}) of load currents along with their average active power component (I_{avg}). The I_{avg} is used further to generate magnitude of reference currents for SAPF.

4.5 COMPARATIVE EVALUATION OF PROPOSED CONTROL SCHEMES

In this chapter, PQ problems and their mitigation using three different control techniques viz. NF, Kalman LMS and Hopfield NN are discussed in detail for a TPTW distribution system. These advanced control algorithms have been implemented on TPTW system and found to be effective in reducing the reactive power burden of the load, harmonic content and unbalancing on the AC supply and also to improve the PF and profile of waveform of supply currents. Performance of the three control techniques on TPTW distribution system feeding linear and non-linear loads have been verified through simulations and hardware results.

Based on the experimental results (Fig. 4.17, 4.20, 4.23, 4.26, 4.29, 4.32), two comparison tables are shown for non-linear and linear load compensation.

Table 4.1 shows that load current has THD around 23%, which has been brought down to a value of 1.90%, 2.8% and 3.4% in the supply current using NF, Kalman-LMS and Hopfield NN control algorithms respectively. Out of all the three control techniques developed, it has been observed that the lowest THD of supply current was obtained with the NF control algorithm. The supply current THD is 1.90% with this algorithm when the supply voltage has a THD of ~ 4.3% in all three cases. The results have been taken under same load conditions, which is around 5.6A of load current having a THD of 23%.

Table 4.2 shows the power balance on the supply, load and compensator side using developed control algorithms. In all cases, the load demand is ~620 W, 350 VARs. The results obtained with the three algorithms show that the supply feeds active power of ~700 W and reactive power supply of ~180 VAR. The supply side PF is nearly the same as 0.95 with all the three control algorithms. Moreover, the load and compensator active power and reactive power are observed to be nearly the same for all three control algorithm under consideration as

Table 4.1 COMPARISON OF CONTROL ALGORITHMS FOR NON-LINEAR LOAD

S.No.	Quantity	Notch Filter	Kalman-LMS	Hopfield
1.	Supply Voltage (v_{sa})	62.4 V, 4.3% THD	60.2 V, 4.5% THD	61.1 V, 4.2% THD
2.	Load Current (i_{La})	5.87 A, 23.0% THD	5.65 A, 23.0% THD	5.486 A, 23.1% THD
3.	Supply Current (i_{sa})	6.21 A, 1.90% THD	5.98 A, 2.8% THD	5.99 A, 3.4% THD

Table 4.2 COMPARISON OF CONTROL ALGORITHMS FOR LINEAR LOAD

S.No.	Quantity	Notch Filter	Kalman-LMS	Hopfield
1.	Supply Power	700 W, 170 VARs, 0.95 P.F.	700 W, 180 VARs, 0.95 P.F.	710 W, 180 VARs, 0.95 P.F.
2.	Load Power	630 W, 370 VARs, 0.86 P.F.	620 W, 360 VARs, 0.86 P.F.	630 W, 350 VARs, 0.87 P.F.
3.	Compensator Power	70 W, 190 VARs, 0.26 P.F.	70 W, 180 VARs, 0.28 P.F.	70 W, 180 VARs, 0.27 P.F.

experimental tests were conducted under similar load conditions. The performance of the developed control algorithms with linear loads is satisfactory and comparable.

The NF and Hopfield NN control algorithm can also be extended for extracting harmonics components of distorted load current.

4.6 CONCLUSIONS

The main contributions of this chapter are to develop new control algorithms such as NF, Kalman LMS and Hopfield NN for mitigating PQ problems in TPTW system. The control algorithms developed have fast response and show improved system performance substantially. Among all three control algorithms developed for implementation, NF based control technique is less complex and the average fundamental current component of load (I_{avg}) takes almost one and half cycles (Fig. 4.22) to settle under dynamic load changes as compared to Kalman LMS which takes three cycles (Fig. 4.28). The Hopfield NN based algorithm takes 5-6 cycles (Fig. 4.34) to settle down under similar dynamic load changes. It is observed that while all the designed control algorithms achieve the desired objectives for shunt compensation, NF based algorithm is much simpler to realize mathematically, followed by Hopfield control and Kalman-LMS algorithm. The complexity of computing adaptive gain of LMS using KF was observed to be the highest. The dynamic performance of NF was observed to be the best under the worst case load change viz. the removal of one phase of the load.

Chapter 5
POWER QUALITY IMPROVEMENT IN THREE PHASE FOUR WIRE DISTRIBUTION SYSTEM

5.0 INTRODUCTION

In this chapter PQ problems occurring in TPFW distribution system are discussed. New control techniques for the mitigation of PQ problems for a variety of load conditions have been developed. These techniques are simulated in a MATLAB/SIMULINK environment for control of shunt compensator. Experimental verification on a prototype hardware system is performed to ensure the effectiveness of the developed control algorithms.

5.1 POWER QUALITY ISSUES IN TPFW DISTRIBUTION SYSTEM

In the previous chapter, PQ issues in TPTW distribution system have been discussed in detail. The TPFW systems are more vulnerable to PQ issues as compared to that of a TPTW due to presence of neutral wire. TPFW systems are used to supply single phase load also. The majority of consumers in TPFW distribution systems are residential and commercial users. The distribution system is prone to various PQ problems such as poor PF, load unbalancing, current harmonics, reactive power demand and additional neutral current compensation.

TPFW systems have been widely used to deliver single phase and three phase loads of domestic, commercial and industrial installations. Due to single phase load, there are unbalance loading among phases and due to this neutral conductor carries excess current which results in overloading of neutral conductor and distribution transformer. If the neutral current is high, the equipment connected in the vicinity gets affected badly. Hence, neural current compensation is required to limit the supply neutral current close to zero. The presence of more and more power electronics equipment with front end rectification are connected in the TPFW system, harmonic current drawn by rectifiers becomes significant which deteriorates PQ further. Several compensation schemes have been developed to

reduce PQ issues in TPFW system such as zig-zag transformer arrangement, SAPF and a combination of zig-zag and SAPF.

It is required to design suitable and effective control techniques for mitigating various PQ issues such as reactive power demand, poor PF, load unbalancing, current harmonics and neutral current compensation in TPFW distribution system.

5.2 DEVELOPMENT AND ANALYSIS OF ADVANCE CONTROL ALGORITHMS FOR TPFW DISTRIBUTION SYSTEM

In this section, new control techniques of SAPF such as Self Tuning Filter (STF), Modified Recursive Gauss Newton (MRGN) and Chebyshev Polynomial based Artificial Neural Network (ChANN) algorithms for PQ problems mitigation in TPFW system are described.

5.2.1 Extraction of Fundamental Active Power Components Using Developed Control Algorithms

The extraction of fundamental active power component (I_{pabc}/I_{avg}) of three phase load currents using developed control algorithms are discussed in this section.

5.2.1.1 Self Tuning Filter Based Control Algorithm

Self Tuning Filter is a class of filters in which the outputs are fed back to the input to determine required frequency component from the input signal. The STF in current research is tuned for fundamental frequency i.e. 314 rad/sec (50 Hz), so STF extracts fundamental component of signal from the distorted input signal. Fig. 5.1 shows the structure of STF. The general structure of STF can be implemented on supply voltages or load currents. A STF is implemented on α-β components of load currents ($i_{L\alpha,}\ i_{L\beta}$). The STF operation produces filtered α-β component $i_{L\alpha f,}\ i_{L\beta f}$ as follows

$$i_{L\alpha f} = \frac{D \times i_{L\alpha} - D \times i_{L\alpha f}}{s} - \frac{\omega \times i_{L\beta f}}{s} \tag{5.1}$$

$$i_{L\beta f} = \frac{D \times i_{L\beta} - D \times i_{L\beta f}}{s} + \frac{\omega \times i_{L\alpha f}}{s} \tag{5.2}$$

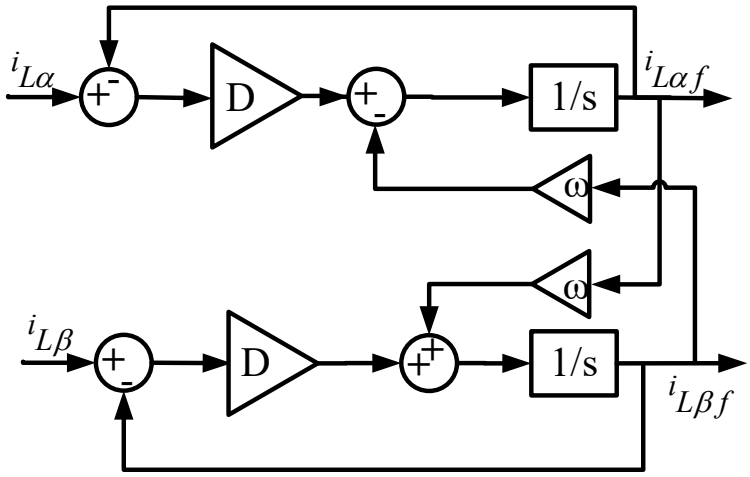

Fig. 5.1 Self Tuning Filter (STF) Block

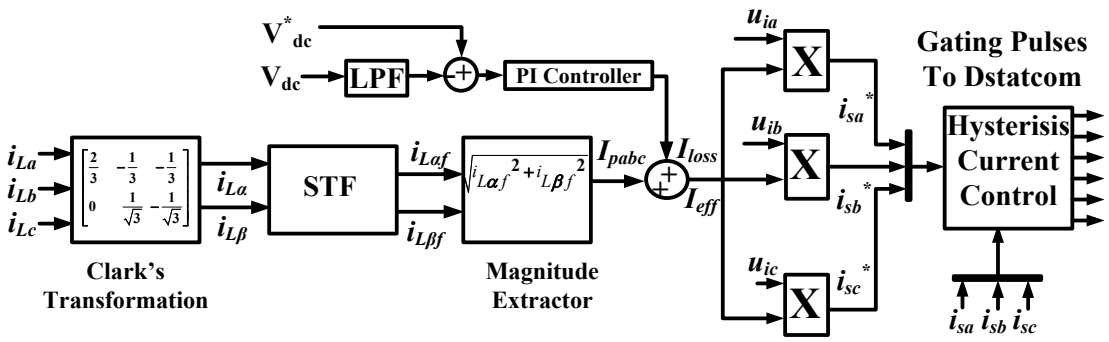

Fig. 5.2 Block diagram of STF based control algorithm implementation

where $i_{L\alpha}$, $i_{L\beta}$ are the Clarke's transformed load currents, D is the gain constant, ω is the frequency of signal to be extracted and taken as 314 rad/sec.

Fig. 5.2 shows the complete block diagram of STF based SAPF control technique to improve PQ in TPFW system. The three phase load currents (i_{La}, i_{Lb}, i_{Lc}) are first transformed into α-β component using Clarke's transformation as:

$$\begin{bmatrix} i_{L\alpha} \\ i_{L\beta} \end{bmatrix} = \sqrt{\frac{2}{3}} \begin{bmatrix} 1 & -\frac{1}{2} & -\frac{1}{2} \\ 0 & \frac{\sqrt{3}}{2} & -\frac{\sqrt{3}}{2} \end{bmatrix} \begin{bmatrix} i_{La} \\ i_{Lb} \\ i_{Lc} \end{bmatrix} \tag{5.3}$$

For the non-linear loads, the transformed α-β components of load currents are also distorted hence they are processed by STF as per Eq. (5.1-5.2) so as to obtain filtered α-β components

of load currents ($i_{L\alpha f,}$ $i_{L\beta f}$). Now. the fundamental active power component (I_{pabc}) is calculated from the $i_{L\alpha f,}$ $i_{L\beta f}$ as

$$I_{pabc} = \sqrt{i_{L\alpha f}^2 + i_{L\beta f}^2} \tag{5.4}$$

The I_{pabc} is added to DC link power loss component I_{loss} so as to obtain effective active power component I_{eff} which is discussed later in this section.

5.2.1.2 Modified Recursive Gauss Newton Based Control Algorithm

Gauss-Newton (GN) method [27] is used for finding minima of a function. In GN Taylor's series expansion and least square method is combined. In GN method there is no need of calculation of second order derivatives of function for minimizing. In this section Recursive Gauss Newton (RGN) and its Modified Recursive Gauss Newton (MRGN) is discussed.

5.2.1.2.1 Recursive Gauss-Newton (RGN) Method

A non-sinusoidal AC current in the power system is expressed as:

$$i_m = M_m \sin(\omega_m t + \gamma_m) + \chi_m \tag{5.5}$$

where i_m= instantaneous value of mth component of current, M_m= peak magnitude of mth component of current, ω_m=angular frequency of mth component of current, γ_m=phase shift of mth component of current and χ_m=zero mean white noise, m=order of harmonic.

For a nonlinear load, current signal has fundamental and harmonics components. An equation error model is required for the determination of peak magnitude (M_m) and phase (γ_m) of mth harmonic component of non-sinusoidal current. Assuming $\theta_k = [M(k) \;\; \gamma(k)]^T$ to be the parameter matrix for fundamental component of current, where M(k) and γ(k) are the magnitude and phase of fundamental component of current at kth instant, the desired parameter matrix at the (k-1)th instant is depicted as $\hat{\theta}_k = [\hat{M}(k-1) \;\; \hat{\gamma}(k-1)]^T$, the equation error model using Eq. (5.5) is described as

$$\rho(k) = i(k) - \hat{M}(k-1)\sin(\omega t + \hat{\gamma}(k-1)) - \chi(k) \tag{5.6}$$

where ρ(k) is error between actual current and estimated current at kth instant, i(k) is actual current at kth instant, ω is 314 rad/sec. A method of modified least squares procedure is used to obtain solution for $\hat{\theta}_k = [\hat{M}(k-1) \quad \hat{\gamma}(k-1)]^T$ in which cost function, E_N is minimized:

$$E_N = \sum_{k=1}^{N} \zeta^{N-k} \rho^2(k) \tag{5.7}$$

where E_N is exponentially weighted cost function, ζ is forgetting factor, whose value lies between (0-1). The minimization of cost function is a nonlinear function for which GN method is followed. Linearizing Eq. (5.7) by Taylor's series expansion in the neighborhood of $\hat{\theta}_k = [\hat{M}(k-1) \quad \hat{\gamma}(k-1)]^T$, we get

$$i(k) = \hat{M}(k-1)\sin(\omega t + \hat{\gamma}(k-1)) + \frac{\partial}{\partial \hat{\theta}(k)}[\hat{M}(k-1)\sin(\omega t + \hat{\gamma}(k-1))]\Delta\hat{\theta}(k) + \chi(k) \tag{5.8}$$

From $\hat{\theta}(k) = [\hat{M}(k-1) \quad \hat{\gamma}(k-1)]^T$, we get

$$\begin{aligned} i(k) = \hat{M}(k-1)\sin(\omega t + \hat{\gamma}(k-1)) &+ \frac{\partial}{\partial \hat{M}(k-1)}[\hat{M}(k-1)\sin(\omega t + \hat{\gamma}(k-1))]\Delta\hat{M}(k-1) \\ &+ \frac{\partial}{\partial \hat{\gamma}(k-1)}[\hat{M}(k-1)\sin(\omega t + \hat{\gamma}(k-1))]\Delta\hat{\gamma}(k-1) + \chi(k) \end{aligned} \tag{5.9}$$

Rearranging Eq. (5.9), we get

$$\begin{aligned} i(k) - \hat{M}(k-1)\sin(\omega t + \hat{\gamma}(k-1)) - \chi(k) = &\frac{\partial}{\partial \hat{M}(k-1)}[\hat{M}(k-1)\sin(\omega t + \hat{\gamma}(k-1))]\Delta\hat{M}(k-1) \\ &+ \frac{\partial}{\partial \hat{\gamma}(k-1)}[\hat{M}(k-1)\sin(\omega t + \hat{\gamma}(k-1))]\Delta\hat{\gamma}(k-1) \end{aligned} \tag{5.10}$$

The LHS is error signal *ρ(k),* So

$$\begin{aligned} \rho(k) = &\frac{\partial}{\partial \hat{M}(k-1)}[\hat{M}(k-1)\sin(\omega t + \hat{\gamma}(k-1))]\Delta\hat{M}(k-1) \\ &+ \frac{\partial}{\partial \hat{\gamma}(k-1)}[\hat{M}(k-1)\sin(\omega t + \hat{\gamma}(k-1))]\Delta\hat{\gamma}(k-1) \end{aligned} \tag{5.11}$$

Putting $\hat{M}(k-1)\sin(\omega t+\hat{\gamma}(k-1))=G(k)$ for simplification

Eq. 5.11 is represented in state space form as

$$\rho(k)=\left[\frac{\partial G(k)}{\partial \hat{M}(k-1)}\ \frac{\partial G(k)}{\partial \hat{\gamma}(k-1)}\right][\Delta \hat{M}(k-1)\quad \Delta \hat{\gamma}(k-1)]^T \tag{5.12}$$

$$\rho(k)=[\Upsilon(k)]\Delta\hat{\theta}(k) \tag{5.13}$$

From Eq. (5.6),(5.12),(5.13)

$$\Upsilon(k)=\frac{\partial G(k)}{\partial \hat{\theta}(k)}=-\frac{\partial \rho(k)}{\partial \hat{\theta}(k)} \tag{5.14}$$

Defining gradient matrix $\Upsilon(k)=-\dfrac{\partial \rho(k)}{\partial \hat{\theta}(k)}$ (5.15)

Putting the value of ρ(k) in Eq. (5.7) from Eq. (5.15)

$$\mathrm{E}_N=\sum_{k=1}^{N}\zeta^{N-k}\{\Upsilon(k)\Delta\hat{\theta}(k)\}^2 \tag{5.16}$$

Since error ρ(k) from Eq. (5.12) is observed of the form Y=AX+BU, so the solution of Eq. (5.13) using standard Least Square method is,

$$\Delta\hat{\theta}(k)=[H(k)]^{-1}\Upsilon^T(k)\rho(k) \tag{5.17}$$

where $H(k)=\sum_{k=1}^{N}\zeta^{N-k}\Upsilon^T(k)\Upsilon(k)$, is called Hessian matrix. (5.18)

The updating equation for estimation of $\hat{\theta}$ is written as

$$\hat{\theta}(k)=\hat{\theta}(k-1)+\Delta\hat{\theta}(k) \tag{5.19}$$

$$\hat{\theta}(k)=\hat{\theta}(k-1)+[H(k)]^{-1}\Upsilon^T(k)\rho(k) \tag{5.20}$$

and updating equation for H(k) is given by modifying Eq. (5.18)

$$H(k)=\zeta H(k-1)+\Upsilon(k)\Upsilon^T(k) \tag{5.21}$$

Eq. (5.20-5.21) are updated recursively so as to minimize the error.

5.2.1.2.2 Modified Recursive Gauss Newton (MRGN) Method

The RGN method is very complex and its memory requirement is also very high due to repetitive calculations using Eqs. (5.20-5.21). So to realize in real system, a simplified RGN method after appropriate simplifications can only be used. This section gives the detailed mathematical analysis of MRGN algorithm.

From Eq. (5.6),(5.14) and (5.15), ϒ(k) is calculated as

$$\Upsilon(k)=\left[-\frac{\partial \hat{M}(k-1)\sin(\omega t+\hat{\gamma}(k-1))}{\partial \hat{M}(k-1)} \quad -\frac{\partial \hat{M}(k-1)\sin(\omega t+\hat{\gamma}(k-1))}{\partial \hat{\gamma}(k-1)}\right] \tag{5.22}$$

$$\Upsilon(k)=\left[-\sin(\omega t+\hat{\gamma}(k-1)) \quad -\hat{M}(k-1)\cos(\omega t+\hat{\gamma}(k-1))\right] \tag{5.23}$$

Putting the value of ϒ(k) in Eq. (5.18)

$$H(k)=\sum_{k=1}^{N}\zeta^{N-k}\left[-\sin(\omega t+\hat{\gamma}(k-1)) \quad -\hat{M}(k-1)\cos(\omega t+\hat{\gamma}(k-1))\right]^{T}\left[-\sin(\omega t+\hat{\gamma}(k-1)) \quad -\hat{M}(k-1)\cos(\omega t+\hat{\gamma}(k-1))\right] \tag{5.24}$$

$$H(k)=\sum_{k=1}^{N}\zeta^{N-k}\begin{bmatrix}\sin^2(\omega t+\hat{\gamma}(k-1)) & \hat{M}(k-1)\sin(\omega t+\hat{\gamma}(k-1))\cos(\omega t+\hat{\gamma}(k-1)) \\ \hat{M}(k-1)\sin(\omega t+\hat{\gamma}(k-1))\cos(\omega t+\hat{\gamma}(k-1)) & \hat{M}^{2}(k-1)\cos^2(\omega t+\hat{\gamma}(k-1))\end{bmatrix} \tag{5.25}$$

Using $\frac{1}{T}\int_0^T s\sin(2\theta)\,d\theta=0$ and $\frac{1}{T}\int_0^T s\sin^2\theta\,d\theta=\frac{1}{2}$

$$H(k)=\frac{1}{2}\begin{bmatrix}\frac{1}{2} & 0 \\ 0 & \frac{\hat{M}^{2}(k-1)}{2}\end{bmatrix}\sum_{k=1}^{N}\zeta^{N-k} \tag{5.26}$$

$$H(k)=\frac{1}{2}\begin{bmatrix}\frac{1}{2} & 0\\ 0 & \frac{\hat{M}^{2}(k-1)}{2}\end{bmatrix}\frac{1-\zeta^{N+1}}{1-\zeta} \tag{5.27}$$

Defining $C(N)=\frac{1-\zeta^{N+1}}{4(1-\zeta)}$ as a constant term, from Eq. (5.27) the inverse of Hessian matrix is calculated as

$$H^{-1}(k)=\frac{1}{C(N)\hat{M}^{2}(k-1)}\begin{bmatrix}\hat{M}^{2}(k-1) & 0\\ 0 & 1\end{bmatrix} \tag{5.28}$$

$$H^{-1}(k)=\frac{1}{C(N)}\begin{bmatrix}1 & 0\\ 0 & \frac{1}{\hat{M}^{2}(k-1)}\end{bmatrix} \tag{5.29}$$

Putting the value of $H^{-1}(k)$ from Eq. 5.29 in Eq. 5.20, and writing the updating eq. for $\hat{\theta}(k)$

$$\hat{\theta}(k)=\hat{\theta}(k-1)+\frac{1}{C(N)}\begin{bmatrix}1 & 0\\ 0 & \frac{1}{\hat{M}^{2}(k-1)}\end{bmatrix}\Upsilon^{T}(k)\rho(k) \tag{5.30}$$

Also from Eq. (5.23)

$$\hat{\theta}(k)=\hat{\theta}(k-1)+\frac{1}{C(N)}\begin{bmatrix}1 & 0\\ 0 & \frac{1}{\hat{M}^{2}(k-1)}\end{bmatrix}\begin{bmatrix}-\sin(\omega t+\hat{\gamma}(k-1)) & -\hat{M}(k-1)\cos(\omega t+\hat{\gamma}(k-1))\end{bmatrix}^{T}\rho(k) \tag{5.31}$$

$$\hat{\theta}(k)=\hat{\theta}(k-1)+\frac{1}{C(N)}\begin{bmatrix}-\sin(\omega t+\hat{\gamma}(k-1))\\ -\frac{\cos(\omega t+\hat{\gamma}(k-1))}{\hat{M}(k-1)}\end{bmatrix}\rho(k) \tag{5.32}$$

Individual updating equation for $\hat{M}(k),\hat{\gamma}(k)$ is

$$\hat{M}(k) = \hat{M}(k-1) - \frac{1}{C(N)}\sin(\omega t + \hat{\gamma}(k-1))\rho(k) \tag{5.33}$$

$$\hat{\gamma}(k) = \hat{\gamma}(k-1) - \frac{1}{C(N)}\frac{\cos(\omega t + \hat{\gamma}(k-1))}{\hat{M}(k-1)}\rho(k) \tag{5.34}$$

From Eq. 5.33 $\hat{M}(k)$ is considered as fundamental active power component of input signal and Eq. 5.34 $\hat{\gamma}(k)$ is phase angle of input signal. Fig 5.3 shows the complete MRGN control algorithm for SAPF in which MRGN is applied on phase 'a', 'b' and 'c' load currents (i_{La}, i_{Lb}, i_{Lc}). The fundamental active power component for each phase 'I_{pa}', 'I_{pb}' and 'I_{pc}' average of fundamental component of three phase load currents is determined as:

$$I_{avg} = \frac{I_{pa} + I_{pb} + I_{pc}}{3} \tag{5.35}$$

This I_{avg} is processed further and discussed in section 5.2.2.

5.2.1.3 Chebyshev Polynomial Based Control Algorithm

In this section, Chebyshev Polynomial based Artificial Neutral Network (ChANN) control algorithm for SAPF is discussed. The Artificial Neural Network (ANN) [115] is trained using Chebyshev Polynomial and back propagation algorithm. Chebyshev polynomials (*ChP*) are

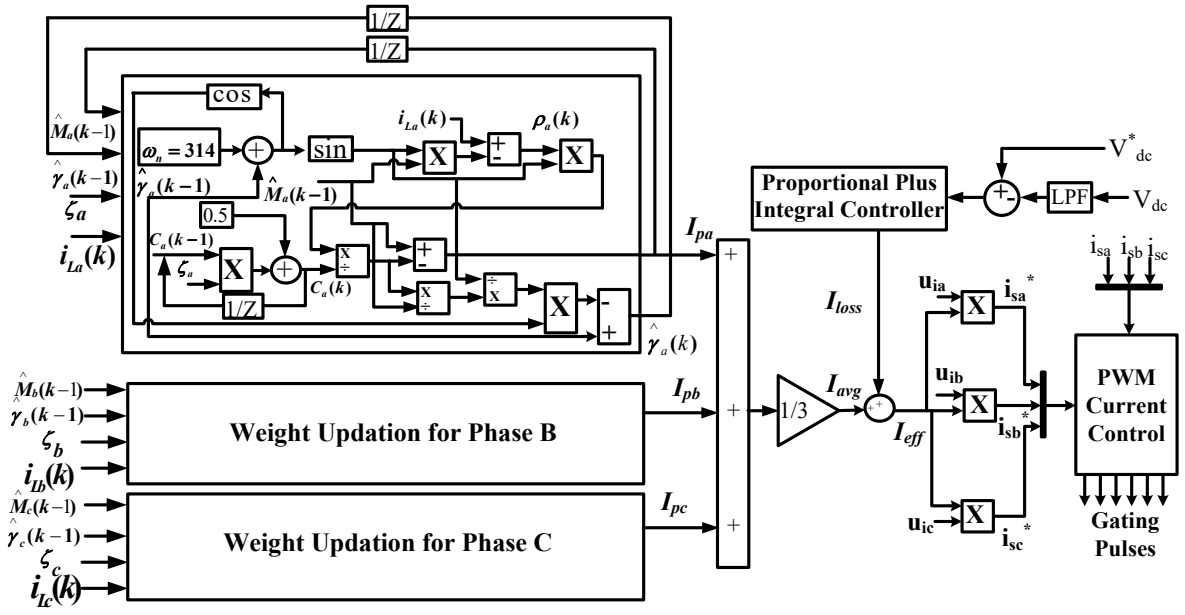

Fig. 5.3 Block diagram of MRGN based control algorithm implementation

used for approximating nonlinear function. The *ChP* form the solution for Chebyshev differential equation given by:

$$(1-x^2)\frac{d^2y}{dx^2}-x\frac{dy}{dx}+\lambda^2 y=0 \tag{5.36}$$

For $x<|1|$, Eq. (5.36) has singularity at -1, 1, and ∞. So solution is obtained using the series expansions which yields

$$y=\sum_{i=0}^{\infty}\kappa_i x^i \tag{5.37}$$

Differentiating Eq. (5.37)

$$\frac{dy}{dx}=\sum_{i=0}^{\infty} i\kappa_i x^{i-1} \tag{5.38}$$

Eq. (5.38) is modified as

$$\frac{dy}{dx}=\sum_{i=0}^{\infty}(i+1)\kappa_{i+1}x^i \tag{5.39}$$

Again differentiating Eq. (5.39) and rearranging

$$\frac{d^2y}{dx^2}=\sum_{i=0}^{\infty}(i+2)(i+1)\kappa_{i+2}x^i \tag{5.40}$$

Substituting Eq. (5.37),(5.39), (5.40) in (5.36) and rearranging

$$(1-x^2)\sum_{i=0}^{\infty}(i+2)(i+1)\kappa_{i+2}x^i-x\sum_{i=0}^{\infty}(i+1)\kappa_{i+1}x^i+\lambda^2\sum_{i=0}^{\infty}\kappa_i x^i=0 \tag{5.41}$$

$$\sum_{i=0}^{\infty}(i+2)(i+1)\kappa_{i+2}x^i-\sum_{i=2}^{\infty}i(i-1)\kappa_i x^i-\sum_{i=1}^{\infty}i\kappa_i x^i+\lambda^2\sum_{i=0}^{\infty}\kappa_i x^i=0 \tag{5.42}$$

On expanding upto i=1

$$(2)(1)\kappa_2+(3)(2)\kappa_3 x-(1)\kappa_1 x+\lambda^2(\kappa_0+\kappa_1 x)+\sum_{i=2}^{\infty}[(i+2)(i+1)\kappa_{i+2}-i(i-1)\kappa_i-i\kappa_i+\lambda^2\kappa_i]x^i=0 \tag{5.43}$$

On simplifying

$$(2\kappa_2 + \lambda^2\kappa_0) + [(\lambda^2 - 1)\kappa_1 + 6\kappa_3]x + \sum_{i=2}^{\infty}[(i+2)(i+1)\kappa_{i+2} + (\lambda^2 - i^2)\kappa_i]x^i = 0 \tag{5.44}$$

From Eq. (5.44)

$$2\kappa_2 + \lambda^2\kappa_0 = 0; (\lambda^2 - 1)\kappa_1 + 6\kappa_3 = 0 \tag{5.45}$$

$$and \quad \kappa_{i+2} = \frac{(i^2 - \lambda^2)\kappa_i}{(i+2)(i+1)} \tag{5.46}$$

From Eq. (5.44),(5.45), it is evident that Eq. (5.45) is special case of Eq. (5.46) so Eq. (5.46) is generalized recurrence equation.

For i=0,2,... even coefficients are obtained as

$$\kappa_2 = -\frac{\lambda^2\kappa_0}{2} \tag{5.47}$$

$$\kappa_4 = \frac{(2^2 - \lambda^2)\kappa_2}{(3)(4)} = \frac{(2^2 - \lambda^2)(-\lambda^2)\kappa_0}{(1)(2)(3)(4)} \tag{5.48}$$

$$and\ in\ general \quad \kappa_{2i} = \frac{[(2i)^2 - \lambda^2)(2i-2)^2 - \lambda^2).....(-\lambda^2)]\kappa_0}{(2i)!} = \frac{\kappa_{even}\kappa_0}{(2i)!} \tag{5.49}$$

Similarly for i=1,3,…., the odd coefficients are obtained as

$$\kappa_3 = \frac{(1 - \lambda^2)\kappa_1}{3!} \tag{5.50}$$

$$\kappa_5 = \frac{(3^2 - \lambda^2)(1^2 - \lambda^2)\kappa_1}{5!} \tag{5.51}$$

$$and\ in\ general \quad \kappa_{2i+1} = \frac{[(2i-1)^2 - \lambda^2)(2i-3)^2 - \lambda^2).....(1^2 - \lambda^2)]\kappa_1}{(2i+1)!} = \frac{\kappa_{odd}\kappa_1}{(2i+1)!} \tag{5.52}$$

The general solution of Eq. 5.36 is obtained using Eq. 5.37, 5.39 and 5.52 as

$$y = [\kappa_0 + \sum_{i=0,1,2..}^{\infty} \kappa_{2i}x^{2i}] + [\kappa_1 x + \sum_{i=0,1,2..}^{\infty} \kappa_{2i+1}x^{2i+1}] \tag{5.53}$$

$$y = \kappa_0[1 + \sum_{i=1,2..}^{\infty} \kappa_{2i}x^{2i}] + \kappa_1[x + \sum_{i=1,2..}^{\infty} \kappa_{2i+1}x^{2i+1}] \tag{5.54}$$

which can be written as

$$y = \kappa_0 \cos(\lambda \sin^{-1} x) + \kappa_1 \sin(\lambda \sin^{-1} x) \tag{5.55}$$

A equivalent form of the solution 5.55 is

$$y = \eta_0 \cos(\lambda \cos^{-1} x) + \eta_1 \sin(\lambda \cos^{-1} x) \tag{5.56}$$

$$y = \eta_0 ChF_n(x) + \eta_1 ChS_n(x) \tag{5.57}$$

where $ChF_n(x)$ is the Chp of the first kind and $ChS_n(x)$ is Chp polynomial of the second kind. In our proposed work $ChF_n(x)$ is used to approximate load current. $ChF_n(x)$ is also calculated using Rodrigue's formula as

$$ChT_n(x) = \frac{(-2)^n n!}{(2n)!} \sqrt{1-x^2}\, \frac{d^n}{dx^n} \sqrt{(1-x^2)^{(n-1)}} \tag{5.58}$$

where $ChT_0(x) = 1, ChT_1(x) = x, Ch_2(x) = 2x^2 - 1, Ch_2(x) = 4x^3 - 3x$, and so on.

By observing the pattern, a general recurrence relationship is developed as follows

$$ChT_{n+1}(x) = 2xChT_n(x) - ChT_{n-1}(x) \qquad n = 1, 2, 3..... \tag{5.59}$$

The *Chp* consist of orthogonal polynomials. Fig. 5.4 shows the proposed Chebyshev Polynomial based Artificial Neural Network (*ChANN*) algorithm in which *ChP* is used to approximate the load current. The weights of ChANN are trained using back-propagation technique. In Fig 5.4, the load current in phase 'a' is approximated by *ChP*, whose output i.e.

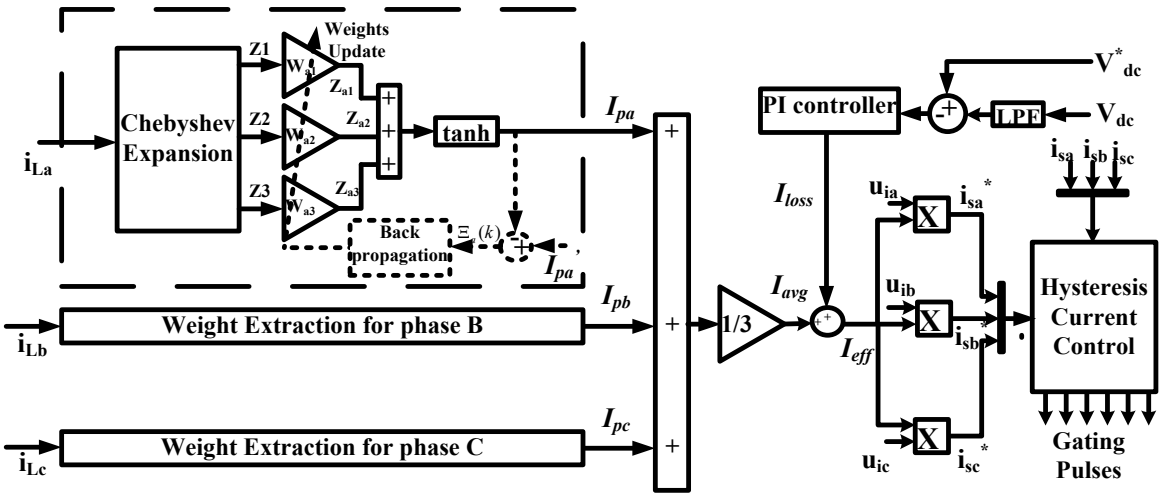

Fig. 5.4 Block diagram of ChANN based control algorithm implementation

Z_1 is multiplied by back-propagation trained ANN weight w_{a1} to obtain weighted Chebyshev expansion Z_{a1}. Similarly, Z_{a2} and Z_{a3} are calculated. Finally, all the product components Z_{a1}, Z_{a2}, Z_{a3} are added and processed by activation function *tanh*. The final output $I_{pa}(k)$ is used further for reference currents calculation.

The following equation is used to train weights of ANN (w_{a1}, w_{a2}, w_{a3}) using back-propagation technique

$$w_{i(k+1)} = w_{i(k)} + \delta \Xi_k (1 - I_{pk})^2 ChP_i(x) \tag{5.60}$$

For phase 'b' and 'c', the fundamental active power component 'I_{pb}', 'I_{pc}' are determined. For the calculation of effective active power component weights corresponding to the all three phases (I_{pa}, I_{pb}, I_{pc}) are averaged to compute an average weight I_{avg}.

$$\boldsymbol{I_{avg}} = \frac{\boldsymbol{I_{pa}} + \boldsymbol{I_{pb}} + \boldsymbol{I_{pc}}}{3} \tag{5.61}$$

The I_{avg} is used further for calculation of reference currents and discussed below.

5.2.2. Generation of Reference Currents for Control of SAPF

A SAPF requires real power from three phase supply to replenish the switching losses in VSC. These losses are modeled as:

$$I_{loss}(k) = I_{loss}(k-1) + K_p\{(e_{dc}(k) - e_{dc}(k-1)\} + K_I[e_{dc}(k)] \tag{3.12}$$

where $e_{dc}(k) = V_{dc}^{*}(k) - V_{dc}(k)$ (3.13)

The I_{loss} is the real power loss in the system, since the IGBT switching losses at high frequency are significant and therefore must be added to I_{pabc}/I_{avg} for effective active power component I_{eff} calculation as follows.

$$I_{eff} = I_{avg} + I_{loss} \tag{5.62}$$

For the generation of reference current for SAPF, unit templates are determined which are used to synchronize the SAPF system to grid voltages. As discussed in chapter 3, the in-phase unit templates are calculated using grid voltages as per Eq. (3.18)

$$u_{ia} = \frac{v_{sa}}{V_t}; u_{ib} = \frac{v_{sb}}{V_t}; u_{ic} = \frac{v_{sc}}{V_t} \tag{3.18}$$

where v_{sa}, v_{sb}, v_{sc} are the three phase supply voltages, and peak value of AC supply voltage V_t is the calculated using

$$V_t = \sqrt{\frac{2}{3}(v_{sa}^2 + v_{sb}^2 + v_{sc}^2)} \tag{3.19}$$

I_{eff} calculated using developed control algorithms is multiplied by unit templates u_{ia}, u_{ib}, u_{ic} to obtain reference currents i_{sa}^*, i_{sb}^*, i_{sc}^*.

$$i_{sa}^* = u_{ia} * I_{eff}; i_{sb}^* = u_{ib} * I_{eff}; i_{sc}^* = u_{ic} * I_{eff} \tag{5.63}$$

Now the reference currents are compared with the actual supply currents sensed through current sensors (i_{sa}, i_{sb}, i_{sc}) to generate switching signals to VSC in HCC. The HCC band is kept at 0.2. Six gating pulses are generated and fed to SAPF for proper operation of SAPF system. The supply currents follow the reference currents and hence become sinusoidal and are balanced and sinusoidal.

5.3 SIMULATION RESULTS

The developed control techniques viz STF, MRGN and ChANN are also simulated in MATLAB/SIMULINK environment. The simulation study on SAPF system is carried out to test the effectiveness of new control techniques for load compensation and PQ improvement in TPFW system. The simulation results for TPFW linear and non-linear loads are discussed in subsequent sections.

5.3.1 Self Tuning Filter Based Control Algorithm

STF based control technique is implemented on a SAPF in a TPFW 110 V, 50 Hz, distribution system with linear and non-linear loads. Fig 5.5 shows the three phase supply voltages (v_{sabc}), three phase supply currents (i_{sabc}), three phase compensating currents (i_{cabc}), three phase non-sinusoidal load currents (i_{Labc}), DC link voltage (V_{dc}) of SAPF and supply

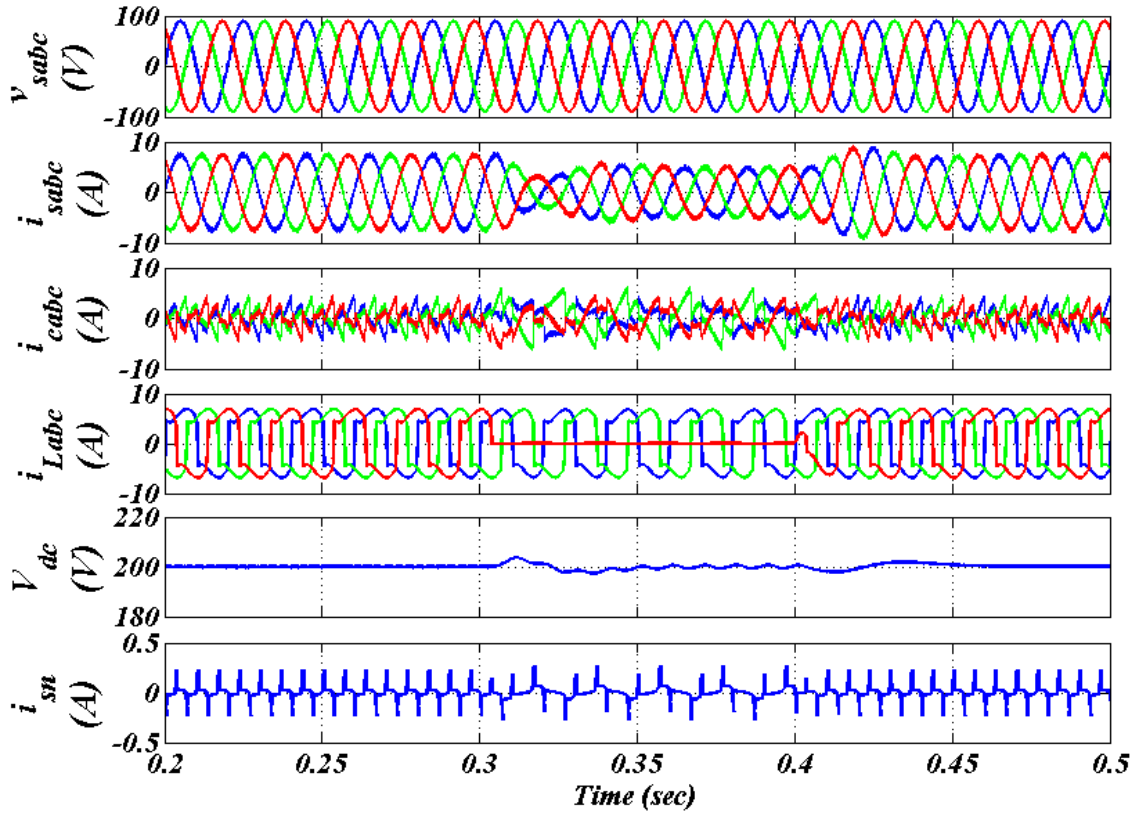

Fig. 5.5 Simulation results using STF based control algorithm for non-linear load.

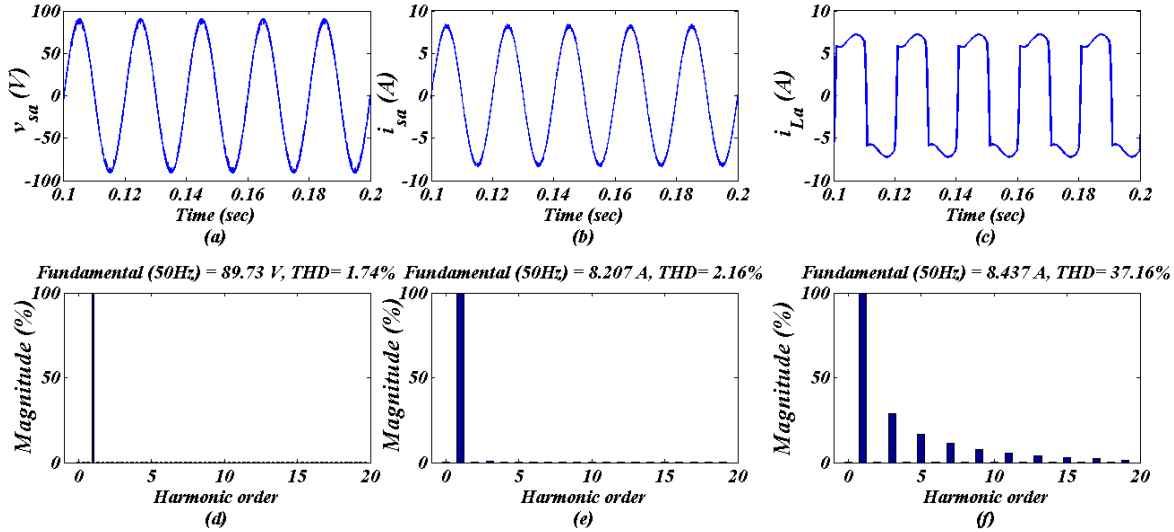

Fig. 5.6 Harmonic analysis using STF based control algorithm (a-c) waveforms of v_{sa}, i_{sa}, i_{La} (d-f) THD of v_{sa}, i_{sa}, i_{La} for non-linear load

neutral current (i_{sn}) with non-linear loads. In TPFW system, three single phase nonlinear loads each comprising of a diode bridge rectifier with a R-L load are considered for analysis. Load currents are distorted and the THD content is higher. An unbalancing at t=0.3 sec to t=0.4 sec is introduced to capture the dynamic performance of SAPF using STF control

technique. The phase 'c' load current is absent during t=0.3 sec to 0.4 sec. The supply currents are perfectly sinusoids. The magnitudes of all source currents are also same which indicates balancing of three phase supply currents on grid side. The DC link is regulated to 200 V and has ripples during unbalancing of loads. The compensating current injected by SAPF helps in improving PQ problem in TPFW supply system. The supply neutral current (i_{sn}) is small during unbalancing period. Figs. 5.6(a)-(c) show waveforms and Figs. 5.6(d)-(f)

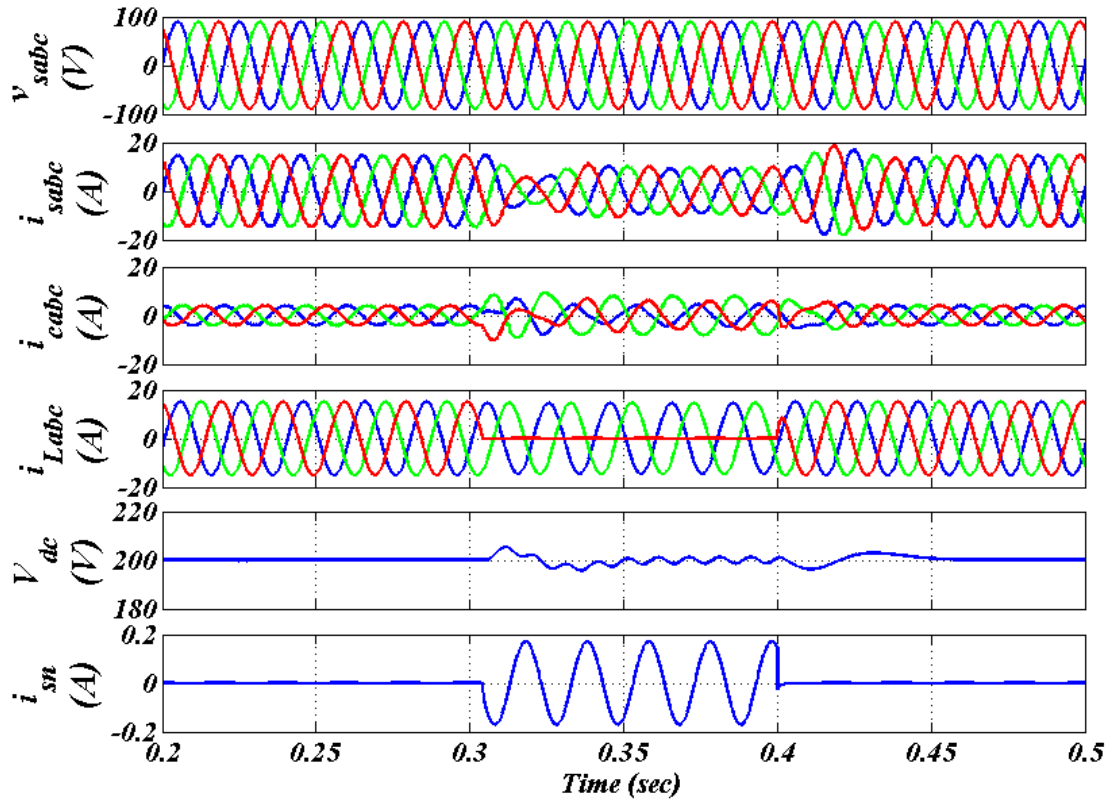

Fig. 5.7 Simulation results using STF based control technique for linear load

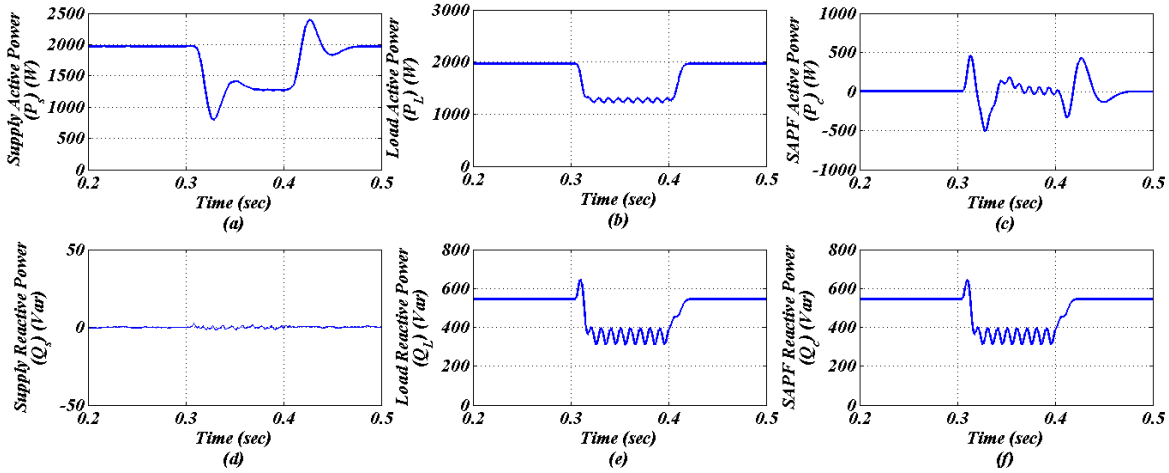

Fig. 5.8 Power flow in TPFW distribution system using STF based control algorithm (a-c) Active power P_s, P_L, P_c (d-f) Reactive Power Q_s, Q_L, Q_c for linear load

show harmonic spectra of phase 'a' supply voltage (v_{sa}), phase 'a' supply current (i_{sa}) and phase 'a' load current (i_{La}) respectively. The phase 'a' supply voltage (v_{sa}), phase 'a' supply current (i_{sa}) and phase 'a' load current (i_{La}) have a THD of 1.74%, 2.16% and 37.16% respectively. The STF algorithm has effectively reduced the harmonics in the TPFW supply system. The currents and voltages have THD content lower than prescribed in IEEE 519 [40].

Fig 5.7 shows the three phase supply voltages (v_{sabc}), three phase supply currents (i_{sabc}), three phase compensating currents (i_{cabc}), three phase lagging PF load currents (i_{Labc}), DC link voltage (V_{dc}) of SAPF and supply neutral current (i_{sn}) with linear load. The load has active power demand of 2000 W and reactive power demand of 550 VARs. The load PF is lagging. An unbalancing at t=0.3 is introduced and restored at t=0.4 sec. However, the supply currents are still balanced and in-phase with the supply voltages. The SAPF provides reactive support and helps to improve supply PF close to unity even though load has a lagging PF. The supply neutral current (i_{sn}) is close to zero and unaffected by unbalancing effect in phase 'c' due to load removal.

Figs. 5.8(a)-(f) show the power balance between supply, load and SAPF compensator. The load demands 2000 W real power and 550 VARs of reactive power, out of which active power is supplied by TPFW supply system and reactive power is provided by compensator. The reactive power drawn from AC supply is nearly zero; and the real power consumed by compensator is quite small. This power balance is also valid during unbalancing period, t=0.3 sec to t=0.4 sec.

5.3.2 Modified Recursive Gauss Newton Based Control Algorithm

The modified RGN based control scheme for SAPF in a 110 V (L-L), 50 Hz, TPFW distribution system with non-linear load is simulated in MATLAB/SIMULINK Fig 5.9 presents the three phase supply voltages (v_{sabc}), three phase supply currents (i_{sabc}), three phase compensating currents (i_{cabc}), three phase non-linear load currents (i_{Labc}), DC link voltage

(V_{dc}) of SAPF and supply neutral current (i_{sn}) in a TPFW distribution system feeding non-linear load. In this case, three, single phase diode bridge rectifiers are used as load and one terminal of all the bridge rectifiers input side is made common and connected to load neutral point. The load currents are non-sinusoidal and distorted. This TPFW distribution system with nonlinear load is subjected to unbalance condition by sudden removal of phase 'c'

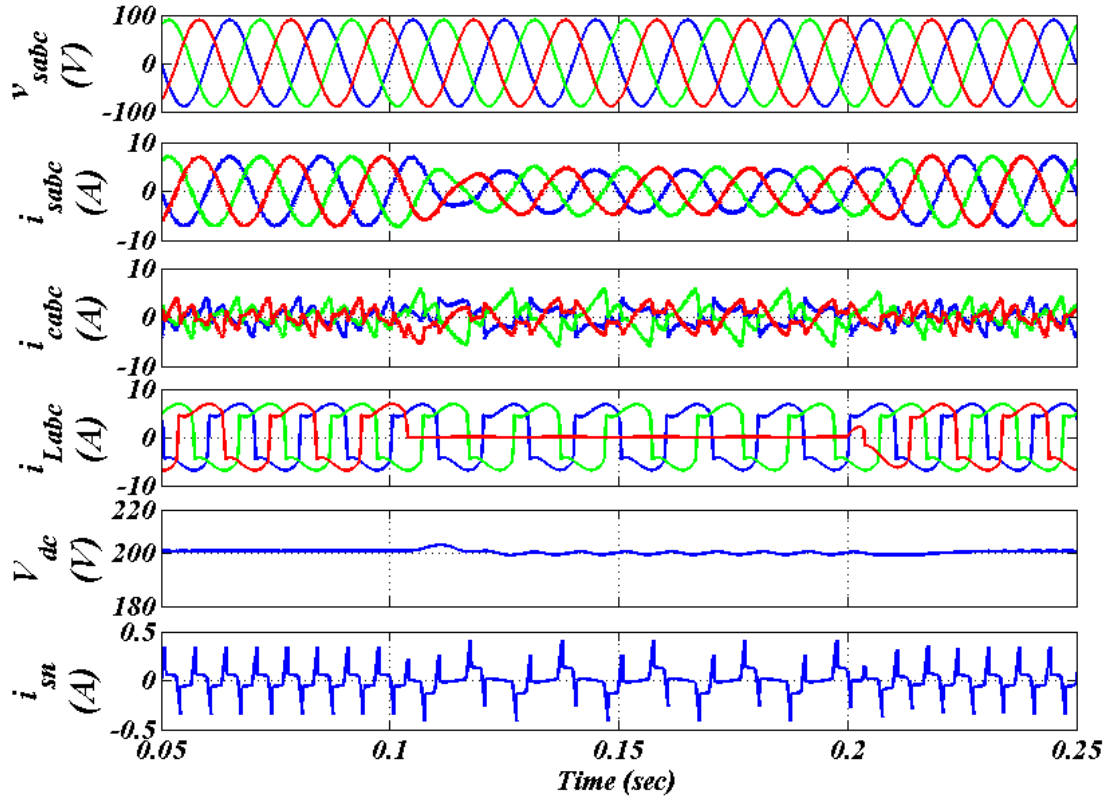

Fig. 5.9 Simulation results using MRGN control algorithm for non-linear load.

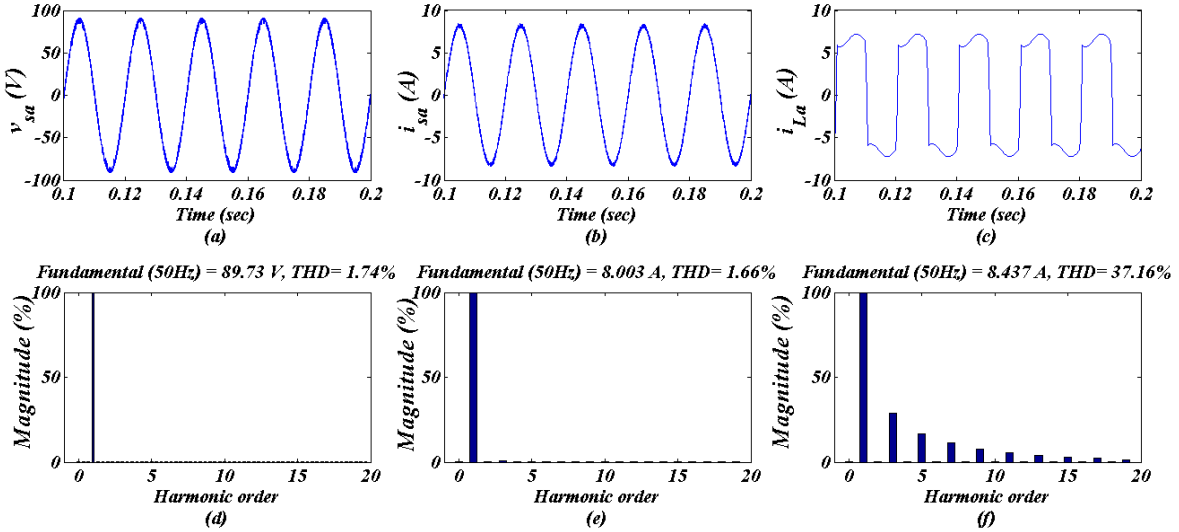

Fig. 5.10 Harmonic analysis using MRGN control algorithm (a-c) waveforms of v_{sa}, i_{sa}, i_{La} (d-f) THD of v_{sa}, i_{sa}, i_{La} for non-linear load

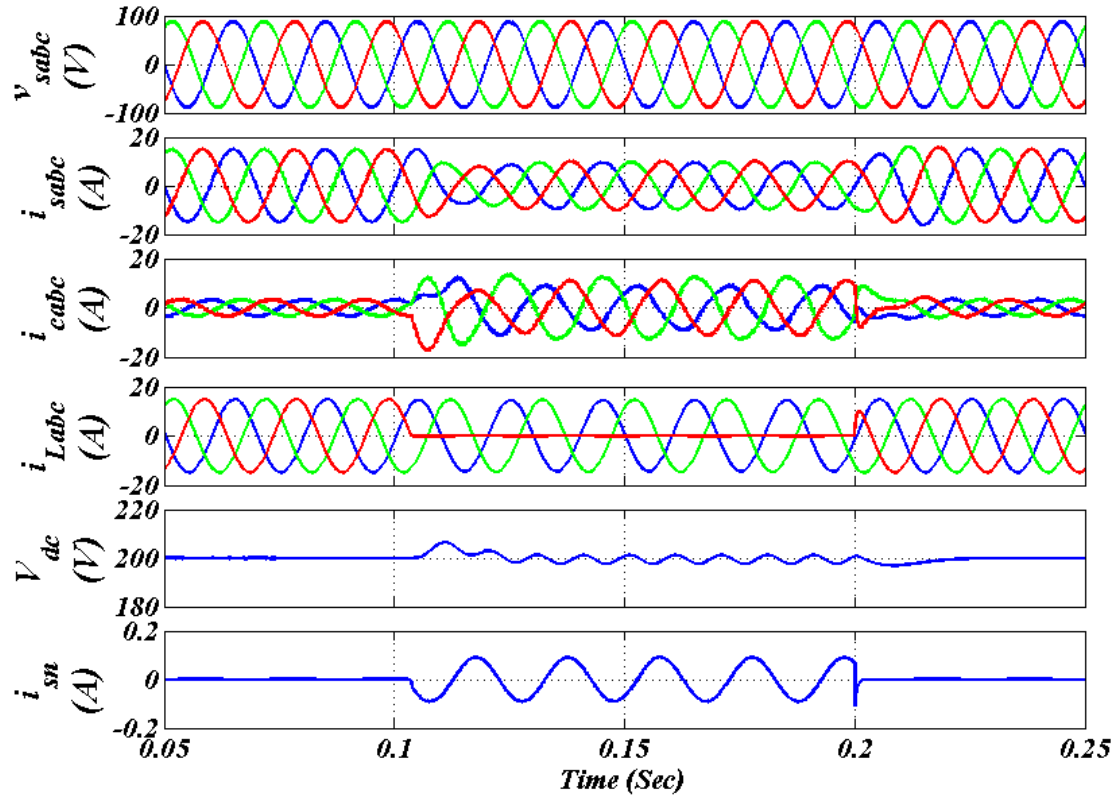

Fig. 5.11 Simulation results using MRGN control algorithm for linear load.

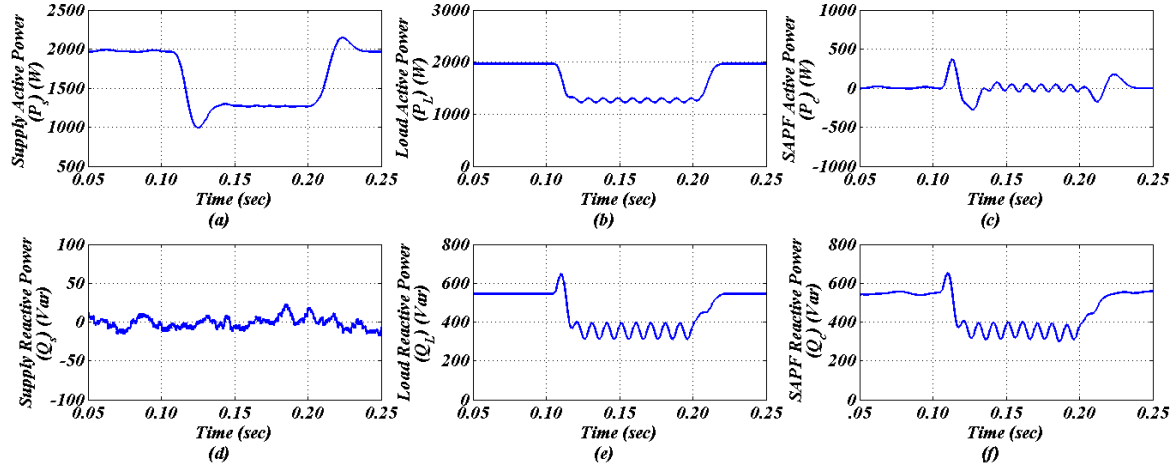

Fig. 5.12 Power flow in TPFW distribution system using MRGN control algorithm (a-c) Active power P_s, P_L, P_c (d-f) Reactive Power Q_s, Q_L, Q_c

during t=0.1 sec to t=0.2 sec. The MRGN based control of SAPF works satisfactorily to generate appropriate reference currents for gating pulses generation of the SAPF. The DC link voltage is maintained constant at 200 V by PI controller. The supply neutral current is also limited during unbalancing. Figs. 5.10(a)-(c) show waveforms of phase 'a' sinusoidal supply voltage (v_{sa}), phase 'a' sinusoidal supply current (i_{sa}) and non-sinusoidal phase 'a' load current (i_{La}) and Figs. 5.10(d)-(f) show their harmonic spectra respectively. The PCC

voltage has a THD of 1.74%. The load currents are non-sinusoidal with a THD of 37.16%. The supply current THD has improved to 1.66% due to harmonic compensation by SAPF.

Fig 5.11 presents the three phase supply voltages (v_{sabc}), three phase supply currents (i_{sabc}), three phase compensating currents (i_{ca}, i_{cb}, i_{cc}), three phase lagging PF load currents (i_{La}, i_{Lb}, i_{Lc}), DC link voltage (V_{dc}) of SAPF and supply neutral current (i_{sn}) with linear load. The load is inductive in nature and has poor power factor. The control algorithm generates reference currents which are in-phase with the grid voltages results in better PF at PCC. SAPF injects compensation currents to improve PQ of the supply. During load unbalancing period t=0.1 sec to 0.2 sec, the supply currents are observed to be balanced and

in-phase with the grid voltages. The load neutral current passes through zigzag transformer neutral path and supply neutral conductor has low current.

Figs. 5.12(a)-(f) present the power flow between supply, load and SAPF in TPFW distribution system. The linear load is inductive and it demands 2000 W active power and 550 VARs reactive power under steady state. The controller to SAPF ensures that real power demand of 2000 W is delivered by the grid. The reactive power demand of load is met from the SAPF compensator and real power demand of the load and also the switching losses within SAPF are delivered by grid. The SAPF on the contrary supplies only reactive power burden of the load. During unbalance load condition i.e. from t=0.1 sec to t=0.2 sec, the active and reactive power requirement of the load is reduced so the active power is delivered from supply and reactive power supplied by SAPF.

5.3.3. *ChANN* Based Control Algorithm

In this section, simulation results of SAPF control using *ChANN* control technique for TPFW 110 V, 50 Hz distribution system are discussed. Fig 5.13 shows the three phase supply voltages (v_{sabc}), three phase supply currents (i_{sabc}), three phase compensating currents (i_{cabc}), three phase non-sinusoidal load currents (i_{Labc}), DC link voltage (V_{dc}) of SAPF and supply

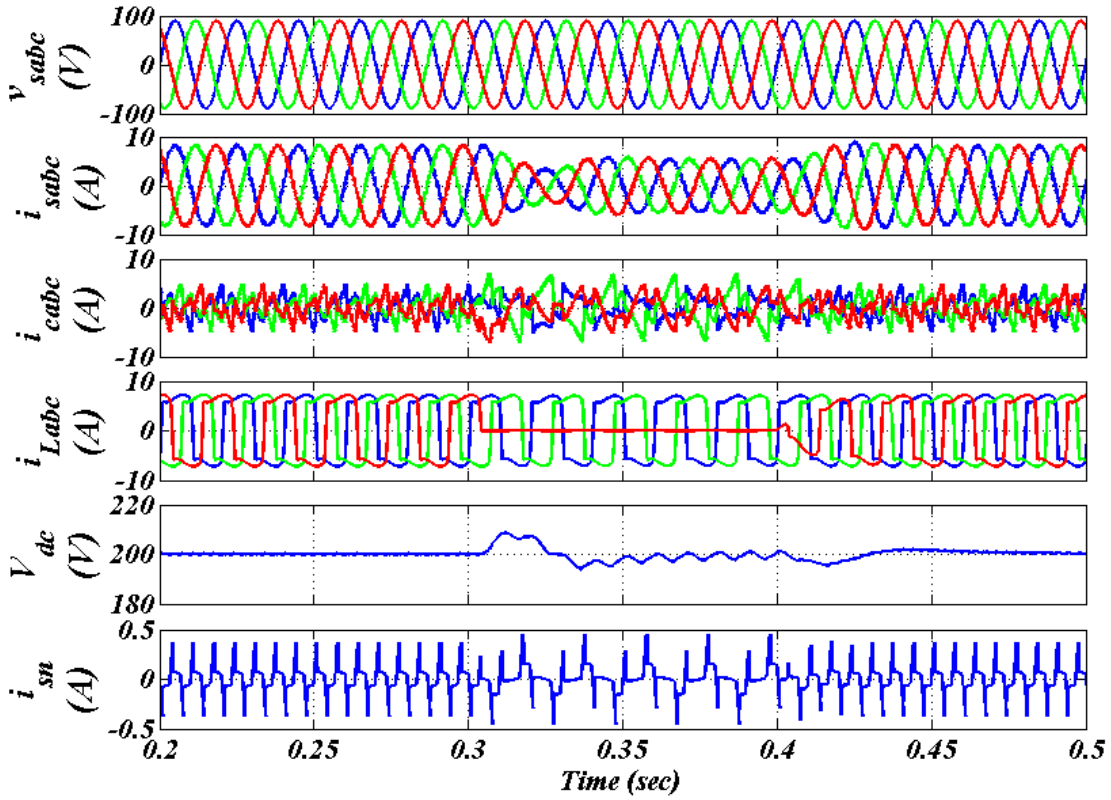

Fig. 5.13 Simulation results using *ChANN* control algorithm for non-linear load.

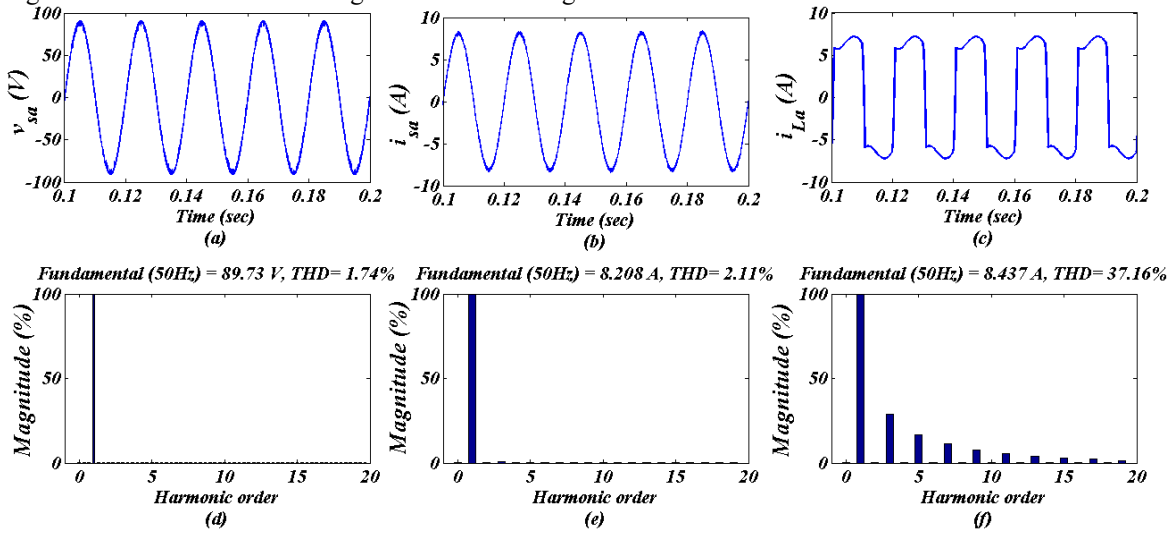

Fig. 5.14 Harmonic analysis using *ChANN* control algorithm (a-c) waveforms of v_{sa}, i_{sa}, i_{La} (d-f) THD of v_{sa}, i_{sa}, i_{La} for non-linear load

neutral current (i_{sn}) of a TPFW system with non-linear load. The grid voltage supply is considered to be sinusoidal and balanced feeding non-linear loads. The supply currents are non-sinusoidal and distorted in absence of SAPF. However, in presence of SAPF the supply currents are distortion free and in-phase with the AC supply. The *ChANN* control technique for SAPF generates appropriate compensating currents and improves PQ on the supply side.

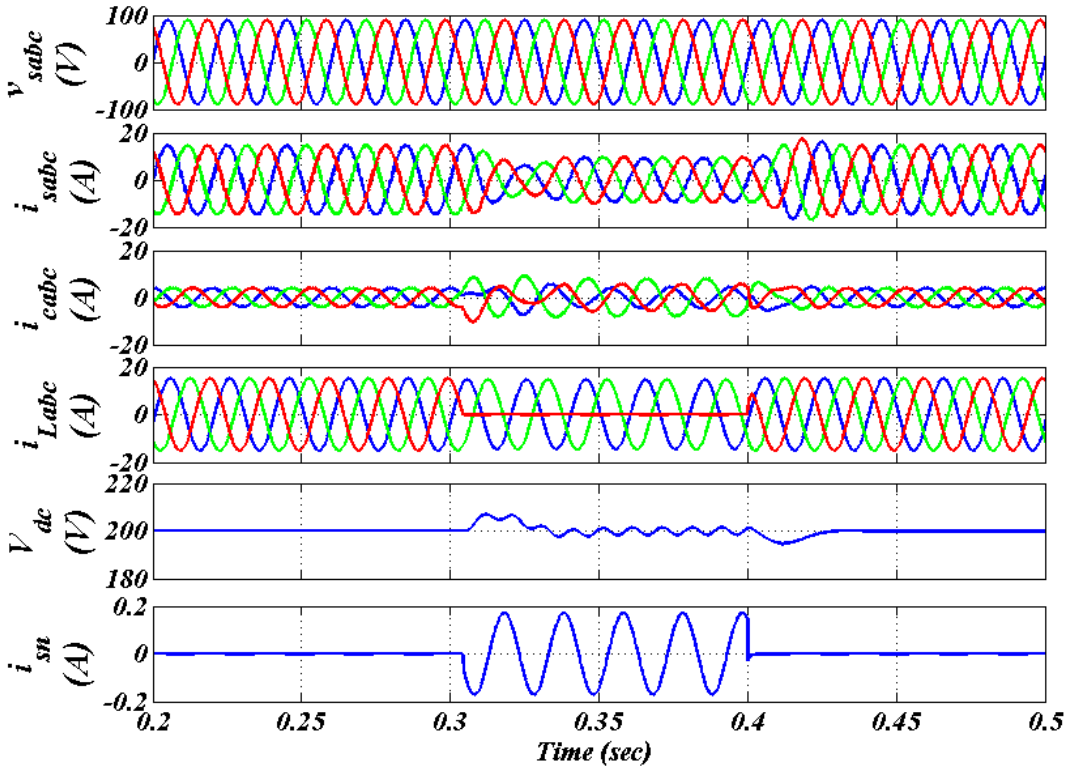

Fig. 5.15 Simulation results using *ChANN* control algorithm for linear load.

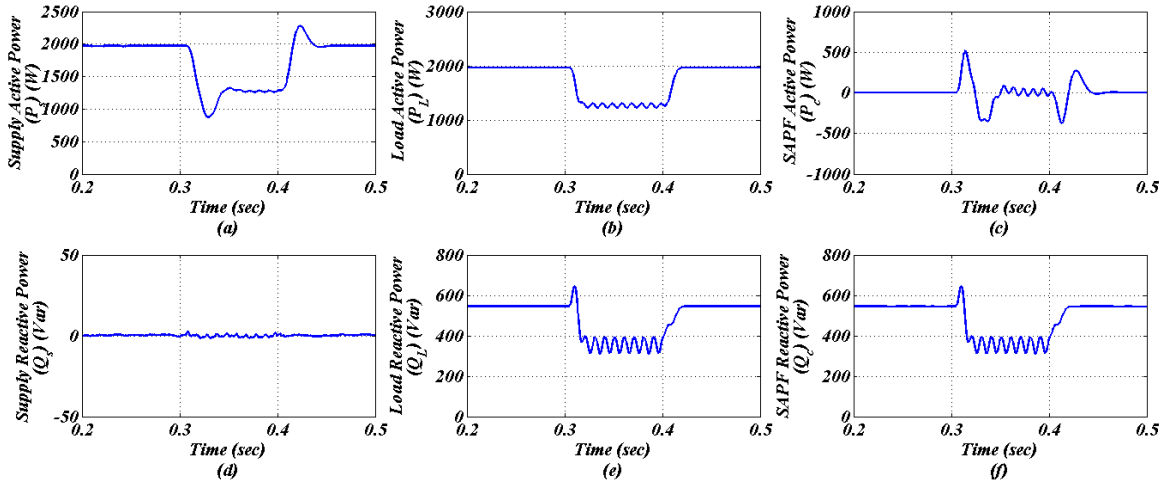

Fig. 5.16 Power flow in TPFW distribution system using *ChANN* control algorithm (a-c) Active power P_s, P_L, P_c (d-f) Reactive Power Q_s, Q_L, Q_c for linear load

Load unbalancing is introduced in the system at t= 0.3 till t= 0.4 sec. The *ChANN* control technique works effectively for load compensation. The DC link voltage is regulated by a P-I controller. The supply neutral current is negligible small.

In Figs. 5.14(a)-(c) waveforms of phase 'a' supply voltage (v_{sa}), phase 'a' shunt compensated supply current (i_{sa}) and phase 'a' non-sinusoidal load current (i_{La}) and in Figs. 5.14(d)-(f) their harmonic spectra are shown. The PCC voltage, supply current and load current have a

THD of 1.74%, 2.11 and 37.16% respectively.

Fig 5.15 shows three phase supply voltages (v_{sabc}), three phase supply currents (i_{sabc}), three phase compensating currents (i_{cabc}), three phase lagging PF load currents (i_{Labc}), DC link voltage (V_{dc}) of SAPF and supply neutral current (i_{sn}) of a TPFW system with linear load. The load is consisting of resistor and inductor and demands reactive power. The PI controller keeps DC link voltage well regulated to its reference value of 200V. SAPF injects necessary compensating currents of proper magnitude using the *ChANN* control technique. The neutral current of supply is observed to be almost zero and the entire neutral current of load passes through the zigzag transformer. Figs. 5.16(a)-(f) show the power flow in TPFW system. The supply active power (P_s), reactive power (Q_s), load active power (P_L), reactive power (Q_L), compensator active power (P_c), reactive power (Q_c) have been plotted. The supply active power includes the load active power demand and compensator losses. The compensator reactive power includes load reactive power demand. The reactive power burden on the grid side is reduced.

5.4 EXPERIMENTAL RESULTS

The developed control algorithms in this chapter have been implemented on prototype hardware controlled using dSPACE1104 DSP controller. The hardware is tested and real time signals have been captured with the help of DSO, single phase power analyzer FLUKE 43B and three phase power analyzer FLUKE 434. The experimental results are discussed in this section.

5.4.1. Self Tuning Filter Based Control Algorithm

A hardware setup for SAPF based compensator in a TPFW system of 110 V (L-L), 50 Hz, feeding nonlinear load is developed and tested under different load conditions. Fig. 5.17(a)-(c) show phase ‘a’ sinusoidal supply current (i_{sa}), phase ‘a’ non-sinusoidal load current (i_{La}) and phase ‘a’ shunt injected compensator current (i_{ca}) along with phase ‘a’ supply voltage

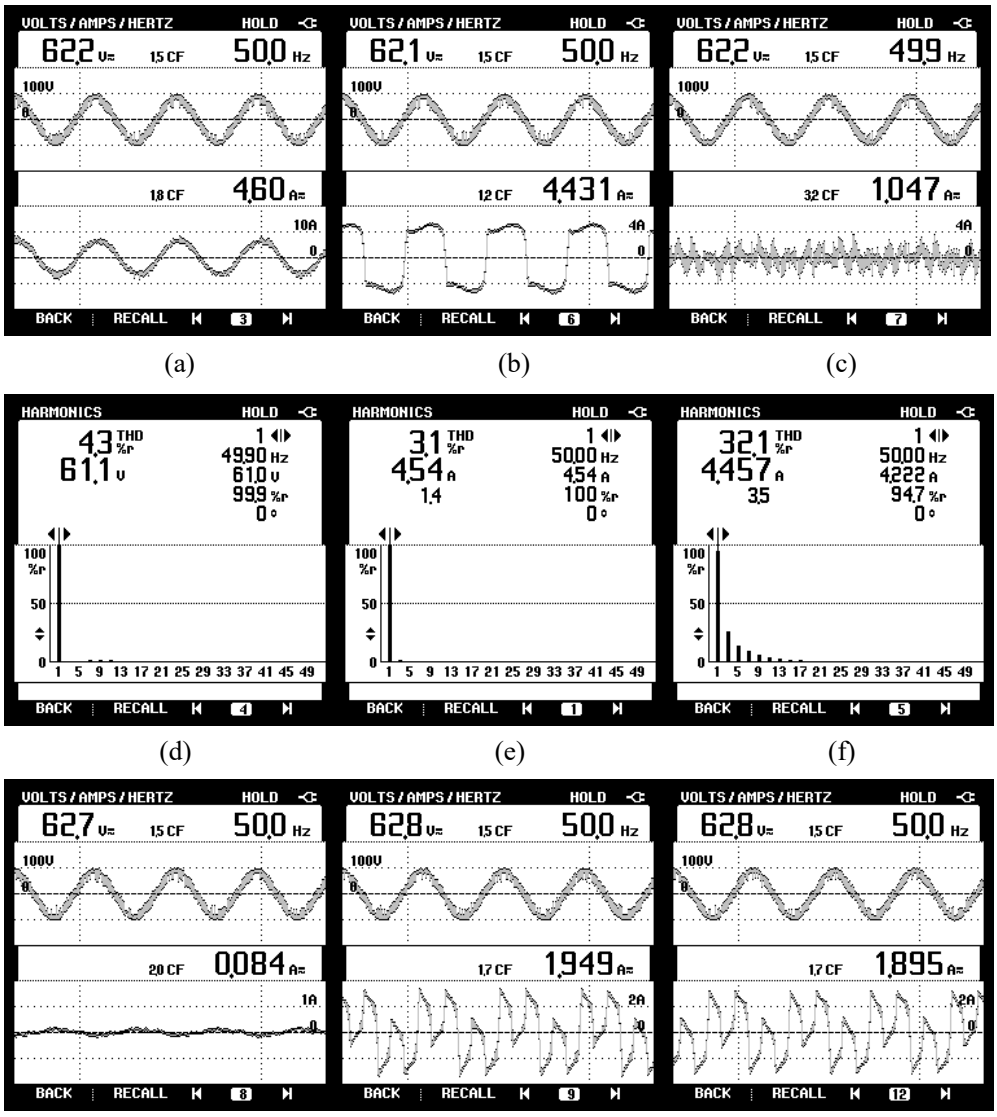

Fig. 5.17 Steady state waveforms for TPFW system using STF based control algorithm (a) v_{sa}-i_{sa} (b) v_{sa}-i_{La} (c) v_{sa}-i_{ca} and (d-f) THD of (d) v_{sa} (e) i_{sa} (f) i_{La} (g-i) neutral current of (g) supply (i_{sn}) (h) load (i_{Ln}) and (i) zigzag transformer (i_{zn}) for non-linear load

(v_{sa}). The load is nonlinear but the supply current has become sinusoidal. Figs. 5.17(d)-(f) show the harmonic content in phase 'a' supply voltage (v_{sa}), phase 'a' supply current (i_{sa}) and phase 'a' load current (i_{La}) respectively. The supply voltage has a THD of 4.3% which is within the prescribed limit of IEEE 519 [40]. The supply current has THD of 3.1%, whereas the load current has a THD of 32.1%. The installation and proper control of SAPF helps in achieving balanced and sinusoidal supply currents. Figs. 5.17(g)-(i) show the supply neutral current (i_{sn}), load neutral current (i_{Ln}) and zigzag transformer neutral current (i_{zn}) along with phase 'a' supply voltage. The supply neutral current is small in magnitude and has a value of

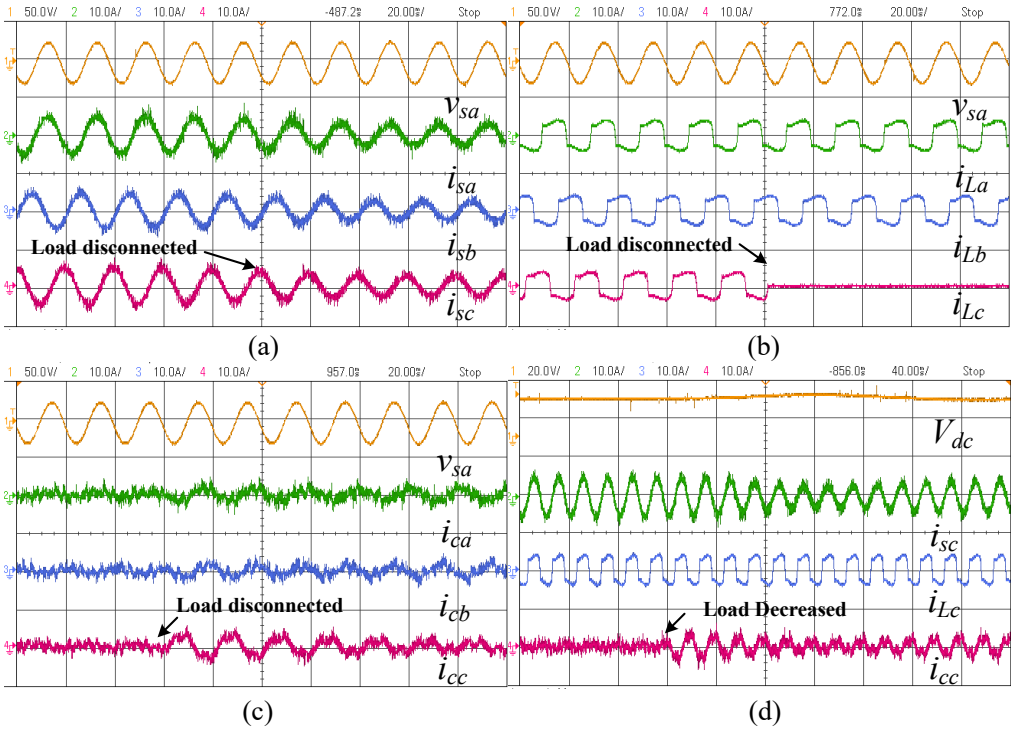

Fig. 5.18 Results showing dynamics in phase 'c' using STF based control algorithm (a) v_{sa}, i_{sa}, i_{sb}, i_{sc} (b) v_{sa}, i_{La}, i_{Lb}, i_{Lc} (c) v_{sa}, i_{ca}, i_{cb}, i_{cc} (d) V_{dc}, i_{sc}, i_{Lc}, i_{cc} for nonlinear load

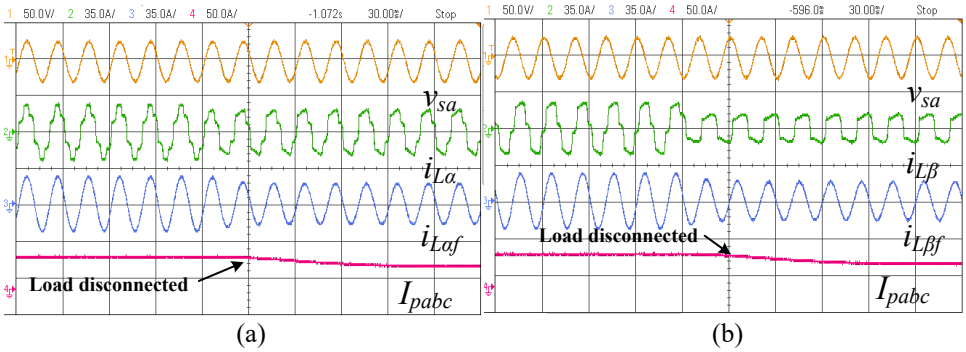

Fig. 5.19 Intermediate signals using STF based control algorithm (a) v_{sa}, i_{La}, i_{Laf}, I_{pabc} (b) v_{sa}, $i_{L\beta}$, $i_{L\beta f}$, I_{pabc} for non-linear load

0.084 A. The neutral current in load and zigzag transformer have almost equal magnitude so all the neutral load current during load unbalancing period gets transferred to zigzag transformer and supply neutral current remains negligible.

Fig. 5.18 shows the dynamic performance of the TPFW system using STF control technique with non-linear load. Fig. 5.18(a) shows phase 'a' supply voltage (v_{sa}) and three phase balanced and sinusoidal supply currents (i_{sa}, i_{sb}, i_{sc}). The supply currents remain are at lower magnitude during load unbalance period. The supply currents are sinusoidal. Fig. 5.18(b)

shows phase ‘a’ supply voltage (v_{sa}) and three phase non-sinusoidal load currents (i_{La}, i_{Lb}, i_{Lc}), which presents the effect of unbalanced load. Fig. 5.18(c) shows phase ‘a’ supply voltage (v_{sa}) and three phase compensator currents (i_{ca}, i_{cb}, i_{cc}). The compensator currents help in balancing the supply currents during unbalancing period and keep it sinusoidal. Fig. 5.18(d) shows DC link voltage (V_{dc}) of SAPF and all three phase ‘c’ supply, load, compensator currents (i_{sc}, i_{Lc}, i_{cc}). It is observed that STF based algorithm has been effective in improving PQ problems and the DC link voltage is maintained at 200 V during varying load conditions. Fig. 5.19 shows the intermediate results in the STF control technique for SAPF with non-linear load. Fig 5.19(a) shows the phase ‘a’ supply voltage (v_{sa}), Clarke’s transformed α-component of load current ($i_{L\alpha}$), load current filtered α-component ($i_{L\alpha f}$) and fundamental active power component of phase ‘c’. The STF has been able to extract fundamental frequency component from the distorted α-component of load current ($i_{L\alpha}$). This helps in generation of appropriate reference currents. Fig. 5.19(b) shows phase ‘a’ supply voltage (v_{sa}), Clark transformed β-component of load current ($i_{L\beta}$), load current filtered β-component ($i_{L\beta f}$) and fundamental active power component of phase ‘c’. The STF has been also able to extract fundamental frequency component from the distorted β-component of load current ($i_{L\beta}$).

Fig. 5.20 shows the steady state waveforms in TPFW distribution system with SAPF feeding linear load. Figs. 5.20(a)-(c) show steady state power flow in TPFW distribution system using STF based control algorithm The active and reactive power are measured with the help of FLUKE434 power quality analyzer. The supply delivers active power (690 W) and reactive power (170 VARs), where the load demands active power 610 W and reactive power demand 350 VARs. The excess active power of supply is used to feed compensator switching losses of 70 W. The SAPF feeds 180 capacitive VARs into the system. Figs. 5.20(d)-(f) present the supply neutral current (i_{sn}), load neutral current (i_{Ln}) and zigzag transformer

neutral current (i_{zn}) and phase 'a' supply voltage (v_{sa}). The supply neutral current is small in magnitude and equal to 0.055 A. The zigzag transformer neutral current is 0.932 A and load neutral current is 0.957 A so a major part of the load neutral current during load unbalancing

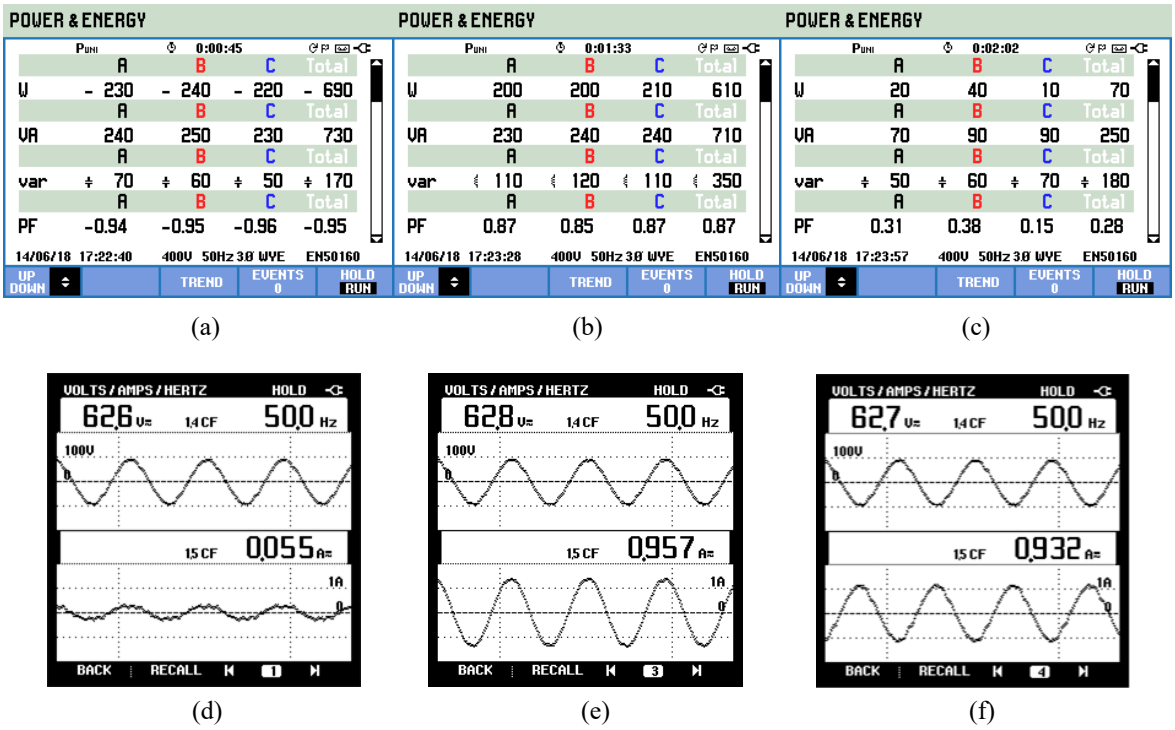

Fig. 5.20 (a-c) Steady state power for TPFW linear system using STF based control algorithm for (a) Supply (b) Load (c) Compensator and (d-f) neutral current of (d) supply (i_{sn}) (e) load (i_{Ln}) and (f) zigzag transformer

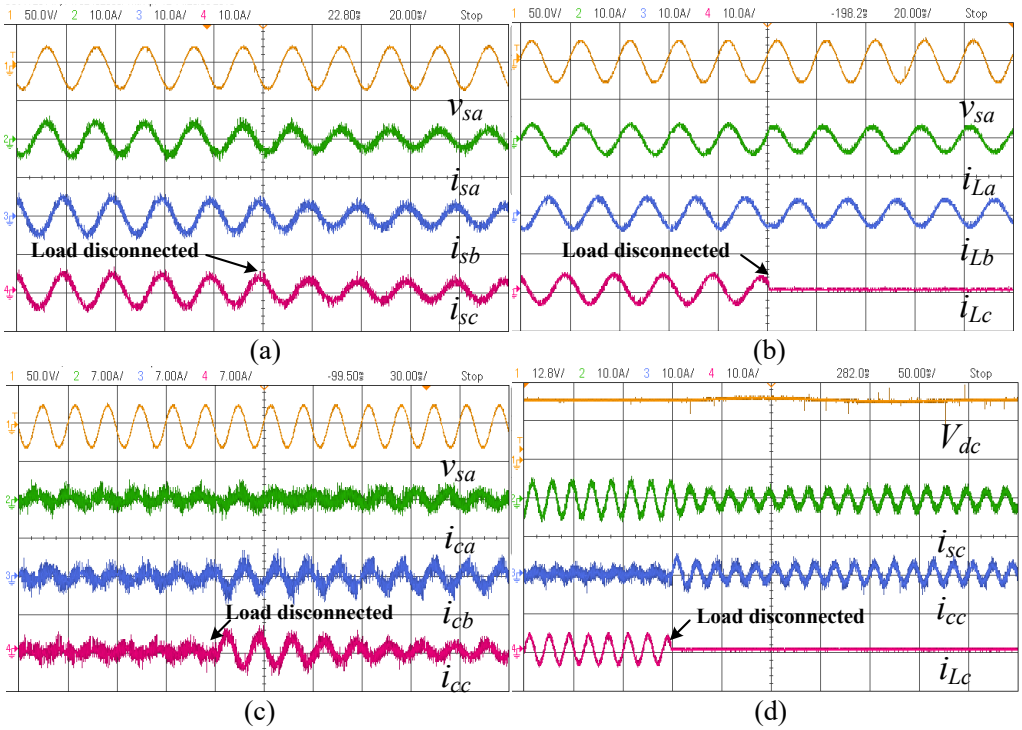

Fig. 5.21 Results showing dynamics for load disconnected in phase 'c' using STF based control algorithm (a) v_{sa}, i_{sa}, i_{sb}, i_{sc} (b) v_{sa}, i_{La}, i_{Lb}, i_{Lc} (c) v_{sa}, i_{ca}, i_{cb}, i_{cc} (d) V_{dc}, i_{sc}, i_{cc}, i_{Lc} for linear load

is transferred to zigzag transformer and only a very small part enters the supply neutral.

Fig. 5.21 shows the dynamic performance of the TPFW system with SAPF using STF control technique and linear loads. Fig. 5.21(a) shows phase 'a' supply voltage (v_{sa}) and SAPF compensated three phase supply currents (i_{sa}, i_{sb}, i_{sc}). The supply currents are observed to be balanced and sinusoidal. Fig. 5.21(b) shows phase 'a' supply voltage (v_{sa}) and three phase lagging PF load currents (i_{La}, i_{Lb}, i_{Lc}). During sudden removal of phase 'c', the phase 'c' load current reduces to zero. 5.21(c) shows phase 'a' supply voltage (v_{sa}) and three phase shunt injected compensator currents (i_{ca}, i_{cb}, i_{cc}). The phase 'c' compensator current is exact replica of supply phase 'c' current during load unbalancing case. 5.21(d) shows DC link voltage (V_{dc}) of SAPF and all three phase 'c' supply, compensator and load currents (i_{sc}, i_{cc}, i_{Lc}). Fig. 5.22 shows the intermediate results for the STF control technique with linear load. Fig 5.22 (a) shows the phase 'a' supply voltage (v_{sa}), Clarke's transformed α-component of load current ($i_{L\alpha}$), load current filtered α-component ($i_{L\alpha f}$) and fundamental active power component of phase 'c' (I_{pc}). The STF extracts the noise free fundamental component from $i_{L\alpha}$. Fig. 5.22(b) shows phase 'a' supply voltage (v_{sa}), Clarke's transformed β-component of load current ($i_{L\beta}$), load current filtered β-component ($i_{L\beta f}$) and fundamental active power component of phase 'c' I_{pc}. The α-component and β-component of load currents are necessary for generation of suitable magnitude of reference currents for providing required compensation.

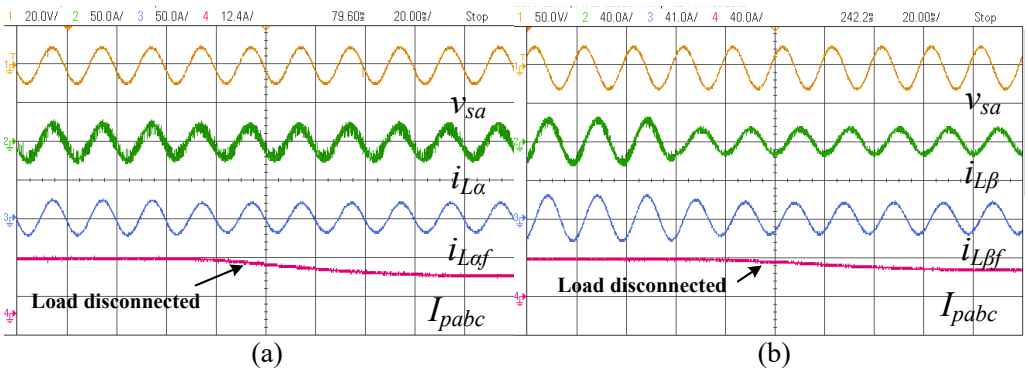

(a) (b)

Fig. 5.22 Intermediate results using STF based control algorithm (a) v_{sa}, i_{La}, $i_{La f}$, I_{pabc} (b) v_{sa}, $i_{L\beta}$, $i_{L\beta f}$, I_{pabc} for linear load

5.4.2. Modified Recursive Gauss Newton Based Control Algorithm

Fig. 5.23 shows the steady state waveforms in TPFW 110 V (L-L), 50 Hz distribution system with SAPF feeding non-linear load using MRGN control Technique. Figs. 5.23(a)-(c) show phase 'a' supply current (i_{sa}), phase 'a' load current (i_{La}) and phase 'a' compensator current (i_{ca}) and phase 'a' supply voltage (v_{sa}). The supply currents are in-phase with supply voltages. Figs. 5.23(d)-(f) show the harmonic content for the phase 'a' supply voltage (v_{sa}), phase 'a' supply current (i_{sa}) and phase 'a' load current (i_{La}). The THD of supply voltage is 4.1%. The supply current has THD of 3.4%, which is higher than that observed with STF control technique under similar loading conditions. The load current has a THD of 32.1%. The

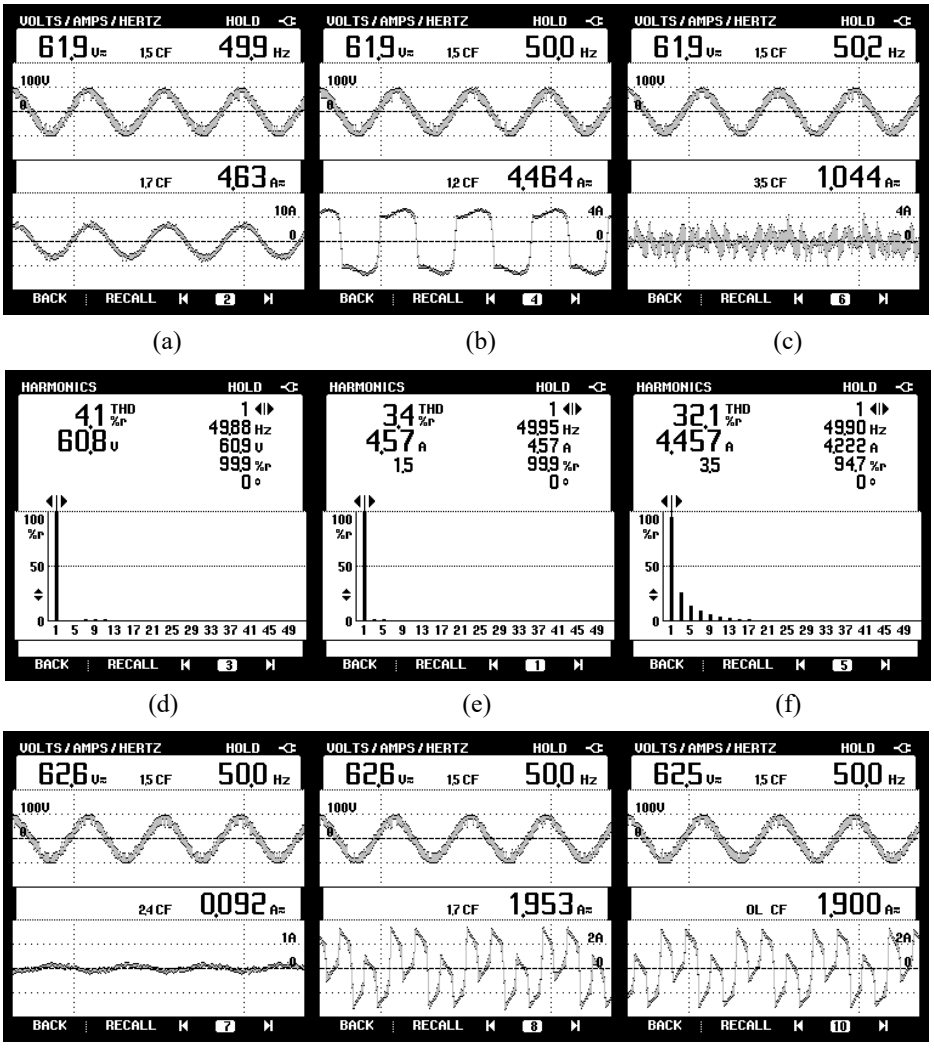

(a) (b) (c)

(d) (e) (f)

(g) (h) (i)

Fig. 5.23 Steady state waveforms for TPFW system using MRGN control algorithm (a) v_{sa}-i_{sa} (b) v_{sa}-i_{La} (c) v_{sa}-i_{ca} and (d-f) THD of (d) v_{sa} (e) i_{sa} (f) i_{La} (g-i) neutral current of (g) supply (i_{sn}) (h) load (i_{Ln}) and (i) zigzag transformer (i_{zn}) for non-linear load

supply current and PCC voltage have low distortions and meet the THD limits as specified by IEEE 519 [40]. Figs. 5.23(g)-(i) show the supply neutral current (i_{sn}), load neutral current (i_{Ln}) and zigzag transformer neutral current (i_{zn}) along with phase 'a' supply voltage (v_{sa}). The supply neutral current like in the case of STF is very small and has a value of 0.092 A. The neutral current in load has magnitude of 1.953 A and zigzag transformer neutral current has magnitude of 1.90 A.

Fig. 5.24 shows the dynamic performance of the TPFW system with SAPF and MRGN control technique for non-linear load. Fig. 5.24(a) shows phase 'a' sinusoidal supply voltage (v_{sa}) and three phase SAPF compensated supply currents (i_{sa}, i_{sb}, i_{sc}). The supply currents are sinusoidal and balanced. Fig. 5.24(b) shows phase 'a' supply voltage (v_{sa}) and three phase non-sinusoidal and unbalanced load currents (i_{La}, i_{Lb}, i_{Lc}). The unbalancing in phase 'c' is introduced by sudden removal of phase 'c' supply. However, it does not affect waveforms of phase 'a' and 'b' currents. 5.24(c) shows phase 'a' supply voltage (v_{sa}) and the three phase compensator currents (i_{ca}, i_{cb}, i_{cc}). The compensator currents are injected by the SAPF so that

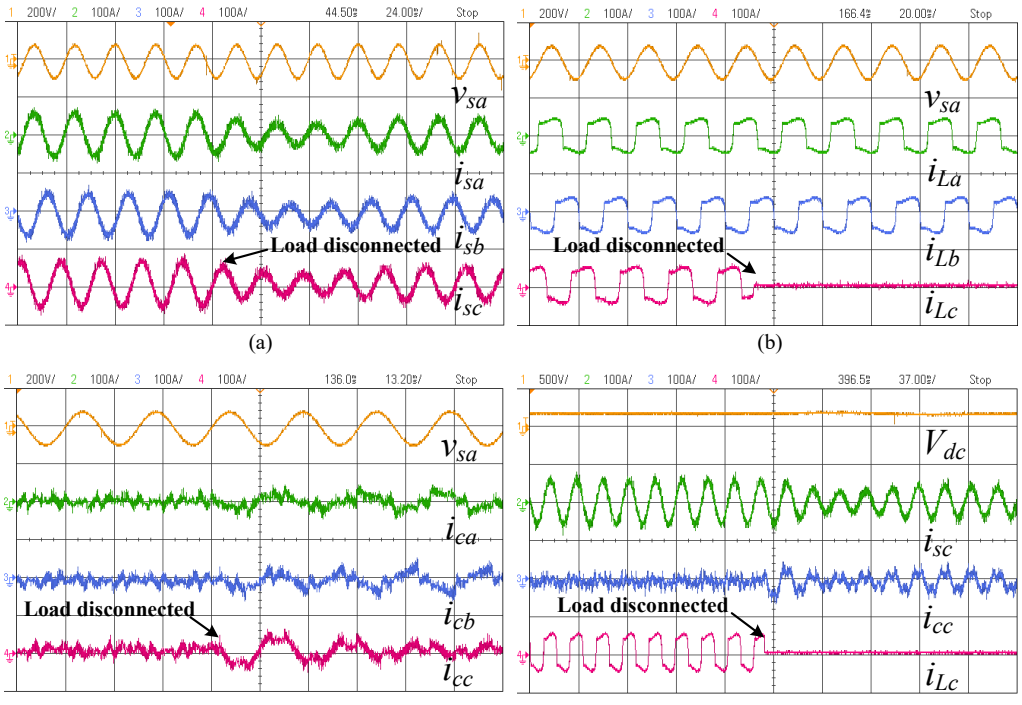

Fig. 5.24 Results showing dynamics for load disconnected in phase 'c' using MRGN control algorithm (a) v_{sa}, i_{sa}, i_{sb}, i_{sc} (b) v_{sa}, i_{La}, i_{Lb}, i_{Lc} (c) v_{sa}, i_{ca}, i_{cb}, i_{cc} (d) V_{dc}, i_{sc}, i_{cc}, i_{Lc} for non-linear load

the supply currents remain balanced and sinusoidal. 5.24(d) shows DC link voltage (V_{dc}) of SAPF and phase 'c' supply current (i_{sc}), compensator current (i_{cc}) and load current (i_{Lc}). The effect of disconnection of phase 'c' of load on three phase AC supply in presence of SAPF has been analyzed. The compensator acts under these conditions and injects higher currents during unbalanced condition compared to that of balanced load condition. The DC link voltage is observed to be changed slightly due to sudden load removal but settles down soon to reference value of 200V. Fig. 5.25 shows the intermediate signals in the MRGN control technique for non-linear load. Fig 5.25(a) shows the average fundamental active power component (I_{avg}), phase 'a' fundamental active power component (I_{pa}), phase 'b' fundamental active power component (I_{pb}) and phase 'c' fundamental active power component (I_{pc}). The fundamental active power component of phase 'a' and 'b' are unaffected and I_{pc} is reduced to zero. Fig. 5.25(b) shows the DC link voltage (V_{dc}) of SAPF, supply neutral current (i_{sn}), neutral current in load (i_{Ln}) and the zigzag transformer neutral current (i_{Zn}). During unbalanced load period, the load and zigzag transformer neutral current are higher but the supply neutral current remains close to zero. This demonstrates the effect of zigzag transformer in achieving neutral current compensation.

Fig. 5.26 shows the steady state power balance between supply, load and SAPF. The supply feeds active power (690 W), reactive power (170 VARs) and SAPF feeds the reactive power (180 VARs), load power demand of 610 W active and 350 VARs reactive. The SAPF

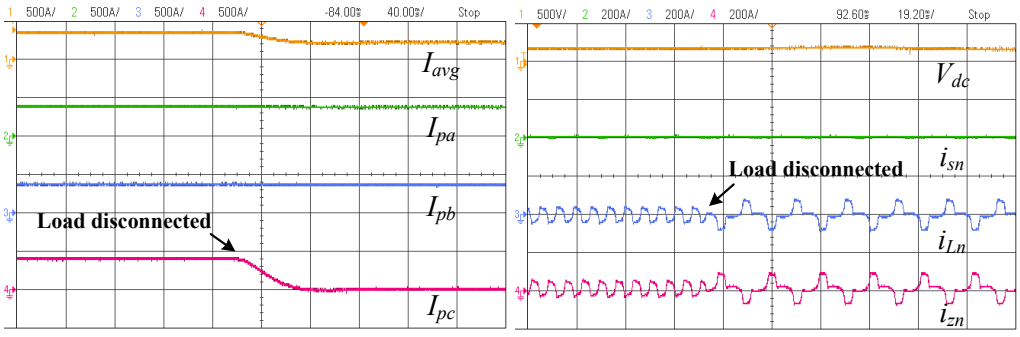

(a) (b)

Fig. 5.25 Intermediate results using MRGN control algorithm (a) I_{avg}, I_{pa}, I_{pb}, I_{pc} (b) V_{dc}, i_{sn}, i_{Ln}, i_{zn} for non-linear load

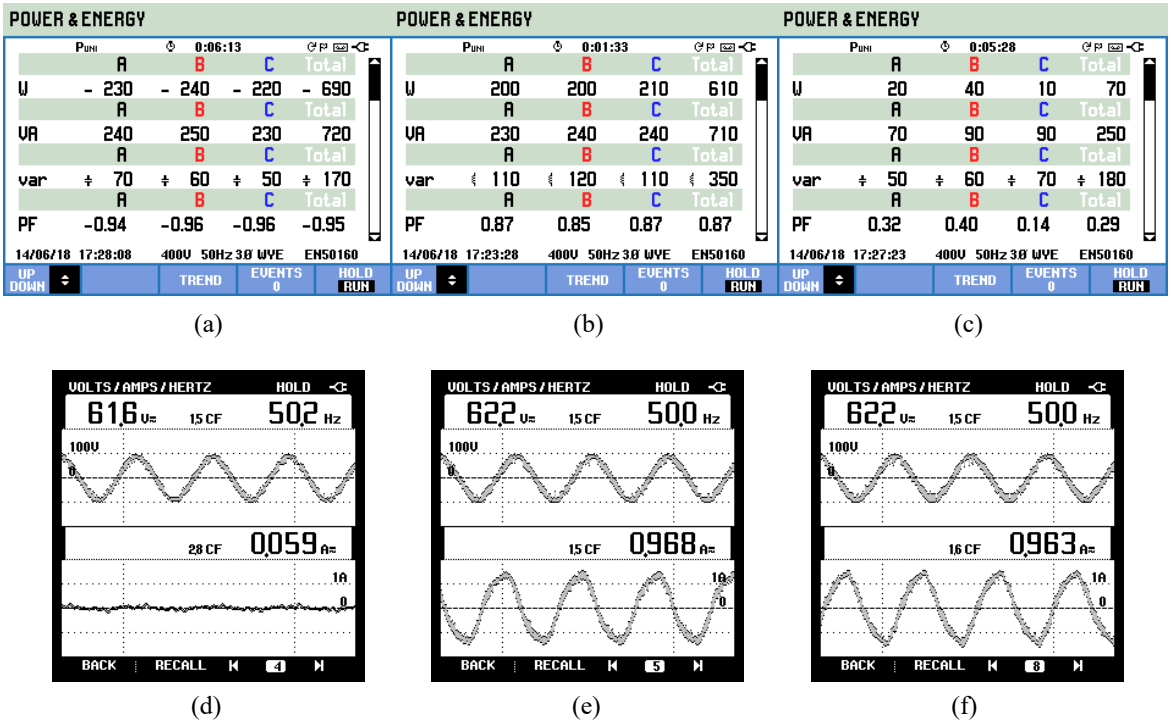

Fig. 5.26 (a-c) Steady state power for TPFW linear system using MRGN based control algorithm for (a) Supply (b) Load (c) Compensator and (d-f) neutral current of (d) supply (i_{sn}) (e) load (i_{Ln}) and (f) zigzag transformer (i_{zn}) *w.r.t* phase 'a' voltage (v_{sa}) in presence of linear load

consumes real power of 70 W to meet the switching losses in SAPF. Figs. 5.26(d)-(f) presents the supply neutral current (i_{sn}), neutral current in load (i_{Ln}) and zigzag transformer neutral current (i_{zn}) along with phase 'a' supply voltage. The supply neutral current is negligible as compared to load current. The load neutral and zigzag transformer neutral has almost equal magnitude as 0.968 A and 0.963 A. This shows that the neutral current compensation has been achieved.

Fig. 5.27 shows the dynamic performance of the TPFW system using MRGN control technique for linear load. Fig. 5.27(a) shows phase 'a' supply voltage (v_{sa}) and three phase shunt compensated supply currents (i_{sa}, i_{sb}, i_{sc}). The supply currents remains balanced and sinusoidal even phase 'c' of load is suddenly removed. Fig. 5.27(b) shows phase 'a' supply voltage (v_{sa}) and three phase lagging PF load currents (i_{La}, i_{Lb}, i_{Lc}) under balanced/unbalanced loads. The phase 'c' load current has become zero during sudden disconnection of phase 'c'. Fig. 5.27(c) shows phase 'a' supply voltage (v_{sa}) and three phase shunt injected compensator

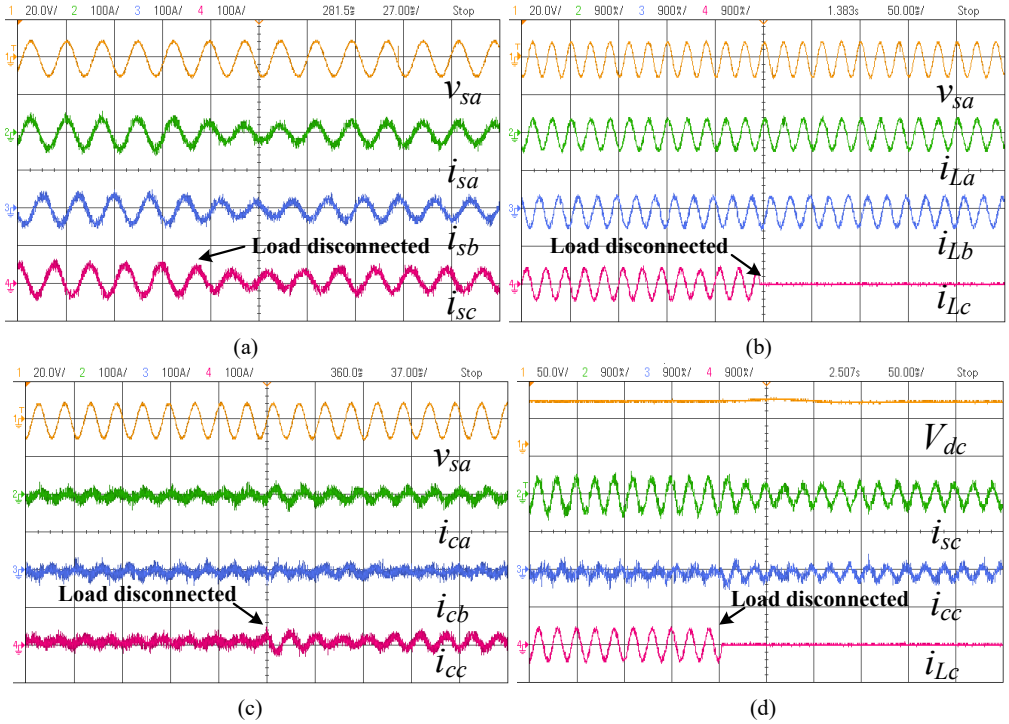

Fig. 5.27 Results showing dynamics for load disconnected in phase 'c' using MRGN control algorithm (a) v_{sa}, i_{sa}, i_{sb}, i_{sc} (b) v_{sa}, i_{La}, i_{Lb}, i_{Lc} (c) v_{sa}, i_{ca}, i_{cb}, i_{cc} (d) V_{dc}, i_{sc}, i_{cc}, i_{Lc} for linear load

currents (i_{ca}, i_{cb}, i_{cc}). The compensator currents for linear loads are less distorted as compared to MRGN technique based control for non-linear loads. Fig. 5.27(d) shows DC link voltage (V_{dc}) of SAPF, and phase 'c' supply current (i_{sc}), phase 'c' compensator currents (i_{cc}) and phase 'c' load current (i_{Lc}). The supply and compensator currents settle very fast after the load in phase 'c' is removed. Fig. 5.28 shows the intermediate signals in MRGN control technique for linear load. Fig 5.28(a) shows the average fundamental active power component (I_{avg}), phase 'a' fundamental active power component (I_{pa}), phase 'b' fundamental active power component (I_{pb}) and phase 'c' fundamental active power component (I_{pc}). The phase 'c' fundamental active power component (I_{pc}) is reduced to zero during load removal. Fig. 5.28(b) shows DC link (V_{dc}) of SAPF, supply neutral current (i_{sn}), neutral current in load (i_{Ln}) and the zigzag transformer neutral current (i_{Ln}). During the unbalanced load conditions, the neutral current in load passes through the zigzag transformer neutral path. The supply neutral current is always well regulated and small in magnitude.

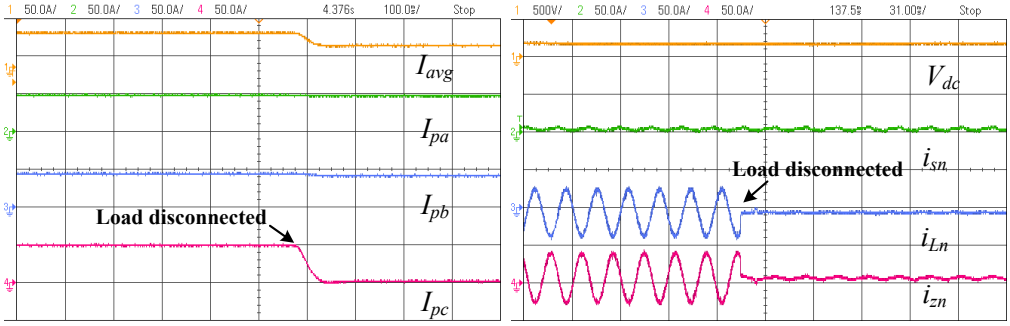

(a) (b)

Fig. 5.28 Intermediate results using MRGN control algorithm (a) I_{avg}, I_{pa}, I_{pb}, I_{pc} (b) V_{dc}, i_{sn}, i_{Ln}, i_{zn} for linear load

5.4.3. ChANN Based Control Algorithm

The Chebyshev Polynomial ANN (*ChANN*) based control was implemented for control of SAPF in a TPFW system at 110 V (L-L), 50 Hz in presence of non-linear loads. Fig. 5.29 shows the steady state waveform using *ChANN* control technique for non-linear load. Figs. 5.29(a)-(c) show phase 'a' sinusoidal supply current (i_{sa}), phase 'a' non-sinusoidal load current (i_{La}) and phase 'a' shunt injected compensator current (i_{ca}) along with phase 'a' sinusoidal supply voltage (v_{sa}). The SAPF compensator improves the profile of supply current waveforms under nonlinear loads. Figs. 5.29(d)-(f) show the THD in the phase 'a' supply voltage (v_{sa}), phase 'a' supply current (i_{sa}) and phase 'a' load current (i_{La}). The THD of supply voltage is 4.1%. The supply current has THD of 4.3%, which is observed to be the highest among all the three control techniques developed and implemented for load compensation in this chapter. The load current has a THD of 32.0%. However, the THD in supply current is still within prescribed limits specified in IEEE 519 [40]. Figs. 5.29(g)-(i) show the supply neutral current (i_{sn}), load neutral current (i_{Ln}) and zigzag transformer neutral current (i_{zn}) along with phase 'a' supply voltage (v_{sa}) for unbalanced load. The supply neutral current is small and has a value of 0.110 A. The neutral current in load is 2.355 A and zigzag transformer neutral current magnitude is 2.282 A.

The dynamic performance of the TPFW system using *ChANN* control technique is shown in Fig. 5.30 for non-linear load. Fig. 5.30(a) shows phase 'a' supply voltage (v_{sa}) and three

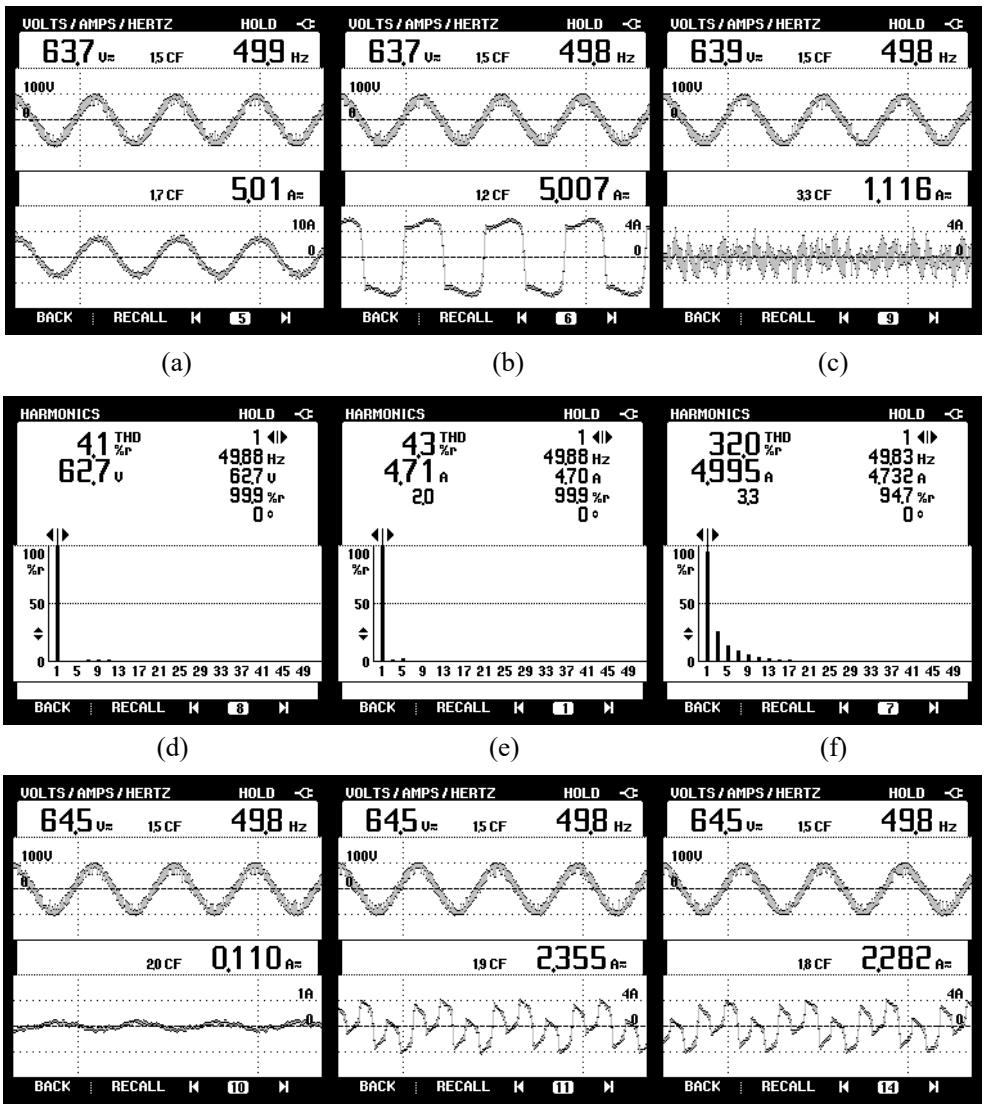

Fig. 5.29 Steady state waveforms for TPFW system using ChANN control algorithm (a) v_{sa}-i_{sa} (b) v_{sa}-i_{La} (c) v_{sa}-i_{ca} and (d-f) THD of (d) v_{sa} (e) i_{sa} (f) i_{La} (g-i) neutral current of (g) supply (i_{sn}) (h) load (i_{Ln}) and (i) zigzag transformer (i_{zn}) for non-linear load

phase SAPF compensated balanced supply currents (i_{sa}, i_{sb}, i_{sc}) under balanced/unbalanced load. The supply currents waveforms are sinusoidal and their magnitudes slightly reduce during unbalancing period. Fig. 5.30(b) shows phase 'a' supply voltage (v_{sa}) and three phase non-sinusoidal and unbalanced load currents (i_{La}, i_{Lb}, i_{Lc}). 5.30(c) shows phase 'a' supply voltage (v_{sa}) and SAPF injected three phase compensator currents (i_{ca}, i_{cb}, i_{cc}). The compensator injects currents at PCC to improve the THD of supply currents. 5.30(d) shows DC link voltage (V_{dc}) of SAPF, phase 'c' supply current (i_{sc}), phase 'c' load current (i_{Lc}) phase 'c' compensator current (i_{cc}). The *ChANN* control technique is observed to be working

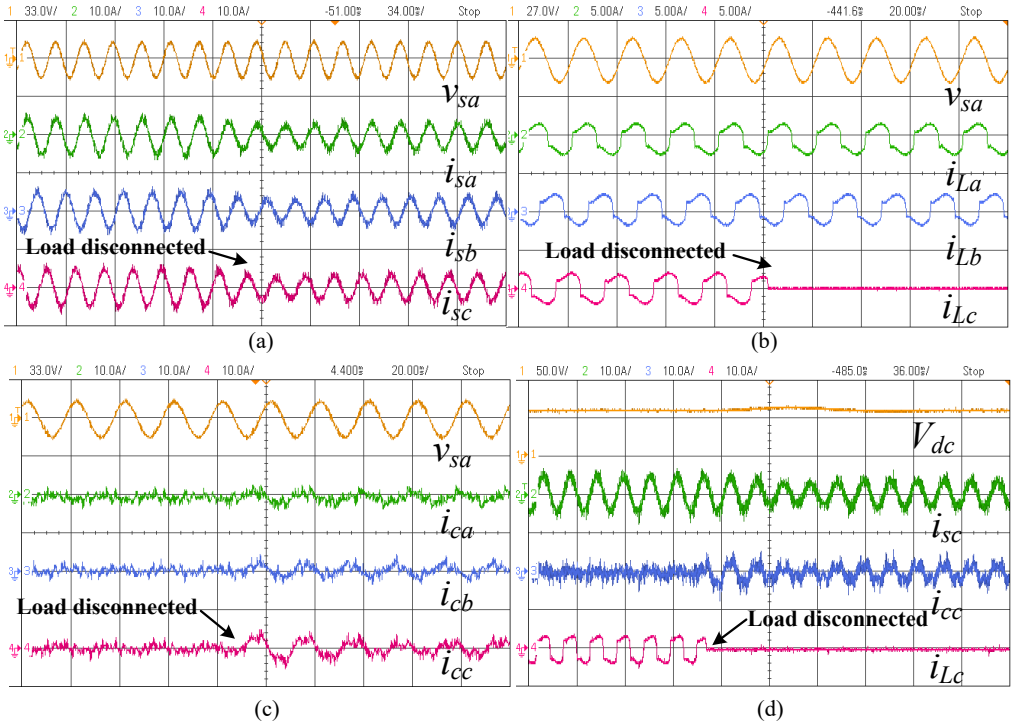

Fig. 5.30 Results showing dynamics for load disconnected in phase 'c' using ChANN control algorithm (a) v_{sa}, i_{sa}, i_{sb}, i_{sc} (b) v_{sa}, i_{La}, i_{Lb}, i_{Lc} (c) v_{sa}, i_{ca}, i_{cb}, i_{cc} (d) V_{dc}, i_{sc}, i_{cc}, i_{Lc} for non-linear load

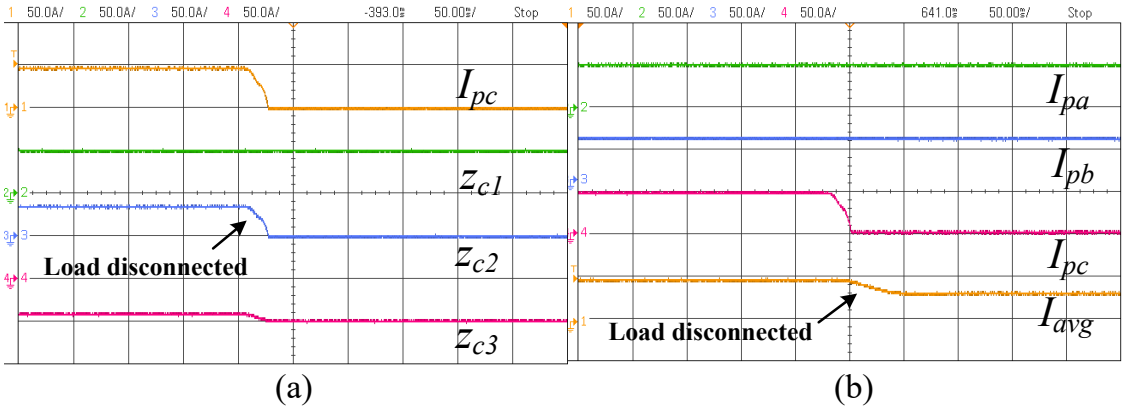

Fig. 5.31 Intermediate results using ChANN control algorithm (a) I_{pc}, Z_{c1}, Z_{c2}, Z_{c3} (b) I_{pa}, I_{pb}, I_{pc}, I_{avg} for non-linear load

well for nonlinear balanced/ unbalanced load case. Fig. 5.31 shows the intermediate signals for the *ChANN* control technique with non-linear load. In Fig 5.31(a) phase 'c' fundamental active power component (I_{pc}) and Chebyshev expansion functions (Z_{c1}, Z_{c1}, Z_{c3}) have been recorded. The Chebyshev expansion functions change according to the change in load and the algorithm is able to extract I_{pc} effectively. In Fig. 5.31(b) the phase 'a' fundamental active power component (I_{pa}), phase 'b' fundamental active power component (I_{pb}), phase 'c' fundamental active power component (I_{pc}) and average fundamental active power component

(I_{avg}) are shown. The fundamental active power component of phase 'c' (I_{pc}) is affected due to load removal.

Fig. 5.32(a-c) shows the steady state power flow among supply load and compensator for linear loads using *ChANN* control technique. The supply feeds active power (690 W) and compensator feeds reactive power (180 VARs) out of total demand of load (620 W, 350 VARs). The compensator draws active power of 70 W from grid to meet switching losses in IGBT switches. The PF of AC supply is 0.95, which is better in comparison to that of the PF of the load. Figs. 5.32(d)-(f) present the supply neutral current (i_{sn}), neutral current of load (i_{Ln}) and zigzag transformer neutral current (i_{zn}) along with phase 'a' supply voltage. The supply neutral current is 0.088 A. The zigzag transformer neutral current and load neutral current have almost equal magnitude of 1.021 A and 1.087 A respectively.

Fig. 5.33 shows the dynamic performance of the TPFW system using *ChANN* control technique for linear load. Fig. 5.33(a) shows phase 'a' supply voltage (v_{sa}) and three phase SAPF compensated supply currents (i_{sa}, i_{sb}, i_{sc}) with balanced/unbalanced load. The supply

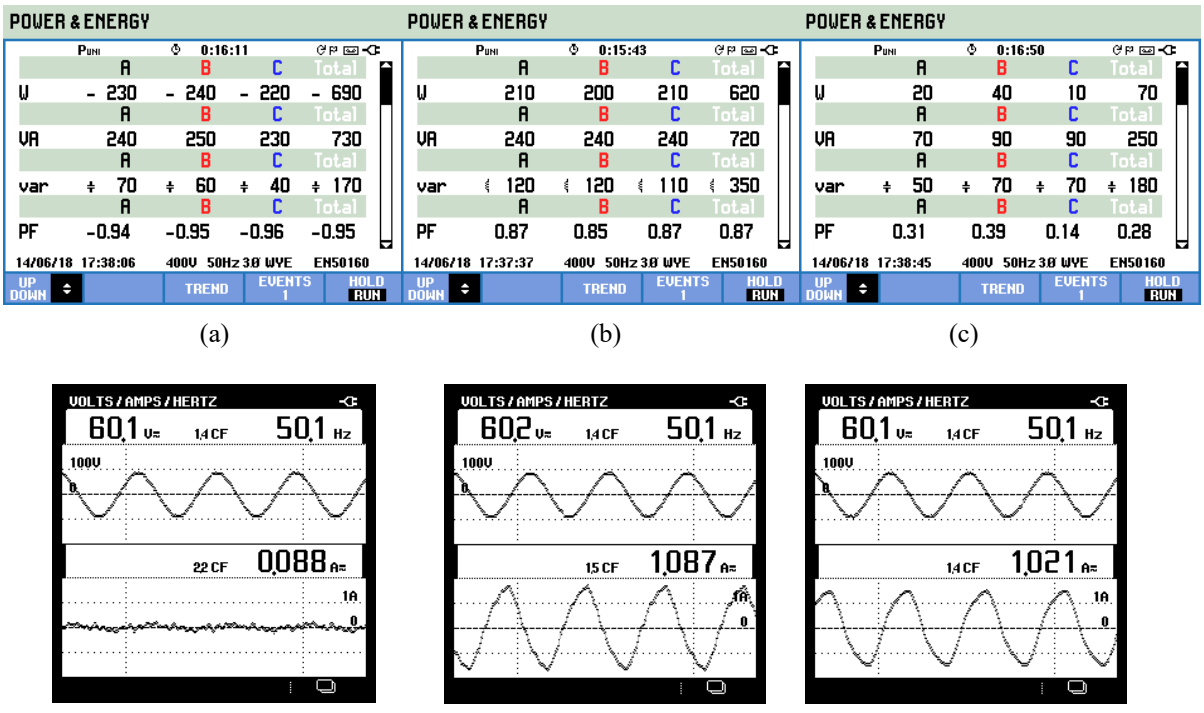

(a) (b) (c)

(d) (e) (f)

Fig. 5.32 (a-c) Steady state power for TPFW linear system using *ChANN* based control algorithm for (a) Supply (b) Load (c) Compensator and (d-f) neutral current of (d) supply (i_{sn}) (e) load (i_{Ln}) and (f) zigzag transformer (i_{zn}) *w.r.t* phase 'a' voltage (v_{sa}) in presence of linear load

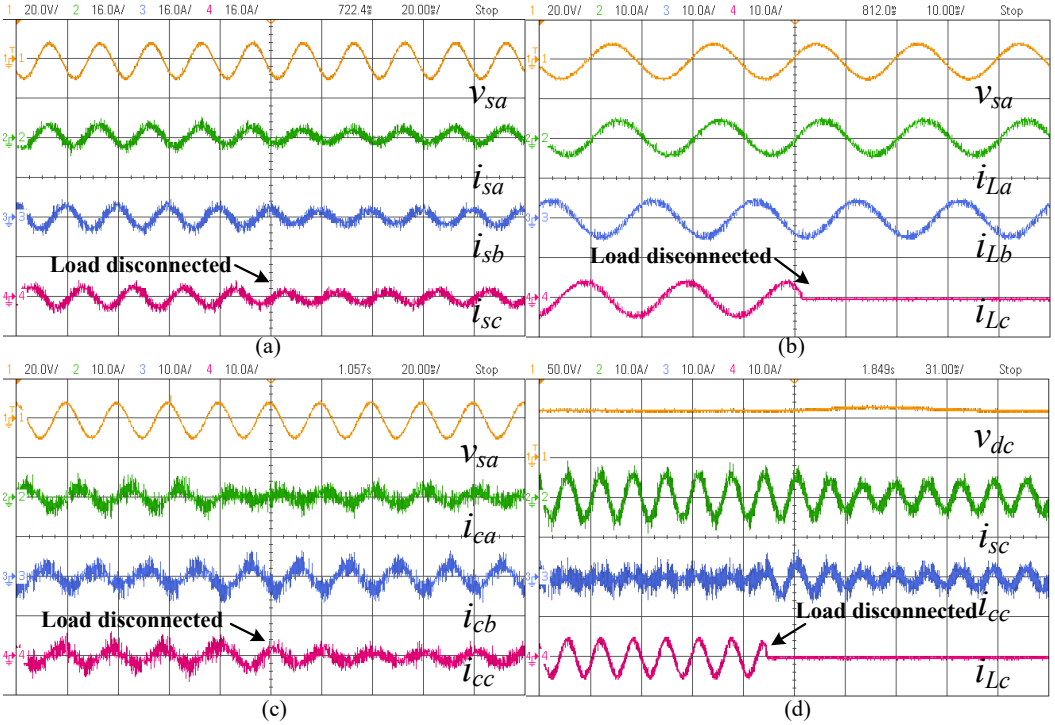

Fig. 5.33 Results showing dynamics for load disconnected in phase 'c' using ChANN control algorithm (a) v_{sa}, i_{sa}, i_{sb}, i_{sc} (b) v_{sa}, i_{La}, i_{Lb}, i_{Lc} (c) v_{sa}, i_{ca}, i_{cb}, i_{cc} (d) V_{dc}, i_{sc}, i_{cc}, i_{Lc} for linear load

currents are sinusoidal and balanced even though for some period load is unbalanced. Fig. 5.33(b) shows phase 'a' supply voltage (v_{sa}) and three phase unbalanced and lagging PF load currents (i_{La}, i_{Lb}, i_{Lc}). 5.33(c) shows phase 'a' supply voltage (v_{sa}) and three phase SAPF injected compensator currents (i_{ca}, i_{cb}, i_{cc}). 5.33(d) shows DC link voltage (V_{dc}) of SAPF and phase 'c' supply current (i_{sc}), load current (i_{Lc}) and compensator current (i_{cc}). These results demonstrate the effectiveness of *ChANN* control technique for control of SAPF. Fig. 5.34 shows the intermediate signals in *ChANN* control technique with linear load. In Fig 5.34(a) phase 'c' fundamental active power component (I_{pc}) and Chebyshev expansion functions (Z_{c1}, Z_{c2}, Z_{c3}) are shown. In Fig. 5.34(b) average active power component (I_{avg}), phase 'a' fundamental active power component (I_{pa}), phase 'b' fundamental active power component (I_{pb}), and phase 'c' fundamental active power component (I_{pc}) are shown. These results are similar to that of non-linear load, so the *ChANN* control technique works well in TPFW linear and non-linear loads.

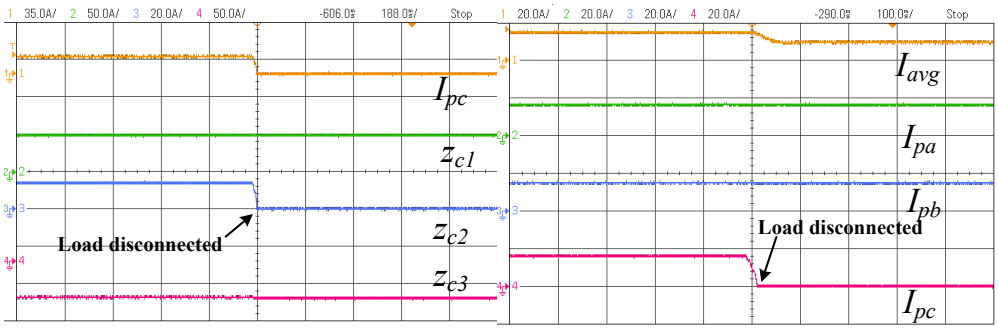

(a) (b)

Fig. 5.34 Intermediate results using ChANN control algorithm (a) I_{pc}, Z_{c1}, Z_{c2}, Z_{c3} (b) I_{pa}, I_{pb}, I_{pc}, I_{avg} for linear load

5.5. COMPARATIVE EVALUATION OF PROPOSED CONTROL SCHEMES

Three new control algorithms viz STF, MRGN and ChANN have been developed and implemented for load compensation in TPFW system. All three techniques have been found effective in mitigating PQ problems to acceptable levels. Table 5.1 and 5.2 show a comparative performance analysis in presence of non-linear and linear loads based on the experimental results (Fig. 5.17, 5.20, 5.23, 5.26, 5.29, 5.32).

Table 5.1 shows a comparison of THD level in supply current obtained using STF, MRGN and ChANN control techniques. The STF gives the lowest THD level in supply current i.e. 3.1% as compared to MRGN and ChANN. The supply side current has been improved to near sinusoidal value with THD of 3.45% with MRGN and 4.3% THD with Chebyshev based algorithm when the load current is distorted and having a high THD of 32.0%. The STF algorithm has been observed to be slightly better in achieving lower THD in supply current than MRGN and Chebyshev based algorithm.

Table 5.2 shows a comparison of power flow in all three techniques under linear load

Table 5.1 COMPARISON OF CONTROL ALGORITHMS FOR NON-LINEAR LOAD

S.No.	Quantity	STF	MRGN	Chebyshev
1.	Supply Voltage (v_{sa})	61.1 V, 4.3% THD	60.8 V, 4.1% THD	62.7 V, 4.1% THD
2.	Load Current (i_{La})	4.457 A, 32.1% THD	4.457 A, 32.1% THD	4.995 A, 32.0% THD
3.	Supply Current (i_{sa})	4.54 A, 3.1% THD	4.57 A, 3.4% THD	4.71 A, 4.3% THD

Table 5.2 COMPARISON OF CONTROL ALGORITHMS FOR LINEAR LOAD

S.No.	Quantity	STF	MRGN	Chebyshev
1.	Supply Power	690 W, 170 VARs, 0.95 P.F.	690 W, 170 VARs, 0.95 P.F.	690 W, 170 VARs, 0.95 P.F.
2.	Load Power	610 W, 350 VARs, 0.87 P.F.	610 W, 350 VARs, 0.87 P.F.	620 W, 350 VARs, 0.87 P.F.
3.	Compensator Power	70 W, 180 VARs, 0.28 P.F.	70 W, 180 VARs, 0.29 P.F.	70 W, 180 VARs, 0.28 P.F.

conditions. Load has a active power demand of 610W, 350 VARs which is measured with a three phase Power Analyzer (Fluke 434). which are recorded in Fig. 5.20, 5.26, 5.32. The active and reactive power flow in the developed control techniques are nearly the same and also P.F. of the supply has been improved from 0.87 lag to 0.95 in all three control techniques.

5.6 CONCLUSIONS

The main contributions of this chapter are to develop improved control techniques such as MRGN, STF and ChANN for TPFW system. This chapter also incorporates neutral current compensation in TPFW using zigzag transformer which is cost effective solution. A fair comparison is performed based on the obtained results. All three control algorithms can be used to extract harmonics from load current. The performance of the algorithms under dynamic load changes (disconnection of load) has been investigated. It has been observed that with MRGN algorithm, the fundamental active power component (I_{pc}) settles quickly in ~ 2 cycles as compared to three cycles for STF and two and half cycles for ChANN. However, the complexity in real time implementation of MRGN and STF was comparable, while ChANN is moderately complex. Overall, performance of MRGN was slightly superior than the other two control algorithms viz. STF and ChANN.

Chapter 6
POWER QUALITY IMPROVEMENT IN DISTORTED LOW VOLTAGE DISTRIBUTION SYSTEM

6.0 INTRODUCTION

In the previous chapters, PQ problems in TPTW and TPFW have been discussed. The development of control algorithms in these chapters are based on the assumption that grid supply is sinusoidal and has low THD. In this chapter, PQ problems of distorted low voltage distribution system are analyzed. New control algorithms for PQ improvement in TPFW distorted distribution system are developed. These techniques are simulated in a MATLAB/SIMULINK environment and experimentally validated on a prototype system developed in the laboratory.

6.1 POWER QUALITY ISSUES IN TPFW DISTORTED LOW VOLTAGE DISTRIBUTION SYSTEM

A detailed analysis of PQ problems and mitigation techniques are described for TPTW and TPFW grid tied distribution system in previous chapters. The supply is considered as stiff and unaffected by the type of load present and amount of current drawn from the supply. The PCC voltages have THD less than 5%. Hence, the generation of unit templates for synchronizing SAPF to the grid can be realized easily.

However, in the case of distorted low voltage distribution system, the supply voltage is not perfectly sinusoidal. The waveforms of PCC voltages are distorted and THD in voltages are also more than allowable limit of 5%. The generation of perfectly sinusoidal unit templates for generation of reference currents for control of SAPF in distorted distribution system is a new challenge. The conventional approach of generating unit templates fails under distorted supply voltage. If unit templates are generated from the distorted supply voltages, then they are also distorted and reference currents generated using these unit templates are also

distorted and it is not possible to achieve a sinusoidal AC supply current through compensation.

Compensation and mitigation of PQ problems requires extraction of fundamental component of supply voltages. This chapter focuses on PQ improvement in TPFW distorted distribution system such as PF correction, harmonic reduction and compensation for neutral current etc. with advanced control techniques.

6.2 DEVELOPMENT AND ANALYSIS OF MODERN CONTROL ALGORITHMS FOR MITIGATION OF PQ ISSUES IN TPFW DISTORTED LOW VOLTAGE DISTRIBUTION SYSTEM

In this section, control techniques for PQ issues and mitigation in TPFW distorted grid system are discussed. These techniques are general and have been implemented on load currents as well as distorted PCC voltages. Details of control techniques such as Multiple Complex Coefficient Filter (MCCF) and Second Order Generalized Integrator (SOGI) is discussed in subsequent sections.

6.2.1. Extraction of Fundamental Active Power Components

The determination of fundamental active power component (I_{pabc}/I_{avg}) using new control algorithms are described in this section.

6.2.1.1. Multiple Complex Coefficient Filter (MCCF) Based Control Algorithm

The Complex Coefficient Filter (CCF) is frequency selective filter and have zero phase shift, unity gain. The CCF transfer function of is given by

$$T.F. = \frac{\omega_b}{s - jn\omega_0 + \omega_b} \tag{6.1}$$

where ω_b is bandwidth of filter, ω_0 is fundamental frequency and 'n' denotes the order of harmonic frequency.

The CCF frequency response characteristic is shown in the Fig 6.1 with bode plot. It is also

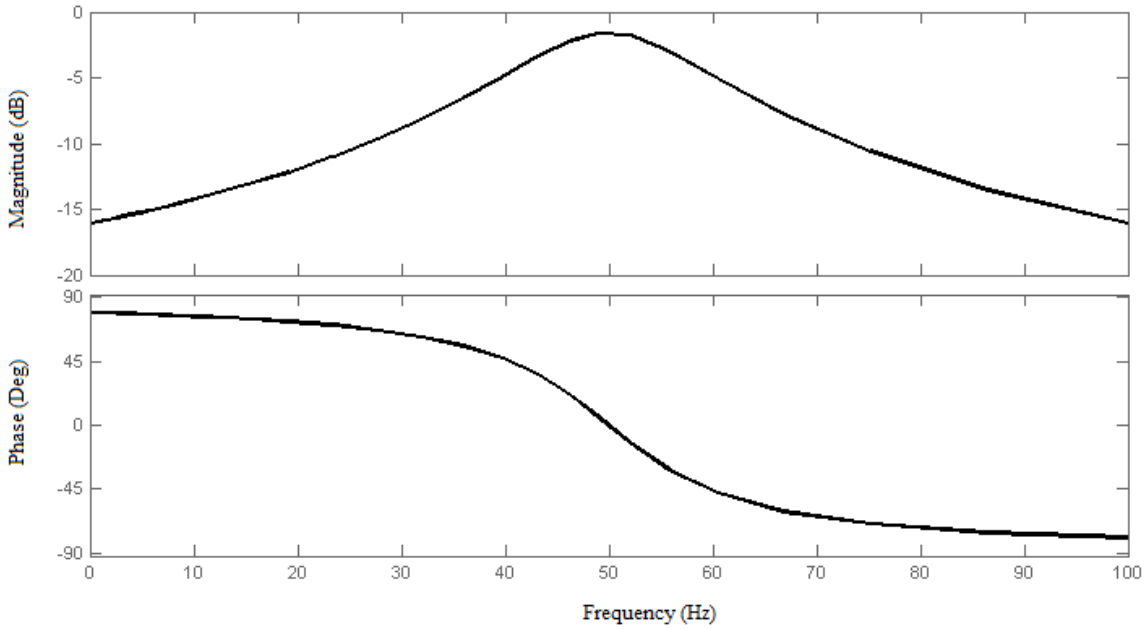

Fig. 6.1 Magnitude and phase plot of Complex Coefficient Filter (CCF)

observed from the figure that corresponding to $\omega_{0,}$ the CCF has zero phase shift and unity gain response, which are desirable characteristics of an ideal filter. The CCF has advantages over other popular filters such as Butterworth Filter (BWF), Moving Average Filter (MAF) etc. of having the ability to differentiate between sequence components such as positive and negative sequence component of individual harmonic as shown in Fig 6.2. A CCF can be used to obtain positive sequence fundamental component of voltage and current signal.

Fig. 6.2 shows the implementation of Multiple CCF (MCCF) filter for positive and negative sequence component of load current fundamental as well as harmonic components. The proposed MCCF filter shown in Fig 6.2 can be expressed by a set of linear frequency domain equations for fundamental component as

$$\dot{i}_{L\alpha f}^{+} = \omega_b i_{L\alpha} - \omega_b i_{L\alpha f}^{+} - \omega_0 i_{L\beta f}^{+} \tag{6.2}$$

$$\dot{i}_{L\beta f}^{+} = \omega_b i_{L\beta} + \omega_0 i_{L\alpha f}^{+} - \omega_b i_{L\beta f}^{+} \tag{6.3}$$

$$\dot{i}_{L\alpha f}^{-} = \omega_b i_{L\alpha} - \omega_b i_{L\alpha f}^{-} + \omega_0 i_{L\beta f}^{-} \tag{6.4}$$

$$\dot{i}_{L\beta f}^{-} = \omega_b i_{L\beta} - \omega_0 i_{L\alpha f}^{-} - \omega_b i_{L\beta f}^{-} \tag{6.5}$$

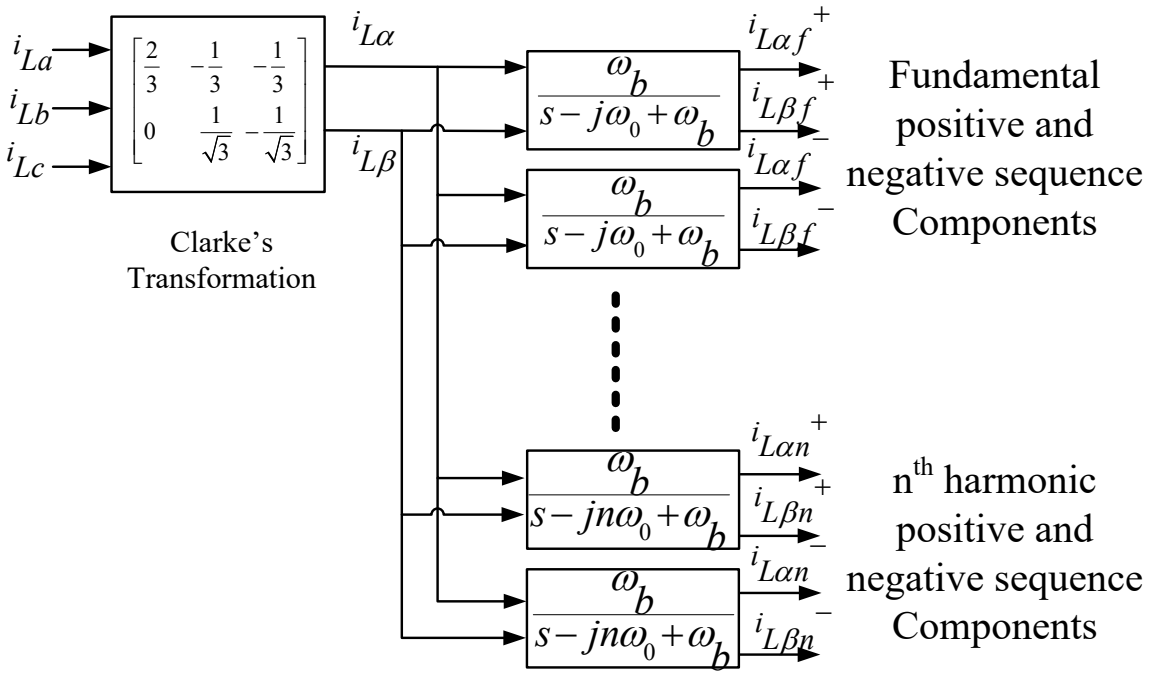

Fig. 6.2 Implementation of MCCF to extract load current fundamental and harmonic sequence components

where $i_{L\alpha}$, $i_{L\beta}$ are the alpha-beta components of load currents, $i_{L\alpha}^{+}$, $i_{L\beta}^{+}$ are the positive sequence fundamental alpha-beta components of load currents, $i_{L\alpha}^{-}$, $i_{L\beta}^{-}$ are the negative sequence fundamental alpha-beta components of load currents.

Similarly for nth order frequency component the positive and negative sequence alpha- beta components of load currents are given by:

$$\dot{i}_{L\alpha n}^{+} = \omega_b i_{L\alpha} - \omega_b i_{L\alpha n}^{+} - \omega_0 i_{L\beta n}^{+} \tag{6.6}$$

$$\dot{i}_{L\beta n}^{+} = \omega_b i_{L\beta} + \omega_0 i_{L\alpha n}^{+} - \omega_b i_{L\beta n}^{+} \tag{6.7}$$

$$\dot{i}_{L\alpha n}^{-} = \omega_b i_{L\alpha} - \omega_b i_{L\alpha n}^{-} + \omega_0 i_{L\beta n}^{-} \tag{6.8}$$

$$\dot{i}_{L\beta n}^{-} = \omega_b i_{L\beta} - \omega_0 i_{L\alpha n}^{-} - \omega_b i_{L\beta n}^{-} \tag{6.9}$$

where 'n' denotes the order of harmonics.

A state space model of system can be represented by

$$\begin{aligned} \dot{X}(t) &= AX(t) + Bu(t) \\ y(t) &= CX(t) + Du(t) \end{aligned} \tag{6.10}$$

where $X(t) = y(t) = [i_{L\alpha f}{}^{+} \;\; i_{L\beta f}{}^{+} \;\; i_{L\alpha f}{}^{-} \;\; i_{L\beta f}{}^{-} \ldots\ldots\ldots\ldots i_{L\alpha n}{}^{+} \;\; i_{L\beta n}{}^{+} \;\; i_{L\alpha n}{}^{-} \;\; i_{L\beta n}{}^{-}]^{T}$,

$u(t) = [i_{L\alpha} \;\; i_{L\beta} \;\; i_{L\alpha} \;\; i_{L\beta} \ldots\ldots\ldots\ldots i_{L\alpha} \;\; i_{L\beta}]^{T}$, $D=0$, $C = [I]_{4n}$, $B = \omega_b [I]_{4n}$

and

$$A = \begin{bmatrix} -\omega_b & -\omega_0 & 0 & 0 & & & & \\ \omega_0 & -\omega_b & 0 & 0 & & & & \\ 0 & 0 & -\omega_b & \omega_0 & & & & \\ 0 & 0 & -\omega_0 & -\omega_b & & & & \\ & & & & :: & & & \\ & & & & & :: & & \\ & & & & & & -\omega_b & -n\omega_0 & 0 & 0 \\ & & & & & & n\omega_0 & -\omega_b & 0 & 0 \\ & & & & & & 0 & 0 & -\omega_b & n\omega_0 \\ & & & & & & 0 & 0 & -n\omega_0 & -\omega_b \end{bmatrix}_{4n \mathrm{X} 4n}$$

The steady state solution of Eq. (6.10) is given by

$$y(t) = X(t) = e^{At} X(0) \tag{6.11}$$

$$y(t) = X(t) = \begin{bmatrix} F_1^{+} \sin(\omega_0 t + \gamma_1^{+}) \\ -F_1^{+} \cos(\omega_0 t + \gamma_1^{+}) \\ F_1^{-} \sin(-\omega_0 t + \gamma_1^{-}) \\ -F_1^{-} \sin(-\omega_0 t + \gamma_1^{-}) \\ :: \\ :: \\ F_n^{+} \sin(n\omega_0 t + \gamma_n^{+}) \\ -F_n^{+} \cos(n\omega_0 t + \gamma_n^{+}) \\ -F_n^{+} \cos(n\omega_0 t + \gamma_n^{+}) \\ -F_n^{-} \sin(-n\omega_0 t + \gamma_n^{+}) \end{bmatrix}_{4n \mathrm{X} 1} \tag{6.12}$$

where F_1^{+}, F_1^{-} maximum value of are the fundamental positive and negative sequence components of load current, similarly F_n^{+}, $F_n^{-}$is for n^{th} harmonic, $\gamma_1^{+} \ldots\ldots \gamma_n^{+}$ denotes the phase shift of particular harmonic signal and 'n' denotes the order of harmonic.

From Eq. 6.12 it is clear that proposed filter is able to extract all the positive as well as negative sequence component of fundamental and all higher order harmonics in distribution system. Fig. 6.3 shows the block diagram of implementation of MCCF filter for PQ

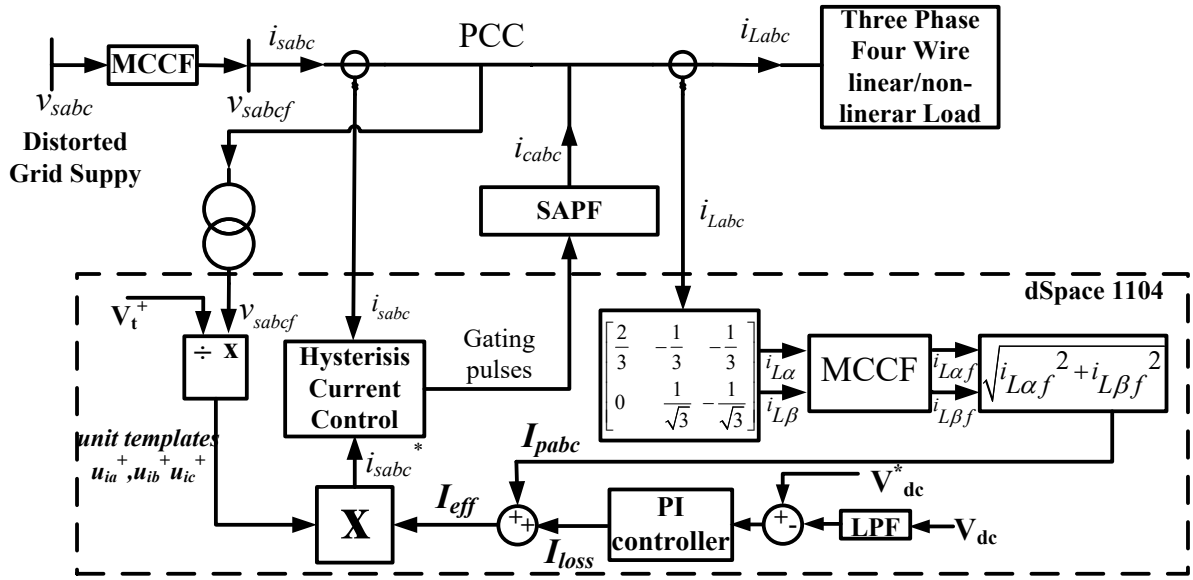

Fig. 6.3 Block diagram of MCCF based control algorithm implementation

improvement in distorted grid system. For the generation of appropriate unit templates the distorted PCC voltages are first transformed into α-β components using Clarke's transformation as

$$\begin{bmatrix} v_{s\alpha} \\ v_{s\beta} \end{bmatrix} = \sqrt{\frac{2}{3}} \begin{bmatrix} 1 & -\frac{1}{2} & -\frac{1}{2} \\ 0 & \frac{\sqrt{3}}{2} & -\frac{\sqrt{3}}{2} \end{bmatrix} \begin{bmatrix} v_{sa} \\ v_{sb} \\ v_{sc} \end{bmatrix} \tag{6.13}$$

where v_{sa},v_{sb},v_{sc} are three phase PCC voltages and $v_{s\alpha}$,$v_{s\beta}$ are transformed voltages. The transformed voltages $v_{s\alpha}$ and $v_{s\beta}$ can further be expanded as follows

$$v_{s\alpha\beta}^{n} = v_{s\alpha\beta}^{n+} + v_{s\alpha\beta}^{n-} + v_{s\alpha\beta}^{n0} \tag{6.14}$$

where 'n' denotes the order of harmonics.

Now the MCCF filter tuned to fundamental positive frequency i.e. 50 Hz, is used to extract fundamental positive component of PCC voltages from distorted voltages $v_{s\alpha}$ and $v_{s\beta}$. The MCCF filters out fundamental positive sequence component $v_{s\alpha}^{+}$ and $v_{s\beta}^{+}$, which is transformed by reverse Clarke's transformation to get fundamental positive sequence three phase voltages v_{saf}^{+}, v_{sbf}^{+}, v_{scf}^{+} as

$$\begin{bmatrix} v_{saf}^{+} \\ v_{sbf}^{+} \\ v_{scf}^{+} \end{bmatrix} = \sqrt{\frac{2}{3}} \begin{bmatrix} 1 & 0 \\ -\frac{1}{2} & \frac{\sqrt{3}}{2} \\ -\frac{1}{2} & -\frac{\sqrt{3}}{2} \end{bmatrix} \begin{bmatrix} v_{s\alpha}^{+} \\ v_{s\beta}^{+} \\ v_{s0} \end{bmatrix} \tag{6.15}$$

where v_{s0} is supply zero sequence component. These (v_{saf}^{+}, v_{sbf}^{+}, v_{scf}^{+}) or simply (v_{saf}, v_{sbf}, v_{scf}) are used to calculate modified unit templates (u_{ia}^{+}, u_{ib}^{+}, u_{ic}^{+}), and discussed later in section 6.2.2.

The load currents are transformed into α-β components for the extraction of fundamental active power component of load current using Clarke's transformation as:

$$\begin{bmatrix} i_{L\alpha} \\ i_{L\beta} \end{bmatrix} = \sqrt{\frac{2}{3}} \begin{bmatrix} 1 & -\frac{1}{2} & -\frac{1}{2} \\ 0 & \frac{\sqrt{3}}{2} & -\frac{\sqrt{3}}{2} \end{bmatrix} \begin{bmatrix} i_{La} \\ i_{Lb} \\ i_{Lc} \end{bmatrix} \tag{6.16}$$

Now these transformed currents ($i_{L\alpha}$, $i_{L\beta}$) are processed by MCCF filter to obtain fundamental positive sequence load components ($i_{L\alpha f}$, $i_{L\beta f}$). The fundamental active power component (I_{pabc}) of combined load is calculated using

$$I_{pabc} = \sqrt{i_{L\alpha f}^2 + i_{L\beta f}^2} \tag{6.17}$$

The component I_{pabc} is added to DC link power loss component I_{loss} to determine effective magnitude (I_{eff}) of compensator currents.

6.2.1.2. Second Order Generalized Integrator (SOGI) Based Control Algorithm

Second Order Generalized Integrator (SOGI) is a general purpose second order transfer function [146]. It is used to calculate in-phase and quadrature phase frequency components of input signal. The input signal may be voltage or current, SOGI outputs two components which are in phase quadrature. Fig. 6.4(a) shows a generalized SOGI block diagram implemented on phase 'a' load current i_{La}. The in-phase and quadrature components of phase 'a' load currents are given as:

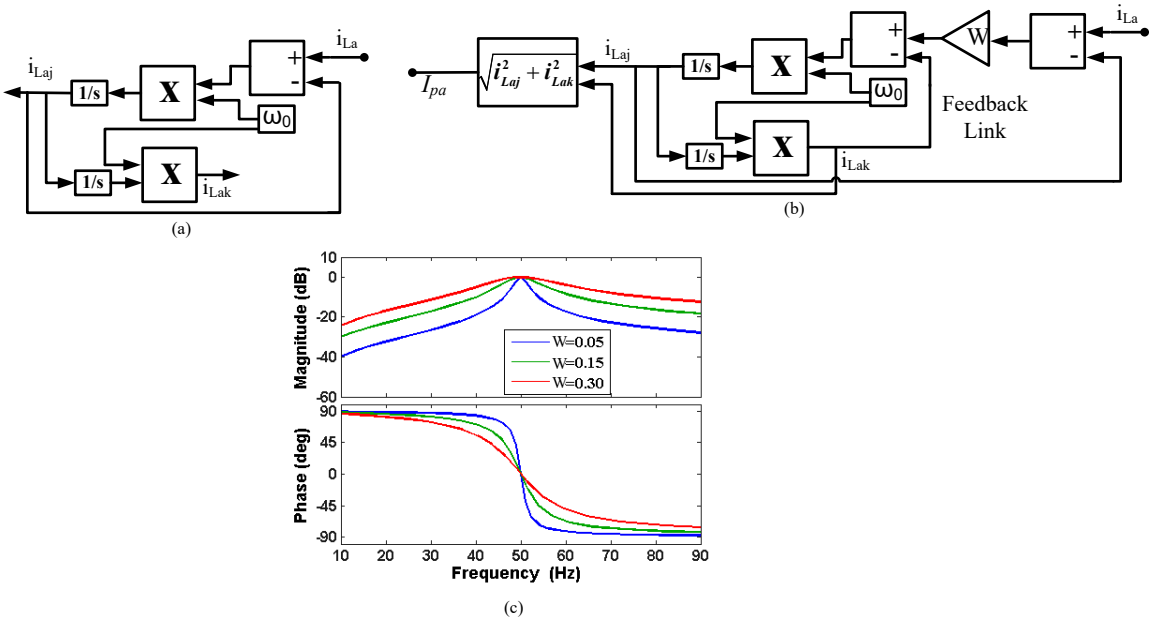

Fig. 6.4 Second Order Generalized Integrator (SOGI) (a) Block diagram without feedback link (b). Block diagram with feedback link (c) Magnitude and phase plot for different gain 'W'

$$\frac{i_{Laj}}{i_{La}} = \frac{\omega_0 s}{s^2 + \omega_0^2} \tag{6.18}$$

$$\frac{i_{Lak}}{i_{La}} = \frac{\omega_0^2}{s^2 + \omega_0^2} \tag{6.19}$$

where ω_0 is fundamental frequency and i_{Laj}, i_{Lak} are the in-phase and phase quadrature outputs generated using SOGI.

The above SOGI realization shows resonance problem due to which the output may increase in uncontrolled manner. A feedback link as shown in Fig. 6.4(b) is introduced to mitigate the resonance phenomenon. For calculation of fundamental active current component I_{pa}, the SOGI in-phase and phase quadrature outputs i_{Laj} and i_{Lak} are obtained. The transfer functions modified after introduction of feedback link as:

$$\frac{i_{Laj}}{i_{La}} = \frac{W\omega_0 s}{s^2 + W\omega_0 s + \omega_0^2} \tag{6.20}$$

$$\frac{i_{Lak}}{i_{La}} = \frac{W\omega_0^2}{s^2 + W\omega_0 s + \omega_0^2} \tag{6.21}$$

where W is constant gain and s is the laplace operator. The SOGI has two outputs which are

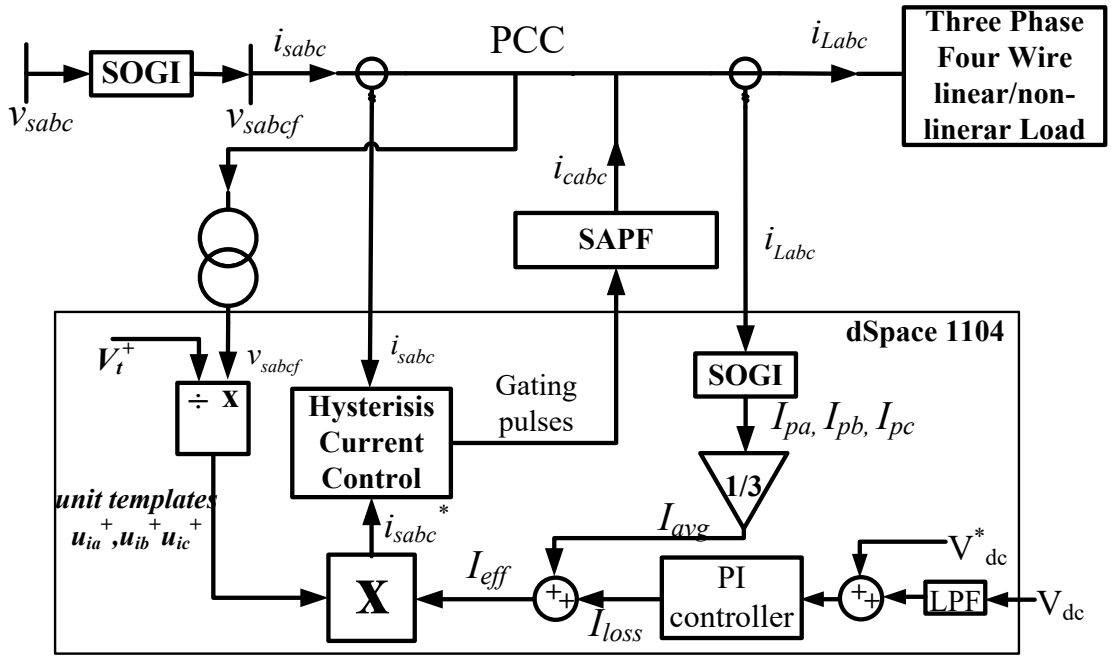

Fig. 6.5 Block diagram of SOGI based control algorithm implementation

always phase quadrature so this structure of SOGI is also called Quadrature Signal Generator(QSG)-SOGI. The gain W determines the bandwidth of SOGI block. For small values of W, band pass of the SOGI block becomes narrower as shown in Fig. 6.4(c), which leads to more filtering but slow dynamic response of the system. And vice versa for large value of W. So value of W is required to be chosen judiciously to achieve good harmonic rejection and fast dynamic response.

Fig. 6.5 shows the complete control technique block diagram using SOGI. The SOGI block is used to compute the fundamental in-phase component of phase 'a' voltage v_{sa} as

$$\frac{v_{saf}}{v_{sa}} = \frac{W\omega_0 s}{s^2 + W\omega_0 s + \omega_0^2} \tag{6.22}$$

where v_{saf} is phase 'a' fundamental in-phase voltage component.

For the extraction of fundamental active component of load, SOGI blocks in phase 'a' is implemented to calculate in-phase and quadrature components of each phase as per Eq. (6.23-2.24).

Now the fundamental active power component for phase 'a' (I_{pa}) is calculated as

$$I_{pa} = \sqrt{i_{Laj}^2 + i_{Lak}^2} \tag{6.23}$$

Similarly fundamental active power component for phase 'b' (I_{pb}) and phase 'c' (I_{pc}) are calculated and average fundamental active power component I_{avg} is calculated as

$$I_{avg} = \frac{I_{pa} + I_{pb} + I_{pc}}{3} \tag{6.24}$$

Now switching losses of IGBT switches (I_{loss}) are added to get effective active power current component and discussed in the next section.

6.2.2. Generation of Reference Currents for Control of SAPF

As discussed in section 3.8.1, the losses occurred in the IGBT switches of SAPF can be determined using the Eq. 3.12, 3.13 which are

$$I_{loss}(k) = I_{loss}(k-1) + K_P\{(e_{dc}(k) - e_{dc}(k-1)\} + K_I[e_{dc}(k)] \tag{3.12}$$

where $e_{dc}(k) = V_{dc}^{*}(k) - V_{dc}(k)$ (3.13)

The I_{loss} is the real power loss component of current in the system, since the IGBT switching losses at high frequency are significant and therefore this loss must be added to I_{pabc}/I_{avg} for effective active power current component I_{eff} calculation as follows.

$$I_{eff} = I_{avg} + I_{loss} \tag{6.25}$$

For the generation of reference current for SAPF, unit templates which are also called synchronizing templates is determined. As discussed in previous sections that conventional way of calculating unit templates as per Eq. (3.18) cannot be directly used because of distorted supply voltage, therefore the fundamental component of supply voltages (v_{saf}, v_{sbf}, v_{scf}) must be calculated using developed control algorithms. The modified in-phase unit templates (u_{ia}^{+}, u_{ib}^{+}, u_{ic}^{+}) are calculated from the extracted fundamental supply voltage (v_{saf}, v_{sbf}, v_{scf}) as per Eq. (6.26)

$$u_{ia}^{+}=\frac{v_{saf}}{V_t^{+}};\quad u_{ib}^{+}=\frac{v_{sbf}}{V_t^{+}};\quad u_{ic}^{+}=\frac{v_{scf}}{V_t^{+}} \tag{6.26}$$

$V_t{}^{+}$is the peak value of fundamental component of supply voltage and calculated using

$$V_t^{+}=\sqrt{\frac{2}{3}(v_{saf}{}^{2}+v_{sbf}{}^{2}+v_{scf}{}^{2})} \tag{6.27}$$

And the reference currents $i_{sa}{}^{*}$, $i_{sb}{}^{*}$, $i_{sc}{}^{*}$ are generated using

$$i_{sa}^{*}=u_{ia}^{+}*I_{eff};\ \ i_{sb}^{*}=u_{ib}^{+}*I_{eff};\quad i_{sc}^{*}=u_{ic}^{+}*I_{eff} \tag{6.28}$$

Now the reference currents generated are compared with the actual supply currents (i_{sa}, i_{sb}, i_{sc}) in the HCC. The HCC band is kept at 0.2. Comparison of reference currents and actual supply currents provide six gating pulses which are fed to SAPF for proper operation of system. The supply currents follows the reference currents and it is sinusoidal and balanced.

6.3. SIMULATION RESULTS

The developed control algorithms viz. MCCF and SOGI based controller are tested for control of SAPF connected TPFW distribution system in MATLAB/SIMULINK environment. Additional source inductance (2 mH) is connected which produces distorted PCC voltages. The simulated results of application in TPFW system under distorted grid condition are analyzed.

6.3.1 Multiple Complex Coefficient Filter Based Control Algorithm

Fig. 6.6 shows the simulation results for implementation of MCCF control technique for SAPF in a distorted distribution system. Fig. 6.6 presents three phase supply voltages (v_{sa}, v_{sb}, v_{sc}), three phase filtered supply voltages (v_{saf}, v_{sbf}, v_{scf}), three phase supply currents (i_{sa}, i_{sb}, i_{sc}), three phase compensator currents (i_{ca}, i_{cb}, i_{cc}), three phase non-sinusoidal load currents (i_{La}, i_{Lb}, i_{Lc}), DC link voltage (V_{dc}) of SAPF and supply neutral current (i_{sn}) for TPFW system with non-linear load. The supply voltages are observed to be highly distorted. The MCCF implementation on supply voltages makes the filtered supply voltages (v_{sabcf}) distortion less

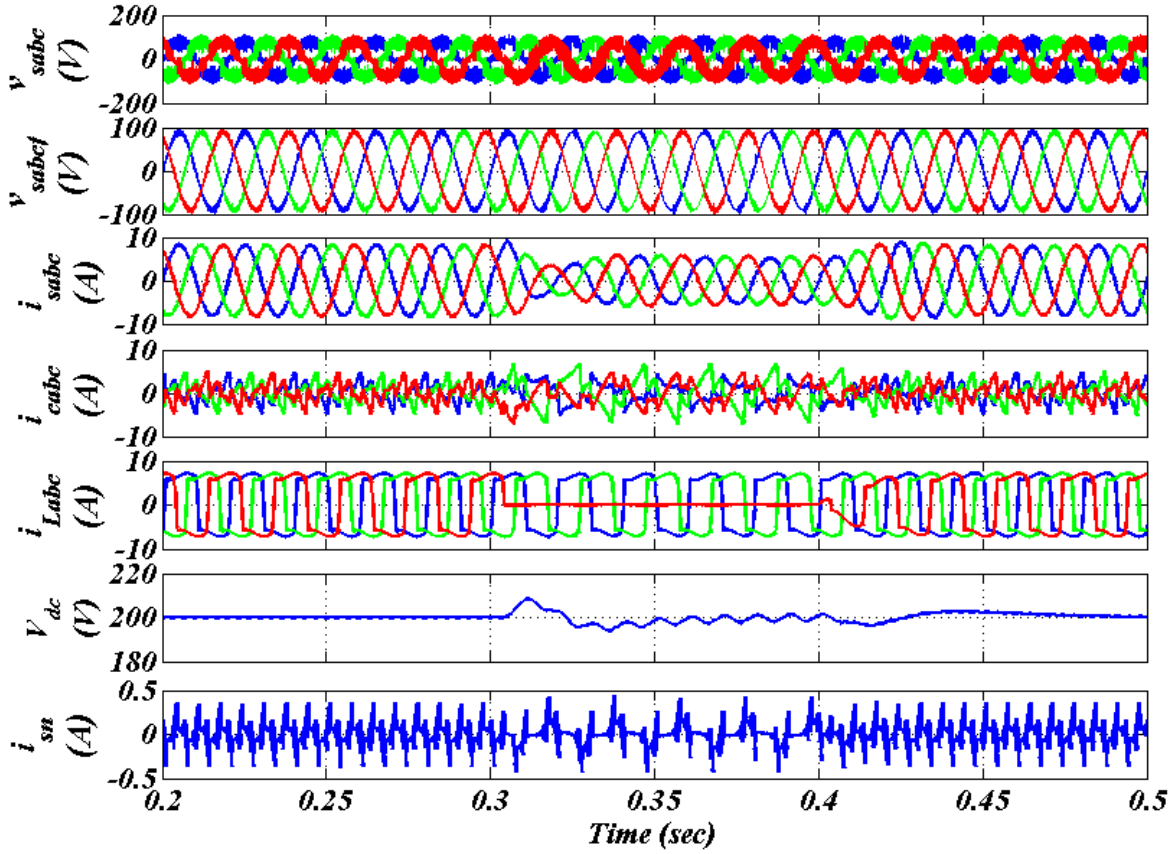

Fig. 6.6 Simulation results using MCCF based control algorithm for non-linear load under distorted grid.

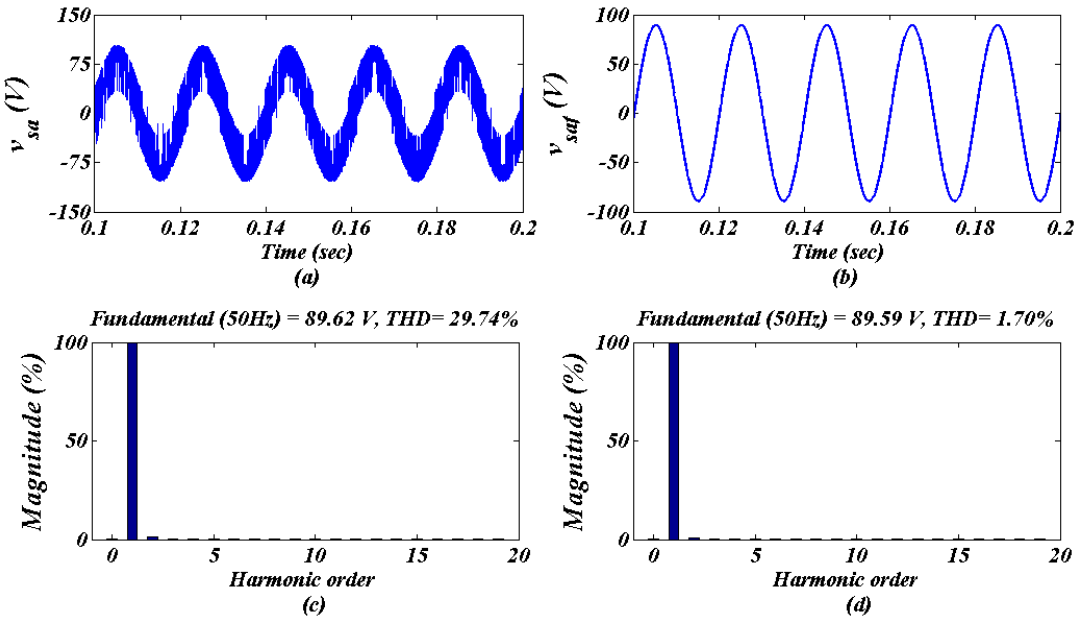

Fig. 6.7 Harmonic analysis using MCCF based control algorithm (a-b) waveforms of v_{sa}, v_{saf} (c-d) THD of v_{sa}, v_{saf} for non-linear load

and sinusoidal. The MCCFs are also implemented on the load currents to get fundamental component of currents. The performance of the controller is observed under steady state condition as well as under a load unbalancing introduced during time t=0.3 sec to 0.4 sec.

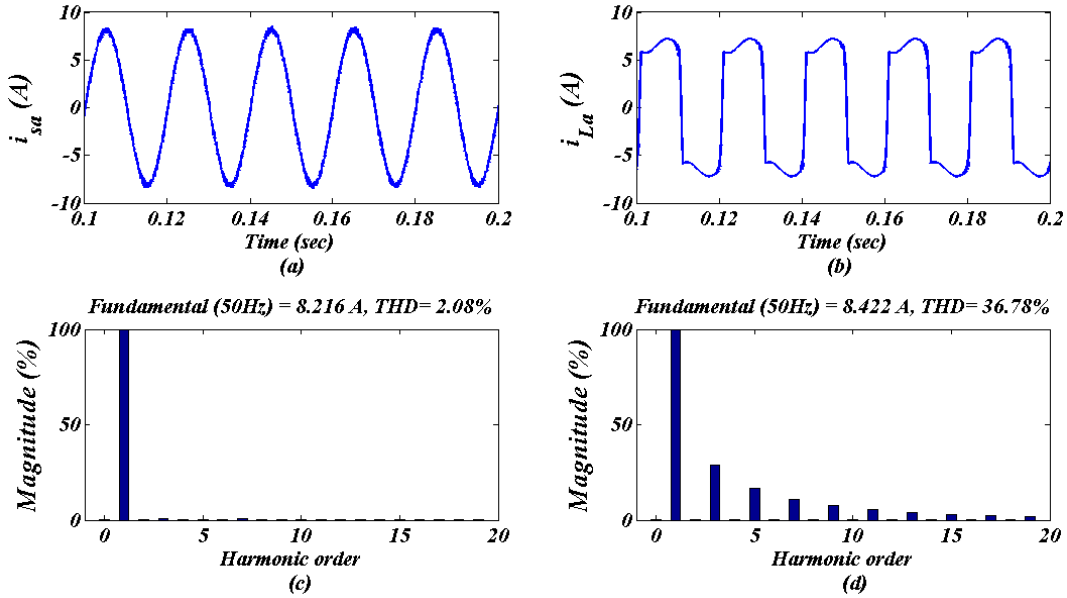

Fig. 6.8 Harmonic analysis using MCCF based control algorithm (a-b) waveforms of i_{sa}, i_{La} (c-d) THD of i_{sa}, i_{La} for non-linear load

Figs. 6.7(a)-(b) show phase 'a' supply voltage (v_{sa}) and phase 'a' filtered supply voltage (v_{saf}) waveforms. Figs. 6.7(c)-(d) show the THD content in phase 'a' supply voltage (v_{sa}) and phase 'a' filtered supply voltage (v_{saf}). The THD of supply voltage is very high (29.74%), which has been reduced to 1.70% by filtering action of MCCF. Figs. 6.8(a)-(b) show waveforms of phase 'a' supply current (i_{sa}) and phase 'a' non-sinusoidal load current (i_{La}). Figs. 6.8(c)-(d) show the THD content of phase 'a' supply current (i_{sa}) and phase 'a' load current (i_{La}). The supply current would be highly distorted with a THD of 36.78% if SAPF is not connected. The SAPF has reduced the THD in supply current to 2.08% by using MCCF based algorithm.

In Fig. 6.9 simulation results for distorted grid condition with MCCF control technique in presence of linear loads are presented. Fig. 6.9 shows three phase supply voltages (v_{sa}, v_{sb}, v_{sc}), three phase filtered supply voltages (v_{saf}, v_{sbf}, v_{scf}), three phase supply currents (i_{sa}, i_{sb}, i_{sc}), three phase compensator currents (i_{ca}, i_{cb}, i_{cc}), three phase lagging load currents (i_{La}, i_{Lb}, i_{Lc}), DC link voltage (V_{dc}) of SAPF and supply neutral current (i_{sn}) for TPFW system with linear load. The MCCF technique controls SAPF effectively for PQ problems mitigation. It

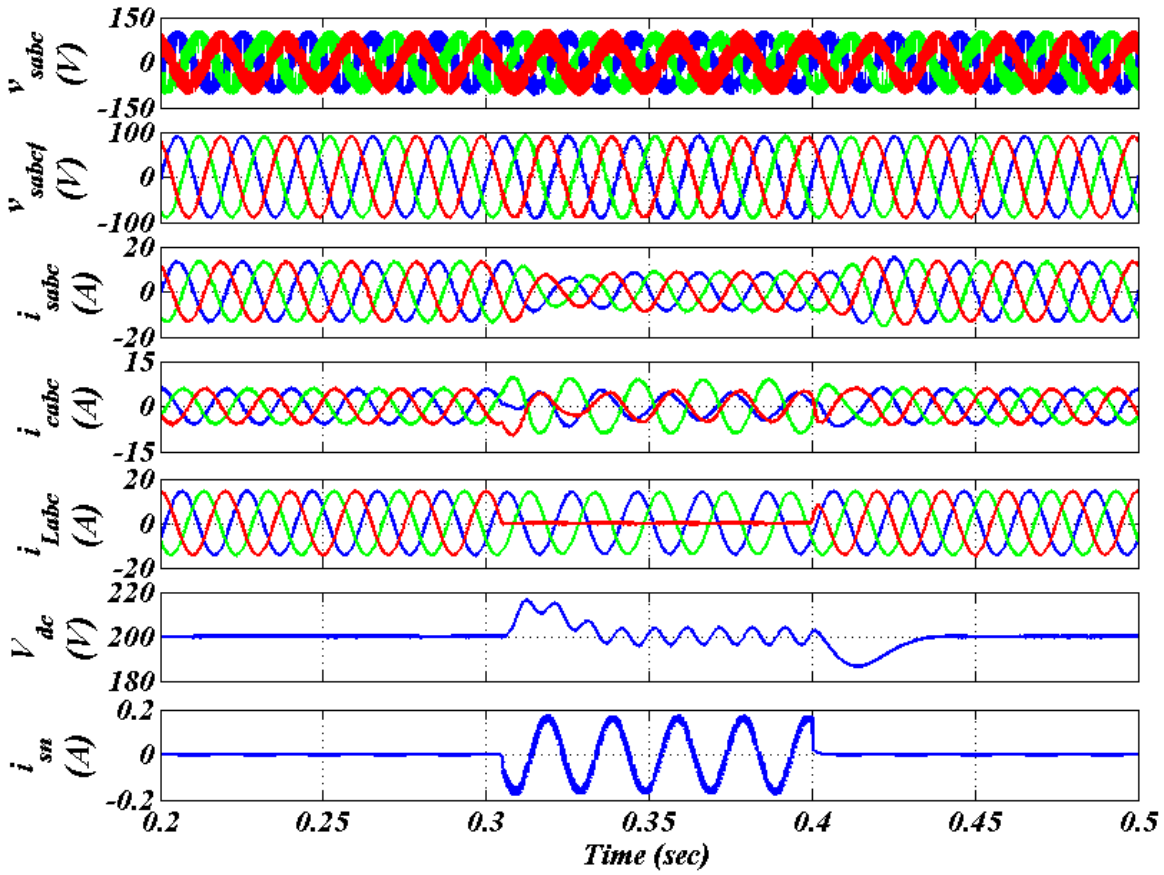

Fig. 6.9 Simulation results using MCCF based control algorithm for linear load under distorted grid.

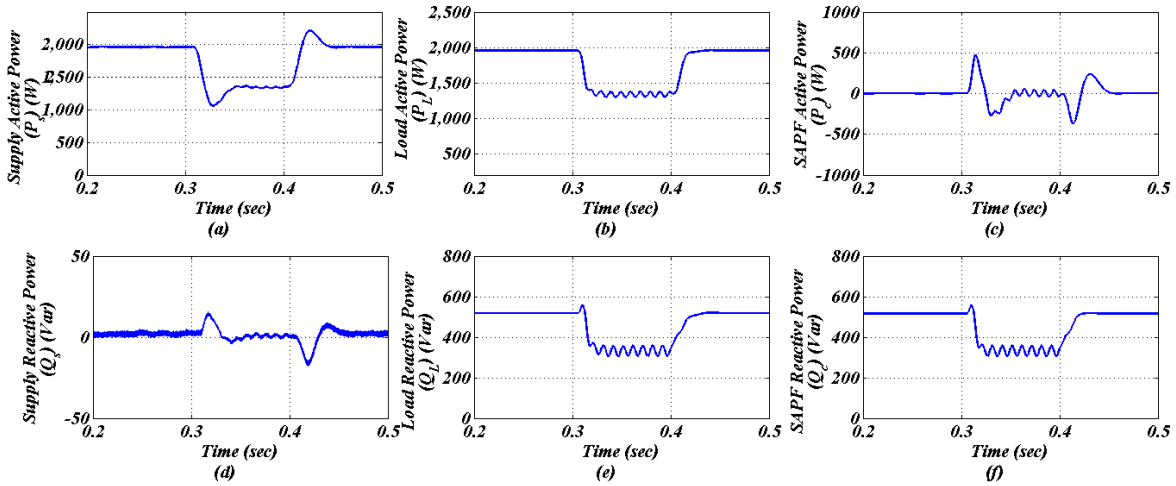

Fig. 6.10 Power flow for TPFW distorted grid system using MCCF based control algorithm (a-c) Active power P_s, P_L, P_c (d-f) Reactive Power Q_s, Q_L, Q_c for linear load

has been observed that the supply currents are balanced and sinusoidal during varying loading condition. The supply neutral current is also limited due to presence of zigzag transformer. Figs. 6.10(a)-(f) show the profiles of power flow for supply (P_s, Q_s), load (P_L, Q_L), and compensator (P_c, Q_c). It is observed that during load unbalancing between t=0.3 sec

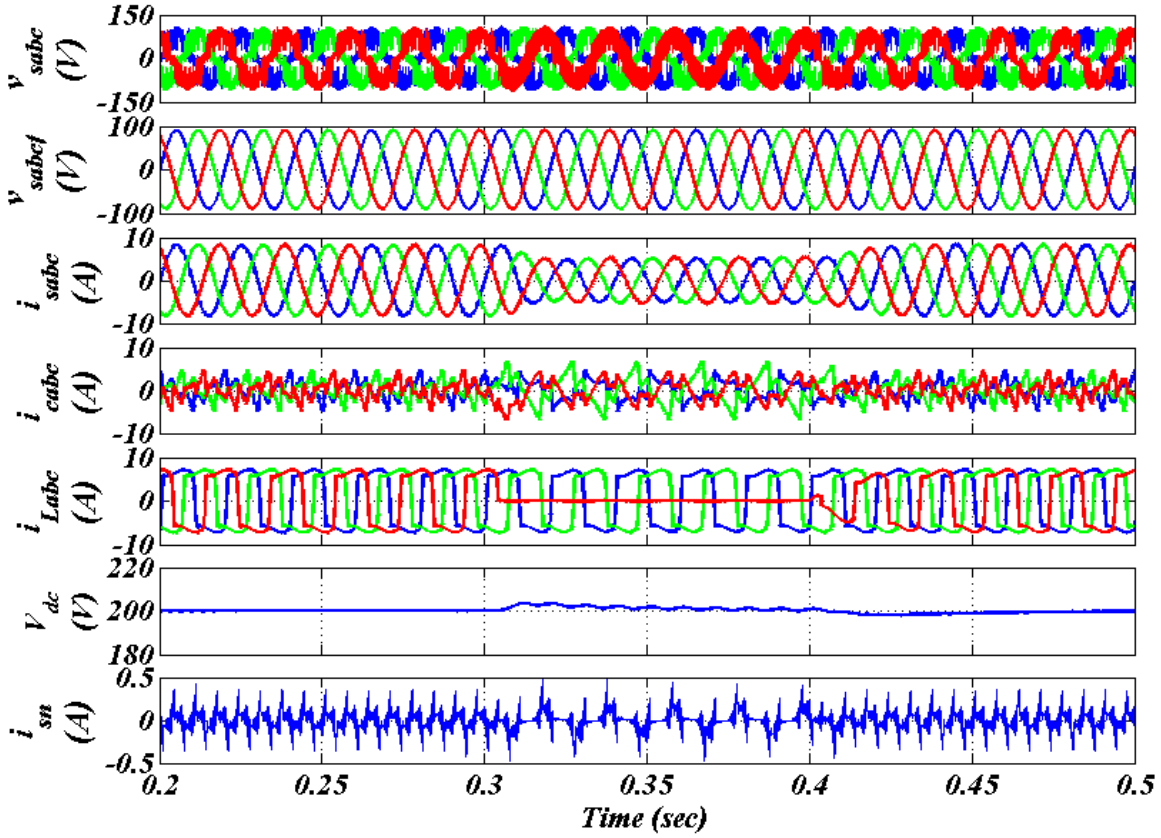

Fig. 6.11 Simulation results using SOGI based control algorithm for non-linear load under distorted grid.

to 0.4 sec, the real power requirement of load is met by the supply whereas reactive power requirement of load is supplied by the compensator. The supply reactive power burden is nearly zero.

6.3.2 Second Order Generalized Integrator Based Control Algorithm

Fig. 6.11 presents simulation results of SOGI based control of SAPF in TPFW system. The load considered is a TPFW non-linear load comprising of three single phase diode bridge rectifiers with R-L load at their output terminals. Fig. 6.11 shows three phase supply voltages (v_{sa}, v_{sb}, v_{sc}), three phase filtered supply voltages (v_{saf}, v_{sbf}, v_{scf}), three phase supply currents (i_{sa}, i_{sb}, i_{sc}), three phase compensator currents (i_{ca}, i_{cb}, i_{cc}), three phase non-sinusoidal load currents (i_{La}, i_{Lb}, i_{Lc}), DC link voltage (V_{dc}) of SAPF and supply neutral current (i_{sn}) for non-linear load. It is observed that the supply voltages are highly distorted and THD content is 29.74%. By using SOGI technique, the filtered supply voltages are extracted. SOGI filters

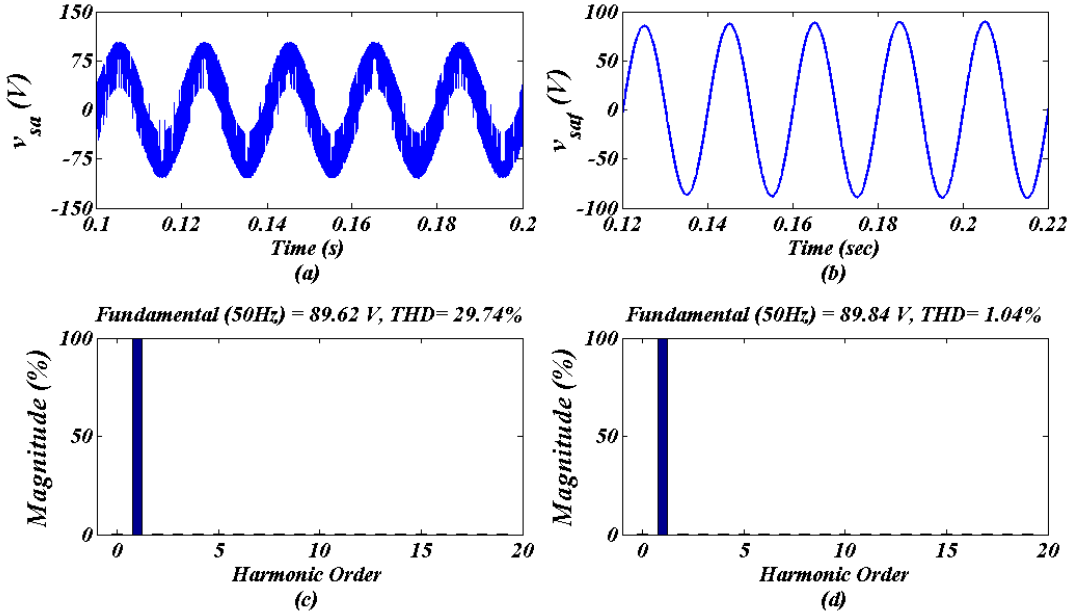

Fig. 6.12 Harmonic analysis using SOGI based control algorithm (a-b) waveforms of v_{sa}, v_{saf} (c-d) THD of v_{sa}, v_{saf} for non-linear load

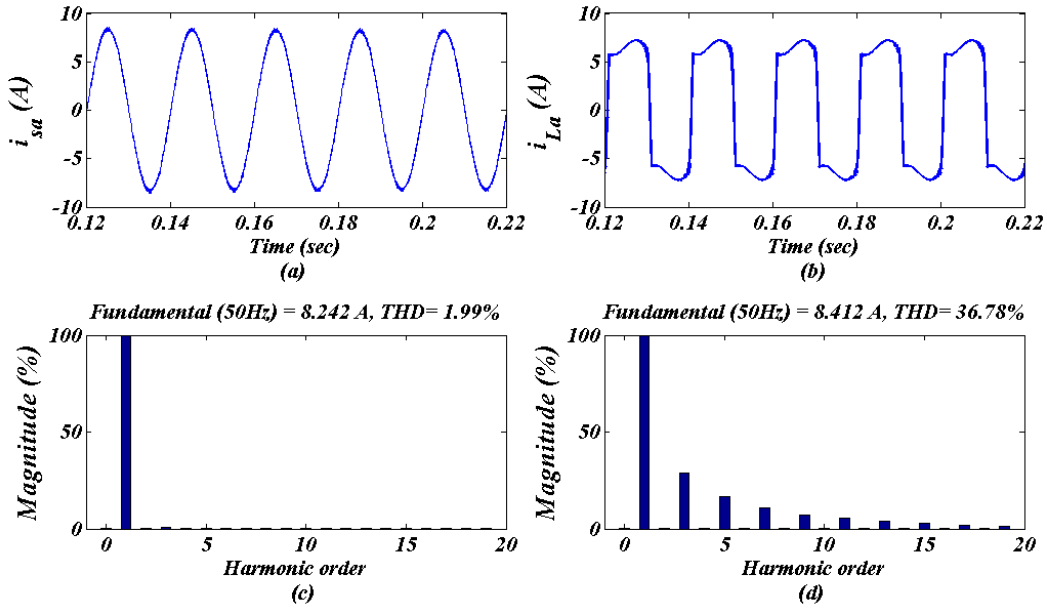

Fig. 6.13 Harmonic analysis using SOGI based control algorithm (a-b) waveforms of i_{sa}, i_{La} (c-d) THD of i_{sa}, i_{La} for non-linear load

are also implemented to extract fundamental component of load currents as shown in Fig. 6.5. Fig. 6.11 shows that during t=0.3 to 0.4 sec, load currents are unbalanced but the supply currents

are balanced and sinusoidal, also DC link voltage is regulated at 200 V. The supply neutral current is also restricted to ±0.2A. Figs. 6.12(a)-(b) show supply voltages (v_{sabc}) and filtered supply voltages (v_{sabcf}) waveforms and Figs. 6.12(c)-(d) show their THD content respectively.

The THD in filtered supply voltage is 1.04%. Figs. 6.13(a)-(b) show phase 'a' supply current (i_{sa}) and phase 'a' load current (i_{La}) waveforms and Figs. 6.13(c)-(d) show their THD respectively. The THD in supply current (i_{sa}) is 1.99%, and in load current is 36.78%. It is observed that the SOGI controller works well for fundamental extraction of voltages and currents.

In Fig. 6.14 simulation results are shown for implementation of SOGI control technique for distorted distribution system with linear load. Fig. 6.14 shows three phase supply voltages (v_{sa}, v_{sb}, v_{sc}), three phase filtered supply voltages (v_{saf}, v_{sbf}, v_{scf}), three phase supply currents (i_{sa}, i_{sb}, i_{sc}), three phase compensator currents (i_{ca}, i_{cb}, i_{cc}), three phase lagging load currents (i_{La}, i_{Lb}, i_{Lc}), DC link voltage (V_{dc}) of SAPF and supply neutral current (i_{sn}) for TPFW system with linear load. The supply currents are in phase with respective supply voltages and have sinusoidal waveform. The supply neutral current is also limited to ±0.2 A and DC bus voltage is maintained to reference value of 200 V. Figs. 6.15(a)-(f) show the plots of power flow for

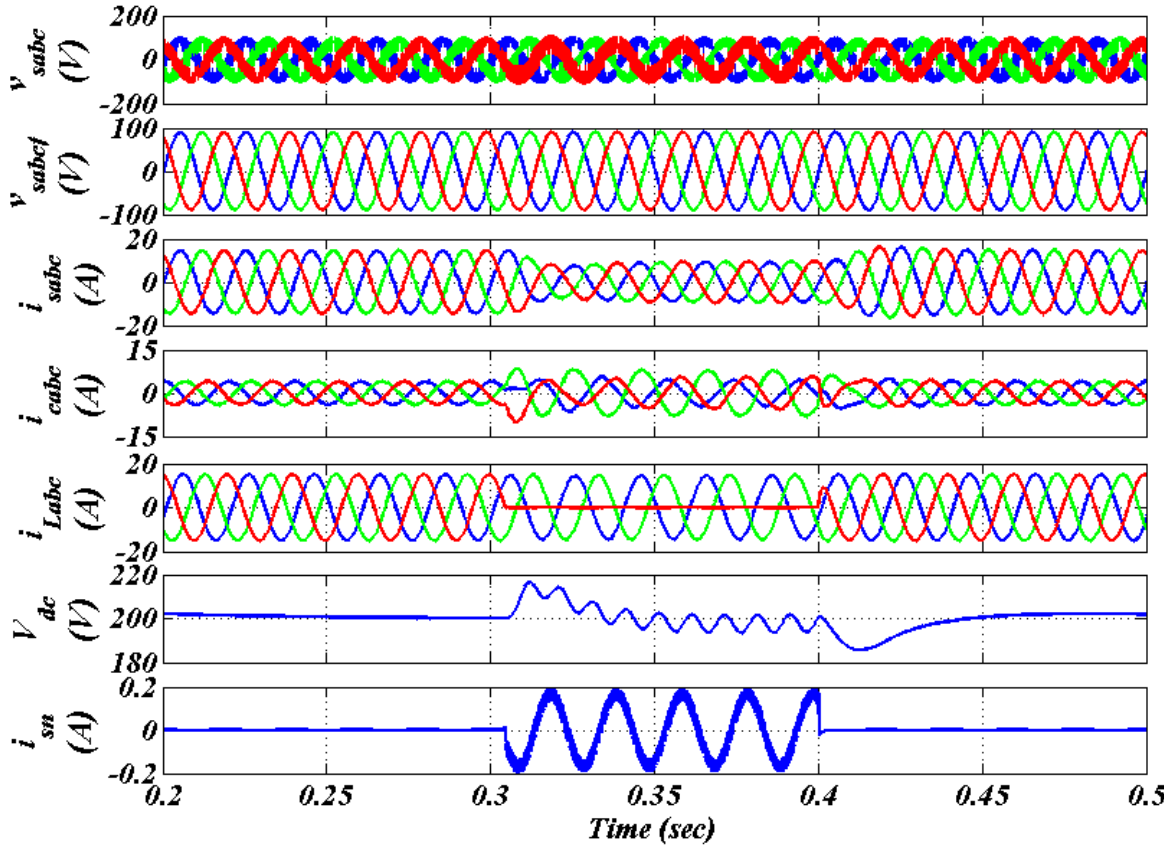

Fig. 6.14 Simulation results using SOGI based control algorithm for linear load under distorted grid.

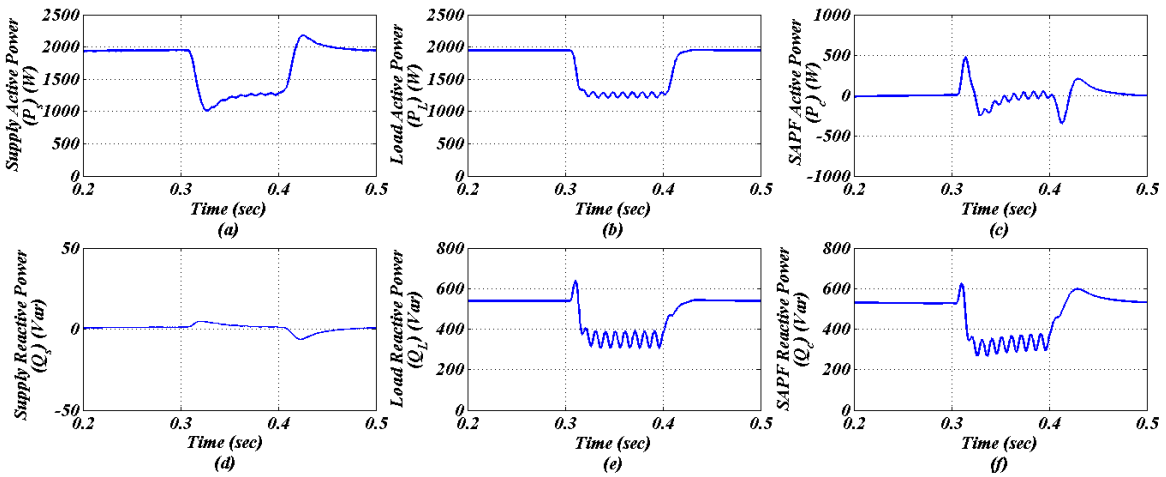

Fig. 6.15 Power flow for TPFW distorted grid system using SOGI based control algorithm (a-c) Active power P_s, P_L, P_c (d-f) Reactive Power Q_s, Q_L, Q_c for linear load

supply (P_s, Q_s), load (P_L, Q_L), and compensator (P_c, Q_c). It indicates that the real power demand of load is met by grid and reactive power demand is met by the compensator during steady state and dynamic conditions.

6.4 EXPERIMENTAL RESULTS

The developed control techniques in this chapter are implemented on prototype hardware using dSPACE1104. Additional inductors are connected in series with the supply voltages to create effect of distortion in the PCC voltage. The hardware is developed and tested and dSPACE1104 DSP controller is used to implement control algorithms on SAPF. The experimental results are recorded and discussed in sub-sections.

6.4.1. Multiple Complex Coefficient Filter Based Control Algorithm

Fig. 6.16 shows the steady state waveforms of a TPFW system with SAPF and MCCF control technique for non-linear loads. Figs. 6.16(a)-(c) show phase 'a' SAPF compensated supply current (i_{sa}), phase 'a' load current (i_{La}) and phase 'a' SAPF injected compensator current (i_{ca}) and phase 'a' supply voltage (v_{sa}). The load current is non-sinusoidal but the supply current is sinusoidal. Figs. 6.16(d)-(f) show the harmonic content in phase 'a' supply voltage (v_{sa}), phase 'a' supply current (i_{sa}) and phase 'a' load current (i_{La}) respectively. The PCC voltage has a THD of 9.7%. The PCC voltages and non-linear load currents are processed in dSAPCE

1104 controller for implementation of MCCF technique to generate reference currents. In presence of SAPF, the phase 'a' supply current has THD of 3.6%, which is below 5% limit, whereas the load current has a THD of 29.9%. The SAPF succeeds is able to reduce THD in supply current even though the PCC voltages are distorted. Figs. 6.16(g)-(i) show the supply neutral current (i_{sn}), load neutral current (i_{Ln}) and zigzag transformer neutral current (i_{zn}) and phase 'a' supply voltage (v_{sa}). The supply neutral current is limited to 0.107 A. The neutral current in load and zigzag transformer neutral current have almost equal magnitude. All the neutral current of the load during load unbalancing is transferred to the neutral wire of the

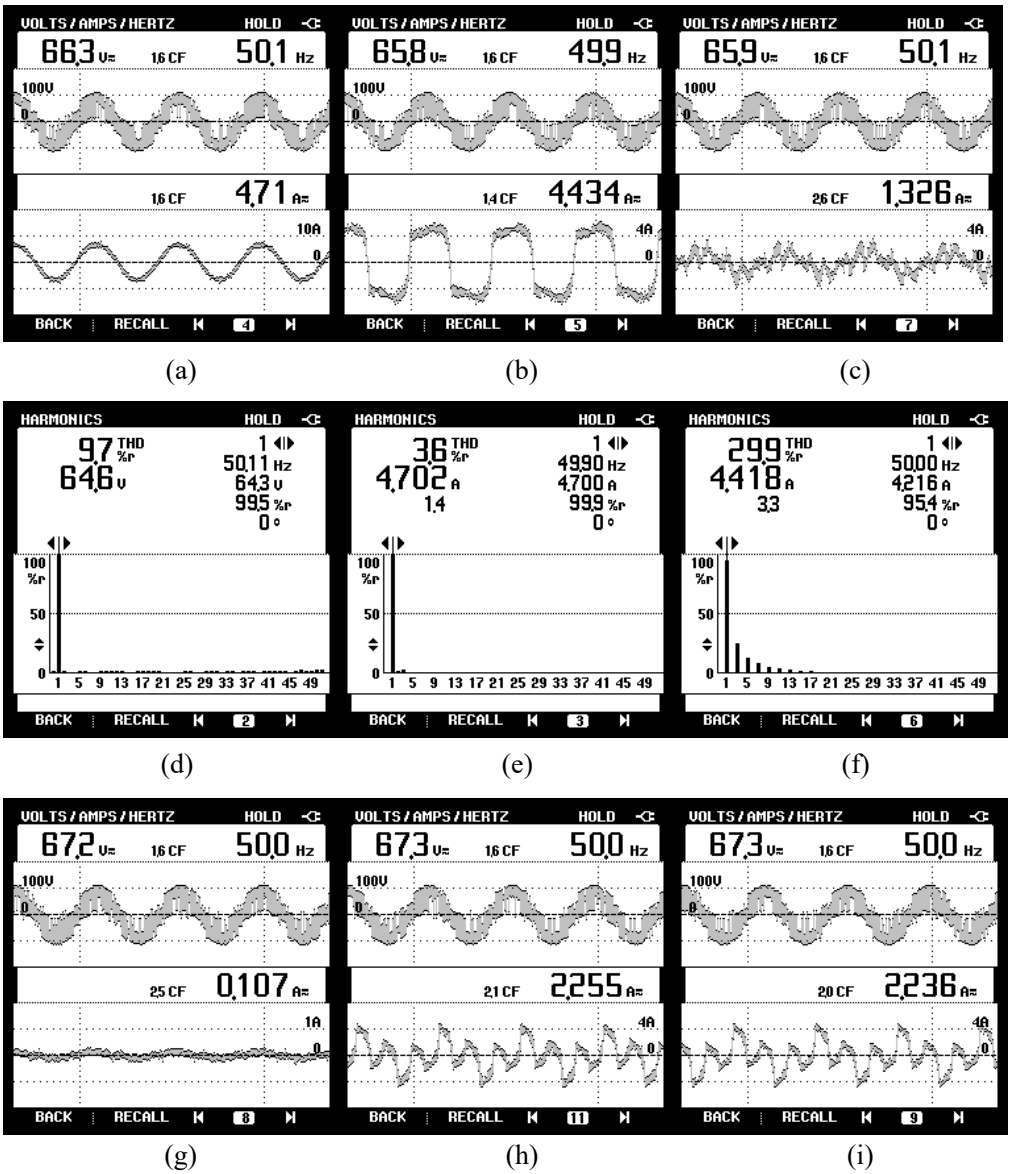

Fig. 6.16 Steady state waveforms for TPFW distorted grid system using MCCF based control algorithm (a) v_{sa}-i_{sa} (b) v_{sa}-i_{La} (c) v_{sa}-i_{ca} and (d-f) THD of (d) v_{sa} (e) i_{sa} (f) i_{La} (g-i) neutral current of (g) supply (i_{sn}) (h) load (i_{Ln}) and (i) zigzag (i_{zn}) for non-linear load

supply and zigzag transformer is restricted to very low value.

Fig. 6.17 shows the dynamic performance of the TPFW system with SAPF using MCCF control technique and non-linear load. Fig. 6.17(a) shows phase 'a' supply voltage (v_{sa}) and three phase shunt compensated supply currents (i_{sa}, i_{sb}, i_{sc}). After compensation the supply currents are observed to be balanced but smaller in magnitude due to unbalanced load. The supply currents are also sinusoidal. Fig. 6.17(b) shows phase 'a' supply voltage (v_{sa}) and three phase non-sinusoidal load currents (i_{La}, i_{Lb}, i_{Lc}). The load unbalancing is observed from this figure when the current in phase 'c' is reduced to zero by sudden removal of phase 'c' supply line. Fig. 6.17(c) shows phase 'a' supply voltage (v_{sa}) and three phase shunt injected compensator currents (i_{ca}, i_{cb}, i_{cc}). The compensator currents helps in balancing the supply currents during unbalancing and making it sinusoidal during all load conditions. Fig. 6.17(d) shows DC link voltage (V_{dc}), phase 'c' supply current (i_{sc}), phase 'c' load current (i_{Lc}) and phase 'c' compensator currents (i_{cc}).

Fig. 6.18 shows the intermediate signals with the MCCF control technique of SAPF for non-

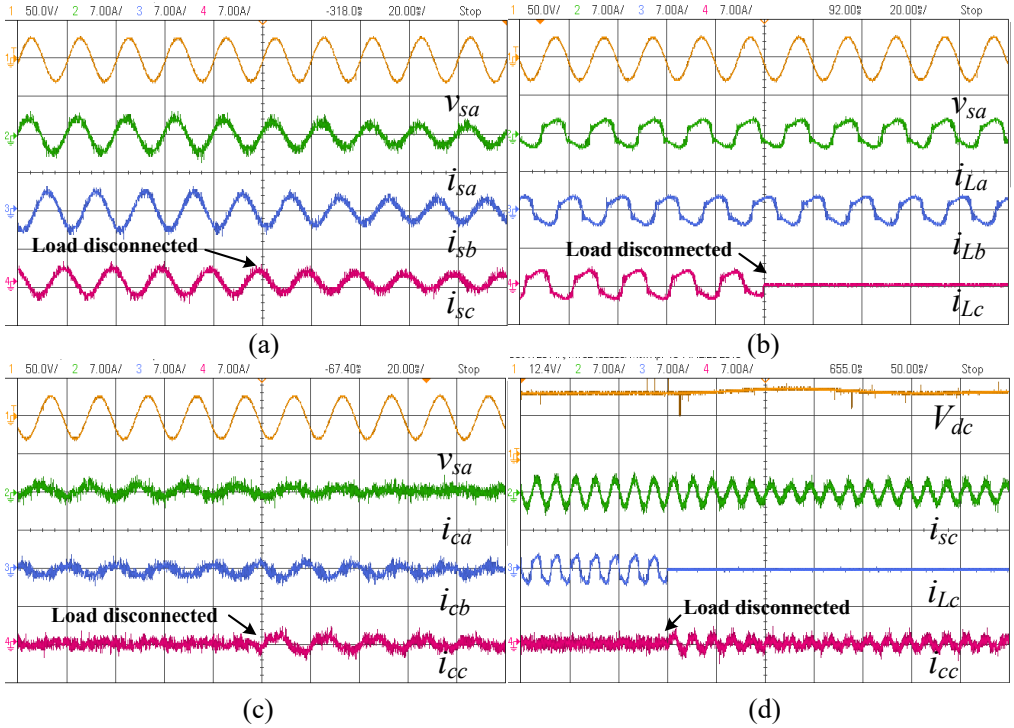

Fig. 6.17 Results showing dynamics for load disconnected in phase 'c' using MCCF based control algorithm (a) v_{sa}, i_{sa}, i_{sb}, i_{sc} (b) v_{sa}, i_{La}, i_{Lb}, i_{Lc} (c) v_{sa}, i_{ca}, i_{cb}, i_{cc} (d) V_{dc}, i_{sc}, i_{Lc}, i_{cc} for non-linear load

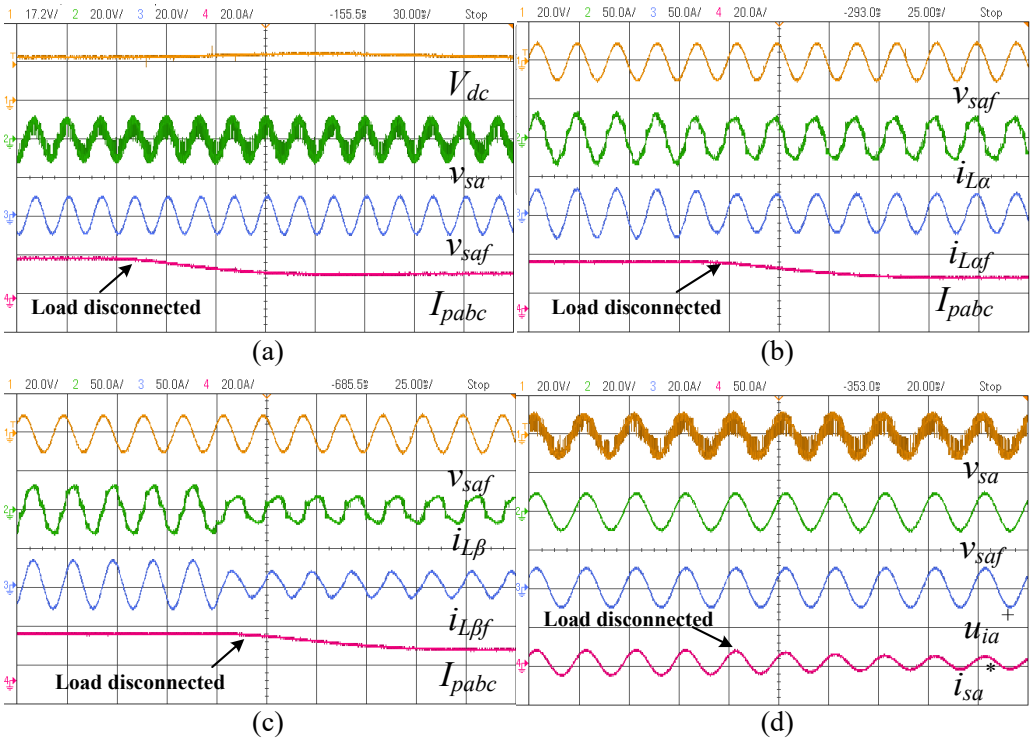

Fig. 6.18 Intermediate results using MCCF based control algorithm (a) V_{dc}, v_{sa},v_{saf}, I_{pabc} (b) v_{saf}, $i_{L\alpha}$, $i_{L\alpha f}$, I_{pabc} (c) v_{saf}, $i_{L\beta}$, $i_{L\beta f}$, I_{pabc} (d) v_{sa}, v_{saf}, u_{ia}^{+}, i_{sa}^{*} for non-linear load

linear load. Fig 6.18(a) shows the DC link voltage (V_{dc}), phase 'a' supply voltage (v_{sa}), filtered phase 'a' supply voltage (v_{saf}) and fundamental active power component of load currents (I_{pabc}). The fundamental voltage component (v_{saf}) has been filtered effectively using MCCF and DC link voltage is regulated to reference value using PI controller. Fig. 6.18(b) shows filtered phase 'a' supply voltage (v_{saf}), load current alpha component ($i_{L\alpha}$), filtered alpha component of load current ($i_{L\alpha f}$) and fundamental active power component (I_{pabc}) of load currents. The MCCF is applied for non-linear load and successfully extracts fundamental α-β components of load current. Fig. 6.18(c) shows filtered phase 'a' supply voltage (v_{saf}), beta component of load current ($i_{L\beta}$), filtered beta component of load current ($i_{L\beta f}$) and fundamental active power component (I_{pabc}) of load currents. Fig. 6.18(d) presents phase 'a' supply voltage (v_{sa}), filtered phase a supply voltage (v_{saf}), modified unit template for phase 'a', (u_{ia}^{+}) and reference current for phase 'a' (i_{sa}^{*}). The reference currents of proper magnitude are generated by MCCF control technique for SAPF connected on PCC voltages

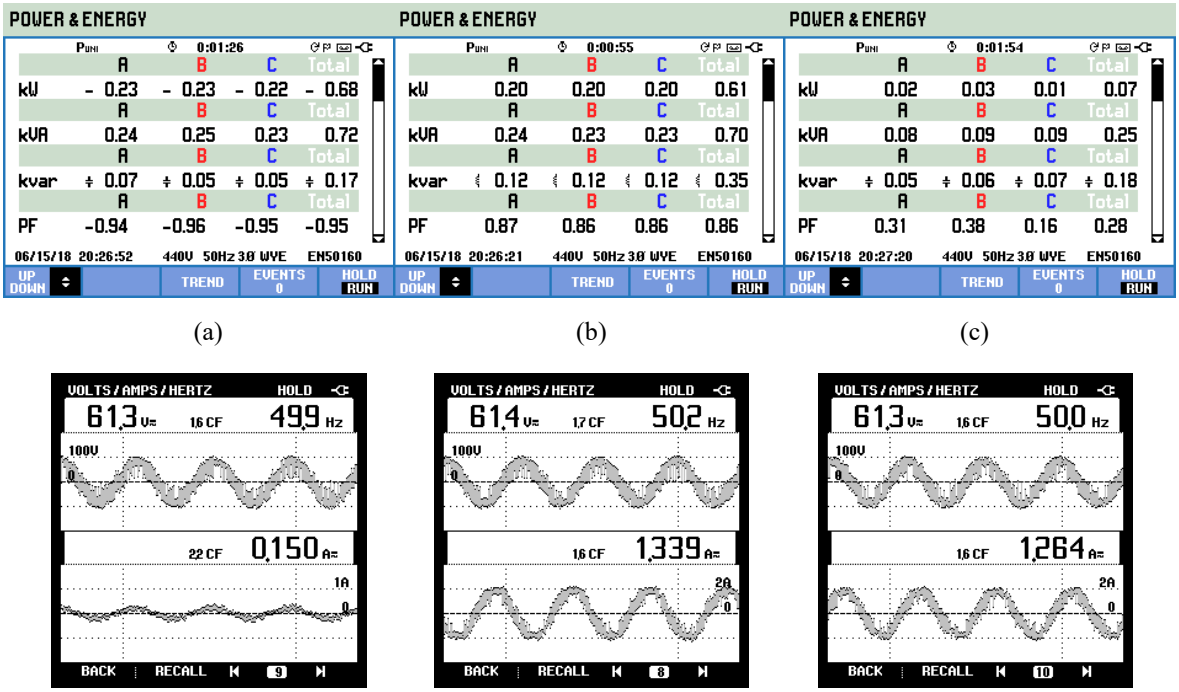

(a) (b) (c)

(d) (e) (f)

Fig. 6.19 (a-c) Steady state power for TPFW linear system using MCCF based control algorithm for (a) Supply (b) Load (c) Compensator and (d-f) neutral current of (d) supply (i_{sn}) (e) load (i_{Ln}) and (f) zigzag (i_{zn}) for linear load

and load currents.

Fig. 6.19 shows the steady state power flow using MCCF control Technique. Figs. 6.19(a)-(c) show steady state power flow from supply, load and SAPF respectively. The supply feeds active power (680 W), reactive power (170 VARs) and compensator provides reactive power (180 VARs) to the load, which has a total power requirement of P_L (610 W) and Q_L (350 VARs). Figs. 6.19(d)-(f) present the supply neutral current (i_{sn}), load neutral current (i_{Ln}) and zigzag transformer neutral current (i_{zn}) and phase 'a' supply voltage (v_{sa}). The supply neutral current is limited to 0.15 A. The entire neutral current of the load passes through the zigzag transformer neutral.

Fig. 6.20 shows the dynamic performance of the TPFW system with SAPF and MCCF control technique for linear load. Fig. 6.20(a) shows phase 'a' supply voltage (v_{sa}) and three phase shunt compensated supply currents (i_{sa}, i_{sb}, i_{sc}). It is observed that supply currents are balanced and sinusoidal. Fig. 6.20(b) shows phase 'a' supply voltage (v_{sa}) and three phase

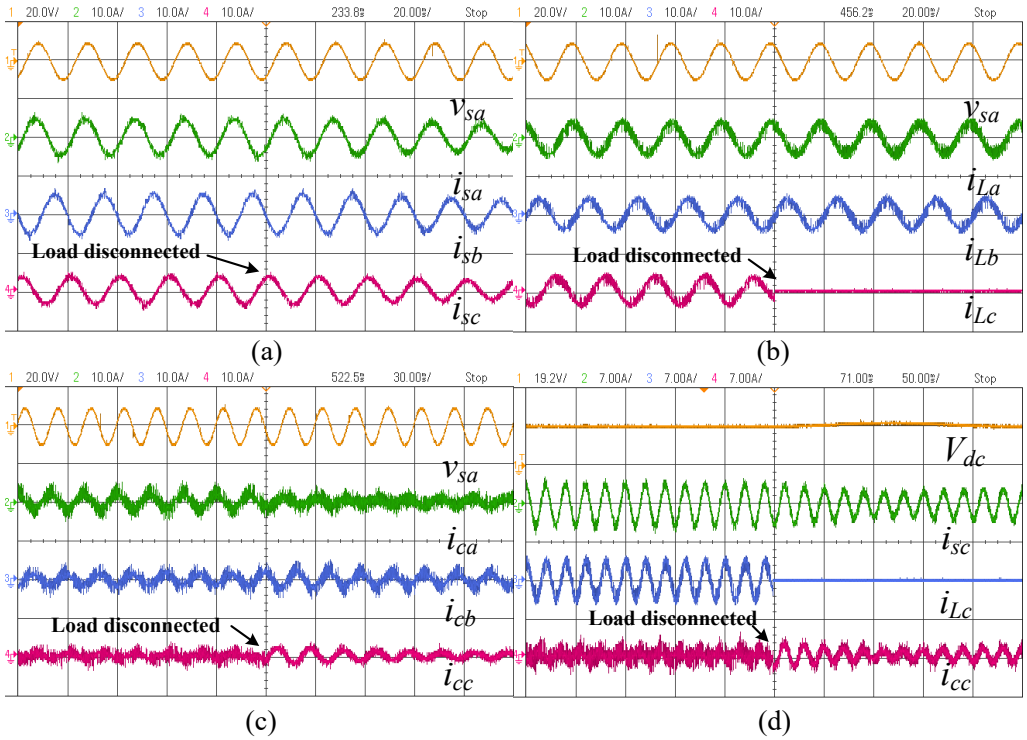

Fig. 6.20 Results showing dynamics for load disconnected in phase 'c' using MCCF based control algorithm (a) v_{sa}, i_{sa}, i_{sb}, i_{sc} (b) v_{sa}, i_{La}, i_{Lb}, i_{Lc} (c) v_{sa}, i_{ca}, i_{cb}, i_{cc} (d) V_{dc}, i_{sc}, i_{Lc}, i_{cc} for linear load

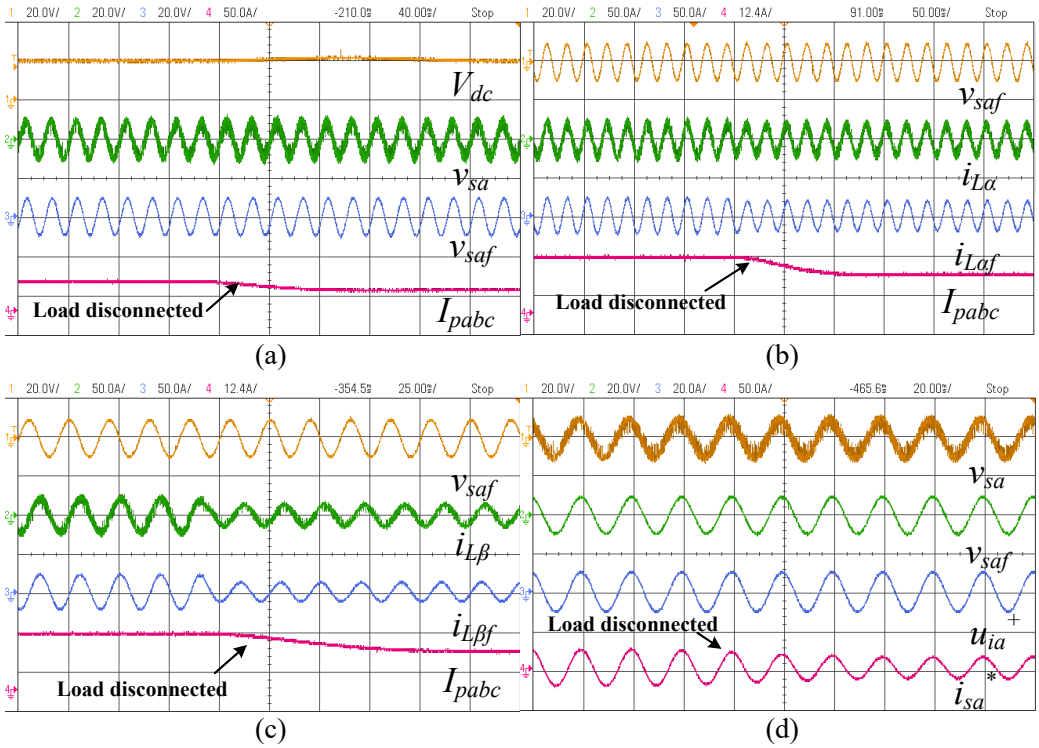

Fig. 6.21 Intermediate results using MCCF based control algorithm (a) V_{dc}, v_{sa},v_{saf}, I_{pabc} (b) v_{saf}, $i_{L\alpha}$, $i_{L\alpha f}$, I_{pabc} (c) v_{saf}, $i_{L\beta}$, $i_{L\beta f}$, I_{pabc} (d) v_{sa}, v_{saf}, u_{ia}^{+}, i_{sa}^{*} for linear load

lagging PF load currents (i_{La}, i_{Lb}, i_{Lc}). The phase 'c' load current is reduced to zero during load removal in phase 'c'. Fig. 6.20(c) shows phase 'a' supply voltage (v_{sa}) and three phase

SAPF injected compensator currents (i_{ca}, i_{cb}, i_{cc}) which are sinusoidal. Fig 6.20(d) shows the DC link voltage (V_{dc}), and phase 'c' supply current (i_{sc}), phase 'c' load current (i_{Lc}) and phase 'c' compensator current (i_{sc}, i_{Lc}, i_{cc}). The DC link voltage increases slightly during load unbalancing period but it is regulated by PI controller to 200 V.

Fig. 6.21 shows the intermediate signals with MCCF based control with linear load. Fig 6.21 (a) shows the DC link voltage (V_{dc}), phase 'a' supply voltage (v_{sa}), filtered phase 'a' supply voltage (v_{saf}) and fundamental active power component of load currents (I_{pabc}). The I_{pabc} decreases in magnitude during unbalanced load. Fig. 6.21(b) shows filtered phase 'a' supply voltage (v_{saf}), alpha component of load current ($i_{L\alpha}$), filtered load current alpha component ($i_{L\alpha f}$) and fundamental active power component (I_{pabc}) of load current. Fig. 6.21(c) shows filtered phase 'a' supply voltage (v_{saf}), load beta component ($i_{L\beta}$), filtered beta component of load current ($i_{L\beta f}$) and fundamental active power component (I_{pabc}). Fig. 6.21(d) presents phase 'a' supply voltage (v_{sa}), phase 'a' filtered supply voltage (v_{saf}) and MCCF extracted unit template for phase 'a', (u_{ia}^{+}) and reference current (i_{sa}^{*}) for phase 'a'. The reference current i_{sa}^{*} decreases in magnitude during sudden disconnection of phase 'c' of the load.

6.4.2. Second Order Generalized Integrator Based Control Algorithm

Fig. 6.22 shows the steady state waveforms using SOGI based control of SAPF in TPFW distribution system feeding non-linear loads. Figs. 6.22(a)-(c) show phase 'a' supply current (i_{sa}), phase 'a' non-sinusoidal load current (i_{La}), phase 'a' compensator current (i_{ca}) and phase 'a' supply voltage (v_{sa}). Figs. 6.22(d)-(f) show the harmonic content in the supply voltage (v_{sa}), supply current (i_{sa}) and load current (i_{La}) respectively. The supply voltage has a high THD of 9.5% due to distorted grid condition. The supply current after compensation has THD of 3.8% obtained with SOGI based control technique. The load current has a THD of 29.6%. Figs. 6.22(g)-(i) show the supply neutral current (i_{sn}), load neutral current (i_{Ln}), zigzag transformer neutral current (i_{zn}) and phase 'a' supply voltage (v_{sa}). The supply neutral

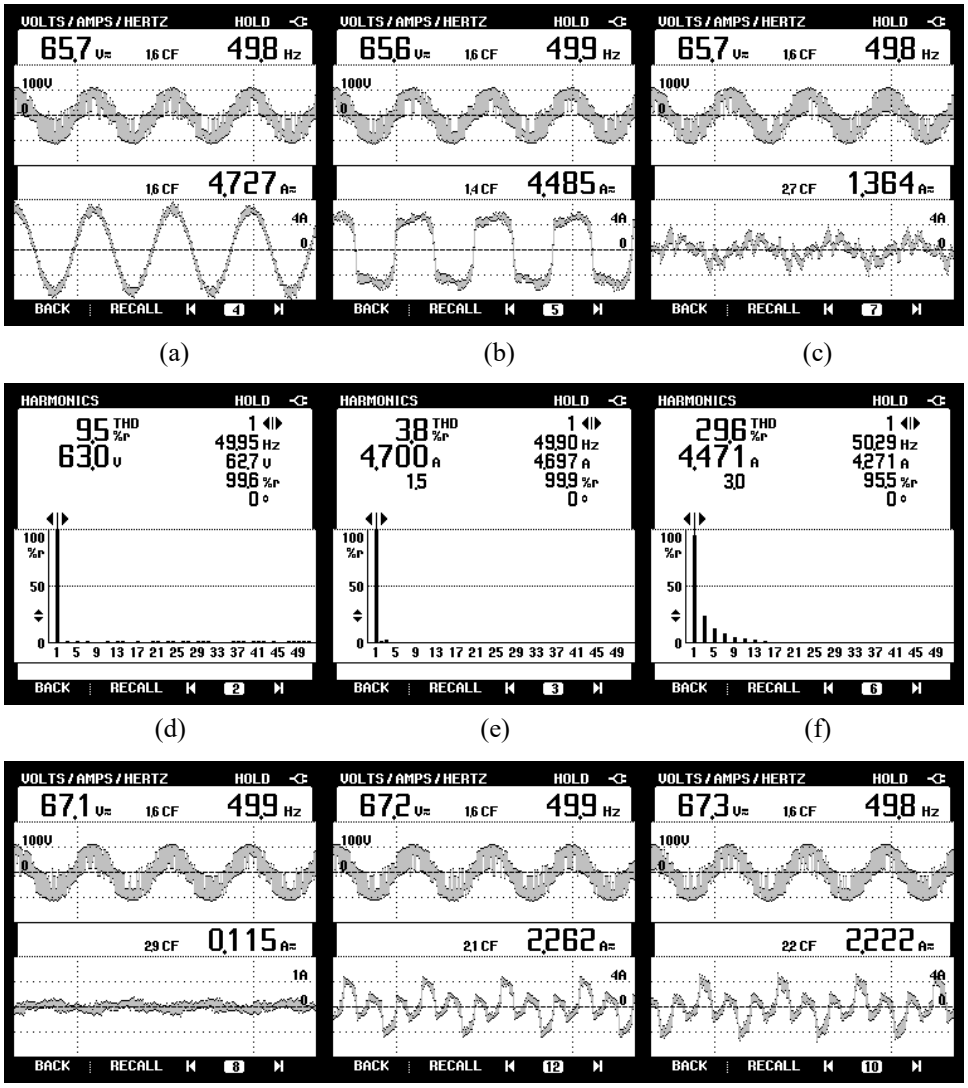

(a) (b) (c)

(d) (e) (f)

(g) (h) (i)

Fig. 6.22 Steady state waveforms for TPFW distorted grid system using SOGI based control algorithm (a) v_{sa}-i_{sa} (b) v_{sa}-i_{La} (c) v_{sa}-i_{ca} and (d-f) THD of (d) v_{sa} (e) i_{sa} (f) i_{La} (g-i) neutral current of (g) supply (i_{sn}) (h) load (i_{Ln}) and (i) zigzag (i_{zn}) for non-linear load

current is limited to 0.115 A. This is due to zigzag transformer connected between load and supply neutral points. The load neutral current has magnitude of 2.262 A and zigzag transformer neutral current has magnitude of 2.222 A. Figs. 23(g)-(i) show the waveforms when one of the load phase is disconnected.

Fig. 6.23 presents the dynamic performance of the TPFW system using SOGI based control technique and non-linear load under distorted distribution system. Fig. 5.24(a) shows phase 'a' supply voltage (v_{sa}) and three phase SAPF compensated supply currents (i_{sa}, i_{sb}, i_{sc}). The compensated supply currents are sinusoidal and balanced even under sudden disconnection of

load. Fig. 6.23(b) shows the phase 'a' supply voltage (v_{sa}) and three phase non-sinusoidal load currents (i_{La}, i_{Lb}, i_{Lc}). Fig. 6.23(c) shows phase 'a' supply voltage (v_{sa}) and three phase

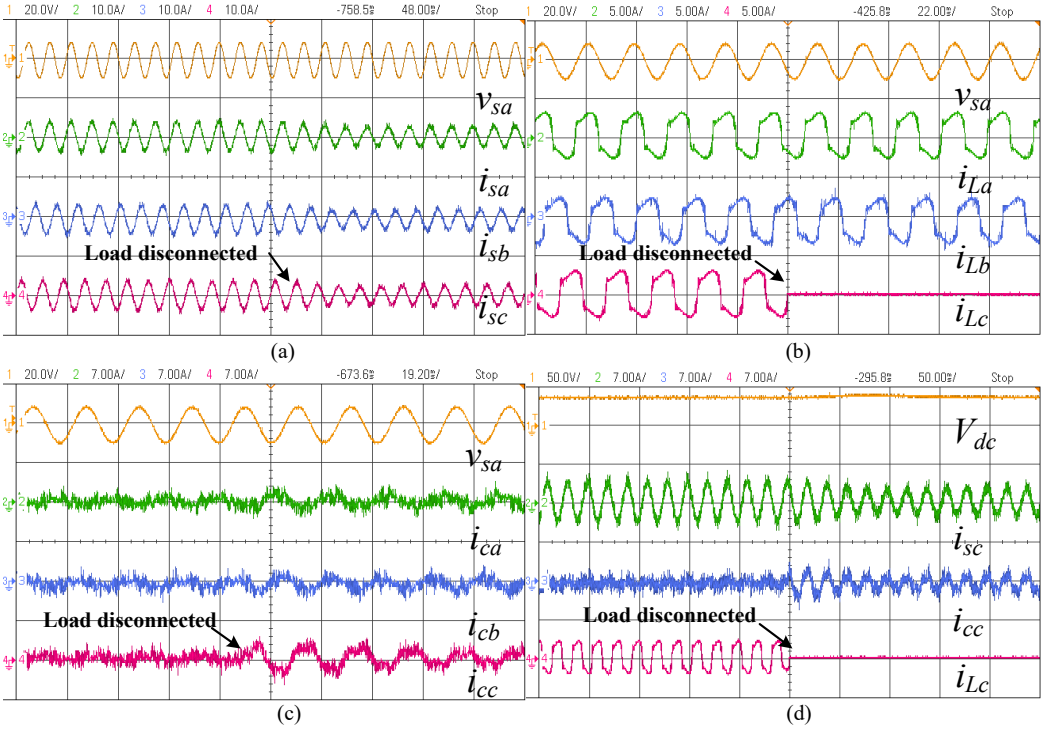

Fig. 6.23 Results showing dynamics for load disconnected in phase 'c' using SOGI based control algorithm (a) v_{sa}, i_{sa}, i_{sb}, i_{sc} (b) v_{sa}, i_{La}, i_{Lb}, i_{Lc} (c) v_{sa}, i_{ca}, i_{cb}, i_{cc} (d) V_{dc}, i_{sc}, i_{cc}, i_{Lc} for non-linear load

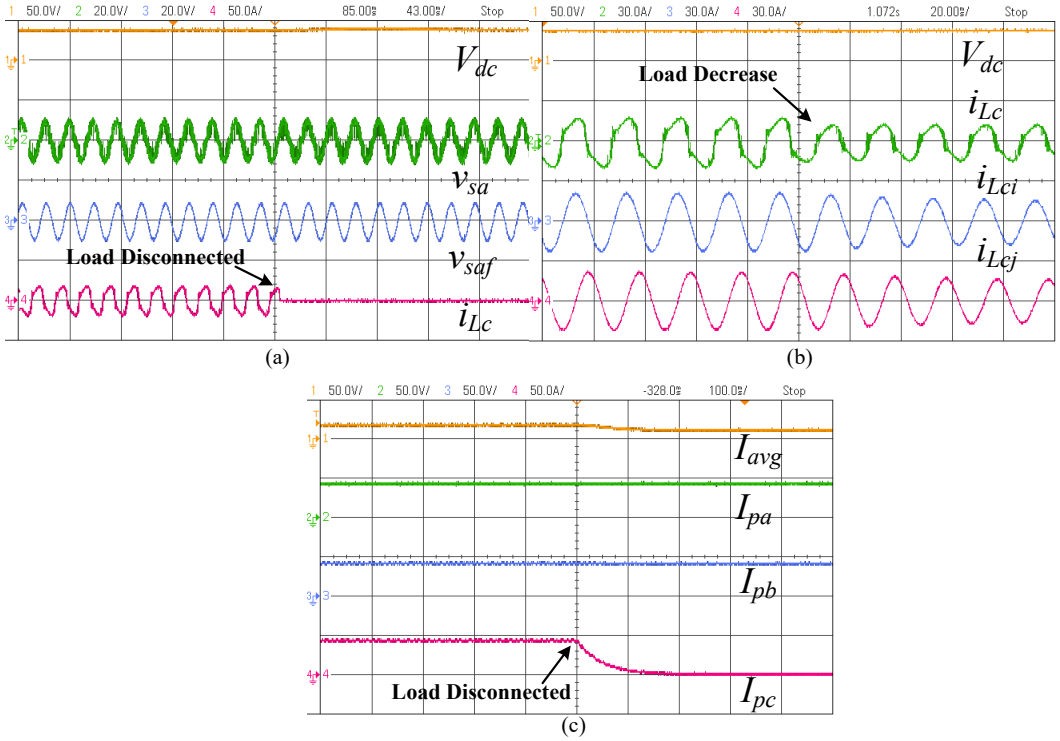

Fig. 6.24 Intermediate signals using SOGI based control technique (a) V_{dc}, v_{sa}, v_{saf}, i_{Lc} (b) (a) V_{dc}, i_{Lc}, i_{Lci}, i_{Lcj} (c) I_{avg}, I_{pa}, I_{pb}, I_{pc} for non-linear load

shunt injected compensator currents (i_{ca}, i_{cb}, i_{cc}). The injected compensator currents make supply currents sinusoidal and balanced. Fig. 6.23(d) shows DC link voltage (V_{dc}) and phase 'c' supply current (i_{sc}), phase 'c' load current (i_{Lc}) and phase 'c' compensator current (i_{cc}). During sudden disconnection of load, action of compensator is demonstrated in this figure. The DC link voltage has some transients but it settle down due to PI controller within few cycles.

Fig. 6.24 shows the intermediate signals in the SOGI control of SAPF in TPFW system feeding non-linear load. Fig 6.24(a) presents the DC link voltage (V_{dc}), phase 'a' supply voltage (v_{sa}), phase 'a' filtered supply voltage (v_{saf}) and the load current of phase 'c' (i_{Lc}). Fig 6.24(b) shows the DC link voltage (V_{dc}), phase 'c' load current (i_{Lc}), in-phase fundamental load current component (i_{Lci}), quadrature-phase fundamental load current component (i_{Lcj}). The SOGI is effective in extracting fundamental components from load current. Fig. 6.24(c) the average fundamental active power component (I_{avg}), phase 'a' fundamental active power component (I_{pa}), phase 'b' fundamental active power component (I_{pb}) and phase 'c' fundamental active power component (I_{pc}). The fundamental active power component of phase 'c' (I_{pc}) reduces during disconnection of load phase 'c'.

Fig. 6.25 shows the steady state power flow among TPFW distribution system, SAPF and load in presence of linear load using SOGI based control technique. Figs. 6.25(a)-(c) show supply, load and compensator steady state power. The load demands 610 W real power and350 VARs reactive power. The supply feed active power 680 W and reactive power 160 VARs. The compensator feeds reactive power 180 VARs to the load. Figs. 6.25(d)-(f) present the supply neutral current (i_{sn}), load neutral current (i_{Ln}), zigzag transformer neutral current (i_{zn}) and phase 'a' supply voltage (v_{sa}). The supply neutral current is limited to 0.135 A. The zigzag transformer neutral current and load neutral current has nearly equal magnitude of 1.385 A and 1.440 A respectively. The supply neutral current is limited due to

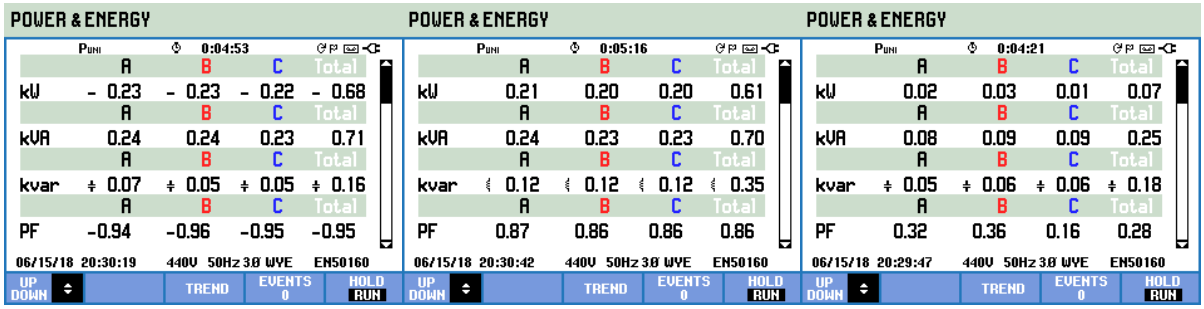

(a) (b) (c)

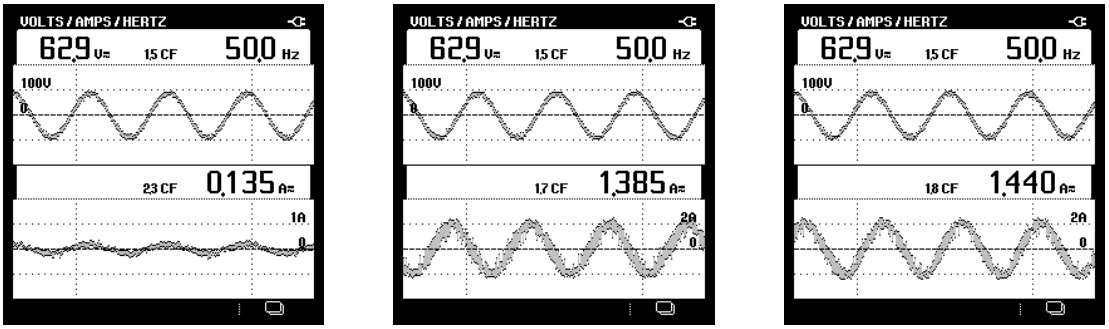

(d) (e) (f)

Fig. 6.25 (a-c) Steady state power for TPFW linear system using SOGI based control algorithm for (a) Supply (b) Load (c) Compensator and (d-f) neutral current of (d) supply (i_{sn}) (e) load (i_{Ln}) and (f) zigzag (i_{zn}) for linear load

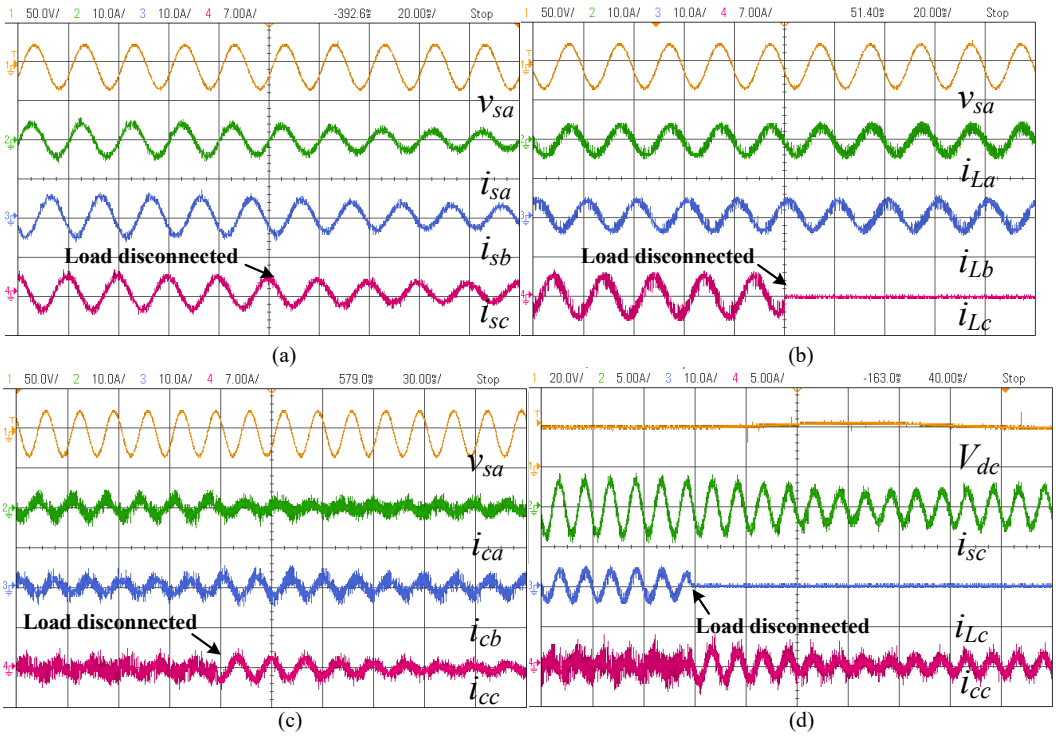

Fig. 6.26 Results showing dynamics for load disconnected in phase 'c' using SOGI based control algorithm (a) v_{sa}, i_{sa}, i_{sb}, i_{sc} (b) v_{sa}, i_{La}, i_{Lb}, i_{Lc} (c) v_{sa}, i_{ca}, i_{cb}, i_{cc} (d) V_{dc}, i_{sc}, i_{Lc}, i_{cc} for linear load

presence of zigzag transformer.

Fig. 6.26 shows the dynamic performance of the TPFW system using SOGI based control

technique for linear load. Fig. 6.26(a) shows phase 'a' supply voltage (v_{sa}) and three phase compensated supply currents (i_{sa}, i_{sb}, i_{sc}). Fig. 6.26(b) shows phase 'a' supply voltage (v_{sa}) and three phase lagging PF load currents (i_{La}, i_{Lb}, i_{Lc}). The phase 'c' load current becomes zero due to sudden removal of load in phase 'c'. 6.26(c) shows phase 'a' supply voltage (v_{sa}) and three phase shunt injected compensator currents (i_{ca}, i_{cb}, i_{cc}). 6.26(d) shows DC link voltage (V_{dc}), and phase 'c' supply current (i_{sc}), phase 'c' load current (i_{Lc}) and phase 'c' compensator current (i_{cc}). The compensator current makes the supply current of phase 'c' balanced and sinusoidal even though the load current (i_{Lc}) is absent.

Fig. 6.27 shows the intermediate signals for the SOGI based control technique for linear loads. Fig 6.27(a) presents DC link voltage (V_{dc}), phase 'a' supply voltage (v_{sa}), phase 'a' filtered supply voltage (v_{saf}) and the phase 'c' load current (i_{Lc}). Fig 6.27(b) shows DC link voltage (V_{dc}), phase 'c' load current (i_{Lc}), in-phase fundamental load current component (i_{Lci}), quadrature-phase fundamental load current component (i_{Lcj}). The SOGI based controller is effective in extracting fundamental components from load currents. Fig. 6.27(c) phase 'a' fundamental active power component (I_{pa}), phase 'b' fundamental active power component

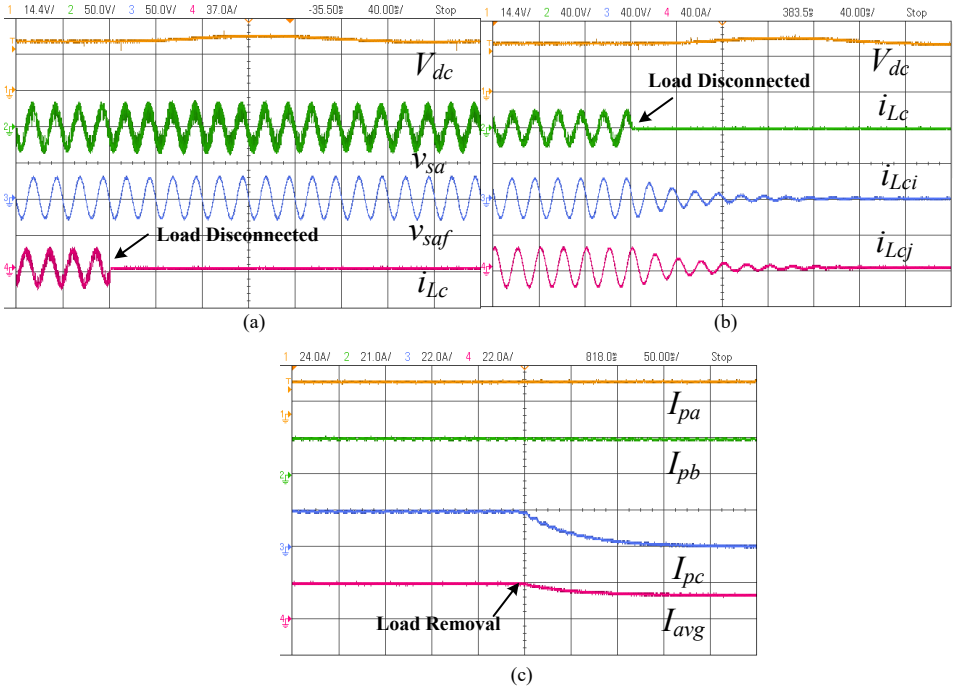

Fig. 6.27 Intermediate signals using SOGI based control technique (a) V_{dc}, v_{sa}, v_{saf}, i_{Lc} (b) (a) V_{dc}, i_{Lc}, i_{Lci}, i_{Lcj} (c) I_{avg}, I_{pa}, I_{pb}, I_{pc} for linear load

(I_{pb}), phase 'c' fundamental active power component (I_{pc}) and average fundamental active power component (I_{avg}). The fundamental active power component of phase 'c' (I_{pc}) is reduced to zero during load unbalancing period.

The effectiveness of SOGI based control techniques for SAPF based mitigation of PQ problems in TPFW distorted distribution system is investigated and discussed.

6.5 COMPARATIVE EVALUATION OF MCCF AND SOGI BASED CONTROL OF SAPF AND TPFW DISTORTED GRID DISTRIBUTION SYSTEM

The mitigation of PQ problems using new control algorithms in TPFW distorted grid distribution system has been considered in this chapter. Two new control algorithms viz MCCF and SOGI have been analyzed in detailed and implemented on hardware prototype system. These algorithms have been used for extraction of fundamental voltage components from distorted supply as well for load compensation. Performance aspect of these controllers is discussed for linear as well as non-linear loads and under dynamic load changes.

Table 6.1 COMPARISON OF CONTROL ALGORITHMS FOR NON-LINEAR LOAD

S.No.	Quantity	MCCF	SOGI
1.	Supply Voltage (v_{sa})	64.6 V, 9.7% THD	63.0 V, 9.5% THD
2.	Load Current (i_{La})	4.418 A, 29.9% THD	4.471 A, 29.6% THD
3.	Supply Current (i_{sa})	4.702 A, 3.6% THD	4.70 A, 3.8% THD

Table 6.2 COMPARISON OF CONTROL ALGORITHMS FOR LINEAR LOAD

S.No.	Quantity	MCCF	SOGI
1.	Supply Power	680 W, 170 VARs, 0.95 P.F.	680 W, 160 VARs, 0.95 P.F.
2.	Load Power	610 W, 350 VARs, 0.86 P.F.	610 W, 350 VARs, 0.86 P.F.
3.	Compensator Power	70 W, 180 VARs, 0.28 P.F.	70 W, 180 VARs, 0.28 P.F.

Table 6.1 shows the comparison of THD content with MCCF and SOGI control of SAPF for non-linear load compensation based on Figs. 6.16, 6.22. The MCCF technique results in a THD of 3.6% in supply currents and THD of 3.8% is obtained with SOGI control technique.

In both the cases load current has THD around 29.6% and supply voltage is distorted having THD of ~9.5%. MCCF is observed to be slightly better when reduction in THD of supply current is considered. The performance comparison of the developed algorithms is also discussed for sharing of power among supply, load and compensator with linear loads. Experimental results based on Fig. 6.19 and Fig. 6.25 have been compiled in Table 6.2. This table shows the power balance between supply, load and compensator side under steady state conditions. It is observed that for a load demand of 610 W and 350 VARs, at a P.F. of 0.86 lag, the compensator installation helps to improve the PF of grid supply to 0.95. The performance of both the algorithms for load compensation has been found to be nearly the same.

6.6 CONCLUSIONS

The main contributions of this chapter are to investigate the performance of TPTW and TPFW system under distorted grid conditions. Robust and simple control techniques such as MCCF and SOGI along with mathematical analysis, simulation studies is presented in this chapter. Both the techniques can be applied for harmonic extraction. It has been observed that implementation of the two algorithms achieve mitigation of power quality problems viz harmonics, load unbalancing, reactive power supply, PF correction and filtering of voltages from distorted grids. Both the algorithms give satisfactory steady state and dynamic performance when tested under similar grid and load conditions.

Chapter 7
DESIGN OF SINGLE PHASE SAPF FOR PV INTEGRATION

7.0 INTRODUCTION

Solar PV integration in grid is rising exponentially during past few decades. This increasing trend is mainly due to fall of prices of solar modules because of mass production of solar cells and also government policies for increasing use of renewable energy to address global warming issues and reduction in Green House Gases (GHG). The conventional energy sources for electricity generation are limited in quantity and will last for next few decades only and usage of alternative electrical energy sources need to be explored. The sun has abundant source of energy and it is also free. Technology must be developed to harvest solar energy. The wind, hydro, biomass etc. are some other Renewable Energy Sources (RES) which are naturally replenished and available in abundance. The control, operation and integration of RES are important issues of concern. This chapter focuses on the design, analysis and control of grid connected single phase PV system.

7.1 DESIGN AND ANALYSIS OF SINGLE PHASE GRID CONNECTED PHOTO VOLTAIC SYSTEM

Fig. 7.1 shows a block diagram of the proposed single phase grid connected PV system integrated to distribution system. The PV is connected at the DC link of single phase VSC. The VSC is controlled to act as a SAPF for the system. The single phase VSC is modeled in H-Bridge configuration. Single phase non-linear load is connected at PCC. Fig. 7.2 shows typical I-V and P-V characteristics of a solar panel. Real power from PV is extracted via a DC-DC boost converter whose duty cycle is varied as per MPPT. A detailed design and analysis of the proposed system is described in this section.

7.1.1 Selection of PV Panels

The selection of PV panels is based on electrical, mechanical, economic, customer and environmental criterion. In the present analysis, two panels of 250 W each are selected for developing gid connected SAPF based PV system. The make of solar panel is VIKRAM SOLAR. The detailed technical description is resented in APPENDIX C.

7.1.1.1 Modeling of PV Panels

Several research papers are available in literature [190-195] for modeling of PV panels based on single diode, two diode model. Fig. 7.3 shows the circuit diagram of a single photovoltaic cell based on single diode model. The PV gets energy from sun to radiate free electrons which in turn help in generating DC voltage. The output current (I_{pv}) of PV cell is given as in Eq. 7.1,

$$I_{pv} = I_{ph} - I_d - I_{sh} \tag{7.1}$$

where *Ipv* denotes the solar cell output current, I_{ph} is the photon current, I_d is the diode current, I_{sh} is the leakage current in the parallel resistor (R_{sh}). Eq. 7.1 can be written as

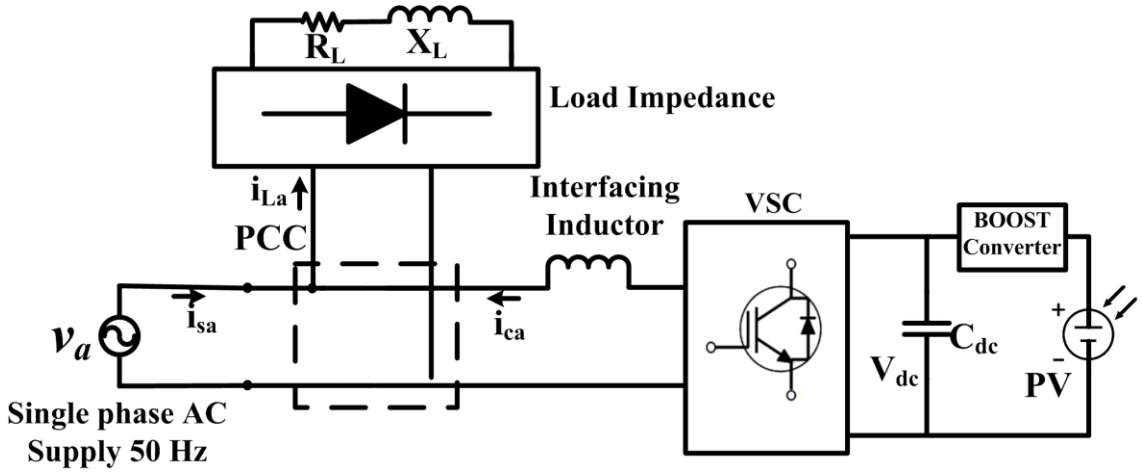

Fig. 7.1 Single phase grid connected PV system under consideration

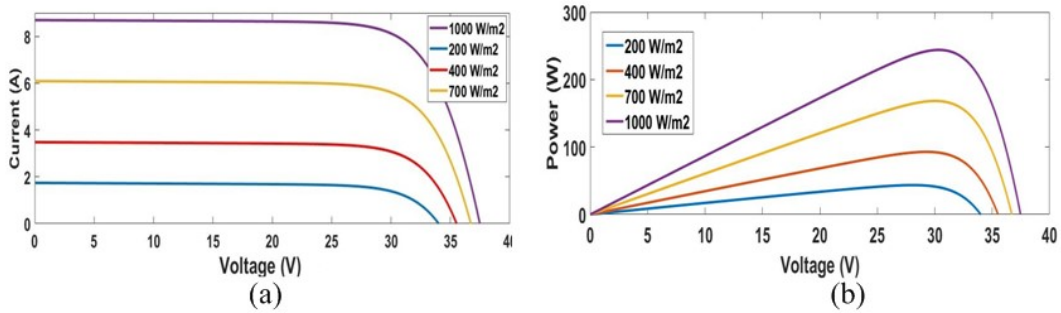

Fig. 7.2 Typical I-V and P-V curve for solar panels

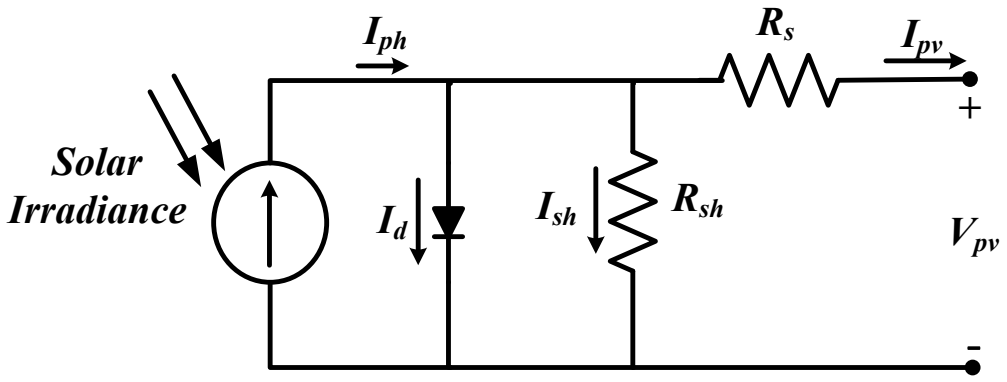

Fig. 7.3 Single cell PV module

$$I_{pv} = \mathrm{I_{ph}} - \mathrm{I_o}\left[\exp\left(\frac{\mathrm{V}_{pv}+I_{pv}\mathrm{R_s}}{£}\right) - 1\right] - \frac{\mathrm{V}_{pv}+I_{pv}\mathrm{R_s}}{\mathrm{R_{sh}}} \quad (7.2)$$

$$\text{and } £ = \frac{\mathrm{N_s}*€*\mathrm{k}*\mathrm{T_c}}{\mathrm{q}} \quad (7.3)$$

where I_0 is reverse saturation current of the diode, R_s is the series resistor, V_{pv} is the PV output voltage and '£' depicts the modified ideality factor. Also, N_s = number of series cells in a PV panel, k = Boltzmann's constant =1.381*10^{-23} J/K and q= electron charge =1.602*10^{-19}C, € is the ideality factor and T_c is temperature of the panel.

As the capacity of PV system increases, we need to design a PV array which consists of number of panels connected in series (N_{ss}) and in parallel(N_{pp}).The PV array equation is modified from PV cell equation and is given as (7.4):

$$I_{pv} = N_{pp}I_{ph} - N_{pp}I_o\left[exp\left(\frac{\mathrm{V}_{pv}+I_{pv}R_s\left(\frac{N_{ss}}{N_{pp}}\right)}{£}\right) - 1\right] - \frac{\mathrm{V}_{pv}+I_{pv}R_s\left(\frac{N_{ss}}{N_{pp}}\right)}{R_{sh}\left(\frac{N_{ss}}{N_{pp}}\right)} \quad (7.4)$$

7.1.2 Design of DC-DC Boost Converter

The output of PV array/system considered is 500 W (max), 75 V (open circuit voltage) and 8.7 A (short circuit current). A DC-DC boost converter is necessary to increase voltage level to 100 V (DC link voltage) for real power transfer between PV and grid. Fig. 7.4 shows the internal structure of boost converter used for the transfer of real power at DC link of the SAPF. The voltage of PV is processed through boost converter after which the voltage is increased by following equation

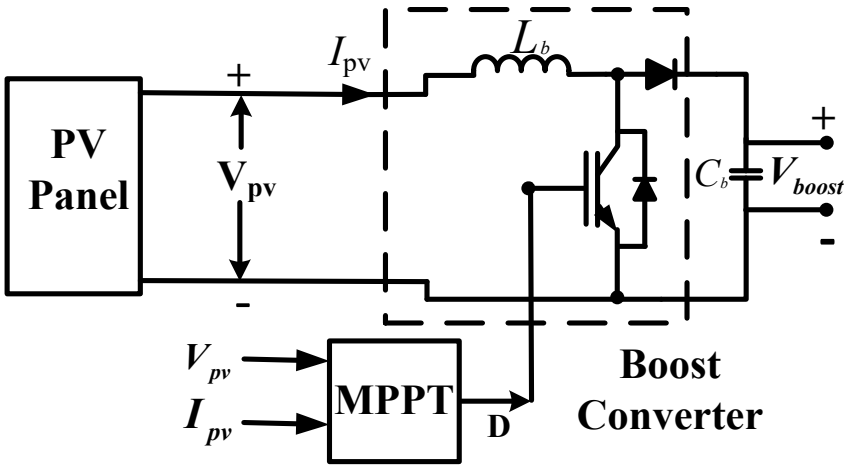

Fig. 7.4 DC-DC boost converter

$$V_{boost} = \frac{1}{1-D} V_{pv} \tag{7.5}$$

where V_{pv}, V_{boost} represent the voltage of PV system before and after boost converter and D is duty cycle of boost converter. In the proposed system, the output of boost converter is fed at DC link of SAPF, so designed value of V_{boost} is equal to DC link voltage, V_{dc} which is 100 V. Conventional Perturb and Observe (P&O) MPPT technique has been used to vary the duty cycle of boost converter for maximum power extraction from the PV.

7.1.2.1 Design of Inductor and Capacitor of Boost Converter

The basic structure of a boost converter comprises the computation of ratings of inductor (L_b) and capacitor (C_b). The inductor value in the boost converter (L_b) is calculated using the following equation.

$$L_b = \frac{v_{mp} \times D}{\Delta I_{pv} \times f_{sw}} \tag{7.6}$$

where v_{mp} is the voltage at maximum power, D is duty cycle, ΔI_{pv} is inductor ripple current, f_{sw} is switching frequency of IGBT switch. From the data sheet of PV panel, v_{mp} is 61.2 V also D is selected as 0.5, ΔI_{pv} is considered 10% as 0.81 A and f_{sw} 10 kHz. The calculated value of L_b is 3.8 mH and selected as 4 mH for hardware setup.

A capacitor (C_b) in DC-DC boost converter is used to smooth out the output voltage. It helps

in filtering out ripples in output boost converter voltage. It is calculated using following equation

$$C_b = \frac{P_{pv}}{2\pi \times f_{sw} \times V_{boost} \times \Delta V_{boost}} \tag{7.7}$$

where P_{pv} is maximum power from PV, V_{boost} is DC-DC boost converter output voltage, ΔV_{boost} ripple in boost output voltage. Taking P_{pv} =500 W, V_{boost} = 100 V, ΔV_{boost} to be 10% as 10 V. C_b is computed as 7.96 μF and taken as 10 μF.

7.1.2.2 Selection of IGBT Switch in DC-DC Boost Converter

IGBT is used as power switch for DC-DC boost converter. The rating of switch depends mainly upon current handling and switching speed. In present analysis switching speed of 10 kHz is considered, and I_{pv} is 50 A (max), the selected IGBT module is SKM50GAL12T4 (Semikron make). Fig. 7.5 shows the internal connection diagram of IGBT switch used in hardware circuit. The specification of IGBT is V_{CES} = 1200V, I_C=50A, f_s = 20 kHz, V_{GES}= 10V, T_{op}= -40°C to 150°C.

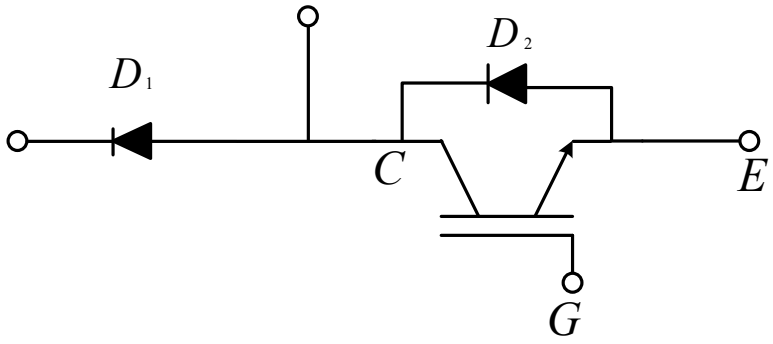

Fig. 7.5 Internal structure of IGBT module SKM50GAL12T4

7.1.3 Design of Single Phase SAPF

A single phase H-bridge converter is used as VSC and controlled as SAPF. The minimum DC link voltage should be more than peak of supply voltage. The peak AC voltage is calculated as

$$V_{peak} = \sqrt{2} V_s \tag{7.8}$$

where V_s is rms value of supply voltage.

Taking supply voltage as 63.5 V rms, V_{peak} is computed as

$$\boldsymbol{V_{peak}} = \sqrt{2} \times 63.5 = 89.8\, \boldsymbol{V} \tag{7.9}$$

The V_{dc} should be more than 89.8 V and selected as 100 V.

The value of DC link capacitor of VSC is calculated using [71]

$$\boldsymbol{C_{dc}} = \frac{\boldsymbol{g}[\boldsymbol{V_{ph}}(\boldsymbol{oI_{ph}})\boldsymbol{t}]}{\frac{1}{2}[\boldsymbol{V_{dc}^2} - \boldsymbol{V_{dc1}^2}]} \tag{7.10}$$

Taking g is constant and taken as 0.05, V_{ph} = 63.5 V, o = 1.2, I_{ph} = 20 A, t=0.02 sec, V_{dc} = 100 V, V_{dc1} = 89.80

From Eq. (7.10) calculated C_{dc} = 1574.41 μF and selected value of C_{dc} is 1600 μF.

Finally the value of AC interfacing inductor is calculated from [71]

$$\boldsymbol{L_i} = \frac{\sqrt{3} * \boldsymbol{m} * \boldsymbol{V_{dc}}}{12 * \boldsymbol{o} * \boldsymbol{f_s} * \boldsymbol{i_{rcpp}}}$$

Assuming m = 1, V_{dc} = 100 V, f_s = 10 kHz and i_{rcpp} = 2 A (10% of output current)

$$\boldsymbol{L_i} = \frac{\sqrt{3} * 1 * 100}{12 * 1.2 * 10000 * 2} = 0.6\, \boldsymbol{mH} \tag{7.11}$$

The selected value of inductor is 1 mH.

The design of voltage and current sensors are already covered in Chapter 3. The complete hardware is developed and grid integration of PV along with PQ improvement is analyzed in single phase distribution system.

7.2 DEVELOPMENT AND ANALYSIS OF CONTROL ALGORITHMS FOR MITIGATION OF POWER QUALITY PROBLEMS IN GRID CONNECTED PV SYSTEM

In this section, control algorithms for PQ problems mitigation in single phase grid connected PV system are discussed. Control algorithms are implemented for load compensation in grid

connected PV system. The simulation results with and without PV are discussed. The details of control algorithms developed are discussed below.

7.2.1. Designing of Maximum Power Point Tracking (MPPT) for PV System

Fig. 7.2 shows the typical I-V and P-V curve of a PV panel under described conditions. The PV power output is maximum at a particular voltage which is called maximum power point voltage (v_{pm}). So to extract maximum power the PV must be operated around this v_{pm}. The control technique used for MPPT is Perturb and Observe (PO). Fig. 7.6 shows the algorithm of PO technique. In this MPPT algorithm power at each step is calculated and it is compared

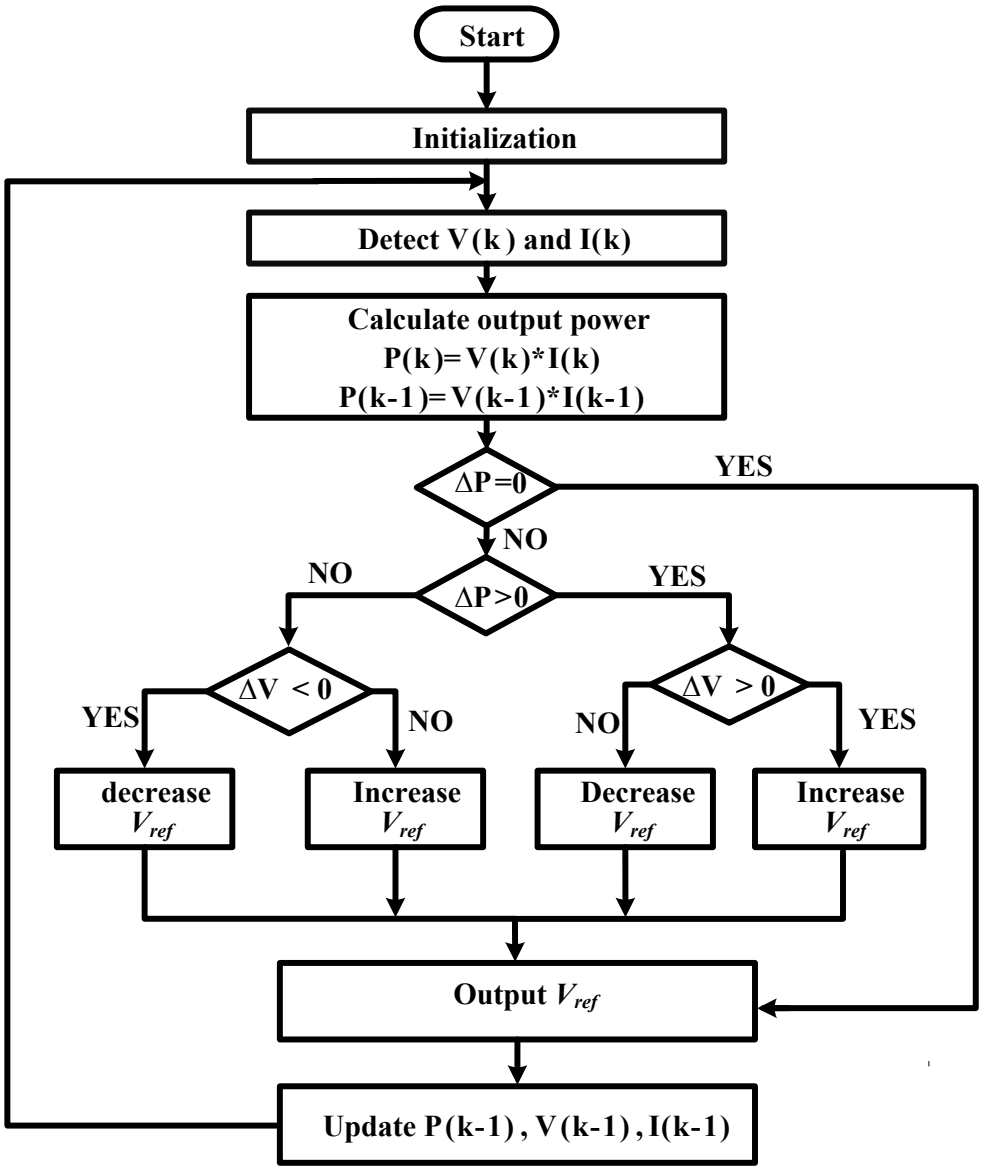

Fig. 7.6 Algorithm for Perturb and Observe (PO)

with the previous value. If the PV power at the k^{th} instance (P_k) is more than PV power at the $(k-1)^{th}$ instance (P_{k-1}) and also the voltage at k^{th} instance (V_k) is more than the voltage at $(k-1)^{th}$ instance then the V_{ref}, which is reference MPPT voltage, is increased. If the PV power at the k^{th} instance (P_k) is more than PV power at the $(k-1)^{th}$ instance (P_{k-1}) but the voltage at k^{th} instance (V_k) is less than the voltage at $(k-1)^{th}$ instance then the V_{ref} is decreased. The reference MPPT voltage is updated as described in flow chart shown in Fig. 7.6 When PV power at the k^{th} instance is less than $(k-1)^{th}$ instance. If the PV power at k^{th} and $(k-1)^{th}$ instances are same then V_{ref} also remains the same. The PO technique provides the reference MPPT voltage which is used further to calculate the duty cycle of boost converter as per Eq. 7.5. The duty cycle is converted to pulses by PWM control by comparing duty cycle with a reference triangular wave. The PWM signal is fed to the gate terminal of IGBT switch which changes output of boost converter accordingly.

7.2.2. Generation of Unit Templates for Single Phase System

For the generation of reference current for SAPF, unit templates or synchronizing templates must be calculated. The unit templates calculation in single phase system is different from computation in a three phase system. Fig. 7.7 shows the unit templates calculation for single phase system. The supply voltage v_s as well as 90˚ phase shifted voltage $v_{s\beta}$ are squared and added. Then square root of the sum is taken, which estimates V_t for single phase system. Now the supply voltage and 90˚ phase shifted voltage are divided by V_t so as to obtain unit templates $sin\theta$ and $cos\theta$. Fig. 7.7 shows the block diagrams used for calculation of V_t and unit

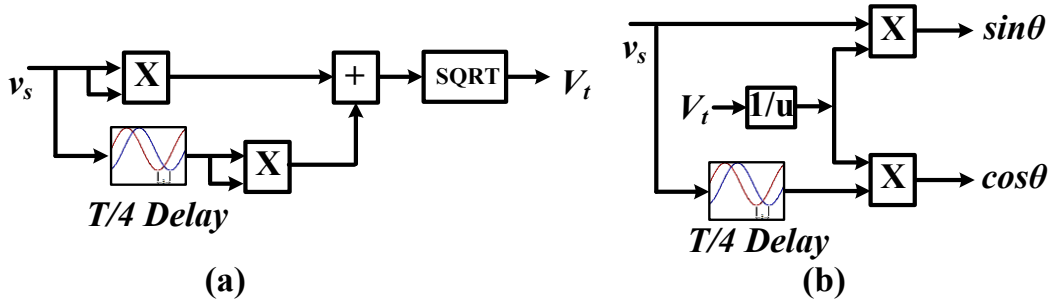

Fig. 7.7 Generation of unit templates for single phase system

templates.

$$V_t = \sqrt{v_s^2 + v_{s\beta}^2} \tag{7.12}$$

$$\sin\theta = \frac{v_s}{V_t}; \cos\theta = \frac{v_{s\beta}}{V_t} \tag{7.13}$$

7.2.3. Calculation of Feed Forward Factor (I_{ff}) for PV

To integrate PV to the grid, a feed forward factor (I_{ff}) is calculated which is subtracted from the fundamental active load component (I_{Ld}/I_p) to compute net magnitude of current required from the grid. The I_{ff} is calculated as

$$I_{ff} = \frac{2 \times V_{mp} \times I_{mp}}{V_t} \tag{7.14}$$

where V_{mp} and I_{mp} are MPPT voltage and current respectively. Since MPPT voltage in grid connected system is to be kept at DC link voltage so Eq. 7.14 is modified as

$$I_{ff} = \frac{2 \times V_{dc} \times I_{pv}}{V_t} \tag{7.15}$$

where *Ipv* is PV output current at voltage V_{dc}. This feed forward factor is used to calculate magnitude of reference current for SAPF.

7.2.4. Extraction of Effective Fundamental Active Power Component and Reference Current Generation

The determination of effective fundamental active power component (I_{eff}) using developed control algorithms viz SRFT, Notch Filter and SOGI are discussed below.

7.2.4.1. Synchronous Reference Frame Theory Based Control Algorithm

Fig. 7.8 shows the modified SRFT control algorithm for single phase grid connected PV system. The load current and 90˚ phase shifted load current are processed by Park's transformation as follows

$$\begin{bmatrix} i_{Ld} \\ i_{Lq} \end{bmatrix} = \sqrt{\frac{2}{3}} \begin{bmatrix} \cos & \sin \\ -\sin & \cos \end{bmatrix} \begin{bmatrix} i_L \\ i_{L\beta} \end{bmatrix} \tag{7.16}$$

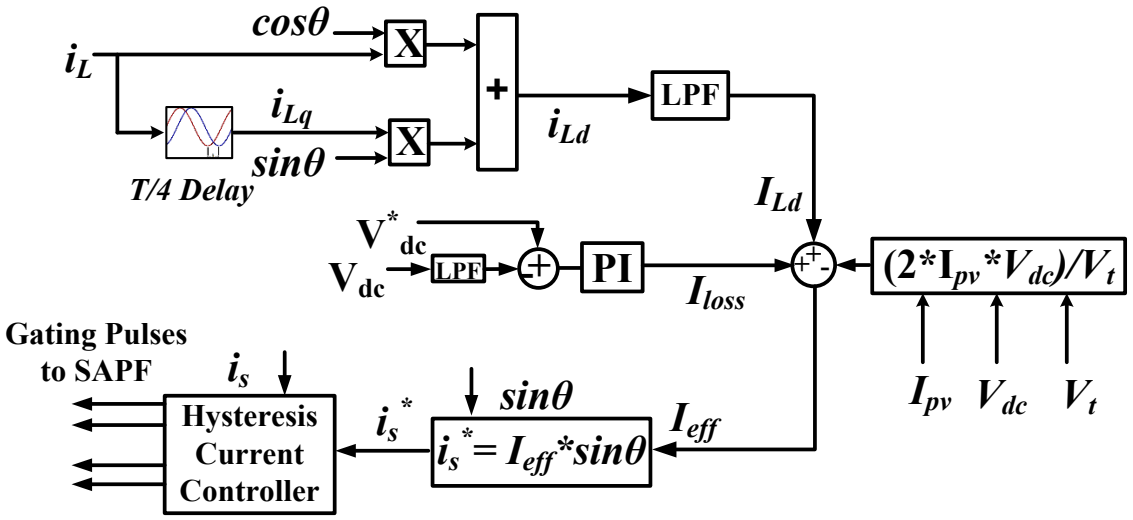

Fig. 7.8 Block diagram of SRFT control algorithm implementation for single phase grid connected PV system

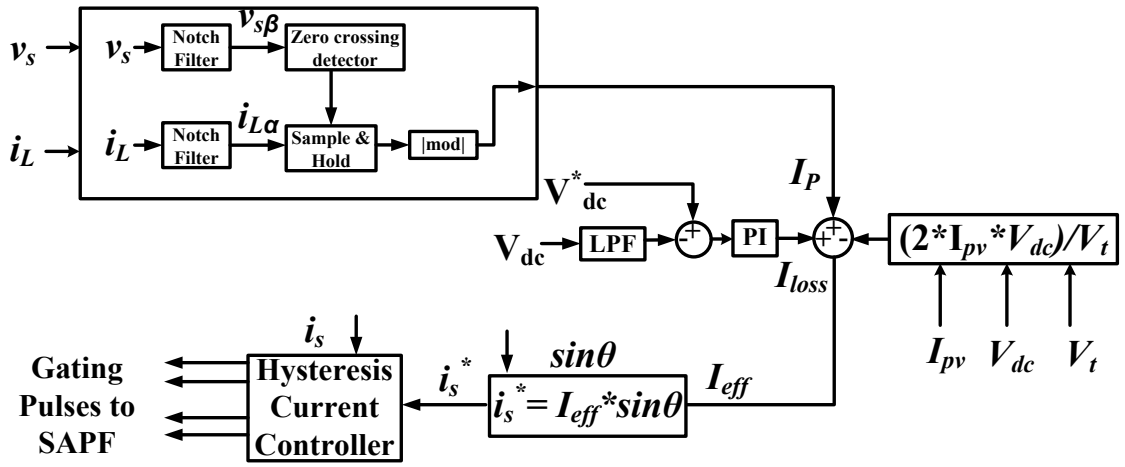

Fig. 7.9 Block diagram of Notch Filter based control algorithm implementation for single phase grid connected PV system

The i_{Ld} component of load current is passed through a low pass filter to obtain $I_{Ld}^{'}$. The DC link power loss component I_{loss} as discussed in section 3.8.2.1 and PV feed forward term I_{ff} are processed to obtain effective fundamental active power component (I_{eff}) as

$$I_{eff}=I_{Ld}^{'}+I_{loss}-I_{ff} \tag{7.17}$$

I_{eff} is multiplied by unit template sinθ to obtain reference current i_s^*.

$$i_s^* = I_{eff} * \sin\theta \tag{7.18}$$

Now the reference current generated by SRFT control technique is compared with the actual supply currents (i_s) in the HCC. The HCC controller outputs four gating pulses for H-bridge

VSC, which are generated for proper operation of system.

7.2.4.2. Notch Filter Based Control Algorithm

Fig. 7.9 shows the Notch Filter (NF) based control algorithm for single phase grid connected PV system. The basic equations are already discussed in section 4.2.1.1 of Chapter 4. The Eq. (4.1) is modified as:

$$i_{L\alpha} = \frac{s\varepsilon\phi}{s^2 + s\varepsilon\phi + \phi^2} i_L \tag{7.19}$$

$$v_{s\beta} = \frac{s\phi^3}{s^2 + s\varepsilon\phi + \phi^2} v_s \tag{7.20}$$

where ϕ is phase angle of I/P signal (i_L and v_s), ε is damping constant of system and 's' denotes the laplace operator.

Sample and hold circuit and zero order hold circuit are used to calculate fundamental active power component of load current I_p. The effective fundamental active power component I_{eff} is calculated as follows

$$I_{eff}=I_P+I_{loss}-I_{ff} \tag{7.21}$$

I_{eff} is multiplied by unit template sinθ to obtain reference currents i_s^*.

$$i_s^* = I_{eff} * \sin\theta \tag{7.22}$$

Now the reference current (i_s^*) is compared with the actual supply currents (i_s) and four gating pulses for H-bridge VSC are generated. The actual supply current follows the reference supply current generated using the Notch based filter.

7.2.4.3. Second Order Generalized Integrator Based Control Algorithm

Fig. 7.10 shows a generalized SOGI block diagram. As already discussed in section 6.2.1.2 of Chapter 6, the in-phase and quadrature fundamental load current component computed from SOGI are

$$\frac{i_{Lj}}{i_L} = \frac{W\omega_0 s}{s^2 + W\omega_0 s + \omega_0^2} \tag{7.23}$$

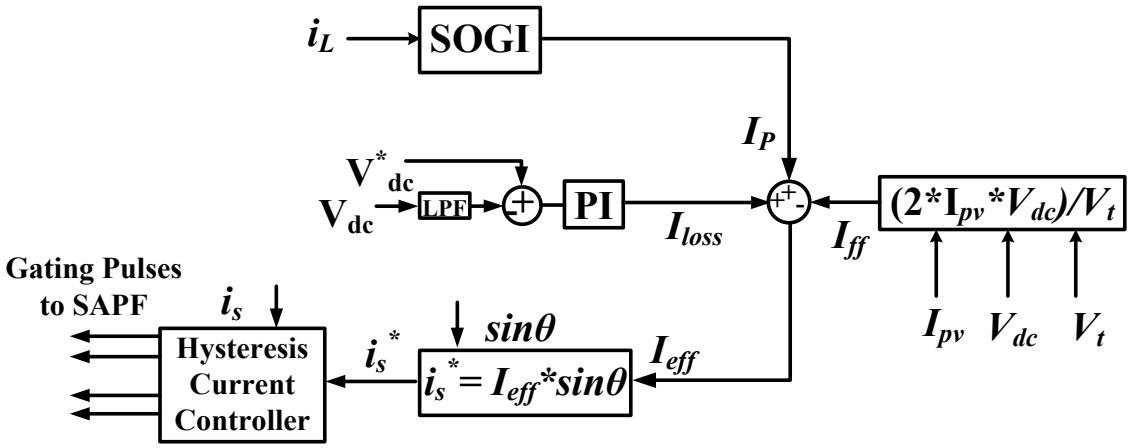

Fig. 7.10 Block diagram of SOGI based control algorithm implementation for single phase grid connected PV system

$$\frac{i_{Lk}}{i_L} = \frac{W\omega_0^2}{s^2 + W\omega_0 s + \omega_0^2} \tag{7.24}$$

where ω_0 is fundamental frequency and i_{Lj}, i_{Lk} are SOGI fundamental in-phase and phase quadrature outputs of load current, W is constant gain.

Now the fundamental active power component (i) is calculated as

$$I_p = \sqrt{i_{Lj}^2 + i_{Lk}^2} \tag{7.25}$$

The DC link loss component (I_{loss}) and PV feed forward factor (I_{ff}) are adjusted as follows

$$I_{eff}=I_P+I_{loss}-I_{ff} \tag{7.26}$$

I_{eff} is multiplied by unit templates sinθ to obtain reference current i_s^*.

$$i_s^* = I_{eff} * \sin\theta \tag{7.27}$$

The reference current (i_s^*) is compared with the actual supply currents (i_s) to generate four gating pulses for VSC and SAPF based compensation is provided for PQ improvement using SOGI controller. The performance analysis of grid integrated PV system using these control algorithms is discussed through simulation results and experimental investigations.

7.3. SIMULATION RESULTS

The developed control algorithms are tested in MATLAB/SIMULINK environment. The modified system considered for simulation comprises a 5kW PV system, which is connected

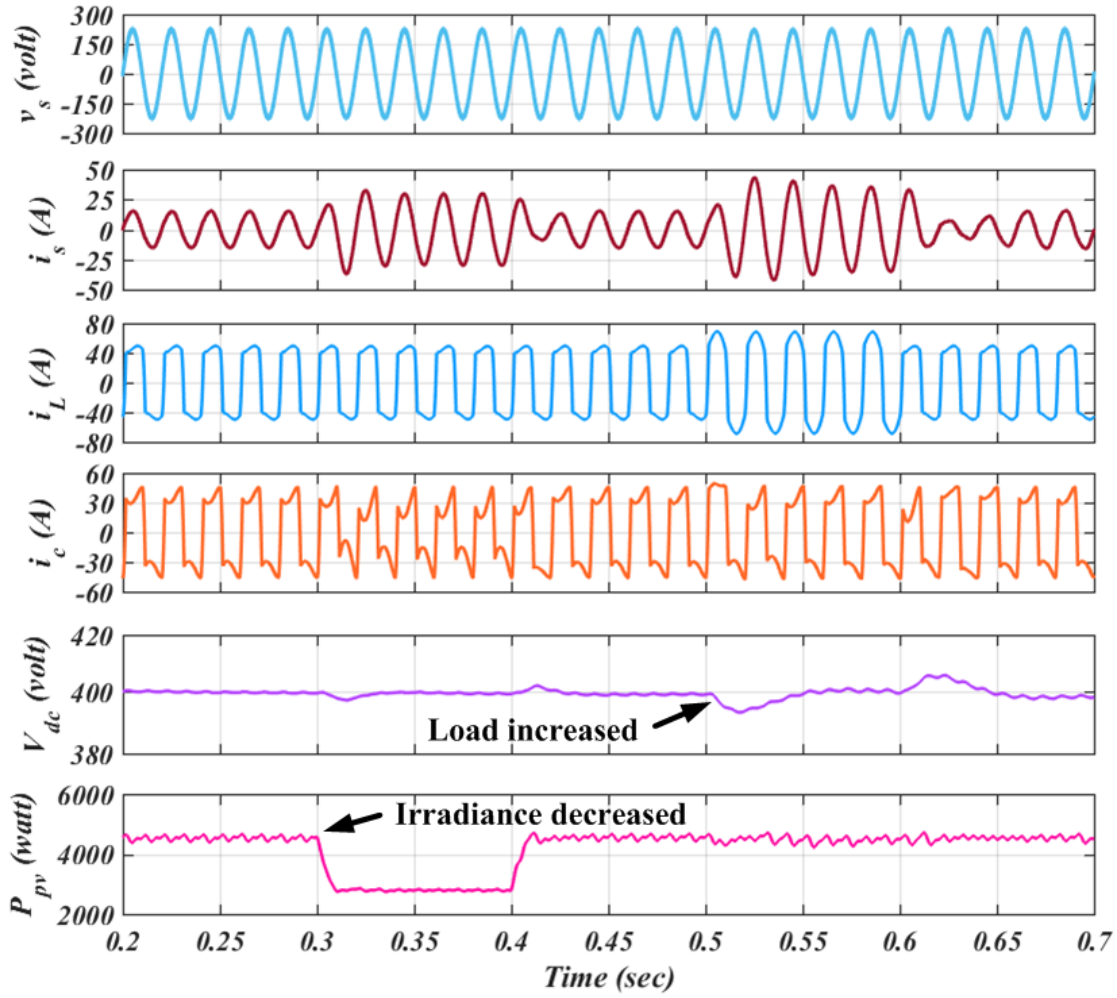

Fig. 7.11 Simulation results for SRFT based control algorithm

to 230 V (peak) single phase grid supply. The effects of variation in load and PV irradiance are observed on the grid system and dynamics performance is discussed.

7.3.1. Synchronous Reference Frame Theory Based Control Algorithm

Fig. 7.11 shows the simulation results for variation in load and solar irradiance level for single phase grid connected SAPF based PV system controlled using SRFT. Fig. 7.11 shows supply voltage (v_s), supply current (i_s), load current (i_L), compensator current (i_c), DC link voltage (V_{dc}) of SAPF and PV output power (P_{pv}). At the start of simulation the solar irradiance is at 1000 W/m^2. At time t=0.3 sec, irradiance is decreased to 600 W/m^2 till t=0.4 sec. It is observed from the Fig. 7.11 that PV output power (P_{pv}) is decreased. Since the load power is same, hence the supply current magnitude is increased during this time. DC link voltage is also affected by irradiance change but settles rapidly. The irradiance is restored

back to 1000 W/m^2 at time t=0.4 sec. At time t=0.5 sec, load is increased and hence an increase in the load current is observed. The PV provides the rated power (4500 W) as before. The DC link shows some transients which get settled due to PI controller action in steady state. The compensator current also changes and the supply current increases to meet the new load demand. During load change as well as irradiance change, the supply current remains sinusoidal even in the presence of distorted load currents. SRFT algorithm successfully improves PQ problems in single phase grid connected PV system.

Figs. 7.12(a)-(c) show the waveforms and Figs. 7.12(d)-(f) show the harmonics content in supply voltage (v_s), supply current (i_s) and load current (i_L) respectively. It is observed that supply current is sinusoidal and in-phase with the grid voltage and supply has Unity Power Factor (UPF). The load current is non-sinusoidal. The THD of supply voltage is 4.41%. The

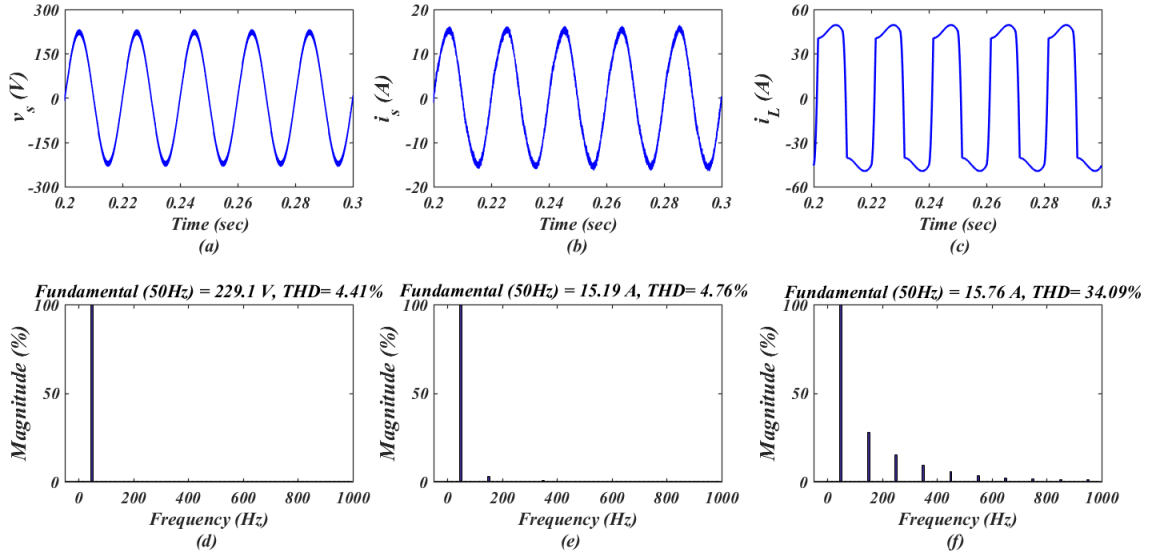

Fig. 7.12 Harmonic analysis using SRFT based control algorithm (a-c) waveforms of v_s, i_s, i_L (d-f) THD of v_s, i_s, i_L for non-linear load

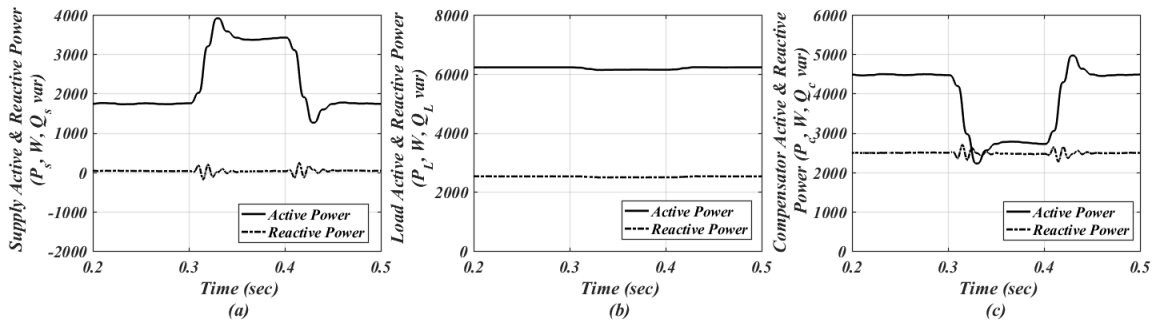

Fig. 7.13 Power flow in single phase grid connected PV system using SRFT based control algorithm (a) Active and reactive supply power P_s, Q_s (b) Active and reactive load power P_L, Q_L (c) Active and reactive compensator power P_c, Q_c

supply current THD is 4.76% after compensation, where the load current THD is 34.09%.

Fig 7.13 shows the power balance between supply, load and PV for variation in solar irradiance. At time t=0.3 sec, irradiance in decreased to 600 W/m^2 from 1000 W/m^2 value. The PV power gets reduced but the supply active output power has increased to meet additional load demand. The supply provides all the real power demand of the load while the reactive power demand of load is met through the SAPF compensator.

7.3.2. Notch Filter Based Control Algorithm

Fig. 7.14 shows the simulation results for Notch Filter based control algorithm. The algorithm is tested for changes in load and irradiance level for single phase grid connected PV system. Fig. 7.14 shows supply voltage (v_s), supply current (i_s), load current (i_L), compensator current (i_c), DC link voltage (V_{dc}) of SAPF and PV power (P_{pv}). At the start of simulation the solar

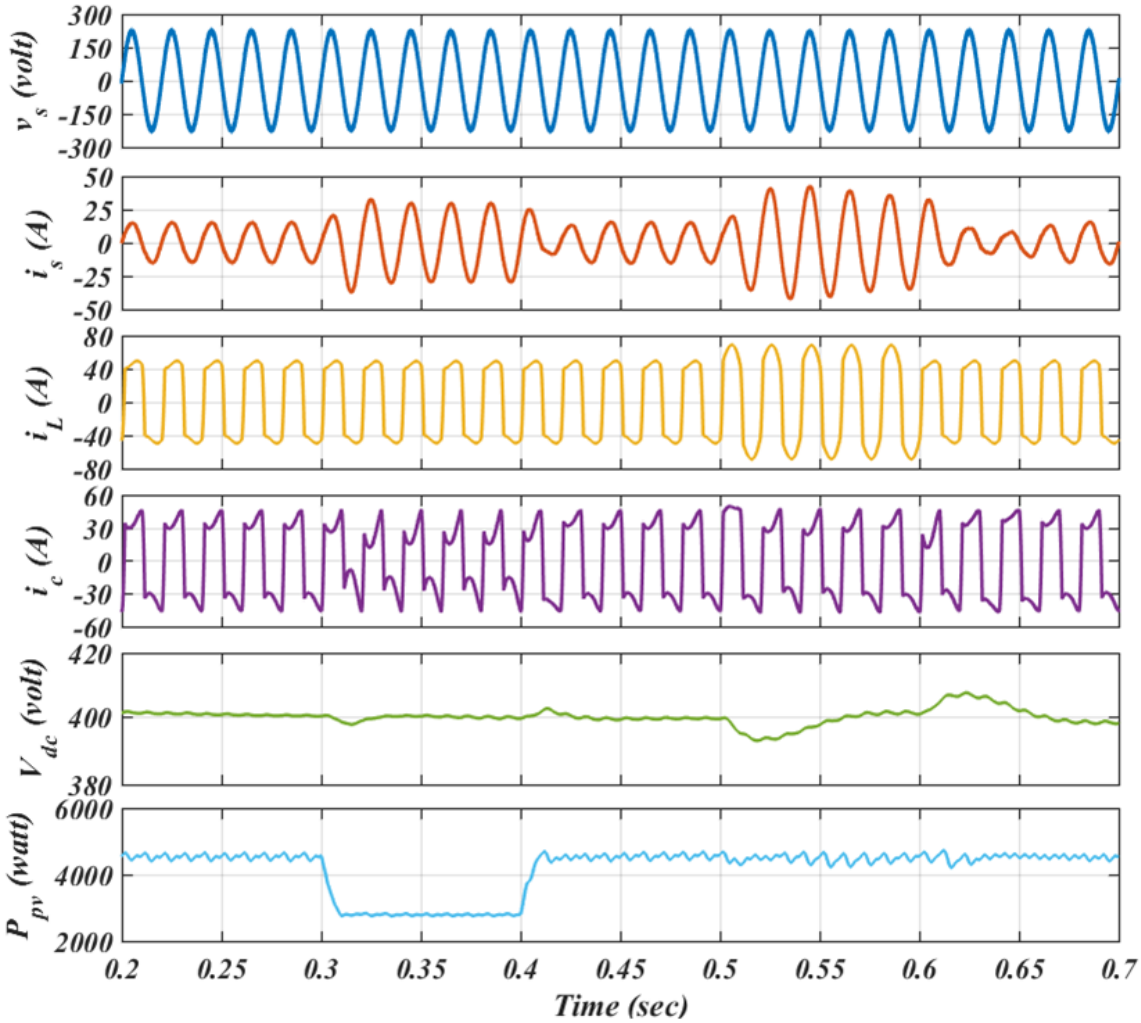

Fig. 7.14 Simulation results for Notch Filter based control algorithm

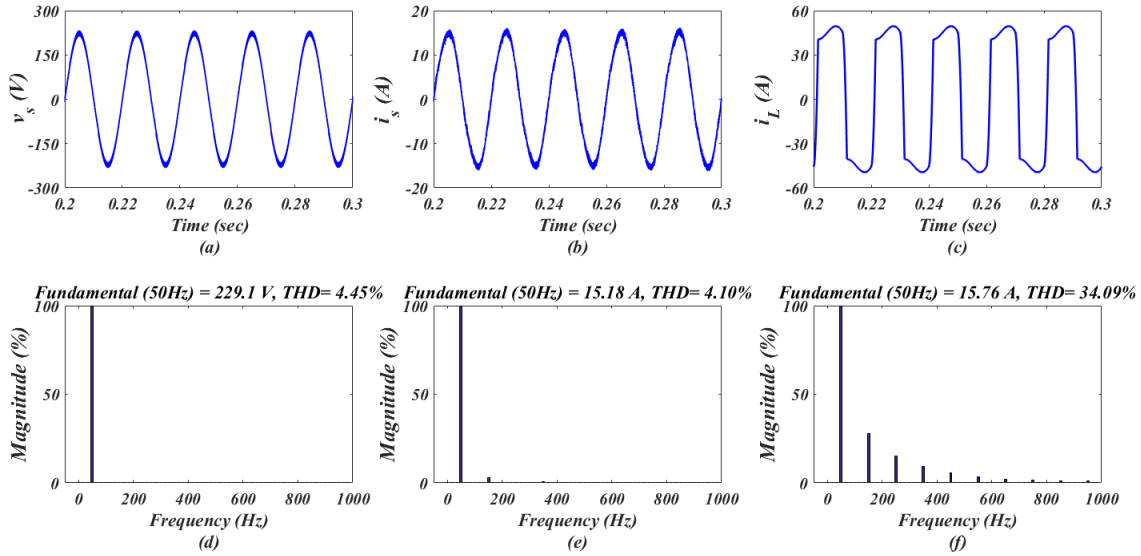

Fig. 7.15 Harmonic analysis using Notch Filter based control algorithm (a-c) waveforms of v_s, i_s, i_L (d-f) THD of v_s, i_s, i_L for non-linear load

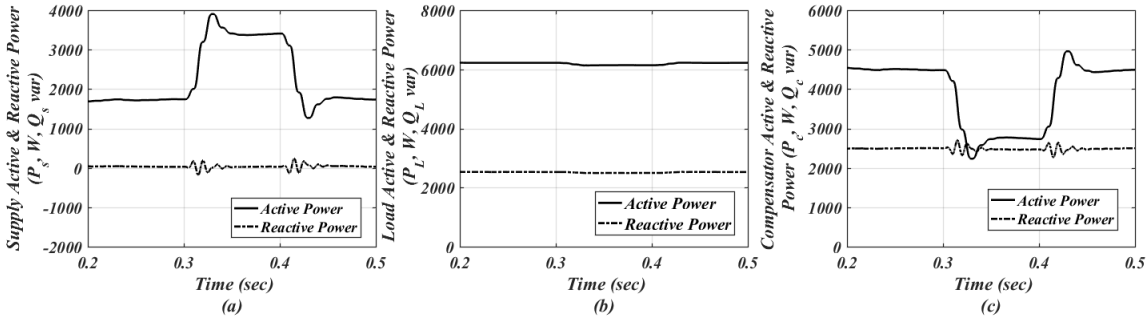

Fig. 7.16 Power flow in single phase grid connected PV system using Notch Filter based control algorithm (a) Active and reactive supply power P_s, Q_s (b) Active and reactive load power P_L, Q_L (c) Active and reactive compensator power P_c, Q_c

irradiance is at 1000 W/m^2. At time t=0.3 sec, irradiance is changed to 600 W/m^2 till t=0.4 sec. Due to change in irradiance the PV output power (P_{pv}) is decreased and therefore the supply delivers more real power (P_{pv}) to the load. The irradiance is restored to 1000 W/m^2 at time t=0.4 sec. At time t=0.5 sec, load is suddenly increased. The supply current (i_s) increases in magnitude due to increase in load demand.

Since, the solar irradiance is constant as 1000 W/m^2, so the PV is giving almost the same power as before. The DC link voltage has some transients during sudden change in load which settles down rapidly. The compensator provides proper compensating currents based on Notch Filter technique to make supply side current (i_s) sinusoidal. The Notch Filter technique works satisfactorily to mitigate PQ problems.

Figs. 7.15(a)-(c) show the waveforms and Figs. 7.15(d)-(f) show the harmonics in supply voltage (v_s), supply current (i_s) and load current (i_L) respectively. The supply voltage and load current has a THD of 4.45% and 34.09% respectively. The THD of supply current is improved in this case to 4.10% as compared to that of SRFT control algorithm.

Fig. 7.16(a-c) shows the plots for both real and reactive power with respect to time balance for supply, load and PV using Notch Filter control technique. The solar irradiance level is changed at time t=0.3 sec from 1000 W/m^2 to 600 W/m^2. The real power from the PV reduces from 4500 W to almost 2800 W, since the load real power demand is constant as 6200 W so real power delivered from supply is increased to 3400 W. The reactive power balance is unaffected by solar irradiance change and the compensator continues to supply all the reactive power demand of the load.

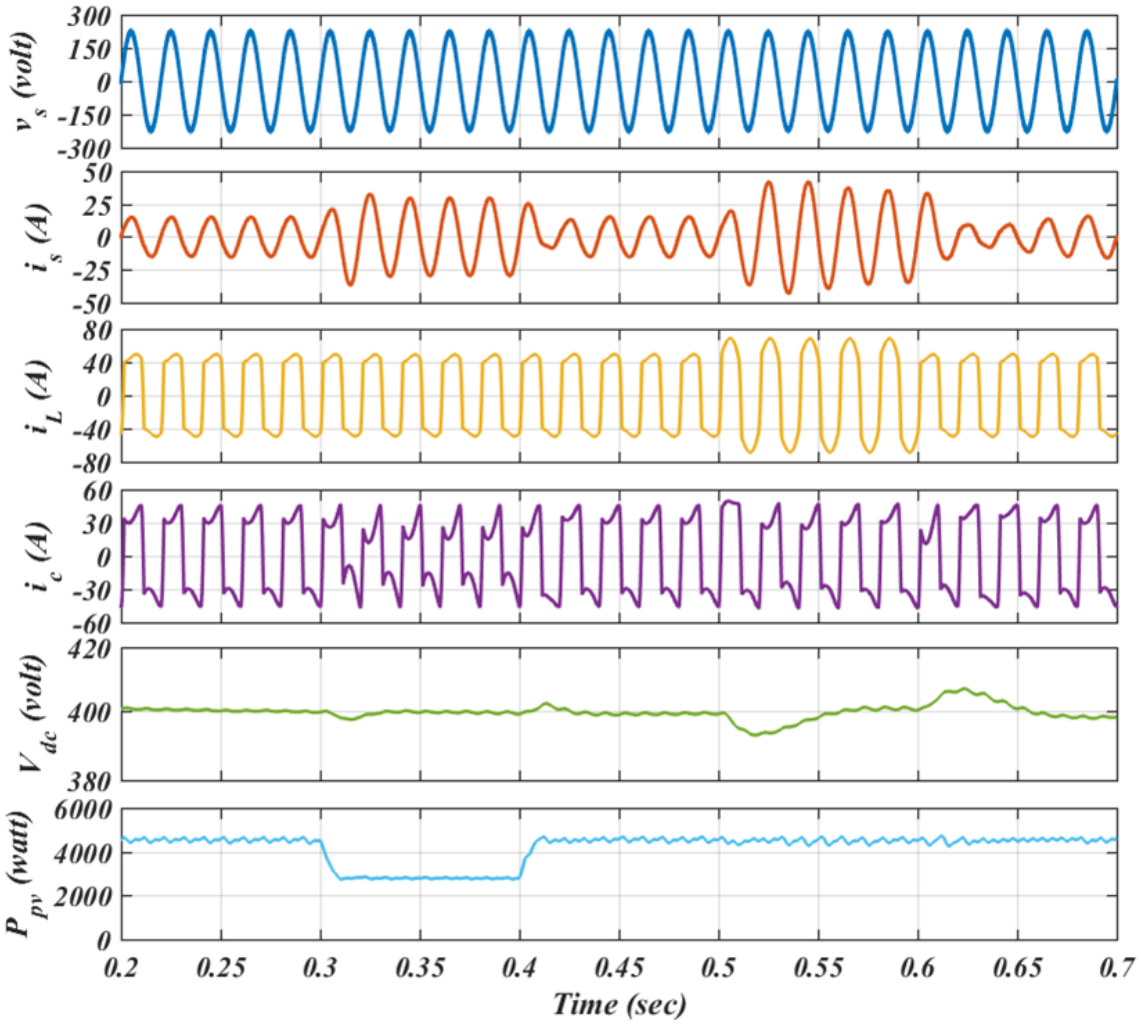

Fig. 7.17 Simulation results for SOGI based control algorithm

7.3.3. Second Order Generalized Integrator Based Control Algorithm

Fig. 7.17 shows supply voltage (v_s), supply current (i_s), load current (i_L), compensator current (i_c), DC link voltage (V_{dc}) of SAPF and PV power (P_{pv}) in SAPF based 5 kW PV system connected to a grid at 230 V (peak). The SAPF is controlled using SOGI based control algorithm. The solar irradiance is changed at t=0.3 sec from 1000 W/m^2 to 600 W/m^2. At time t=0.3 sec, when the irradiance is changed to 600 Wt/m^2 from 1000 W/m^2, the PV output power (P_{pv}) is decreased from 4500 W to 2800 W. The supply has to feed more real power to the load. At t=0.4 sec, the solar irradiance level is again 1000 W/m^2 and the PV system generates its rated power of 4500 W. At time t=0.5 sec, load current (i_L) is suddenly increased. The supply current (i_s) is increased but PV is providing almost the same power as before. The DC link voltage shows dip/increase during variation of load and irradiance level

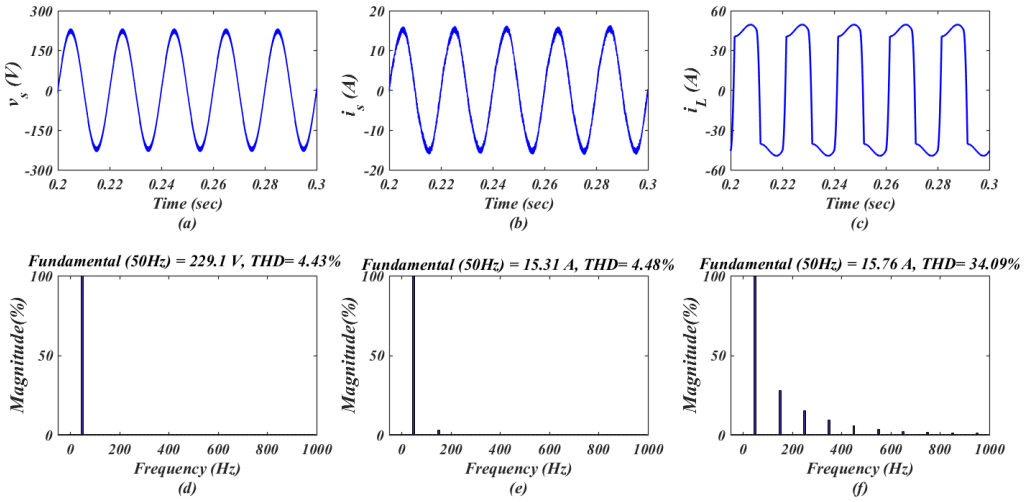

Fig. 7.18 Harmonic analysis using SOGI based control algorithm (a-c) waveforms of v_s, i_s, i_L (d-f) THD of v_s, i_s, i_L for non-linear load

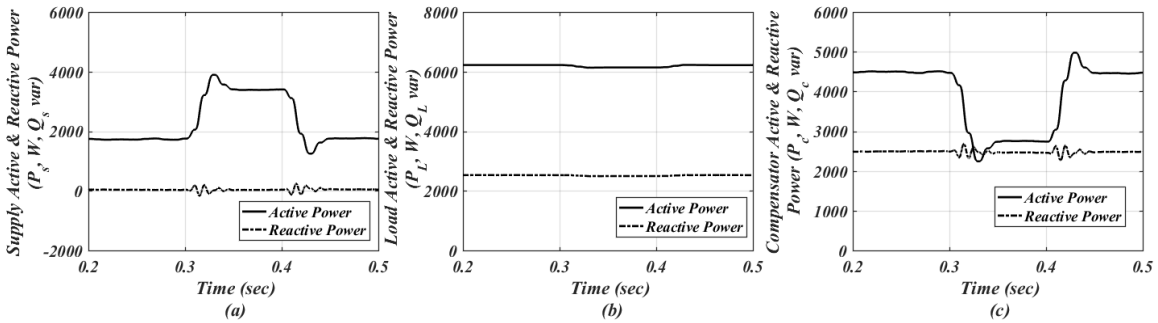

Fig. 7.19 Power flow in single phase grid connected PV system using SRFT based control algorithm (a) Active and reactive supply power P_s, Q_s (b) Active and reactive load power P_L, Q_L (c) Active and reactive compensator power P_c, Q_c

but maintained at 400 V by PI regulator. The compensator improves PQ of the grid by making supply current sinusoidal and also in-phase with the grid voltage.

Figs. 7.18(a)-(c) show the waveforms and Figs. 7.18(d)-(f) show the harmonics in supply voltage (v_s), supply current (i_s) and load current (i_L) respectively. The supply voltage and load current have a THD of 4.43% and 34.09% respectively. The THD of supply current is improved to 4.48% with SAPF compensator.

Fig. 7.19 shows the power balance between supply, load and PV for SOGI based control of SAPF. The solar irradiance is changed from 1000 W/m^2 to 600 W/m^2 from t=0.3 sec to t=0.4 sec. The real power from PV is reduces to 2800 W from 4500 W and increases in supply real power is 3400 W from 1700 W. Moreover the entire reactive power demand of load (2300 VARs) is met locally from SAPF controlled using SOGI algorithm.

7.4. EXPERIMENTAL RESULTS

The control algorithms discussed above are implemented on prototype hardware using dSPACE1104. The hardware results are recorded with the help of power analyzer and DSO.

7.4.1. Synchronous Reference Frame Theory Based Control Algorithm

A SRFT based control scheme for PQ improvement and grid integration of 500 W PV system was implemented on the prototype hardware setup of 63.5 V, 50 Hz, single phase distribution system feeding non-linear load. Fig. 7.20 shows the steady state experimental results in single phase grid connected SAPF-PV system with PV disconnected. Figs. 7.20(a)-(c) show supply current (i_s), load current (i_L) and compensator current (i_c) along with supply voltage (v_s) respectively. The supply current is observed to be sinusoidal and in-phase with the supply voltage. Figs. 7.20(d)-(f) show harmonics content of supply voltage (v_s), supply current (i_s) and load current (i_L). The THD of supply current is 4.8% whereas the load current has THD of 24.7%. The supply voltage has THD of 3.2%. Figs. 7.20(g)-(i) show power flow between supply, load and compensator. It is observed that supply delivers 500 W of real power and 60

VARs of reactive power. The load has a demand of 450 W of real power and 250 VARs of reactive power. The compensator is providing 240 VARs of reactive power but it is consuming 30 W of real power to replenish switching losses.

Fig. 7.21 shows the steady state hardware results of SAPF-PV system connected to non-linear and controlled through SRFT. Figs. 7.21(a)-(c) show supply current (i_s), load current (i_L) and compensator current (i_c) along with supply voltage (v_s) respectively. The supply current magnitude is reduced due to active power injection from PV source. This shows real power flow between PV system and load. Figs. 7.21(d)-(f) show harmonic content of supply voltage (v_s), supply current (i_s) and load current (i_L). The supply current THD obtained in this case is 4.9% which is less than 5% as prescribed in IEEE 519. Figs. 7.21(g)-(i) show power flow

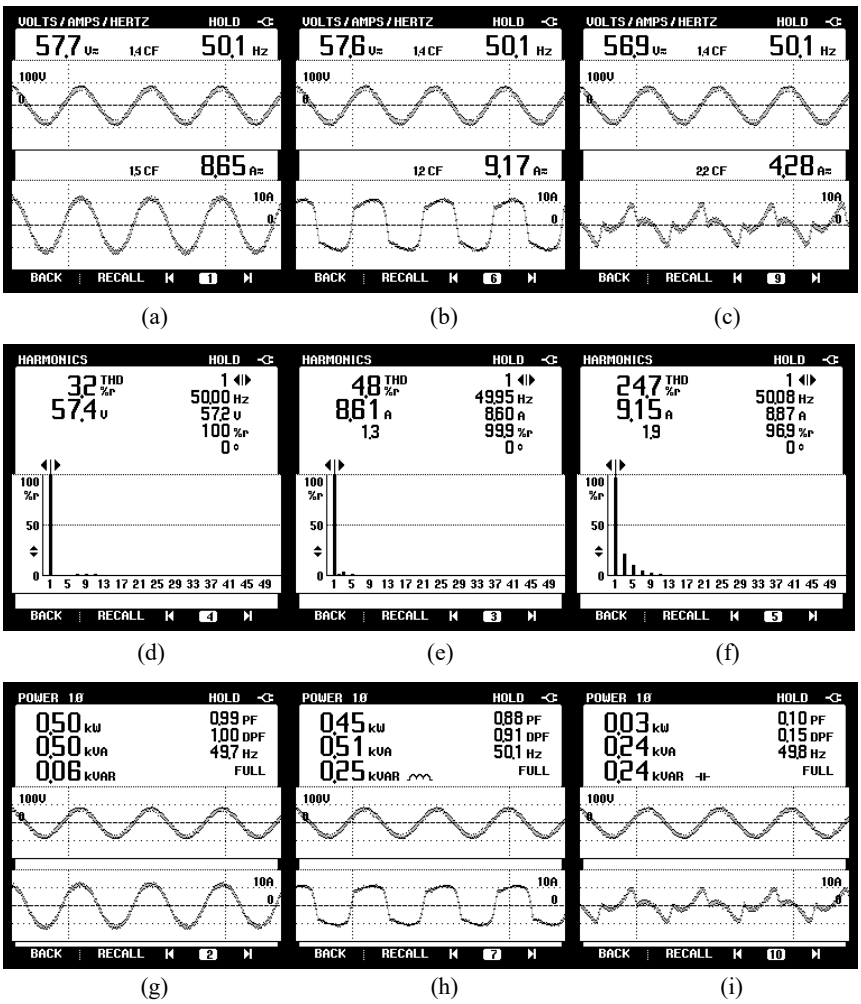

(a) (b) (c)

(d) (e) (f)

(g) (h) (i)

Fig. 7.20 Steady state waveforms for single phase system without PV using SRFT control algorithm (a-c) Waveforms of (a) supply current (i_s) (b) load current (i_L) (c) compensator current (i_c) (d-f) THD analysis (d) supply voltage (v_s) (e) supply current (i_s) (f) load current (i_L) (g-i) Active and reactive power for (g) supply (h) load (i) compensator

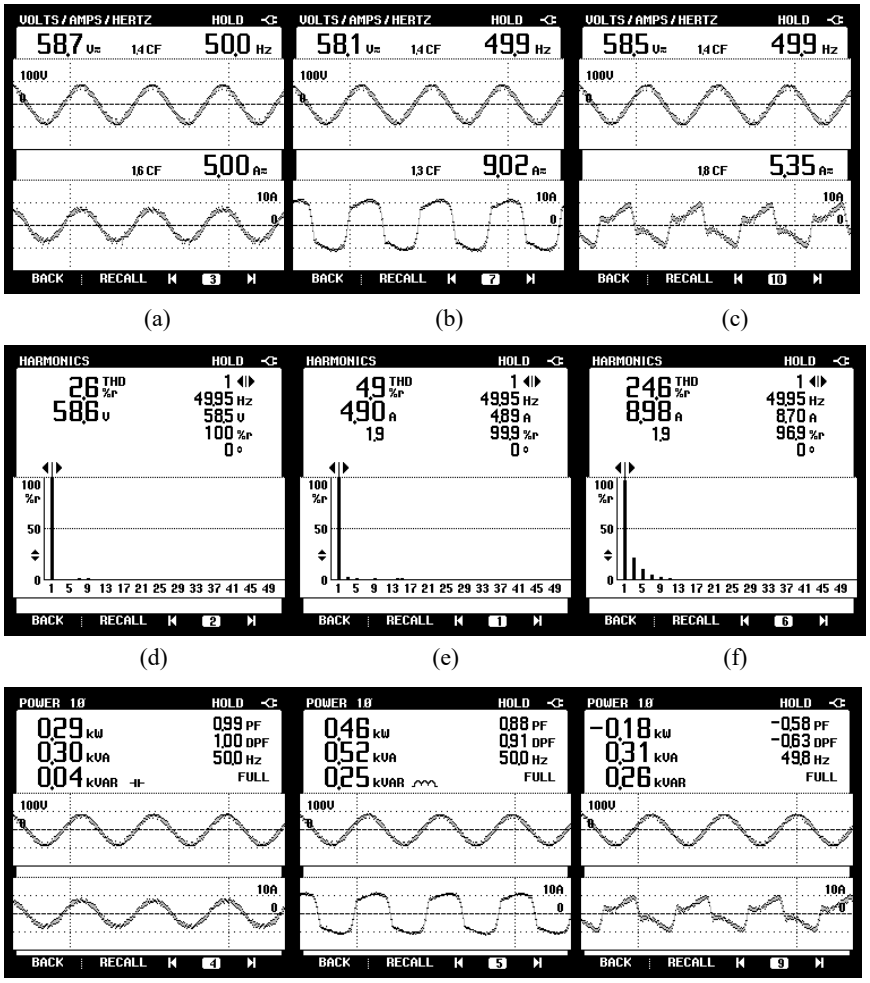

Fig. 7.21 Steady state waveforms for single phase system grid connected PV system using SRFT control algorithm (a-c) Waveforms of (a) supply current (i_s) (b) load current (i_L) (c) compensator current (i_c) (d-f) THD analysis (d) supply voltage (v_s) (e) supply current (i_s) (f) load current (i_L) (g-i) Active and reactive power for (g) supply (h) load (i) compensator

between supply, load and compensator. The supply delivers 290 W of real power and 40 VARs of reactive power at PF close of 0.99. The load has demand of 460 W of real power and 250 VARs of reactive power. The SAPF based compensator with PV interfaced at DC link provides 180 W real power and 260 VARs reactive power.

Fig. 7.22 shows the waveforms with SRFT control technique under dynamic conditions. Fig. 7.22 (a) shows supply voltage (v_s), supply current (i_s), load current (i_L) and compensator current (i_c). When the load is disconnected, it is seen that supply current and compensator current change their phase. Now the supply voltage and supply current are out of phase. This means that the excess PV power enters the grid. Fig. 7.22(b) shows supply voltage (v_s),

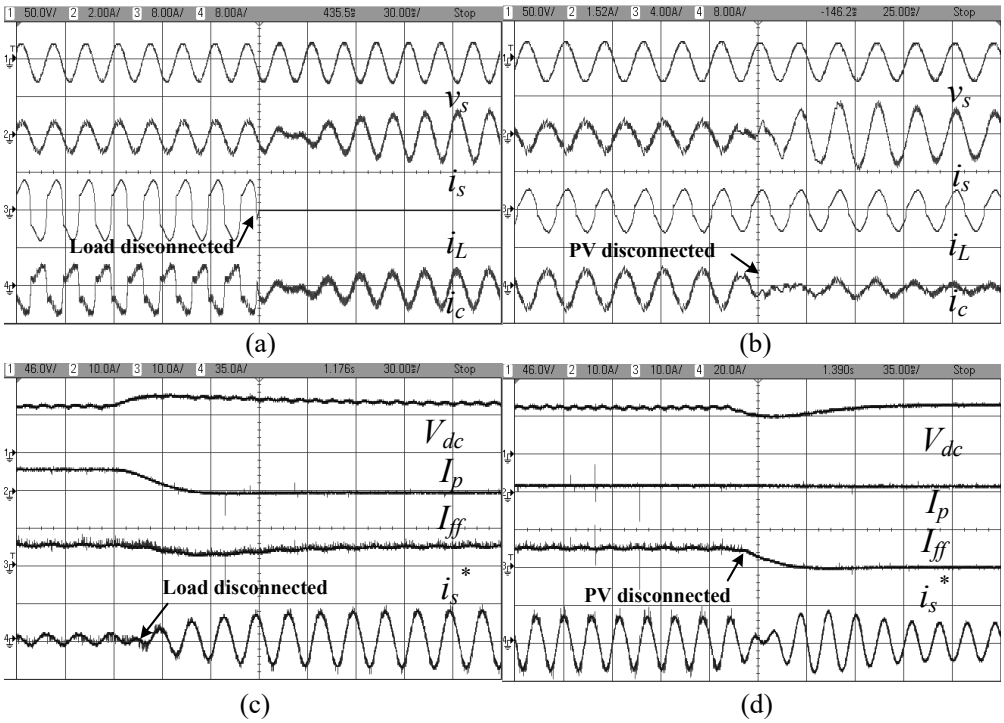

Fig. 7.22 Results showing dynamics for single phase grid connected PV system using SRFT control technique for non-linear load (a) v_s, i_s, i_L, i_c (b) v_s, i_s, i_L, i_c (c) V_{dc}, I_P, I_{ff}, i_s^* (d) V_{dc}, I_P, I_{ff}, i_s^*

supply current (i_s), load current (i_L) and compensator current (i_c). When PV source is disconnected and it is observed that compensator current reduces in magnitude significantly. Also the compensator is consuming power instead of delivering it because of absence of PV. The supply current is also in-phase with the supply voltage indicating supply is feeding power to the load. Fig. 7.22(c) shows DC link voltage (V_{dc}), fundamental active power component ($I_d^{'}$), PV feed forward factor (I_{ff}) and reference current (i_s^*). The DC link settles down to the set reference value and the I_d reduces to zero and I_{ff} is almost the same. The reference current has phase reversal. This indicates that the power flow from PV to grid. Fig. 7.22(d) shows DC link voltage (V_{dc}), fundamental active power component ($I_d^{'}$), PV feed forward factor (I_{ff}) and reference current (i_s^*). The PV output power is more than real power required by load. When the PV is disconnected, I_{ff} is reduced to zero but I_d remains the same. The reference current phase gets reversed due to absence of PV output and load gets real power fed directly from grid.

7.4.2. Notch Filter Based Control Technique

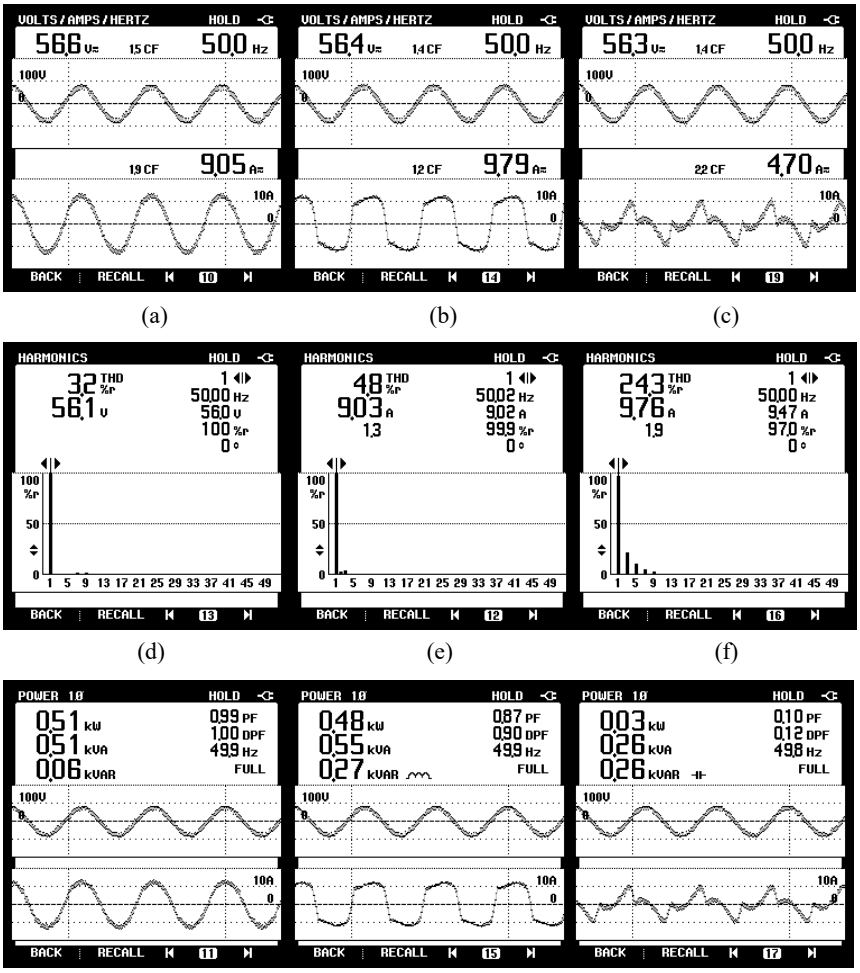

Fig. 7.23 Steady state waveforms for single phase system without PV using Notch Filter control algorithm (a-c) Waveforms of (a) supply current (i_s) (b) load current (i_L) (c) compensator current (i_c) (d-f) THD analysis (d) supply voltage (v_s) (e) supply current (i_s) (f) load current (i_L) (g-i) Active and reactive power for (g) supply (h) load (i) compensator

Fig. 7.23 shows the steady state experimental results of SAPF connected 63.5 V, 50 Hz, single phase distribution system feeding non-linear load using Notch Filter control technique. In Figs. 7.23(a)-(c) supply current (i_s), load current (i_L) and compensator current (i_c) along with supply voltage (v_s) are shown. The supply current obtained is in-phase with the supply voltage and sinusoidal. In Figs. 7.23(d)-(f) harmonics content of supply voltage (v_s), supply current (i_s) and load current (i_L) are shown. The supply current THD is 4.8% and the load current THD is 24.3%. The supply voltage has THD of 3.2%. Figs. 7.23(g)-(i) show power flow between supply, load and compensator. The supply delivers 510 W of real power and 60 VARs of reactive power. The load has a demand of 480 W of real power and 270 VARs of

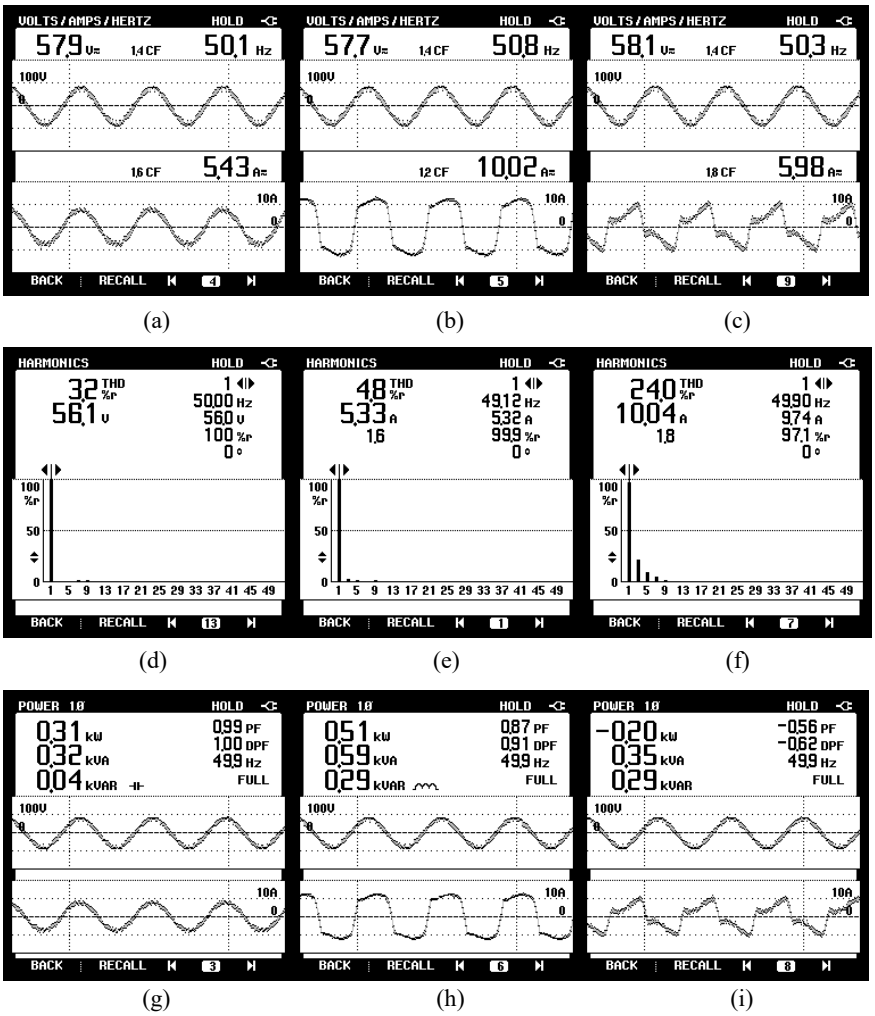

Fig. 7.24 Steady state waveforms for single phase grid connected PV system using Notch Filter control algorithm (a-c) Waveforms of (a) supply current (i_s) (b) load current (i_L) (c) compensator current (i_c) (d-f) THD analysis (d) supply voltage (v_s) (e) supply current (i_s) (f) load current (i_L) (g-i) Active and reactive power for (g) supply (h) load (i) compensator

reactive power. The compensator provides 260 VARs of reactive power and consumes 30 W of real power.

Fig. 7.24 shows the steady state hardware results with PV connected for non-linear load using Notch Filter control technique. Figs. 7.26(a)-(c) show supply current (i_s), load current (i_L) and compensator current (i_c) and supply voltage (v_s). The supply current reduces in magnitude and compensator current increases in magnitude during power flow from PV to PCC. In Figs. 7.24(d)-(f) harmonics content of supply voltage (v_s), supply current (i_s) and load current (i_L) are shown. The supply current THD is 4.8%. The supply voltage THD is 3.2%. Figs. 7.24(g)-(i) show power flow between supply, load and compensator when PV is connected to the

system. The supply delivers a reduced real power of 310 W and 40 VARs of reactive power. The load has demand of 510 W of real power and 290 VARs of reactive power. The compensator now provides 200 W of real power and 290 VARs of reactive power. The load and compensator reactive power is almost the same.

Fig. 7.25 shows the dynamics results using Notch Filter control technique. Fig 7.25(a) shows supply voltage (v_s), supply current (i_s), load current (i_L) and compensator current (i_c) are shown. The effect of sudden load disconnection is investigated. It is observed that when the load current is zero the supply current and compensator current become equal. The PV feeds power to the grid. In Fig 7.25(b) supply voltage (v_s), supply current (i_s), load current (i_L) and compensator current (i_c) are shown. The effect of sudden PV disconnection is also studied. It is observed that compensator current reduces in magnitude significantly. The load active power demand is also being supplied from the grid. In Fig. 7.25(c) DC link voltage (V_{dc}), fundamental active power component ($I_p^{'}$), PV feed forward factor (I_{ff}) and reference current (i_s^*) are presented. When the load is disconnected the fundamental active power component

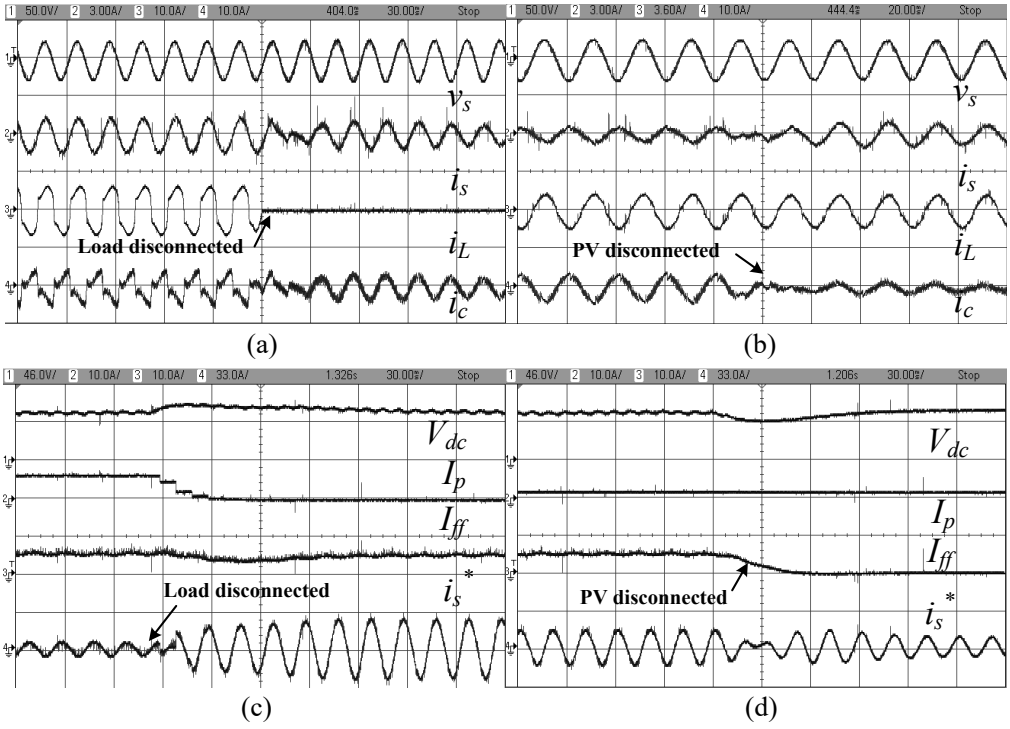

Fig. 7.25 Results showing dynamics for single phase grid connected PV system using Notch Filter based control algorithm for non-linear load (a) v_s, i_s, i_L, i_c (b) v_s, i_s, i_L, i_c (c) V_{dc}, I_P, I_{ff}, i_s^* (d) V_{dc}, I_P, I_{ff}, i_s^*

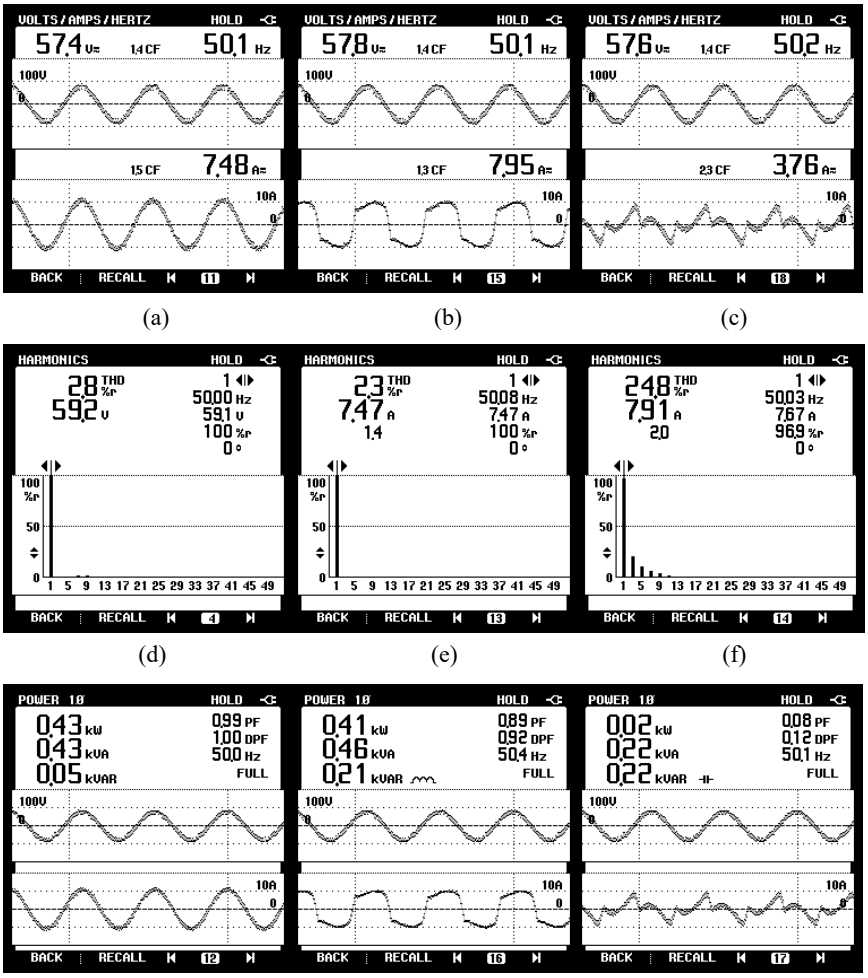

Fig. 7.26 Steady state waveforms for single phase system without PV using SOGI based control algorithm (a-c) Waveforms of (a) supply current (i_s) (b) load current (i_L) (c) compensator current (i_c) (d-f) THD analysis (d) supply voltage (v_s) (e) supply current (i_s) (f) load current (i_L) (g-i) Active and reactive power for (g) supply (h) load (i) compensator

(I_P) is reduced to zero and I_{ff} which denotes PV contribution does not change. In Fig. 7.25(d), DC link voltage (V_{dc}), fundamental active power component (I_p'), PV feed forward factor (I_{ff}) and reference current (i_s^*) are shown for the case when PV is disconnected. The DC link takes 3-4 cycles to settle down to reference value. The fundamental active power component I_P does not change and I_{ff} is reduced to zero due to sudden PV disconnection. The reference current (i_s^*) profile is shown in Fig. 7.25 (d) using Notch Filter algorithm, which is reduced and phase inverted during PV disconnection period.

7.4.3. Second Order Generalized Integrator Based Control Algorithm

Fig. 7.26 shows the steady state hardware results of 63.5 V, 50 Hz, single phase grid

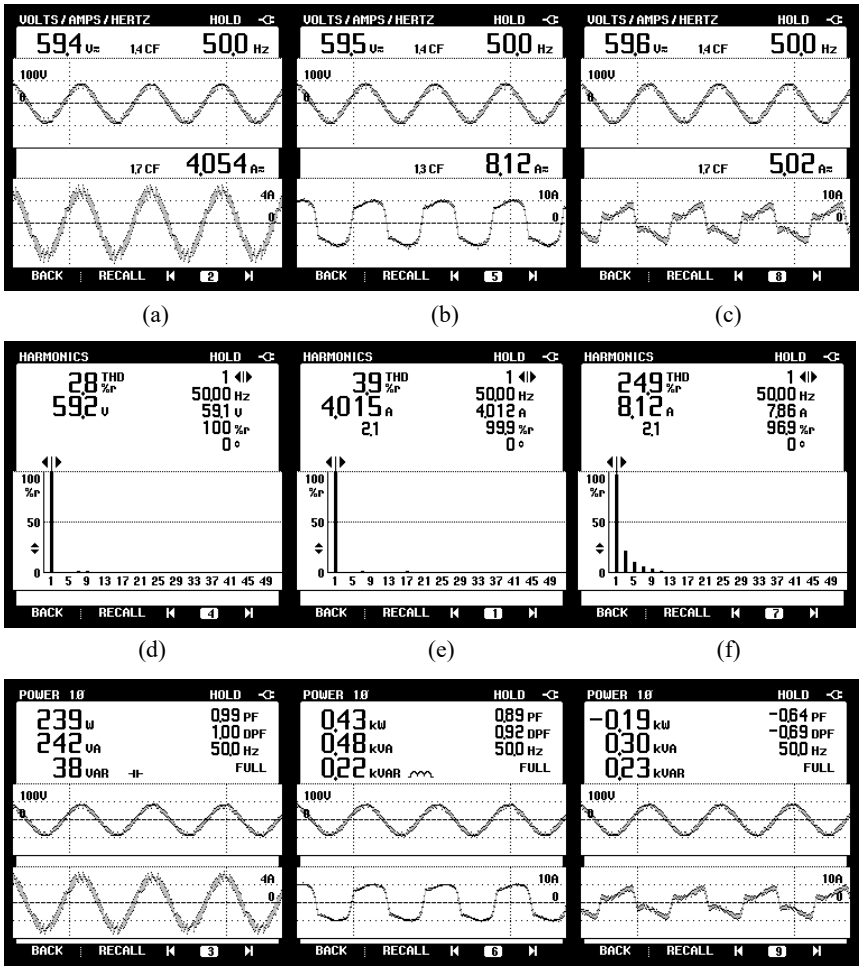

Fig. 7.27 Steady state waveforms for single phase grid connected PV system using SOGI based control algorithm (a-c) Waveforms of (a) supply current (i_s) (b) load current (i_L) (c) compensator current (i_c) (d-f) THD analysis (d) supply voltage (v_s) (e) supply current (i_s) (f) load current (i_L) (g-i) Active and reactive power for (g) supply (h) load (i) compensator

connected SAPF system feeding non-linear load using SOGI control algorithm. Figs. 7.26 (a)-(c) show supply current (i_s), load current (i_L), compensator current (i_c) and supply voltage (v_s). The supply current is sinusoidal and in-phase with the supply voltage. Figs. 7.26(d)-(f) show the harmonics content of supply voltage (v_s), supply current (i_s) and load current (i_L).

The supply current THD is 2.3% whereas the THD of load current is 24.8%. The supply voltage has THD of 2.8%. Figs. 7.26(g)-(i) show power flow between supply, load and compensator. The supply is observed to deliver 430 W of real power and 50 VARs of reactive power when the load has a demand of 410 W of real power and 210 VARs reactive power. The compensator provides 220 VARs of reactive power. It consumes 20 W of

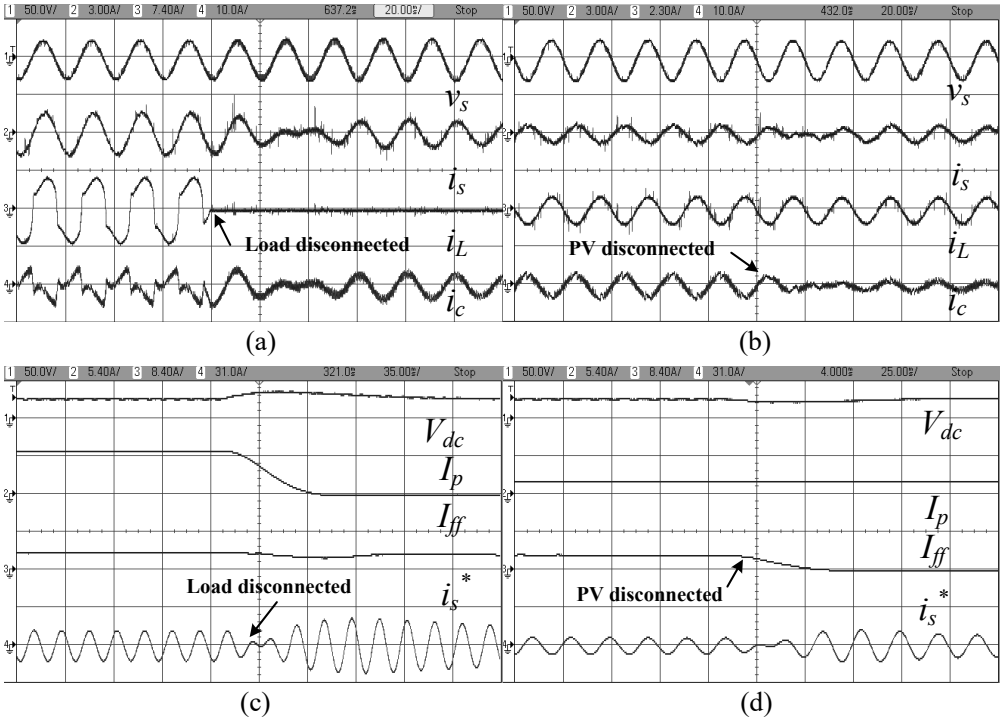

Fig. 7.28 Results showing dynamics for single phase grid connected PV system using SOGI based control algorithm for non-linear load (a) v_s, i_s, i_L, i_c (b) v_s, i_s, i_L, i_c (c) V_{dc}, I_P, I_{ff}, i_s^* (d) V_{dc}, I_P, I_{ff}, i_s^*

real power.

Fig. 7.27 shows the steady state experimental results with grid integration of PV and feeding non-linear load. The SAPF is controlled using SOGI control technique. Figs. 7.27(a)-(c) show supply current (i_s), load current (i_L) and compensator current (i_c) along with supply voltage (v_s). From Fig. 7.26 and Fig. 7.27 it is observed that the supply current magnitude has reduced from 7.48 A to 4.054 A, even though at same load condition. The compensator current magnitude has increased from 3.76 A to 5.02 A. This implies real power flow between PV and PCC. Figs. 7.27(d)-(f) show harmonic content in supply voltage (v_s), supply current (i_s) and load current (i_L) respectively. The supply current THD is 3.9% whereas the THD of load current and PCC voltage are 24.9% and 2.8% respectively. Figs. 7.27(g)-(i) show real and reactive power flow between supply, load and compensator. The supply delivers 239 W of real power and 38 VARs of reactive power at 0.99 PF. The load has demand of 430 W of real power and 220 VARs of reactive power. The compensator provides 190 W of real power and 230 VARs of reactive power. It is inferred that out of total real and reactive power demand of the load, the PV interfaced SAPF meets the total reactive power

demand of the load. The PV source injects real power as per its capability. The remaining real power demand of the load is met from the grid.

Fig. 7.28 shows the dynamics performance of SAPF using SOGI control technique. Fig. 7.28 (a) shows supply voltage (v_s), supply current (i_s), load current (i_L) and compensator current (i_c). When the load is suddenly disconnected, excess PV power is fed into the grid. This is observed as supply current has phase reversal. Fig. 7.28(b) shows supply voltage (v_s), supply current (i_s), load current (i_L) and compensator current (i_c). In this case the PV source is suddenly disconnected and it is observed that the PV power is not available. The switching loss of compensator is provided by supply side. Fig. 7.28(c) shows DC link voltage (V_{dc}), fundamental active power component ($I_p^{'}$), PV feed forward factor (I_{ff}) and reference current (i_s^*). When the load is disconnected, the DC link voltage has some transients but it settles after a couple of cycles. It is observed that I_P reduces to zero and I_{ff} is the same. Power flow from PV source to the grid is observed after load disconnection. A sudden phase change in reference current (i_s^*) is clearly visible. Fig. 7.28(d) shows the DC link voltage (V_{dc}), fundamental active power component ($I_p^{'}$), PV feed forward factor (I_{ff}) and reference current (i_s^*). In this case the PV source is disconnected. The I_P remains the same and I_{ff} is reduced to zero. In this case also, the reversal of reference current phase is observed. The PV is no longer able to provide any real power to the system since it is disconnected.

The performance evaluation of three control algorithm viz SRFT, Notch Filter and SOGI have been investigated on a single phase PV interfaced grid connected system. A comparison of different performance aspects is described in detail in the next section.

7.5 PERFORMANCE EVALUATION OF SRFT, NF AND SOGI BASED CONTROL ALGORITHMS WITH SAPF

A comparison of all three control algorithms SRFT, NF and SOGI is carried out through simulation and experimental studies for a single phase grid connected PV system. The PV

Table 7.1 COMPARISON OF CONTROL ALGORITHMS WITH PV DISCONNECTED (THD)

S. No.	Quantity	SRFT	Notch Filter	SOGI
1.	Supply Voltage (v_{sa})	57.4 V, 3.2% THD	56.1 V, 3.2% THD	59.2 V, 2.8% THD
2.	Load Current (i_{La})	9.15 A, 24.7% THD	9.76, 24.3% THD	7.91 A, 24.8% THD
3.	Supply Current (i_{sa})	8.61 A, 4.8% THD	9.03 A, 4.8% THD	7.47 A, 2.3% THD

Table 7.2 POWER FLOW USING DIFFERENT CONTROL ALGORITHM WITH PV DISCONNECTED

S.No.	Quantity	SRFT	Notch Filter	SOGI
1.	Supply Power	500 W, 60 VARs, 0.99 P.F.	520 W, 60 VARs, 0.99 P.F.	430 W, 50 VARs, 0.99 P.F.
2.	Load power	450 W, 250 VARs, 0.88 P.F.	480 W, 270 VARs, 0.87 P.F.	410 W, 210 VARs, 0.89 P.F.
3.	Compensator Power	30 W, 240 VARs	30 W, 260 VARs	20 W, 220 VARs

system is integrated to the grid and mitigation of PQ problems using a single phase H bridge based SAPF have been studied. The three control techniques under consideration are SRFT, NF and SOGI. Based on the experimental results, performance of the algorithms has been investigated in presence of non-linear and linear loads under similar test conditions.

Tables (7.1-7.4) have been compiled for a suitable comparison of the algorithms. Table 7.1 shows a comparison of control algorithms when PV system is disconnected and only non-linear load is considered. Experimental results shown in Fig. 7.20, 7.23, 7.26 have been compared. The THD in the supply current obtained using SRFT, Notch Filter, SOGI technique are 4.8%, 4.8% and 2.3% respectively. The load current THD under similar test conditions has THD of 24.7%, 24.3% and 24.8% respectively. The supply voltage has THD of 3.2%, 3.2% and 2.8% respectively. The THD obtained using SOGI control algorithm is found to be the least than obtained with the SRFT and Notch Filter based algorithm.

Table 7.3 COMPARISON OF CONTROL ALGORITHMS WITH PV CONNECTED (THD)

S.No.	Quantity	SRFT	Notch	SOGI
1.	Supply Voltage (v_{sa})	58.6 V, 2.6% THD	56.1 V, 3.2% THD	59.2 V, 2.8% THD
2.	Load Current (i_{La})	8.98 A, 24.6% THD	10.0, 24.0% THD	8.12 A, 24.9% THD
3.	Supply Current (i_{sa})	4.90 A, 4.9% THD	5.33 A, 4.8% THD	4.015 A, 3.9% THD

Table 7.4 POWER FLOW USING DIFFERENT CONTROL ALGORITHM WITH PV CONNECTED

S.No.	Quantity	SRFT	Notch Filter	SOGI
1.	Supply Power	290 W, 40 VARs, 0.99 P.F.	310 W, 40 VARs, 0.99 P.F.	239 W, 38 VARs, 0.99 P.F.
2.	Load power	460 W, 250 VARs, 0.88 P.F.	510 W, 290 VARs, 0.87 P.F.	430 W, 220 VARs, 0.89 P.F.
3.	Compensator Power	-180 W, 260 VARs	-200 W, 290 VARs	-190 W,230 VARs

Table 7.2 shows comparison of the steady state power of the supply, load and SAPF when PV is disconnected from the developed system. It can be observed from the table that the grid supply feeds real power demand of load and compensator feeds a major part of load reactive power requirement. The supply P.F. is improved to 0.99 in all the three cases when the load P.F. is 0.87 lag. The power factor of the supply is considerably improved to nearly unity with all the three developed algorithms.

Table 7.3 shows a comparison of control algorithms for grid connected PV system in presence of non-linear load. The results in this table have been compiled on the basis of experimental results shown in Fig. 7.21, 7.24 and 7.27. It has been observed that the supply current THD obtained using SRFT, Notch Filter, SOGI technique is 4.9%, 4.8% and 3.9% respectively. The load current THD in these cases are 24.6%, 24.0% and 24.9% respectively. The supply voltage has THD 2.6%, 3.2% and 2.8% respectively. As observed form the Table, the THD obtained using SOGI control algorithm is comparatively better than obtained using SRFT and Notch Filter with PV integrated to the system.

Table 7.4 shows the steady state power flow between supply, load and SAPF when PV system is connected.

7.6 CONCLUSIONS

The main contributions of this chapter are to develop a grid integrated single phase PV system. It has been observed that the PV system feeds real power into the system due to which active power delivered from grid is effectively reduced. Different control algorithms considered in this chapter include SRFT, NF and SOGI. For all control algorithms developed and implemented, the grid supply feeds the real power demand of load and compensator supplies major part of load reactive power requirement. The supply feed most of the active power required by SAPF. Active power provided by PV in all three cases is almost same. The performance of all three control algorithms is compared and nearly UPF is maintained at the AC supply. The performance of Notch controller is observed to be slightly better than SOGI and Notch Filter based algorithms.

Chapter 8
MAIN CONCLUSIONS AND FUTURE SCOPE OF WORK

8.0 GENERAL

PQ problems in TPTW and TPFW distribution system and their mitigation techniques using conventional and modern control algorithms have been addressed in this thesis. PQ problems have been studied in detailed in MATLAB/SIMULINK environment for TPTW and TPFW systems. MATLAB based SIMULINK models have been developed and tested for various PQ problems such as load unbalancing, harmonics elimination, PF improvement and distortion in voltage etc. After successful development of control algorithm in SIMULINK model, experimental prototype hardware is developed in laboratory and tested with conventional control algorithms for PQ problem mitigation. Further, new control techniques have been developed and tested first in MATLAB/SIMULINK environment and also validated experimentally. The loads considered are non-linear and linear load combinations for analysis of SAPF system with modern control algorithm. Experimental setup for TPTW and TPFW distribution systems has been also tested under load dynamics by creating unbalancing in loads. The introduction of distortion in supply voltage and effective control of SAPF under distorted grid condition is also demonstrated. This study has also been performed in TPFW system with linear and non-linear loads. Performance analysis of filtering techniques for distorted grid voltage and generating synchronizing signals has been discussed. Further, a single phase grid integrated PV system has been analyzed for integration to grid and mitigation of PQ problems. Various control algorithms have been successfully implemented for control of VSC for PQ mitigation and real power extraction from the PV source.

8.1 MAIN CONCLUSIONS

The work of this thesis has been broadly classified into four parts. The first part deals with development of control algorithms for TPTW distribution system. Three control techniques namely Notch Filter, Kalman-LMS and Hopfield NN have been developed for load balancing, power factor improvement and harmonics reduction. All the control algorithms effectively improve PQ of TPTW system. In case of non-linear loads, the supply side THD content is considerably improved up-to 1.90% and harmonics have been effectively filtered with the help of SAPF. The experimentally obtained results showed a THD of 1.90%, 2.8% and 3.4% in source current with the Notch Filter, Kalman-LMS and Hopfield NN respectively when the load current had THD of 23.0%. The performance of these three algorithms is similar with linear loads. The supply side P.F. is improved drastically from 0.86 to 0.95 by connecting SAPF. The steady state as well as dynamics performance of SAPF proves the effectiveness of developed control techniques for mitigating PQ problems. The complexities of developed control algorithms have also been investigated through mathematical calculations and dynamics performance analysis. It has been shown that fundamental component extraction is fastest in case of Notch Filter as compared to Kalman-LMS and Hopfield NN based algorithm which is least complex and can be executed easily using dSPACE 1104.

In the second part of the thesis work, TPFW distribution system experimental setup has been developed and tested for PQ problems such as load unbalancing, PF correction, harmonics reduction and neutral current compensation. Three control algorithms have been developed for TPFW system viz. STF, MRGN and ChANN. A conventional TPTW SAPF with three legs has been used along with a zigzag transformer to avoid costly four leg SAPF structure. The zigzag transformer provides a path to the flow of load neutral current under unbalanced conditions. The supply neutral is controlled to be zero irrespective of the variations in loads.

By using developed control algorithms, balanced currents in supply side have been obtained by all control algorithms. The SAPF has been able to compensate for harmonics in loads and poor PF with different loads. The reactive power requirement of load has been met locally by SAPF. Besides mitigating PQ issues, all the control algorithms can be used to extract harmonic components from non-linear load currents. The control algorithms have been developed to extract the fundamental active power component of the load current and generate six switching pulses. All the control algorithms have been able to improve supply side currents profile from non-sinusoidal to nearly sinusoidal profile. Based on the performance and complexity of control techniques discussed in Chapter 5, MRGN control algorithm has been found to perform better as compared to STF and ChANN *wrt* improved convergence under dynamic load changes. The supply current has shown THD of 3.1%, 3.4% and 4.3% with nonlinear loads using STF, MRGN and ChANN based algorithms.

In the third part of the thesis, distortion in supply voltages has been considered additionally. Conventional methods to obtain synchronizing templates for generation of reference currents fail due to high distortion in PCC voltages. Hence, two control techniques viz MCCF and SOGI have been developed and implemented on load currents as well as PCC voltages. They have been used to extract the fundamental component of PCC voltages so that the reference currents can be generated. Non-linear and/or linear loads have been considered for performance analysis of the controllers. The MCCF and SOGI have also been implemented for extracting fundamental component of load current and its use in reference supply current generation. Steady state experimental results with MCCF and SOGI have shown good performance for load compensation. The THD in supply current has improved from 29.9% to 3.6% with MCCF and 3.8% with SOGI algorithm. Dynamic performance of SAPF has shown that both control algorithms are effective for PQ problems mitigation in distorted grid system.

In the fourth part of the thesis, besides PQ problems, grid integration of PV system is also discussed and analyzed in detail. Single phase grid connected PV system has been developed using simulation and validated using experimental analysis. Since, the integration of RES to grid is an emerging area of research, SAPF topology has been slightly modified with PV integrated at the DC bus. Three control algorithms viz SRFT, Notch Filter and SOGI have been implemented for single phase grid connected PV system. A feed forward factor has been determined to estimate the real power extracted from PV source. Simulation as well as experimental results with/ without PV have been recorded and investigated. It has been observed that besides mitigating PQ issues such as harmonics in supply currents, poor PF etc. real power demand of load has also been met partially by PV. Steady state performance of SAPF showing supply voltage, load and supply currents with and without PV system is discussed in detail. The THD of 4.9%, 4.8% and 3.8% in supply current using the three algorithms namely SRFT, Notch Filter and SOGI is obtained. In all the cases, supply side current THD is reduced significantly and it is less than the limit prescribed in standard IEEE 519. Low THD in supply side current also indicates effective filtering action of SAPF. Notch Filter has been found to be most simple and effective for real time implementation on a single phase grid connected PV system.

8.2 FUTURE SCOPE OF WORK

In this thesis, SAPF having conventional two level VSC is considered. SAPF having three or higher (multilevel) VSC configuration can be used to mitigate PQ problems in TPTW and TPFW systems. Multilevel VSC based SAPF can be used for higher voltage and power level applications.

The P&O MPPT technique is used to extract maximum power from solar PV system. New and modern control techniques for MPPT can be implemented which are more efficient than conventional control techniques in terms of complexity and application.

In this thesis single phase grid connected PV system is discussed. Presence of large number of single phase PV systems can cause unbalanced operation of three phase grid which is not desirable. So three phase grid connected PV system can be developed for efficient power system operation. Such integration of PV systems with TPTW, TPFW distribution systems should comply with the grid code. Besides PV system, several other RES such as wind, biomass, hydro can be connected to single phase as well as three phase distribution systems.

In this dSPACE 1104 is used for DSP which processes all input signals and produces the desired output. It is most critical part of the shunt compensation system. There is a scope of low cost FPGA based DSP development, which is cost effective and have faster operation as compared to dSAPCE1104. This new development will lead to more accurate development of modern control techniques.

Besides all above, study on fault ride through capabilities of distribution system supported with distributed generation can be studied. This will allow practical implementation of such system in real world on a large scale.

Following are the some publications in journals and conferences out of this research work.

❖ Publications in National/International Journals

[1] **Prakash Chittora**, Alka Singh, Madhusudan Singh, "Gauss–Newton-based fast and simple recursive algorithm for compensation using shunt active power filter," in IET Generation, Transmission & Distribution, vol. 11, no. 6, pp. 1521-1530, 4 20 2017. doi: 10.1049/iet-gtd.2016.1222.

[2] **Prakash Chittora**, Alka Singh, Madhusudan Singh, "Performance evaluation of digital filters in distribution static compensator for non-linear loads," in IET Power Electronics, vol. 10, no. 14, pp. 1915-1923, 11 17 2017.

[3] **Prakash Chittora**, Alka Singh, Madhusudan Singh,"Simple and efficient control of DSTATCOM in three-phase four-wire polluted grid system using MCCF-SOGI based controller," in IET Generation, Transmission & Distribution, vol. 12, no. 5, pp. 1213-1222, 3 13 2018.

[4] **Prakash Chittora**, Alka Singh and Madhusudan Singh, "Chebyshev Functional Expansion Based Artificial Neural Network Controller for Shunt Compensation," in IEEE Transactions on Industrial Informatics, Vol. 14, no. 9, pp. 3792-3800, 2018. doi: 10.1109/TII.2018.2793347

[5] **Prakash Chittora**, Alka Singh, Madhusudan Singh, "Application of Hopfield Neural Network for Harmonic Current Estimation and Shunt Compensation," in Electric Power Components and Systems. Vol. 46, no. 13, pp. 290-301, 2018. doi 10.1080/15325008.2018.

❖ Publications in National/International Conferences

[1] **Prakash Chittora**, Alka Singh, Madhusudan Singh, "Modeling and analysis of power quality problems in electric arc furnace," 2015 Annual IEEE India Conference (INDICON), New Delhi, 2015, pp. 1-6. doi: 10.1109/INDICON.2015.7443638

[2] **Prakash Chittora**, Alka Singh, Madhusudan Singh, "Harmonic Current Extraction and Compensation in Three Phase Three Wire System Using Notch Filter", 2015 IEEE Recent Advances in Intelligent Computational Systems (RAICS), Trivandrum, 2015, pp. 422-427. doi: 10.1109/RAICS.2015.7488453.

[3] **Prakash Chittora**, Alka Singh, Madhusudan Singh, "Performance evaluation of a new Kalman filter based least mean square algorithm for power quality improvement," in IEEE 1st International Conference on Power Electronics, Intelligent Control and Energy Systems (ICPEICES), Delhi, 2016, pp. 1-5. doi: 10.1109/ICPEICES.2016.7853382.

[4] **Prakash Chittora**, Alka Singh, Madhusudan Singh, "Application of Self Tuning Filter for Power Quality Improvement in Three-Phase-Three-Wire Distorted Grid System", in 7th International Conference on Power Systems (ICPS), Pune, 2017, pp. 313-318. doi: 10.1109/ICPES.2017.8387312

[5] **Prakash Chittora**, Alka Singh, Madhusudan Singh, "Multi-functional Capabilities of Self Tuned Filter in Three Phase Four Wire Polluted Grid Distribution System", in IEEE 2nd International Conference on Power Electronics, Intelligent Control and Energy Systems (ICPEICES), Delhi, 2018, pp. 1-6.

REFERENCES

1. BOOKS

[1] B. Singh, A. Chandra, K. Al-Haddad, “Power Quality:Problems and Mitigation Techniques”, John Wiley and Sons, U.K., 2015.

[2] Ewald F. Fuchs and Mohammad A. S. Mausoum, “Power Quality in Power Systems and Electrical Machines”, Elsevier Academic Press, London, UK, 2008.

[3] Antonio Moreno-Munoz, “Power Quality: Mitigation Technologies in a Distributed Environment”, Springer-Verlag London limited, London, 2007.

[4] G. Arindam and L. Gerard, “Power Quality Enhancement using Custom Power Devices”, Springer International Edition ed. Delhi, India: Springer, 2009.

[5] E.Acha, V.G. Agelids, O. Anaya-Lara, T.J.E. Miller, “Power Electronic Control in Electric Systems”, Newness Power engineering series, 1st Edition, Oxford, 2002.

[6] F. F. Ewald andA. S.M.Mohammad, “Power Quality in Power Systems and Electrical Machines. London, U.K.: Elsevier Academic Press, 2008.

[7] H. Akagi, E H Watanabe and M Aredes, “Instantaneous power theory and applications to power conditioning, John Wiley & Sons, New Jersey, USA, 2007.

[8] N.G. Hingorani, L. Gyugyi, 1999, “Understanding FACTS: Concepts and Technology of Flexible AC Transmission Systems,” IEEE Press, New York.

[9] K. R. Padiyar, “FACTS Controllers in Power Transmission and Distribution,” New Age International (P) Limited, Publishers, New Delhi, 2007.

2. Power Quality Problems

[10] M. F. McGranaghan, D. R. Mueller and M. J. Samotyj, "Voltage sags in industrial systems," in IEEE Transactions on Industry Applications, vol. 29, no. 2, pp. 397-403, Mar/Apr 1993.doi: 10.1109/28.216550.

[11] P. Wang, N. Jenkins and M. H. J. Bollen, "Experimental investigation of voltage sag mitigation by an advanced static VAr compensator," in IEEE Transactions on Power Delivery, vol. 13, no. 4, pp. 1461-1467, Oct 1998.doi: 10.1109/61.714772

[12] R. T. Ugale, Y. BalaKrishna and B. N. Chaudhari, "Effects of short power interruptions and voltage sags on the performance of line start permanent magnet synchronous motor," 2008 4th IET Conference on Power Electronics, Machines and Drives, York, 2008, pp. 184-188.doi: 10.1049/cp:20080508

[13] P. G. Therond, I. Joly and M. Volker, "Superconducting magnetic energy storage (SMES) for industrial applications-comparison with battery systems," in IEEE Transactions on Applied Superconductivity, vol. 3, no. 1, pp. 250-253, March 1993. doi: 10.1109/77.233718

[14] P. Y. Or and K. N. Leung, "An Output-Capacitorless Low-Dropout Regulator With Direct Voltage-Spike Detection," in IEEE Journal of Solid-State Circuits, vol. 45, no. 2, pp. 458-466, Feb. 2010.doi: 10.1109/JSSC.2009.2034805

[15] J. M. Wang, S. T. Wu, S. C. Yen and H. J. Chiu, "A Simple Inverter for Arc-Welding Machines With Current Doubler Rectifier," in IEEE Transactions on Industrial Electronics, vol. 58, no. 11, pp. 5278-5281, Nov. 2011.doi: 10.1109/TIE.2011.2126538
[16] H. Mokhtari and M. Hejri, "A new three phase time-domain model for electric arc furnaces using MATLAB," IEEE/PES Transmission and Distribution Conference and Exhibition, 2002, pp. 2078-2083 vol.3. doi: 10.1109/TDC.2002.1177781
[17] A. M. O. Haruni, K. M. Muttaqi and M. Negnevitsky, "Analysis of harmonics and voltage fluctuation using different models of Arc furnace," 2007 Australasian Universities Power Engineering Conference, Perth, WA, 2007, pp. 1-6. doi: 10.1109/AUPEC.2007.4548105
[18] Y. J. Hsu, K. H. Chen, P. Y. Huang and C. N. Lu, "Electric Arc Furnace Voltage Flicker Analysis and Prediction," in IEEE Transactions on Instrumentation and Measurement, vol. 60, no. 10, pp. 3360-3368, Oct. 2011. doi: 10.1109/TIM.2011.2134910
[19] M. Torabian Esfahani and B. Vahidi, "A New Stochastic Model of Electric Arc Furnace Based on Hidden Markov Model: A Study of Its Effects on the Power System," in IEEE Transactions on Power Delivery, vol. 27, no. 4, pp. 1893-1901, Oct. 2012. doi: 10.1109/TPWRD.2012.2206408
[20] D. C. Bhonsle and R. B. Kelkar, "Simulation of electric arc furnace characteristics for voltage flicker study using MATLAB," 2011 International Conference on Recent Advancements in Electrical, Electronics and Control Engineering, Sivakasi, 2011, pp. 174-181.doi: 10.1109/ICONRAEeCE.2011.6129773
[21] S. I. Deaconu, G. N. Popa, A. I. Toma and M. Topor, "Modeling and Experimental Analysis for Modernization of 100-t EAF," in IEEE Transactions on Industry Applications, vol. 46, no. 6, pp. 2259-2266, Nov.-Dec. 2010. doi: 10.1109/TIA.2010.2072977
[22] G. C. Montanari, M. Loggini, A. Cavallini, L. Pitti and D. Zaninelli, "Arc-furnace model for the study of flicker compensation in electrical networks," in IEEE Transactions on Power Delivery, vol. 9, no. 4, pp. 2026-2036, Oct 1994. doi: 10.1109/61.329535
[23] P. P. Barker, T. A. Short, C. a Warren, J. J. Burke, R. T. Mancao, and J. J. Siewierski, "Power quality monitoring of a distribution system," in IEEE Transactions on Power Delivery, vol. 9, no. 2, pp. 1136-1142, Apr 1994. doi: 10.1109/61.296300

3. Power Quality Estimation

[24] V. Terzija and V. Stanojevic, "STLS algorithm for power quality indices estimation," 2008 IEEE Power and Energy Society General Meeting - Conversion and Delivery of Electrical Energy in the 21st Century, Pittsburgh, PA, 2008, pp. 1-1. doi: 10.1109/PES.2008.4596952
[25] M. Biswal and P. K. Dash, "Estimation of time-varying power quality indices with an adaptive window-based fast generalised S-transform," in IET Science, Measurement & Technology, vol. 6, no. 4, pp. 189-197, July 2012. doi: 10.1049/iet-smt.2011.0202

[26] P. S. Wright, A. Bergman, A. P. Elg, M. Flood, P. Clarkson and K. Hertzberg, "Onsite Measurements for Power-Quality Estimation at the Sweden–Poland HVDC Link," in IEEE Transactions on Power Delivery, vol. 29, no. 1, pp. 472-479, Feb. 2014. doi: 10.1109/TPWRD.2013.2276408

[27] V. Terzija and S. Vladimir, "Two-Stage Improved Recursive Newton Type Algorithm for Power Quality Indices Estimation," 2007 IEEE Power Engineering Society General Meeting, Tampa, FL, 2007, pp. 1-1. doi: 10.1109/PES.2007.385727

[28] A. Bagheri, M. Mardaneh, A. Rajaei and A. Rahideh, "Detection of Grid Voltage Fundamental and Harmonic Components Using Kalman Filter and Generalized Averaging Method," in IEEE Transactions on Power Electronics, vol. 31, no. 2, pp. 1064-1073, Feb. 2016. doi: 10.1109/TPEL.2015.2418271

[29] R. Cisneros-Magaña, A. Medina, V. Dinavahi and A. Ramos-Paz, "Time-Domain Power Quality State Estimation Based on Kalman Filter Using Parallel Computing on Graphics Processing Units," in IEEE Access, vol. 6, pp. 21152-21163, 2018. doi: 10.1109/ACCESS.2018.2823721

[30] A. A. Girgis, W. B. Chang and E. B. Makram, "A digital recursive measurement scheme for online tracking of power system harmonics," in IEEE Transactions on Power Delivery, vol. 6, no. 3, pp. 1153-1160, Jul 1991. doi: 10.1109/61.85861

[31] M. Mojiri and A. R. Bakhshai, "Estimation of n Frequencies Using Adaptive Notch Filter," in IEEE Transactions on Circuits and Systems II: Express Briefs, vol. 54, no. 4, pp. 338-342, April 2007. doi: 10.1109/TCSII.2006.889724

[32] K. B. Nazirov, G. V. Shvedov, S. R. Chorshanbiev and S. D. Dzhuraev, "Study of the operating modes of the 0.4 kV main distribution network, in Dushanbe city of the Republic of Tajikistan, with distributed solar generation for power losses and power quality estimation," 2018 IEEE Conference of Russian Young Researchers in Electrical and Electronic Engineering (EIConRus), Moscow, 2018, pp. 737-742. doi: 10.1109/EIConRus.2018.8317197

[33] N. Anandh, P. A. D'sa, M. V. Gautam and V. S. Sandeep, "Power quality estimation, analysis and improvement for uninterrupted power supply," 2016 International Conference on Control, Instrumentation, Communication and Computational Technologies (ICCICCT), Kumaracoil, 2016, pp. 26-31. doi: 10.1109/ICCICCT.2016.7987914

[34] P. V. Morozov and Y. V. Morozov, "Statistical methods application in signals spectral classification for power quality estimation in power transmission lines with fast changing loads," 2017 18th International Conference of Young Specialists on Micro/Nanotechnologies and Electron Devices (EDM), Erlagol, 2017, pp. 393-395. doi: 10.1109/EDM.2017.7981780

[35] S. Ali, K. Wu, K. Weston and D. Marinakis, "A Machine Learning Approach to Meter Placement for Power Quality Estimation in Smart Grid," in IEEE Transactions on Smart Grid, vol. 7, no. 3, pp. 1552-1561, May 2016. doi: 10.1109/TSG.2015.2442837

[36] Q. Ai, Y. Zhou, W. Xu, “Adaline and its application in power quality disturbances detection and frequency tracking”, in Electric Power Systems Research, Vol. 77, No. 5–6, Pages 462-469, April 2007. doi: 10.1016/j.epsr.2006.04.007
[37] I. S. Ilie, I. Hernando-Gil and S. Z. Djokic, "Theoretical interruption model for reliability assessment of power supply systems," in IET Generation, Transmission & Distribution, vol. 8, no. 4, pp. 670-681, April 2014. doi: 10.1049/iet-gtd.2013.0339
[38] D. Andrews, M. T. Bishop and J. F. Witte, "Harmonic measurements, analysis, and power factor correction in a modern steel manufacturing facility," in IEEE Transactions on Industry Applications, vol. 32, no. 3, pp. 617-624, May/Jun 1996. doi: 10.1109/28.502174
[39] S.K. Singh , N. Sinha , A.K. Goswami and N. Sinha, “Variable Constraint based Least Mean Square algorithm for power system harmonic parameter estimation”, in International Journal of Electrical Power & Energy Systemsm vol. 73, pp. 218–228, 2015. doi 10.1016/j.ijepes.2015.04.018.

4. PQ Standards

[40] IEEE Recommended Practice and Requirements for Harmonic Control in Electric Power Systems," in IEEE Std 519-2014 (Revision of IEEE Std 519-1992) , pp.1-29, June 11 2014. doi: 10.1109/IEEESTD.2014.6826459
[41] W. E. Reid, "Power quality issues-standards and guidelines," in IEEE Transactions on Industry Applications, vol. 32, no. 3, pp. 625-632, May/Jun 1996.
[42] IEEE Recommended Practice for Monitoring Electric Power Quality," in IEEE Std 1159-2009 (Revision of IEEE Std 1159-1995) , vol., no., pp.c1-81, June 26 2009
[43] IEEE Recommended Practice for Powering and Grounding Electronic Equipment (IEEE Emerald Book) (Superseded by IEEE 1000-2005)," in IEEE Std P1100/D2 , 2005.
[44] IEEE standard definitions for the measurement of electric power quantities under sinusoidal, non-sinusoidal, balanced, or unbalanced conditions," IEEE std. 1459, Mar, 19, 2010.
[45] Electromagnetic compatibility (EMC) - Part 3-2: Limits - Limits for harmonic current emissions (equipment input current ≤16 A per phase) IEC Std. 61000, 3-2, 2018.
[46] Electromagnetic compatibility (EMC) - Part 4-15: Testing and measurement techniques - Flickermeter - Functional and design specifications, IEC Std. 61000, 4-15, 2010.

5. Conventional Mitigation techniques

[47] J. Miret, A. Camacho, M. Castilla, J. L. García de Vicuña and J. de la Hoz, "Reactive current injection protocol for low-power rating distributed generation sources under voltage sags," in IET Power Electronics, vol. 8, no. 6, pp. 879-886, 6 2015. doi: 10.1049/iet-pel.2014.0593
[48] S. S. Choi, J. D. Li and D. M. Vilathgamuwa, "A generalized voltage compensation strategy for mitigating the impacts of voltage sags/swells," in IEEE Transactions on

Power Delivery, vol. 20, no. 3, pp. 2289-2297, July 2005. doi: 10.1109/TPWRD.2005.848442

[49] H. Ghosh, P. Kumar Saha and G. Kumar Panda, "Performance comparison between DVR and DSTATCOM used for load voltage control in distribution side," 2012 International Conference on Advances in Power Conversion and Energy Technologies (APCET), Mylavaram, Andhra Pradesh, 2012, pp. 1-6. doi: 10.1109/APCET.2012.6302026

[50] A. Elnady and M. M. A. Salama, "Unified approach for mitigating voltage sag and voltage flicker using the DSTATCOM," in IEEE Transactions on Power Delivery, vol. 20, no. 2, pp. 992-1000, April 2005. doi: 10.1109/TPWRD.2004.837670

[51] B. Singh, R. Niwas and S. K. Dube, "Load Leveling and Voltage Control of Permanent Magnet Synchronous Generator-Based DG Set for Standalone Supply System," in IEEE Transactions on Industrial Informatics, vol. 10, no. 4, pp. 2034-2043, Nov. 2014. doi: 10.1109/TII.2014.2341952

[52] V. Virulkar and M. Aware, "Analysis of DSTATCOM with BESS for mitigation of flicker," 2009 International Conference on Control, Automation, Communication and Energy Conservation, Perundurai, Tamilnadu, 2009, pp. 1-7.

[53] X. Yu, M. R. Starke, L. M. Tolbert and B. Ozpineci, "Fuel cell power conditioning for electric power applications: a summary," in IET Electric Power Applications, vol. 1, no. 5, pp. 643-656, Sept. 2007. doi: 10.1049/iet-epa:20060386

[54] T. L. Baldwin, T. Hogans, S. D. Henry, F. Renovich and P. T. Latkovic, "Reactive-power compensation for voltage control at resistance welders," in IEEE Transactions on Industry Applications, vol. 41, no. 6, pp. 1485-1492, Nov.-Dec. 2005. doi: 10.1109/TIA.2005.858301

[55] H. Samet and A. Mojallal, "Enhancement of electric arc furnace reactive power compensation using Grey-Markov prediction method," in IET Generation, Transmission & Distribution, vol. 8, no. 9, pp. 1626-1636, Sept. 2014. doi: 10.1049/iet-gtd.2013.0698

[56] A. Garcia-Cerrada, P. Garcia-Gonzalez, R. Collantes, T. Gomez and J. Anzola, "Comparison of thyristor-controlled reactors and voltage-source inverters for compensation of flicker caused by arc furnaces," in IEEE Transactions on Power Delivery, vol. 15, no. 4, pp. 1225-1231, Oct 2000. doi: 10.1109/61.891507

[57] A. Alzate, A. Escobar and J. J. Marulanda, "Application of a D-STATCOM to mitigate arc furnaces power quality problems," 2011 IEEE Trondheim PowerTech, Trondheim, 2011, pp. 1-6. doi: 10.1109/PTC.2011.6019382

[58] P. R. Kasari, M. Paul, B. Das and A. Chakraborti, "Analysis of D-STATCOM for power quality enhancement in distribution network," TENCON 2017 - 2017 IEEE Region 10 Conference, Penang, 2017, pp. 1421-1426. doi: 10.1109/TENCON.2017.8228081

[59] A. Yazdani, M. L. Crow and J. Guo, "An Improved Nonlinear STATCOM Control for Electric Arc Furnace Voltage Flicker Mitigation," in IEEE Transactions on Power Delivery, vol. 24, no. 4, pp. 2284-2290, Oct. 2009. doi: 10.1109/TPWRD.2009.2027508

[60] K. Sedraoui, K. Al-haddad and G. Olivier, "Flicker Compensation in Arc Furnace Power systems Using the UPFC," 2006 IEEE International Symposium on Industrial Electronics, Montreal, Que., 2006, pp. 1864-1868. doi: 10.1109/ISIE.2006.295856

[61] T. S. Saggu, L. Singh and B. Gill, "Harmonics Mitigation in a Steel Industry Using 11-Level Cascaded Multilevel Inverter-Based DSTATCOM," in Canadian Journal of Electrical and Computer Engineering, vol. 40, no. 2, pp. 110-115, Spring 2017. doi: 10.1109/CJECE.2017.2681686

[62] J. M. Kanieski, R. Cardoso, H. Pinheiro and H. A. Gründling, "Kalman Filter-Based Control System for Power Quality Conditioning Devices," in IEEE Transactions on Industrial Electronics, vol. 60, no. 11, pp. 5214-5227, Nov. 2013. doi: 10.1109/TIE.2012.2226412

[63] Leon H. Beverly, Richad D. Hance, Alexander L. Kristalinski, Age T. Visser, "Method and apparatus for reducing the harmonic currents in alternating current distribution networks, " US Patent, 5576942, 19th Nov. 1996.

[64] G. Karmiris, G. Tsengenes, G. Adamidis, "A multifunction control scheme for current harmonic elimination and voltage sag mitigation using a three phase three level flying capacitor inverter," in Simulation Modelling Practice and Theory", Volume 24, Pages 15-34, 2012. Doi: 10.1016/j.simpat.2012.01.007

[65] K. P. Basu and S. A. Hafidz, "Mitigation of single-phase voltage sag and swell with zigzag transformer," 2008 Third International Conference on Electric Utility Deregulation and Restructuring and Power Technologies, Nanjuing, 2008, pp. 2369-2373. doi: 10.1109/DRPT.2008.4523808

[66] K. Selvajyothi and P. A. Janakiraman, "Reduction of Voltage Harmonics in Single Phase Inverters Using Composite Observers," in IEEE Transactions on Power Delivery, vol. 25, no. 2, pp. 1045-1057, April 2010. doi: 10.1109/TPWRD.2009.2035917

[67] S. Gautam, P. Yunqing, Y. Kafle, M. Kashif, S. Ul Hasan, "Evaluation of Fundamental d-q Synchronous Reference Frame Harmonic Detection Method for Single Phase Shunt Active Power Filter", in International Journal of Power Electronics and Drive System (IJPEDS), Vol. 4, No. 1, March 2014 pp. 112-126.

[68] V. Rajagopal, B. Singh and G. K. Kasal, "Electronic load controller with power quality improvement of isolated induction generator for small hydro power generation," in IET Renewable Power Generation, vol. 5, no. 2, pp. 202-213, March 2011. doi: 10.1049/iet-rpg.2010.0081

[69] H. Hu, W. Shi, Y. Lu and Y. Xing, "Design Considerations for DSP-Controlled 400 Hz Shunt Active Power Filter in an Aircraft Power System," in IEEE Transactions on Industrial Electronics, vol. 59, no. 9, pp. 3624-3634, Sept. 2012. doi: 10.1109/TIE.2011.2165452

[70] P. Mitra and G. K. Venayagamoorthy, "An Adaptive Control Strategy for DSTATCOM Applications in an Electric Ship Power System," in IEEE Transactions on Power Electronics, vol. 25, no. 1, pp. 95-104, Jan. 2010. doi: 10.1109/TPEL.2009.2024152

6. Configuration and Design of SAPF

[71] B. Singh, S. R. Arya,"Design and control of a DSTATCOM for power quality improvement using cross correlation function approach", International Journal of Engineering, Science and Technology, Vol. 4, No. 1, pp. 74-86, 2012. doi: 10.4314/ijest.v4il.9s

[72] S. K. Khadem, M. Basu and M. F. Conlon, "Harmonic power compensation capacity of shunt active power filter and its relationship with design parameters," in IET Power Electronics, vol. 7, no. 2, pp. 418-430, February 2014. doi: 10.1049/iet-pel.2013.0098

[73] G. Zhao, J. Liu and Z. Wang, "An analysis on the influence of interface inductor to STATCOM system with phase-shift control and corresponding design considerations," 2009 IEEE 6th International Power Electronics and Motion Control Conference, Wuhan, 2009, pp. 2339-2344. doi: 10.1109/IPEMC.2009.5157794

[74] D. Kumar and Rajesh, "Modelling, Analysis and Performance of a DSTATCOM for Unbalanced and Non-Linear Load," 2005 IEEE/PES Transmission & Distribution Conference & Exposition: Asia and Pacific, Dalian, 2005, pp. 1-6. doi: 10.1109/TDC.2005.1547142.

[75] T. Tian-yuan, J. Qi-rong, L. Gang and L. Yu-xiang, "Comparison of Direct and Indirect Current Control Strategy for DSTATCOM," 2006 International Conference on Power System Technology, Chongqing, 2006, pp. 1-8. doi: 10.1109/ICPST.2006.321895

[76] R. Panigrahi, P. C. Panda and B. D. Subudhi, "Comparison of performances of hysteresis and dead beat controllers in active power filtering," 2012 IEEE Third International Conference on Sustainable Energy Technologies (ICSET), Kathmandu, 2012, pp. 287-292. doi: 10.1109/ICSET.2012.6357413.

[77] C. Kumar and M. K. Mishra, "A control algorithm for flexible operation of DSTATCOM for power quality improvement in voltage and current control mode," 2012 IEEE International Conference on Power Electronics, Drives and Energy Systems (PEDES), Bengaluru, 2012, pp. 1-6. doi: 10.1109/PEDES.2012.6484392

[78] C. Kumar and M. K. Mishra, "A Voltage-Controlled DSTATCOM for Power-Quality Improvement," in IEEE Transactions on Power Delivery, vol. 29, no. 3, pp. 1499-1507, June 2014. doi: 10.1109/TPWRD.2014.2310234

[79] C. A. Sepúlveda, J. A. Muñoz, J. R. Espinoza, M. E. Figueroa and C. R. Baier, "FPGA v/s DSP Performance Comparison for a VSC-Based STATCOM Control Application," in IEEE Transactions on Industrial Informatics, vol. 9, no. 3, pp. 1351-1360, Aug. 2013. doi: 10.1109/TII.2012.2222419

[80] S. Srikanthan and M. K. Mishra, "DC Capacitor Voltage Equalization in Neutral Clamped Inverters for DSTATCOM Application," in IEEE Transactions on Industrial Electronics, vol. 57, no. 8, pp. 2768-2775, Aug. 2010.doi: 10.1109/TIE.2009.2022069

[81] C. A. Sepulveda, J. A. Munoz, J. R. Espinoza, M. E. Figueroa and P. E. Melin, "All-on-Chip dq-Frame Based D-STATCOM Control Implementation in a Low-Cost FPGA," in

IEEE Transactions on Industrial Electronics, vol. 60, no. 2, pp. 659-669, Feb. 2013. doi: 10.1109/TIE.2012.2206353

[82] R. T. Hock, Y. R. De Novaes and A. L. Batschauer, "A voltage regulator based in a voltage-controlled DSTATCOM with minimum power point tracker," 2014 IEEE Energy Conversion Congress and Exposition (ECCE), Pittsburgh, PA, 2014, pp. 3694-3701. doi: 10.1109/ECCE.2014.6953903.

[83] N. Voraphonpiput, I. Ngamroo, S. Chatratana, and N. Science, “Control System Design for a STATCOM using Complex Transfer Function,” in Proceedings of the 6th WSEAS International Conference on Instrumentation, Measurement, Circuits and Systems, pp. 186–192, 2007.

[84] B. Singh, P. Jayaprakash and D. P. Kothari, "Isolated H-bridge VSC Based 3-phase 4-wire DSTATCOM for power quality improvement," 2008 IEEE International Conference on Sustainable Energy Technologies, Singapore, 2008, pp. 366-371. doi: 10.1109/ICSET.2008.4747034

[85] S. Kumar, B. Singh, "Control of 3 Leg VSC Based 3Phase 4Wire DSTATCOM using Modified Instantaneous Symmetrical Component Theory," in International Journal of Automation and Power Engineering (IJAPE) Vol. 2 No. 6, September 2013

[86] S. Kumar and B. Singh, "Control of 4-Leg VSC based DSTATCOM using modified Instantaneous Symmetrical Component Theory," 2009 International Conference on Power Systems, Kharagpur, 2009, pp. 1-6. doi: 10.1109/ICPWS.2009.5442769

[87] A. Dheepanchakkravarthy, Jebasalma, “A Modern Approach of a Three Phase Four Wire Dstatcom for Power Quality Improvement Using T Connected Transformer”, in International Journal of Engineering Inventions, Vol. 1, No. 4 pp: 80-90, 2012

[88] B. Singh, P. Jayaprakash and D. P. Kothari, "A T-Connected Transformer and Three-leg VSC Based DSTATCOM for Power Quality Improvement," in IEEE Transactions on Power Electronics, vol. 23, no. 6, pp. 2710-2718, Nov. 2008. doi: 10.1109/TPEL.2008.2004273

[89] P. Jayaprakash, B. Singh and D. P. Kothari, "Implementation of an Isolated Three-Leg VSC with Star/Hexagon Transformer Based Three-Phase Four-Wire DSTATCOM," 2009 Second International Conference on Emerging Trends in Engineering & Technology, Nagpur, 2009, pp. 533-538. doi: 10.1109/ICETET.2009.122

[90] J. M. Kanieski, R. Cardoso, H. Pinheiro and H. A. Gründling, "Kalman Filter-Based Control System for Power Quality Conditioning Devices," in IEEE Transactions on Industrial Electronics, vol. 60, no. 11, pp. 5214-5227, Nov. 2013. doi: 10.1109/TIE.2012.2226412

[91] U. R. Babu, V. V. K. Reddy and S. T. Kalyani, "Power quality improvement in RDS using smart DSTATCOM," 2017 IEEE PES Asia-Pacific Power and Energy Engineering Conference (APPEEC), Bangalore, 2017, pp. 1-6. doi: 10.1109/APPEEC.2017.8308966

[92] B. Singh, K. Al-Haddad and A. Chandra, "A review of active filters for power quality improvement," in IEEE Transactions on Industrial Electronics, vol. 46, no. 5, pp. 960-971, Oct 1999. doi: 10.1109/41.793345

[93] B. Singh, P. Jayaprakash, D. P. Kothari, A. Chandra and K. A. Haddad, "Comprehensive Study of DSTATCOM Configurations," in IEEE Transactions on Industrial Informatics, vol. 10, no. 2, pp. 854-870, May 2014. doi: 10.1109/TII.2014.2308437

[94] Y. Yoldaş, A. Teke, and M. Barghi Latran, "Erratum: Mitigation of power quality problems using distribution static synchronous compensator: a comprehensive review," in IET Power Electronics, vol. 8, no. 10, pp. 2065-2065, 10 2015. doi: 10.1049/iet-pel.2015.0358.

7. SAPF Control Techniques

7.1. Conventional control techniques

[95] H. Akagi, Y. Kanazawa and A. Nabae, "Instantaneous Reactive Power Compensators Comprising Switching Devices without Energy Storage Components," in IEEE Transactions on Industry Applications, vol. IA-20, no. 3, pp. 625-630, May 1984. doi: 10.1109/TIA.1984.4504460

[96] Fang Zheng Peng, G. W. Ott and D. J. Adams, "Harmonic and reactive power compensation based on the generalized instantaneous reactive power theory for three-phase four-wire systems," in IEEE Transactions on Power Electronics, vol. 13, no. 6, pp. 1174-1181, Nov 1998. doi: 10.1109/63.728344

[97] S. Bhattacharya and D. Divan, "Synchronous frame based controller implementation for a hybrid series active filter system," Industry Applications Conference, 1995. Thirtieth IAS Annual Meeting, IAS '95., Conference Record of the 1995 IEEE, Orlando, FL, 1995, pp. 2531-2540 vol.3. doi: 10.1109/IAS.1995.530625

[98] B. Singh and V. Verma, "Selective Compensation of Power-Quality Problems Through Active Power Filter by Current Decomposition," in IEEE Transactions on Power Delivery, vol. 23, no. 2, pp. 792-799, April 2008. doi: 10.1109/TPWRD.2007.911108

[99] M. Labeeb and B. S. Lathika, "Design and analysis of DSTATCOM using SRFT and ANN-fuzzy based control for power quality improvement," 2011 IEEE Recent Advances in Intelligent Computational Systems, Trivandrum, 2011, pp. 274-279. doi: 10.1109/RAICS.2011.6069317

[100] P. Gharde, N. Pande and P. D. Debre, "Load compensation of a stiff system using ISCT based D-STATCOM under unbalanced and non-linear load condition," 2017 International Conference on Innovations in Information, Embedded and Communication Systems (ICIIECS), Coimbatore, 2017, pp. 1-4. doi: 10.1109/ICIIECS.2017.8276117

[101] B. N. Singh, B. Singh, A. Chandra and K. Al-Haddad, "Design and digital implementation of active filter with power balance theory," in IEE Proceedings - Electric Power Applications, vol. 152, no. 5, pp. 1149-1160, 9 Sept. 2005. doi: 10.1049/ip-epa:20050097

[102] S. Rechka, E. Ngandui, Jianhong Xu and P. Sicard, "Analysis of harmonic detection algorithms and their application to active power filters for harmonics compensation and resonance damping," in Canadian Journal of Electrical and Computer Engineering, vol. 28, no. 1, pp. 41-51, January 2003. doi: 10.1109/CJECE.2003.1426073

[103] R. L. d. A. Ribeiro, T. d. O. A. Rocha, R. M. de Sousa, E. C. dos Santos and A. M. N. Lima, "A Robust DC-Link Voltage Control Strategy to Enhance the Performance of Shunt Active Power Filters Without Harmonic Detection Schemes," in IEEE Transactions on Industrial Electronics, vol. 62, no. 2, pp. 803-813, Feb. 2015. doi: 10.1109/TIE.2014.2345329

[104] Z. Yuan and X. Mingchao, "A study on DC capacitor voltage control strategy of cascade circuit DSTATCOM," IEEE PES Innovative Smart Grid Technologies, Tianjin, 2012, pp. 1-4. doi: 10.1109/ISGT-Asia.2012.6303184

[105] H. Myneni, G. Siva Kumar and D. Sreenivasarao, "Dynamic dc voltage regulation of split-capacitor DSTATCOM for power quality improvement," in IET Generation, Transmission & Distribution, vol. 11, no. 17, pp. 4373-4383, 11 30 2017. doi: 10.1049/iet-gtd.2017.0494

[106] B. Singh and J. Solanki, "A Comparison of Control Algorithms for DSTATCOM," in IEEE Transactions on Industrial Electronics, vol. 56, no. 7, pp. 2738-2745, July 2009. doi: 10.1109/TIE.2009.2021596

7.2. Adaptive Control Algorithms

[107] S. Haykin and T. Kailath, “Adaptive Filter Theory”, Pearson education, New Delhi, India, 2003.

[108] A. Singh, M. Badoni and B. Singh, "Application of least means square algorithm to shunt compensator: An experimental investigation," 2014 IEEE International Conference on Power Electronics, Drives and Energy Systems (PEDES), Mumbai, 2014, pp. 1-6. doi: 10.1109/PEDES.2014.7042044

[109] S. R. Arya and B. Singh, "Performance of DSTATCOM Using Leaky LMS Control Algorithm," in IEEE Journal of Emerging and Selected Topics in Power Electronics, vol. 1, no. 2, pp. 104-113, June 2013. doi: 10.1109/JESTPE.2013.2266372

[110] M. Badoni, A. Singh and B. Singh, "Comparative Performance of Wiener Filter and Adaptive Least Mean Square-Based Control for Power Quality Improvement," in IEEE Transactions on Industrial Electronics, vol. 63, no. 5, pp. 3028-3037, May 2016. doi: 10.1109/TIE.2016.2515558.

[111] J. B. Evans, P. Xue and B. Liu, "Analysis and implementation of variable step size adaptive algorithms," in IEEE Transactions on Signal Processing, vol. 41, no. 8, pp. 2517-2535, Aug 1993. doi: 10.1109/78.229885.

[112] J. F. Liu, Z. Q. Jiang, J. Li and X. Huo, “A Novel Variable Step-Size LMS Adaptive Filtering Algorithm Based on Lorentzian Function,” in Command Control and Simulation, vol. 31, issue. 2, pp. 42-44, 2009.

[113] M. Badoni, A. Singh and B. Singh, "Adaptive Neurofuzzy Inference System Least-Mean-Square-Based Control Algorithm for DSTATCOM," in IEEE Transactions on Industrial Informatics, vol. 12, no. 2, pp. 483-492, April 2016. doi: 10.1109/TII.2016.2516823

[114] B. Singh, S. K. Dube and S. R. Arya, "Hyperbolic tangent function-based least mean-square control algorithm for distribution static compensator," in IET Generation, Transmission & Distribution, vol. 8, no. 12, pp. 2102-2113, 12 2014. doi: 10.1049/iet-gtd.2014.0172

7.3. Neural Network Control Techniques

[115] S. Haykin, “Neural networks and learning machines”, Pearson Education, Inc., Upper Saddle River, New Jersey 07458, 2009.

[116] C.T. Lin and Lee, C. S. G., Neural Fuzzy Systems, A Neuro–Fuzzy Synergism to Intelligent Systems. Englewood Cliffs, NJ: Prentice-Hall, pp. 533–607.

[117] S. R. Arya and B. Singh, "Neural Network Based Conductance Estimation Control Algorithm for Shunt Compensation," in IEEE Transactions on Industrial Informatics, vol. 10, no. 1, pp. 569-577, Feb. 2014. doi: 10.1109/TII.2013.2264290

[118] R. Waswani, K. Fegade, A. Singh and R. Patel, "Power quality improvement by artificial neural network using dstatcom in electric ship," 2017 International Conference on Innovations in Information, Embedded and Communication Systems (ICIIECS), Coimbatore, 2017, pp. 1-4. doi: 10.1109/ICIIECS.2017.8276072

[119] L. T. Teng, F. j. Lin, H. c. Chiang and J. w. Lin, "Recurrent wavelet neural network controller with improved particle swarm optimisation for induction generator system," in IET Electric Power Applications, vol. 3, no. 2, pp. 147-159, March 2009. doi: 10.1049/iet-epa:20080038

[120] M. Cirrincione, M. Pucci, G. Vitale and A. Miraoui, "Current Harmonic Compensation by a Single-Phase Shunt Active Power Filter Controlled by Adaptive Neural Filtering," in IEEE Transactions on Industrial Electronics, vol. 56, no. 8, pp. 3128-3143, Aug. 2009. doi: 10.1109/TIE.2009.2022070

7.4. Modern Control Techniques

[121] R. Panigrahi, P. C. Panda and B. D. Subudhi, "New strategy for generation of reference current in Active Power Filters with distortion in line voltage," 2012 IEEE 7th International Conference on Industrial and Information Systems (ICIIS), Chennai, 2012, pp. 1-5. doi: 10.1109/ICIInfS.2012.6304814.

[122] R. L. de Araujo Ribeiro, C. C. de Azevedo and R. M. de Sousa, "A Robust Adaptive Control Strategy of Active Power Filters for Power-Factor Correction, Harmonic Compensation, and Balancing of Nonlinear Loads," in IEEE Transactions on Power Electronics, vol. 27, no. 2, pp. 718-730, Feb. 2012. doi: 10.1109/TPEL.2011.2161334

[123] P. C. Loh, Y. Tang, F. Blaabjerg and P. Wang, "Mixed-frame and stationary-frame repetitive control schemes for compensating typical load and grid harmonics," in IET

Power Electronics, vol. 4, no. 2, pp. 218-226, February 2011. doi: 10.1049/iet-pel.2009.0222

[124] Z. X. Zou, K. Zhou, Z. Wang and M. Cheng, "Frequency-Adaptive Fractional-Order Repetitive Control of Shunt Active Power Filters," in IEEE Transactions on Industrial Electronics, vol. 62, no. 3, pp. 1659-1668, March 2015. doi: 10.1109/TIE.2014.2363442

[125] G. A. Ramos and R. Costa-Castello, "Power factor correction and harmonic compensation using second-order odd-harmonic repetitive control," in IET Control Theory & Applications, vol. 6, no. 11, pp. 1633-1644, July 19 2012. doi: 10.1049/iet-cta.2011.0272

[126] N. Hoffmann and F. W. Fuchs, "Online grid impedance estimation for the control of grid connected converters in inductive-resistive distributed power-networks using extended kalman-filter," 2012 IEEE Energy Conversion Congress and Exposition (ECCE), Raleigh, NC, 2012, pp. 922-929. doi: 10.1109/ECCE.2012.6342720

[127] R. Cardoso, J. Kanieski, H. Pinheiro and H. A. Grundling, "Reference Generation for Shunt Active Power Filters Based on Optimum Filtering Theory," 2007 IEEE Industry Applications Annual Meeting, New Orleans, LA, 2007, pp. 1621-1627. doi: 10.1109/07IAS.2007.250

[128] B. Singh and S. R. Arya, "Back-Propagation Control Algorithm for Power Quality Improvement Using DSTATCOM," in IEEE Transactions on Industrial Electronics, vol. 61, no. 3, pp. 1204-1212, March 2014. doi: 10.1109/TIE.2013.2258303

8. Shunt Compensation in TPTW Distribution System

[129] T. Jin and K. M. Smedley, "Operation of One-Cycle Controlled Three-Phase Active Power Filter With Unbalanced Source and Load," in IEEE Transactions on Power Electronics, vol. 21, no. 5, pp. 1403-1412, Sept. 2006. doi: 10.1109/TPEL.2006.880264

[130] S. A. Verne and M. I. Valla, “Active power filter for medium voltage networks with predictive current control,” Electric Power Systems Research, vol. 80, no. 12, pp. 1543–1551, 2010. doi: 10.1016/j.epsr.2010.06.019.

[131] S. Rahmani, A. Hamadi and K. Al-Haddad, "A Lyapunov-Function-Based Control for a Three-Phase Shunt Hybrid Active Filter," in IEEE Transactions on Industrial Electronics, vol. 59, no. 3, pp. 1418-1429, March 2012. doi: 10.1109/TIE.2011.2163370

[132] B. Singh and S. R. Arya, "Implementation of Single-Phase Enhanced Phase-Locked Loop-Based Control Algorithm for Three-Phase DSTATCOM," in IEEE Transactions on Power Delivery, vol. 28, no. 3, pp. 1516-1524, July 2013. doi: 10.1109/TPWRD.2013.2257876

[133] N. Dhyani, A. Singh and M. Badoni, "Implemention of distribution energy source as a compensator based on power balance control algorithm," 2014 International Conference on Signal Propagation and Computer Technology (ICSPCT 2014), Ajmer, 2014, pp. 732-737. doi: 10.1109/ICSPCT.2014.6884964

[134] S. K. Kesharvani, A. Singh and M. Badoni, "Conductance based fryze algorithm for improving power quality for non-linear loads," 2014 International Conference on Signal Propagation and Computer Technology (ICSPCT 2014), Ajmer, 2014, pp. 703-708. doi: 10.1109/ICSPCT.2014.6884965

[135] S. R. Arya, B. Singh, A. Chandra and K. Al-Haddad, "Learning-Based Anti-Hebbian Algorithm for Control of Distribution Static Compensator," in IEEE Transactions on Industrial Electronics, vol. 61, no. 11, pp. 6004-6012, Nov. 2014. doi: 10.1109/TIE.2014.2321341

[136] M. T. Ahmad, N. Kumar and B. Singh, "Fast multilayer perceptron neural network-based control algorithm for shunt compensator in distribution systems," in IET Generation, Transmission & Distribution, vol. 10, no. 15, pp. 3824-3833, 11 17 2016. doi: 10.1049/iet-gtd.2016.0328

[137] A. Panda Kumar and M. Mangaraj, "DSTATCOM employing hybrid neural network control technique for power quality improvement," in IET Power Electronics, vol. 10, no. 4, pp. 480-489, 3 31 2017. doi: 10.1049/iet-pel.2016.0556

[138] B. Singh, S. K. Dube, and S. R. Arya, “An improved control algorithm of DSTATCOM for power quality improvement,” in International Journal of Electrical Power & Energy Systems, vol. 64, pp. 493–504, 2015. doi: 10.1016/j.ijepes.2014.07.055

[139] M. Badoni, A. Singh and B. Singh, "Variable Forgetting Factor Recursive Least Square Control Algorithm for DSTATCOM," in IEEE Transactions on Power Delivery, vol. 30, no. 5, pp. 2353-2361, Oct. 2015. doi: 10.1109/TPWRD.2015.2422139

[140] R. B. Roy, J. Cros, E. Basher and S. Akhter, "Power compensation by DSTATCOM plus SCESS," 2017 4th International Conference on Advances in Electrical Engineering (ICAEE), Dhaka, 2017, pp. 32-37. doi: 10.1109/ICAEE.2017.8255322

[141] M. T. Ahmad, N. Kumar and B. Singh, "A discrete derivative control technique for DC link voltage in shunt compensator," 2015 Annual IEEE India Conference (INDICON), New Delhi, 2015, pp. 1-5. doi: 10.1109/INDICON.2015.7443429

[142] M. Badoni, A. Singh and B. Singh, "DSP based implementation of an immune feedback algorithm for control of shunt compensator," 2016 IEEE 6th International Conference on Power Systems (ICPS), New Delhi, 2016, pp. 1-6. doi: 10.1109/ICPES.2016.7584008

[143] P. Doley, S. K. Patel, S. R. Arya and U. K. Kalla, "Control algorithm based on amplitude adaptive filter for DSTATCOM," 2016 IEEE 7th Power India International Conference (PIICON), Bikaner, 2016, pp. 1-6. doi: 10.1109/POWERI.2016.8077448

[144] M. Badoni, B. Singh and A. Singh, "Implementation of Echo-State Network-Based Control for Power Quality Improvement," in IEEE Transactions on Industrial Electronics, vol. 64, no. 7, pp. 5576-5584, July 2017. doi: 10.1109/TIE.2017.2677359

[145] S. Bhattacharya and B. A. Shimray, "Power quality improvement and mitigation of harmonic distortion using DSTATCOM with PI and Fuzzy Logic Controller," 2017 International Conference on Smart grids, Power and Advanced Control Engineering (ICSPACE), Bangalore, 2017, pp. 183-189. doi: 10.1109/ICSPACE.2017.8343426

[146] B. Singh, K. Mathuria, I. Hussain and S. Kumar, "Implementation of demodulation-SOGI control algorithm for improving the power quality," IECON 2017 - 43rd Annual Conference of the IEEE Industrial Electronics Society, Beijing, 2017, pp. 2540-2545. doi: 10.1109/IECON.2017.8216427

[147] M. G. Kumari and K. Gnanambal, "Mitigation of power quality events using deadbeat predictive controller based distribution static compensator," 2017 International Conference on Innovations in Green Energy and Healthcare Technologies (IGEHT), Coimbatore, 2017, pp. 1-6. doi: 10.1109/IGEHT.2017.8094052

[148] M. T. Ahmad, N. Kumar and B. Singh, "AVSF-based control algorithm of DSTATCOM for distribution system," in IET Generation, Transmission & Distribution, vol. 11, no. 13, pp. 3389-3396, 9 7 2017. doi: 10.1049/iet-gtd.2017.0225

[149] M. Mangaraj and A. K. Panda, "NBP-based icosϕ control strategy for DSTATCOM," in IET Power Electronics, vol. 10, no. 12, pp. 1617-1625, 10 6 2017. doi: 10.1049/iet-pel.2017.0129

[150] M. T. Ahmad, N. Kumar and B. Singh, "Generalised neural network-based control algorithm for DSTATCOM in distribution systems," in IET Power Electronics, vol. 10, no. 12, pp. 1529-1538, 10 6 2017. doi: 10.1049/iet-pel.2016.0680

9. Shunt Compensation in TPFW Distribution System

[151] P. Jayaprakash, B. Singh and D. P. Kothari, "DSP based implementation of a three-phase four-wire DSTATCOM for voltage regulation and power quality improvement," 2009 35th Annual Conference of IEEE Industrial Electronics, Porto, 2009, pp. 3660-3665. doi: 10.1109/IECON.2009.5415140

[152] B. Singh and S. Kumar, "Control of DSTATCOM using IcosΦ algorithm," 2009 35th Annual Conference of IEEE Industrial Electronics, Porto, 2009, pp. 322-327. doi: 10.1109/IECON.2009.5414942

[153] V. George and M. K. Mishra, "Design and Analysis of User-Defined Constant Switching Frequency Current-Control-Based Four-Leg DSTATCOM," in IEEE Transactions on Power Electronics, vol. 24, no. 9, pp. 2148-2158, Sept. 2009. doi: 10.1109/TPEL.2009.2019821

[154] T. Zaveri, B. Bhalja, N. Zaveri, “Comparison of control strategies for DSTATCOM in three-phase, four-wire distribution system for power quality improvement under various source voltage and load conditions”, in International Journal of Electrical Power & Energy Systems, Vol. 43, No. 1, pp. 582-594, 2012. doi: 10.1016/j.ijepes.2012.06.044.

[155] B. Singh and S. R. Arya, "Composite observer-based control algorithm for distribution static compensator in four-wire supply system," in *IET Power Electronics*, vol. 6, no. 2, pp. 251-260, Feb. 2013. doi: 10.1049/iet-pel.2012.0412

[156] M. Kumar, A. Swarnkar, N. Gupta and K. R. Niazi, "Design and operation of DSTATCOM for power quality improvement in distribution systems," in The Journal of Engineering, vol. 2017, no. 13, pp. 2328-2333, 2017. doi: 10.1049/joe.2017.0747

[157] M. Mangaraj, T. Penthia and A. K. Panda, "Power quality improvement by a 3-phase 4-leg supercapacitor based DSTATCOM," 2016 IEEE Uttar Pradesh Section International Conference on Electrical, Computer and Electronics Engineering (UPCON), Varanasi, 2016, pp. 91-97. doi: 10.1109/UPCON.2016.7894631

[158] D. Suresh, D. M. Rao and G. D. Sukumar, "Reduced rating hybrid DSTATCOM for three phase four wire distribution system," 2016 IEEE 1st International Conference on Power Electronics, Intelligent Control and Energy Systems (ICPEICES), Delhi, 2016, pp. 1-4. doi: 10.1109/ICPEICES.2016.7853646

[159] H. Myneni, G. S. Kumar and D. Sreenivasarao, "Adaptive dc-link voltage regulation for DSTATCOM under load variations," 2016 IEEE Region 10 Conference (TENCON), Singapore, 2016, pp. 2909-2913. doi: 10.1109/TENCON.2016.7848577

[160] P. Y. Tooski, B. Eskandari and M. R. Azizi, "Three-phase four-wire compensator in distribution system; Detailed simulation for implementation," 2018 9th Annual Power Electronics, Drives Systems and Technologies Conference (PEDSTC), Tehran, 2018, pp. 206-211. doi: 10.1109/PEDSTC.2018.8343797

[161] A. Mus-ab and M. K. Mishra, "Wavelet transform based algorithms for load compensation using DSTATCOM," 2017 IEEE PES Asia-Pacific Power and Energy Engineering Conference (APPEEC), Bangalore, 2017, pp. 1-6. doi: 10.1109/APPEEC.2017.8309012

[162] B. Singh, K. Kant and S. R. Arya, "Notch filter-based fundamental frequency component extraction to control distribution static compensator for mitigating current-related power quality problems," in *IET Power Electronics*, vol. 8, no. 9, pp. 1758-1766, 9 2015. doi: 10.1049/iet-pel.2014.0486

[163] S. K. Patel, S. R. Arya, R. Maurya and B. C. Babu, "Control Scheme for DSTATCOM based on Frequency Adaptive Disturbance Observer," in IEEE Journal of Emerging and Selected Topics in Power Electronics. doi: 10.1109/JESTPE.2018.2808191.

[164] S. Singhai, M. N. Ansari and M. Jain, "Application of DSTATCOM for power quality improvement using isolated zig-zag/star transformer under varying consumer load," 2016 International Conference on Electrical Power and Energy Systems (ICEPES), Bhopal, 2016, pp. 270-275. doi: 10.1109/ICEPES.2016.7915942

[165] Y. Rohilla and Y. Pal, "T-connected transformer integrated three-leg VSC based 3P4W DSTATCOM for power quality improvement," 2013 Nirma University International Conference on Engineering (NUiCONE), Ahmedabad, 2013, pp. 1-7. doi: 10.1109/NUiCONE.2013.6780146.

[166] B. Singh, P. Jayaprakash, S. Kumar and D. P. Kothari, "Implementation of Neural-Network-Controlled Three-Leg VSC and a Transformer as Three-Phase Four-Wire DSTATCOM," in IEEE Transactions on Industry Applications, vol. 47, no. 4, pp. 1892-1901, July-Aug. 2011. doi: 10.1109/TIA.2011.2153811

[167] B. Singh, S. R. Arya, C. Jain and S. Goel, "Implementation of four-leg distribution static compensator," in IET Generation, Transmission & Distribution, vol. 8, no. 6, pp. 1127-1139, June 2014. doi: 10.1049/iet-gtd.2013.0582

10. Shunt Compensation in Distorted Grid Distribution System

[168] G. D. Marques, "A comparison of active power filter control methods in unbalanced and non-sinusoidal conditions," *Industrial Electronics Society, 1998. IECON '98. Proceedings of the 24th Annual Conference of the IEEE*, Aachen, 1998, pp. 444-449 vol.1. doi: 10.1109/IECON.1998.724284

[169] U. K. Rao, M. K. Mishra and A. Ghosh, "Control Strategies for Load Compensation Using Instantaneous Symmetrical Component Theory Under Different Supply Voltages," in IEEE Transactions on Power Delivery, vol. 23, no. 4, pp. 2310-2317, Oct. 2008. doi: 10.1109/TPWRD.2008.923053

[170] N. Gupta , S. P. Singh & R. C. Bansal , "A Digital Signal Processor Based Performance Evaluation of Three-phase Four-wire Shunt Active Filter for Harmonic Elimination, Reactive Power Compensation, and Balancing of Non-linear Loads under Noni deal Mains Voltages", in Electric Power Components and Systems, Vol 40, No. 10, pp. 1119-1148, doi: 10.1080/15325008.2012.682248

[171] N. S. Pande, S. P. Gawande and M. R. Ramteke, "Control of D-STATCOM under unbalanced and distorted voltages using Synchronous Detection method for load compensation," International Conference on Recent Advances and Innovations in Engineering (ICRAIE-2014), Jaipur, 2014, pp. 1-6. doi: 10.1109/ICRAIE.2014.6909302

[172] K. Srinivas and S. S. Tulasi Ram, "A fast dynamic response of three phase four wire shunt active power filter under unbalanced non stiff source," 2014 International Conference on Smart Electric Grid (ISEG), Guntur, 2014, pp. 1-8. doi: 10.1109/ISEG.2014.7005387.

[173] N. Beniwal, I. Hussain and B. Singh, "Implementation of DSTATCOM with i-PNLMS based control algorithm under abnormal grid conditions," 2016 7th India International Conference on Power Electronics (IICPE), Patiala, 2016, pp. 1-5. doi: 10.1109/IICPE.2016.8079475.

[174] S. Mishra, S. K. Dash and P. K. Ray, "Performance analysis of L-type PV-DSTATCOM under ideal and distorted supply voltage," 2016 IEEE Students' Technology Symposium (TechSym), Kharagpur, 2016, pp. 180-185. doi: 10.1109/TechSym.2016.7872678

[175] N. Beniwal, I. Hussain and B. Singh, "Hybrid VSS–LMS–LMF based adaptive control of SPV-DSTATCOM system under distorted grid conditions," in IET Renewable Power Generation, vol. 12, no. 3, pp. 311-322, 2 26 2018. doi: 10.1049/iet-rpg.2016.0868

[176] I. Hussain, R. K. Agarwal and B. Singh, "MLP Control Algorithm for Adaptable Dual-Mode Single-Stage Solar PV System Tied to Three-Phase Voltage-Weak Distribution Grid," in IEEE Transactions on Industrial Informatics. doi: 10.1109/TII.2018.2811485

[177] R. K. Agarwal, I. Hussain and B. Singh, "Application of LMS-Based NN Structure for Power Quality Enhancement in a Distribution Network Under Abnormal Conditions," in IEEE Transactions on Neural Networks and Learning Systems, vol. 29, no. 5, pp. 1598-1607, May 2018. doi: 10.1109/TNNLS.2017.2677961

11. Solar Photo-Voltaic and other Renewable Energy System

[178] C.S. Solanki, “Solar Photovoltaics: Fundamentals Technologies And Applications”, Prentice-Hall Of India Pvt. Limited, 2009.

[179] M. Liserre, T. Sauter and J. Y. Hung, "Future Energy Systems: Integrating Renewable Energy Sources into the Smart Power Grid Through Industrial Electronics," in IEEE Industrial Electronics Magazine, vol. 4, no. 1, pp. 18-37, March 2010. doi: 10.1109/MIE.2010.935861.

[180] Y. Wu, V. K. N. Lau, D. H. K. Tsang, L. P. Qian and L. Meng, "Optimal Energy Scheduling for Residential Smart Grid With Centralized Renewable Energy Source," in IEEE Systems Journal, vol. 8, no. 2, pp. 562-576, June 2014. doi: 10.1109/JSYST.2013.2261001

[181] “Scope of the work in progress includes irradiance and temperature performance measurements and power rating for PV module performance testing and energy rating,” in IEC standard 61853, part 1, 2011.

[182] Photovoltaic (PV) systems - Requirements for testing, documentation and maintenance - Part 1: Grid connected systems - Documentation, commissioning tests and inspection, in IEC standard 62446, part 1, 2016.

[183] Photovoltaic system performance - Part 1: Monitoring” in IEC standard 61724, part-1, 2017

[184] Photovoltaic system performance - Part 2: Capacity evaluation method in IEC standard 61724, part -2, 2016

[185] Photovoltaic system performance - Part 3: Energy evaluation method in IEC standard 61724, part -3, 2016

[186] IEEE Standard for Interconnection and Interoperability of Distributed Energy Resources with Associated Electric Power Systems Interfaces," in IEEE Std 1547-2018 (Revision of IEEE Std 1547-2003) , vol., no., pp.1-138, April 6 2018. doi: 10.1109/IEEESTD.2018.8332112

[187] B. Subudhi and R. Pradhan, "A Comparative Study on Maximum Power Point Tracking Techniques for Photovoltaic Power Systems," in IEEE Transactions on Sustainable Energy, vol. 4, no. 1, pp. 89-98, Jan. 2013. doi: 10.1109/TSTE.2012.2202294.

[188] V. Kokaew, S. M. Sharkh and M. Moshrefi-Torbati, "Maximum Power Point Tracking of a Small-Scale Compressed Air Energy Storage System," in IEEE Transactions on Industrial Electronics, vol. 63, no. 2, pp. 985-994, Feb. 2016. doi: 10.1109/TIE.2015.2477344

[189] L. M. Elobaid, A. K. Abdelsalam and E. E. Zakzouk, "Artificial neural network-based photovoltaic maximum power point tracking techniques: a survey," in IET Renewable Power Generation, vol. 9, no. 8, pp. 1043-1063, 11 2015. doi: 10.1049/iet-rpg.2014.0359.

[190] Ravi Nath Tripathi, A. Singh and M. Badoni, "A MATLAB-simulink-based solar photovoltaic array (SPVA) module with MPPT," *2013 International Conference on Emerging Trends in Communication, Control, Signal Processing and Computing Applications (C2SPCA)*, Bangalore, 2013, pp. 1-6. doi: 10.1109/C2SPCA.2013.6749383

[191] J. Rathinadurai Louis, S. Shanmugham, K. Gunasekar, N. R. Atla and K. Murugesan, "Effective utilisation and efficient maximum power extraction in partially shaded photovoltaic systems using minimum-distance-average-based clustering algorithm," in IET Renewable Power Generation, vol. 10, no. 3, pp. 319-326, 3 2016. doi: 10.1049/iet-rpg.2014.0316.

[192] M. B. Shadmand, M. Mosa, R. S. Balog and H. A. Rub, "An improved MPPT technique for high gain DC-DC converter using model predictive control for photovoltaic applications," 2014 IEEE Applied Power Electronics Conference and Exposition - APEC 2014, Fort Worth, TX, 2014, pp. 2993-2999. doi: 10.1109/APEC.2014.6803730

[193] N. Saxena, B. Singh and A. L. Vyas, "Single-phase solar PV system with battery and exchange of power in grid-connected and standalone modes," in IET Renewable Power Generation, vol. 11, no. 2, pp. 325-333, 2 8 2017. doi: 10.1049/iet-rpg.2016.0143.

[194] M. S. Pádua, S. M. Deckmann, G. S. Sperandio, F. P. Marafão, and D. Colón, "Comparative analysis of Synchronization Algorithms based on PLL, RDFT and Kalman Filter," 2007 IEEE International Symposium on Industrial Electronics, Vigo, 2007, pp. 964-970. doi: 10.1109/ISIE.2007.4374728.

[195] L. G. Barbosa Rolim, D. Rodrigues da Costa and M. Aredes, "Analysis and Software Implementation of a Robust Synchronizing PLL Circuit Based on the pq Theory," in IEEE Transactions on Industrial Electronics, vol. 53, no. 6, pp. 1919-1926, Dec. 2006. doi: 10.1109/TIE.2006.885483

[196] S. Deo, C. Jain and B. Singh, "A PLL-Less Scheme for Single-Phase Grid Interfaced Load Compensating Solar PV Generation System," in IEEE Transactions on Industrial Informatics, vol. 11, no. 3, pp. 692-699, June 2015. doi: 10.1109/TII.2015.2425138.

[197] S. Kumar, A. K. Verma, I. Hussain, B. Singh and C. Jain, "Better Control for a Solar Energy System: Using Improved Enhanced Phase-Locked Loop-Based Control Under Variable Solar Intensity," in *IEEE Industry Applications Magazine*, vol. 23, no. 2, pp. 24-36, March-April 2017. doi: 10.1109/MIAS.2016.2600730

[198] B. Singh, P. Shah and I. Hussain, "ISOGI-Q Based Control Algorithm for a Single Stage Grid Tied SPV System," in IEEE Transactions on Industry Applications, vol. 54, no. 2, pp. 1136-1145, March-April 2018. doi: 10.1109/TIA.2017.2784374

[199] F. Gonzalez-Espin, I. Patrao, E. Figueres and G. Garcera, "An Adaptive Digital Control Technique for Improved Performance of Grid Connected Inverters," in IEEE

Transactions on Industrial Informatics, vol. 9, no. 2, pp. 708-718, May 2013. doi: 10.1109/TII.2012.2225437

[200] B. Singh, C. Jain, S. Goel, A. Chandra and K. Al-Haddad, "A Multifunctional Grid-Tied Solar Energy Conversion System With ANF-Based Control Approach," in IEEE Transactions on Industry Applications, vol. 52, no. 5, pp. 3663-3672, Sept.-Oct. 2016. doi: 10.1109/TIA.2016.2582141

[201] R. K. Agarwal, I. Hussain and B. Singh, "LMF-Based Control Algorithm for Single Stage Three-Phase Grid Integrated Solar PV System," in IEEE Transactions on Sustainable Energy, vol. 7, no. 4, pp. 1379-1387, Oct. 2016. doi: 10.1109/TSTE.2016.2553181

[202] M. Singh and A. Chandra, "Real-Time Implementation of ANFIS Control for Renewable Interfacing Inverter in 3P4W Distribution Network," in IEEE Transactions on Industrial Electronics, vol. 60, no. 1, pp. 121-128, Jan. 2013. doi: 10.1109/TIE.2012.2186103

[203] Y. Liu, B. Ge, H. Abu-Rub and H. Sun, "Hybrid Pulsewidth Modulated Single-Phase Quasi-Z-Source Grid-Tie Photovoltaic Power System," in IEEE Transactions on Industrial Informatics, vol. 12, no. 2, pp. 621-632, April 2016. doi: 10.1109/TII.2016.2524561

[204] T. F. Wu, C. H. Chang, L. C. Lin and C. L. Kuo, "Power Loss Comparison of Single- and Two-Stage Grid-Connected Photovoltaic Systems," in IEEE Transactions on Energy Conversion, vol. 26, no. 2, pp. 707-715, June 2011. doi: 10.1109/TEC.2011.2123897

[205] F. Wu, X. Li, F. Feng and H. B. Gooi, "Modified Cascaded Multilevel Grid-Connected Inverter to Enhance European Efficiency and Several Extended Topologies," in IEEE Transactions on Industrial Informatics, vol. 11, no. 6, pp. 1358-1365, Dec. 2015. doi: 10.1109/TII.2015.2486623

[206] M. Mahdianpoor, A. Kiyoumarsi, M. Ataei and R. A. Hooshmand, "Robust Implementation of Distribution Static Compensator Along With Bridge Type Fault Current Limiter for Fault Ride Through Enhancement of Fixed Speed Wind Turbines," in IEEE Access, vol. 5, pp. 14490-14501, 2017. doi: 10.1109/ACCESS.2017.2696884

APPENDIX A

SYSTEM DATA FOR THREE PHASE THREE WIRE SYSTEM

Grid Supply: 110V, 3-ph, 50Hz. SAPF rating: 25kVA. DC link voltage: V_{dc} = 200V, Interfacing inductor: L_f=3.1mH, Linear load: 10 kW, 0.8 p.f., Nonlinear load: 3-phase uncontrolled diode rectifier with R=20-120 Ω, L=80 mH, Capacitance of dc bus: C_{dc}=1500μF.

APPENDIX B

SYSTEM DATA FOR THREE PHASE FOUR WIRE SYSTEM

Grid Supply: 110V, 3-ph, 50Hz. SAPF rating: 25kVA. DC link voltage: V_{dc} = 200V, Interfacing inductor: L_f=3.1mH, Linear load:10 kW, 0.8 p.f., Nonlinear load: 3-phase uncontrolled diode rectifier with R=20-120 Ω, L=80 mH, Capacitance of dc bus: C_{dc}=1500μF, Zigzag Transformer: three single phase 110/110 V, 2.5 kVA each.

APPENDIX C

SYSTEM DATA FOR SINGLE PHASE GRID CONNECTED SYSTEM

Grid Supply: 63.5 V, 1-ph, 50Hz. SAPF rating: 10 kVA. DC link voltage: V_{dc} = 100V, Interfacing inductor: L_f=1 mH, Nonlinear load: single-phase uncontrolled diode rectifier with R=20-120 Ω, L=80 mH, Capacitance of dc bus: C_{dc}=1600μF, PV panels: make Vikram Solar, P_{max}=250W, V_{oc}=37.5V, I_{sc}=8.7A, V_{mp}=30.6V, I_{mp}=8.18A.